Investigation of Molikpaq 1986 Ice Loading Events & Evaluation of Load Measuring Devices

FINAL REPORT

Submitted to:

Canadian Hydraulics Centre

National Research Council of Canada

Ottawa, ON

Canada K1A 0R6

By:

Ian Jordaan and Associates Inc.

7 East Middle Battery Road

St. John's, NL

Canada A1A 1A3

January 14, 2010

This page is intentionally left blank

Investigation of Molikpaq 1986 Ice Loading Events
& Evaluation of Load Measuring Devices

Final Report

Submitted to:
Canadian Hydraulics Centre
National Research Council of Canada
Ottawa On
Canada K1A 0R6

Submitted by:
Ian Jordaan & Associates
7 East Middle Battery Road
St John's NL
Canada A1A 1A3

Jonathon Bruce, C-CORE
Mark Fuglem, C-CORE
Rocky Taylor, C-CORE (Chapter 6)
Ian Jordaan, Project Manager   January 14, 2010

Executive Summary

The project focuses on the measurements of load on the Molikpaq structure during the 1986 deployment at the Amauligak I65 location. The structure consists of a steel annulus, octagonal in form, serving as a caisson to support drilling operations. The structure was instrumented so as to obtain estimates of ice loads. These have been based on Medof panels attached to the outer steel surface, strain gauges installed on the steel structure, extensometers measuring the deformation of the caisson as well as inferences from the geotechnical design and performance of the structure. In past work, there has been a tendency to use the Medof panels to estimate loads, but at the same time, discrepancies have been noted over the years. In particular, Kevin Hewitt has drawn attention to the fact that geotechnical information suggests lower loads than those estimated from the Medof panels using the original calibrations of these panels. According to Hewitt, the difference could be as high as 300 MN (500 MN as compared to about 200 MN).

Subsequent to the ice loading events of 1986, a Joint Industry Project was carried out to study the events and associated measurements of the Molikpaq. This is referred to as the "1986 JIP". The measurements on the Molikpaq together with the 1986 JIP and its original set of reports have formed the basis of the present study. The IJA project team has concluded that the results of the 1986 JIP need reconsideration. The key aspect that should be reconsidered is the strong reliance on the original calibrations of the Medof panels in the 1986 JIP. The recent report by Klohn Crippen Berger (2009) provides a summary of this JIP. The team is consequently in disagreement with the Klohn Crippen Berger interpretation, which is closely aligned with the 1986 JIP reports. It is considered that the arguments in the report supporting the original Medof calibration are not well-founded.

The IJA project team has acknowledged that there are uncertainties in the Sandwell structural stiffness finite element results (used in conjunction with displacements measured by extensometers in the present study to provide an alternative estimate of ice loads on the Molikpaq structure), but these are outweighed by the far greater uncertainties in the Medof panel results. In fact, the points raised by Klohn Crippen Berger have been dealt with in our work. The ice mechanics in the report omits reference to work after the 1986 JIP in which the behaviour and failure of high-pressure zones have been discovered. The ice mechanics, as a result, are out of date. No cause to change the present approach has been found in the Klohn Crippen Berger report.

The extensometer readings have also been found to give lower loads than those deduced from the Medof panels, and in some reports, there is an indication that strain gauges have also given low values. This is broadly in agreement with the geotechnical information summarized in the first paragraph above. The supposition in the present study was that probabilistic averaging of local loads might explain part of these differences, at least between the extensometers and the Medof panels. The averaging technique takes into account the fact that for many failure modes, crushing in particular, the spatial variation of pressures across the face of the structure is highly uncorrelated, except locally. This

means that the standard deviation of global loads is much less than that for the locally measured loads (or pressures).

The data from the Medof panels on the Molikpaq were subjected to statistical analysis to determine the variation of correlation with distance. This was carried out for creep and crushing events. The values of the correlation coefficient were used in an analysis to account for the averaging effect, resulting in a model of probabilistic averaging. Then the events were analyzed to determine the effect of probabilistic averaging, as compared to linear (or simple) averaging. The latter is based on extrapolation of the averaged Medof panel loads to the full structure width by the ratio of structure width to Medof panel total width. It is noted that the Medof panel width is about 10% of the structure width.

Results are shown in the following table, where LA = linear averaging and PA = probabilistic averaging. The values are face loads, but are not given dimensions because of the uncertainty in the Medof panel calibration constant (the original calibration was used). Although reduced global ice loads were found, probabilistic averaging had little effect on creep loads (as expected) but a greater effect in the case of crushing ice failures. The reduction in load was of the order of 15-20%. This was not enough to account for the differences in load estimates noted above.

Event	Failure Mode	Maximum Nominal Load		Maximum Nominal Load	
		LA	LA	PA	PA
		No Bottom	Uniform	No Bottom	Uniform
Mar-25-N-1	Creep	103.1	103.1	101.9	101.9
Apr-12-E-1	Crushing	168.6	168.6	139.1	139.1
Apr-12-E-2	Crushing	187.5	374.5	158.2	319.6
Apr-12-E-3	Crushing	83.9	92.1	73.3	82.4
May-12-N-1	Crushing	168	343.9	140.9	295.9
May-22-N-1	Creep	108.4	140.3	107.4	139.2
May-22-N-2	Crushing	123.1	213.8	103.2	180.1
Jun-02-E-1	Crushing	127.7	128.9	113.9	115.8
Jun-02-E-2	Creep	86.3	87.2	84.8	85.8

In the table, an adjustment has been made for the fact that in some cases, loads were measured on the lower Medof panels. These did not cover the same lateral width as the main set of panels, in fact were only present on one set of Medof panels per face. The term "Uniform" in the table is a method of allowing for the fact that the lower Medof panel is present for only one set of Medof panels, using a linear extrapolation. The "No Bottom" results do not account for bottom panel loads. Another method, the Ratio method, extrapolates on the basis of the ratio of the lower Medof load to the other loads above it. Neither of these methods (Uniform or Ratio) is satisfactory, particularly for ice crushing. The ice failure process consists of high-pressure zones generally concentrated near the centre of the ice sheet, with occasional excursions towards the edges. Both methods fail to recognize this, and generally overestimate the face loads. It is considered that the increase in loads in the table above under the heading "Uniform", where there are bottom loads, is overestimated.

A review has been conducted of the load measuring devices. The strain gauges have been calibrated to the Medof panel loads in the past, as have the extensometers. The strain gauge readings correlate well with the Medof panel loads, but the calibration factor varies considerably. The figure below, based on the data from all S09 strain gauges, shows the uncertainty in calibration factor (CF). Some differences can be explained by differences in structural details but individual gauges show substantial variation, and taken overall, the figure gives a reasonable illustration of the uncertainty. The variance in the calibration factor results from the fact that the same strain can be achieved in the gauge from a multitude of local ice loads at various positions and intensity.

An investigation into the past recalibrations of the Medof panels at the Tarsuit location (Tarsiut Island Research Program, 1982-3) has been undertaken. This led to the conclusion that softening of this material has very likely taken place. The conclusion is reinforced by the very high variability of stiffness in the calibration reports indicating variability in manufacturing quality. In addition there was evidence of softening in the recalibrations and under repeated loadings.

A review was undertaken of the behaviour of the polyurethane material used as part of the construction of the Medof panels. The panels were composed of two parallel steel plates with Adiprene L100 urethane buttons sandwiched between the plates. The outside plate had a thickness of 12.5 mm (1/2") while the Adiprene L100 buttons had a thickness of 2.54mm (1/10") and a diameter of 9.5 mm (3/8") while the back plate had a thickness of 4.5mm (0.179in). This was in contact with the hull of the structure and welded to it. The urethane buttons were closely spaced at 12.7 mm (1/2") centre to centre, and carried most of the load from the outer surface to the structure.

The original calibration was carried out at a maximum nominal stress on the panel of about 1.86 MPa, resulting in a maximum stress on the polyurethane buttons of about 4 MPa. These stress levels, if uniformly distributed over the panel, might lead to acceptable performance, possibly with small damage or nonlinearity in the material. At the same time, creep is significant for longer term loadings. The original calibrations did not show nonlinearity but nonlinearity was identified in later work by Spencer. In all cases, the stress levels were too low to identify any softening, and none of the programs included meaningful repeated-load tests. A viscoelastic model was developed by Spencer based on his tests, but this is applicable only to low stress levels and one-time loading. The Medof panels in the field received many cycles of loading and high stress levels as will now be outlined.

Ice crushing in particular and mixed-mode failure involve highly localized pressures, so that the pressures are significantly amplified over regions of the panel under these ice failure modes. Crushing in particular will apply loadings akin to "panel beating" with repeated and randomly placed high-pressure zones across the face of the panel. In the literature, and particularly the work of Qi and Boyce, it is found that the stress and strain under plausible conditions for the Medof panels, reached levels that would result in nonlinearities in stress-strain behaviour and in softening associated with the Mullins effect. Further, in most instances, the loads were repeated in many cycles, which would add to the softening effect.

Many results have in the past been premised on the basis that the Medof panels are strictly correct. The analysis in this report shows this to be a questionable assumption as a result of possible softening of the panels. Data gathered using other instruments may form a better basis of load estimation. The following hypotheses were proposed in this work for consideration.

1. The Medof panels form the basis of load estimation, with other devices calibrated to them.
2. The extensometer readings form the basis of load estimation, with other devices calibrated to them.
3. The strain gauges form the basis of load estimation, with other devices calibrated to them.
4. A best estimate compromise between the three estimates form the basis of load estimation.

Our evaluation based on the evidence is that the extensometers form the best method of calibration (item 2 above), with a much higher credibility than the other devices. It is a reasonable conclusion that the Medof panel calibrations changed with time, in the sense of a softening process, giving readings that indicated higher loads than previously thought. The errors are of the order of magnitude two.

It is accepted generally that hydraulically placed sand pumped through a pipeline is loose and not dilative (see Hewitt, 2009), and furthermore, prone to liquefaction. While there are disagreements as to the precise state of the sand core, the estimates based on a loose fill agree in essentials with our current estimates of load. In general terms: our advice from Ryan Phillips is that the three significant load events (March 7/8, April 12, and May 12) exceeded the "basal shear resistance" (say 140 to 180 MN), "but not by very much" (C-CORE Technical Memorandum, July 14, 2009). Our current best estimates of global load for these events based on the extensometer readings are somewhat less than 180 MN (120-160 MN) except for the April 12 event which is greater (about 235 MN). The decelerating floe analysis suggests that the load in the May 12 event might be substantially less than 180 MN, but other estimates are closer to this value. The geotechnical estimates fall more in line with these values and all estimates are beginning to fall into the same "ballpark".

The Medof panels have been used for the calibration of the correlation model used for probabilistic averaging. If panels have softened, the correlation structure should remain unchanged, even if different softening of two panels has occurred. If two panels softened in a significantly different way during a loading event, this might have some effect on the correlation analysis. But this scenario is unlikely since most of the softening would have occurred in the early stages of loading, in the 1984-5 season or early in the 1985-6 season, and the change thereafter not very rapid.

The main factors affecting the choice of stiffness are:

1. core stiffness, and
2. proportion and distribution of load on the base and the consequent load path.

It is difficult to obtain a definitive estimate of the structure stiffness from the Sandwell report for use with the extensometer readings. In our calibration work, the values of stiffness (Load Distortion Ratio) equal to 2.2, 2.6 and 3.0 $MNmm^{-1}$ have been chosen. Our best estimate is of the order of 2.6 $MNmm^{-1}$ but the surrounding uncertainty has been taken into account by using a range of values. The values just quoted are for face loads. In the case of global loads, the inclusion of a lateral force in the Sandwell analysis of the forces on the corners tends to make the structure stiffer than it is in reality. As a result, the load distortion ratios for global loads would tend to be too high and exaggerate them.

The loading pattern in the loading case under consideration must be carefully considered in choosing the appropriate factor. A methodology based on matrix methods for dealing with biaxial loading and superposition on multiple faces has been developed successfully, but does suffer from difficulties in the calibration based on the Sandwell report mentioned in the preceding paragraph.

A new finite element analysis with well chosen boundary conditions would be most useful.

In the following, a summary is presented of the main conclusions of the analysis of the three selected events, as decided by clients in the June, 2008 meeting.

May 12th Floe Deceleration Event

The event of May 12th, in which a large floe in open water impacted the Molikpaq, presented a unique opportunity to assess independently the stiffness of the Molikaq in terms of global load versus extensometer readings. Because the floe was in open water, and the size and velocity of the floe were provided, the initial kinetic energy of floe can be estimated. Assuming that the load during the interaction is proportional to the north-south ring distortion and assuming a linear response, the stiffness (in MN applied force per mm ring distortion) required so that the floe stops in the observed time can be calibrated. The necessary global stiffness (load distortion ratio) is 2.2 $MNmm^{-1}$, corresponding to a maximum load of 105 MN. Our best estimate of the value of load

distortion ratio (2.6 MNmm^{-1}) results in a load of 123 MN. This is a face load, and in the present event the loading was mainly concentrated on the north-east face of the structure.

A sensitivity analysis of uncertainty in the time during which the floe deceleration proper occurred, was undertaken. To do this, the first 12 minutes of the impact was removed. The contribution for these first 12 minutes appears to correspond to small loads based on the extensometer ring distortion. It was assumed that the floe stopped in 15 minutes as opposed to the 27 minute approach described previously. A structural stiffness of 2.9 MNmm^{-1} with a maximum global load of 130 MN is the result of this analysis. The matrix model has also been applied to the May 12, 1986 data set. Using this approach a global load estimate of 126 MN results. This approach considers the predominant loading on the North face in addition to the loading occurring on the North East and East faces. In reality, the load seems to have been mainly a face load so that this is likely to be an overestimate.

The deceleration analysis supports the case that ice loads have been overestimated, giving grounds for using significantly lower stiffness values (load distortion ratios).

Analysis of March 25 Event

On March 25th, there were two significant creep loading ice events which were analyzed. For the first event, a face load of 34 MN was obtained, with a value of 55 MN in the second. The second creep event from March 25 was considered in further detail to examine the reasons for the bilinear slope between the Medof loads and ring distortions and the apparent hysteresis effect. By plotting the Medof column loads against ring distortion for given loading and unloading cycles of the north face, it is seen that there is first loading on the east side of the north face, then the west side and finally the center. The difference in loading times may result from the direction of ice movement and the observed fact that in creep type loads, loading occurs at the edges of a face before the center. The net effect is to produce an apparent bilinear slope in the curve giving total Medof load as a function of ring distortion. The analysis also showed that there were considerable differences in the Medof loads for adjacent columns, and that the non-zero intercepts for the Medof load versus ring distortion may be a function of differences in the time of loading and the fact that only 10% of the face was instrumented.

Analysis of March 7th Event

On March 7th there were two significant events which were considered. The ice came from the North impacting the North, North West and West faces. Due to the loading being on the West face, there were no Medof panels to consider. As a result of there being loading on more than one face, the method of calibrating Medof loads on the North face to the face load determined from the N-S ring distortion was not successful. The matrix method was also used as this has the capability of using extensometer ring distortions from multiple faces. The result was very sensitive to the initial offsets which were chosen. The resulting load was 165 MN for the first event and 95 MN for second. The table below lists the factors which were used to adjust the Medof panel loads for softening. These were achieved by calibrating the Medof panels to the face loads

determined by the extensometers for various ring distortion ratios chosen based on the results presented by Sandwell (1991). The Medof panel loads include appropriate averaging.

Event Number	Date	Fast File	Max Face Load for 2.6 MN/mm Ring Distortion Ratio	Factor used to reduce the Medof panel face load to account for softening		
				Ring Distortion Ratio = 2.2	Ring Distortion Ratio = 2.6	Ring Distortion Ratio = 3.0
0325A	25-Mar-86	f603250801	34 MN	0.27	0.32	0.37
0325B	25-Mar-86	f603251302	55 MN	0.44	0.52	0.60
0512A	12-May-86	f605120301	123 MN	0.44	0.52	0.60
0307A	7-Mar-86	f603071520	100 MN	N/A	N/A	N/A
0307B	7-Mar-86	f603071603	81 MN	N/A	N/A	N/A

Note: Those events with N/A were events for which this method was considered to be inappropriate as there was load on multiple faces and limited contact with Medof panels. The matrix method was adopted for these cases.

With regard to the matrix method, the authors feel that the method is promising, and could be much improved by more work on zeroing, and by adjustments to the stiffness matrix.

While there are disagreements as to the precise state of the sand core, the estimates based on a loose fill agree in essentials with our current estimates of load. In general terms: our advice from Ryan Phillips is that the three significant load events (March 7/8, April 12, and May 12) exceeded the "basal shear resistance" (say 140-180 MN), "but not by very much" (C-CORE Technical Memorandum, July 14, 2009). The state of the core would also be affected by the dynamic shaking during these events. Our current best estimates of load for these events based on the extensometer readings are somewhat less than 200 MN except for the April 12 event which is somewhat greater. The decelerating floe and other analyses suggest that the load in the May 12 event is less than 140 MN. But the geotechnical estimates are beginning to fall into the same "ballpark" as other estimates.

In the absence of a correction for Medof panel softening, the trends of the Molikpaq data are not consistent with the other data. Figure A below, with power-law trendlines illustrates the discrepancy. Accounting for panel softening yields results that are much more consistent with those observed from the STRICE, JOIA and Cook Inlet datasets. Based on a comparison with other data sets, it has been concluded that a panel of constant width experiences decreasing pressure over the loaded area for increasing ice thickness. This is consistent with the well known pressure-area scale effect for ice.

The main conclusion of the work is that design pressures based on the Medof panels attached to the Molikpaq structure, for the 1985-86 deployment, overestimate the loads by about 50%. The more detailed approach based on probabilistic methods, given in our Appendix IJA – A, should also be adjusted to give appropriate input values. The methodology for local pressures, as analyzed in the paper (Jordaan, Bruce, Masterson and Frederking, 2010, Cold Regions Science and Technology, in press) based on the Medof panels, is also relevant for this future work.

STRICE and Molikpaq Column Mean Pressure vs. Ice Thickness Data

Figure A

Table of Contents

List of Tables

List of Figures

1   BACKGROUND AND MOTIVATION

1.1   The Molikpaq Structure

The Molikpaq structure is illustrated in Figure 1-1, Figure 1-2 and Figure 1-3. In brief outline, the structure consists of a steel annulus, octagonal in form, serving as a caisson to support drilling operations. The structure consists of inner and outer steel plate structure connected by bulkheads. The structure rests upon a sand berm, and the core is filled with hydraulically pumped sand, uncompacted in the case of the Amauligak I65 location. The box girder deck rests upon the steel annulus, with rubber bearings between the deck and the main structure. The Molikpaq structure was placed at the Amauligak I65 location during 1986.

Details of the instrumentation are shown in Figure 1-2 and Figure 1-3 (Jefferies and Wright, 1988). Because the structure was heavily instrumented, it has served as a valuable source of information for determining design pressures for ice loading. This is the main focus of the present report, in which loads on the Molikpaq exerted by multiyear ice during the 1986 year of deployment at Amauligak I-65 are analyzed.

Many analyses in the past have relied upon the Medof panels as the primary load-measuring device. Load estimates higher than 500 MN during key events such as that on April 12, 1986, have been suggested (Jefferies and Wright, 1988). An opposing point of view has been taken by other writers, notably by Hewitt (1994; also see Hewitt's 2009 report in the present project and Appendix IJA - D to the present report). Hewitt estimated the maximum load at about 200 MN or less, for the event just noted.

Figure 1-1   The Molikpaq at location with ice crushing against two sides
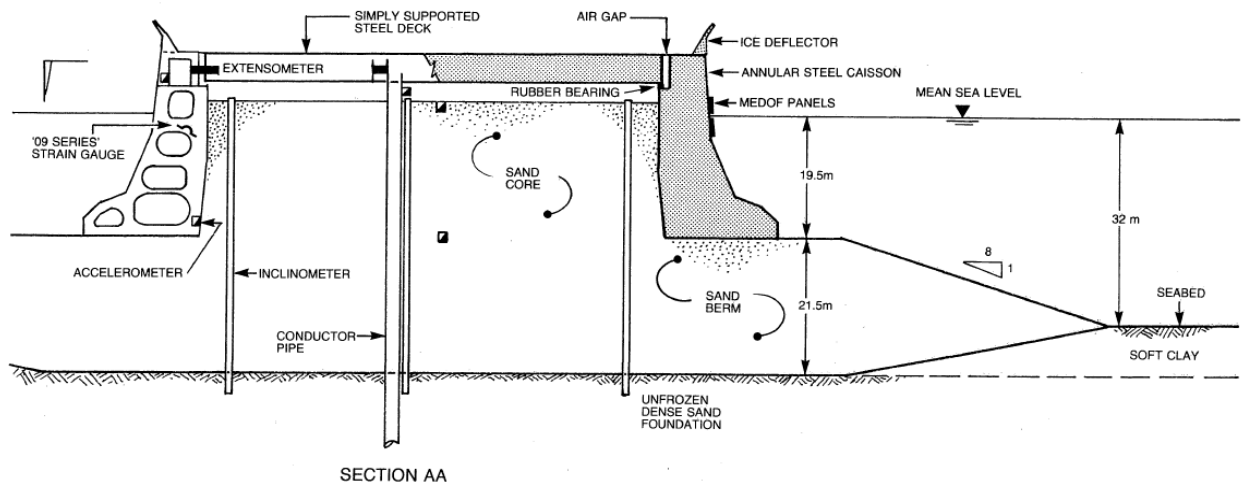
SECTION AA

Figure 1-2   Illustration of the Molikpaq and instrumentation (from Jefferies and Wright, 1988); for section AA details see Figure 1-3

PLAN XX
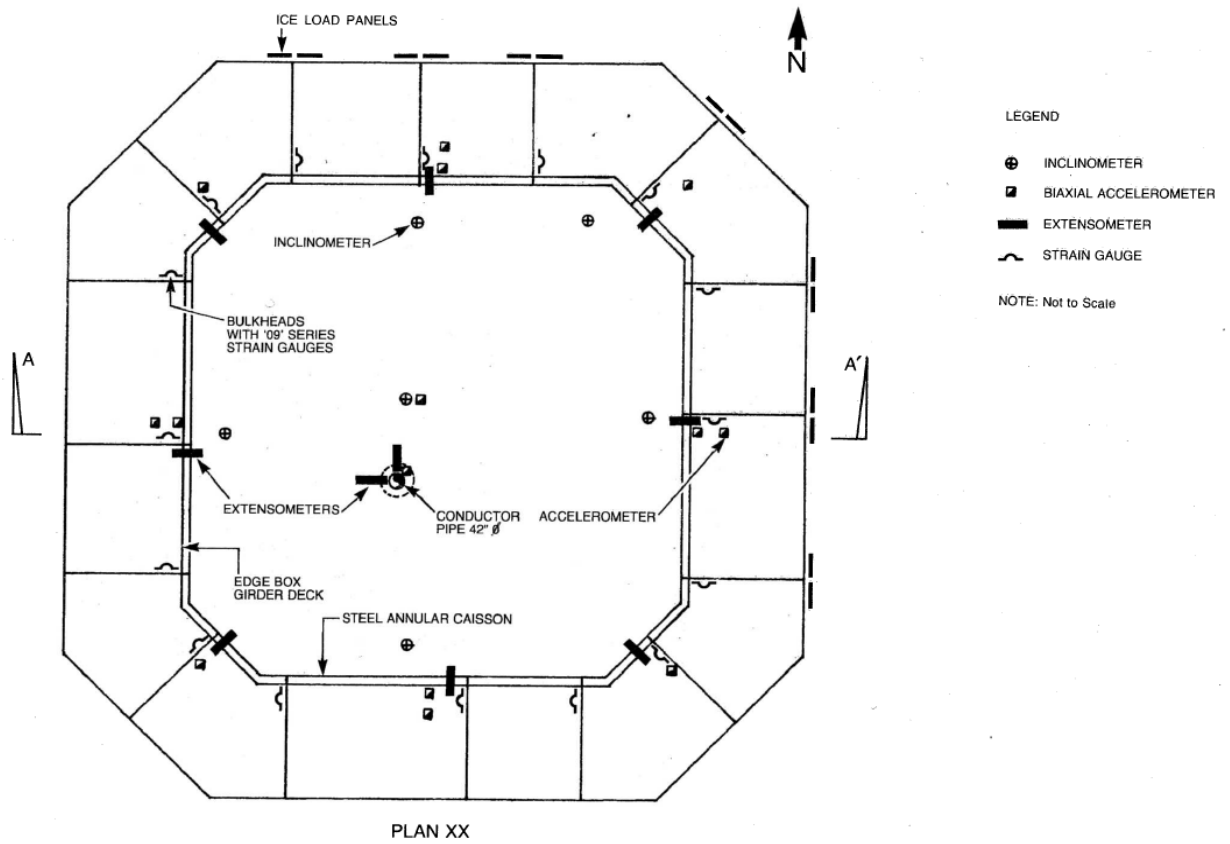
Figure 1-3   Plan view of Molikpaq (from Jefferies and Wright, 1988)

1.2 Use of Ice pressures in Design

The study of ice pressures resulting from multiyear ice acting against structures with a vertical face is important for the design of future offshore structures for arctic areas. Figure 1-4 shows a typical framework of an analysis procedure aimed at probabilistic estimates of design loads. The key, and very important parameter concerned with force, to be studied in this report, is highlighted. Appendix IJA - A summarizes values that are suitable for probabilistic load simulations. This information needs to be updated as a result of the present study.

The Molikpaq data form the basis of many design equations, and of analyses such as that in Figure 1-4 and it is of great importance to resolve the questions raised regarding the level of loads during key events. This is the subject of the present report.

For each of NSIM years
　For each month
　　• Calculate expected number of impacts given ice concentration, floe sizes and floe velocities
　　　For each impact:
　　　　• Randomly select MY floe size, thickness profile, velocity and impact offset
　　　　• Determine driving forces due to wind, current, and ice rubble
　　　　• Determine penetration given initial floe kinetic energy, driving forces, thickness profile and random ice strength
　　　　• Identify maximum load during impact

Store maximum annual loads

Determine loads with specified probabilities of exceedance (return periods)

Figure 1-4:   Example framework for probabilistic model. Highlighted parameter assisted by modeling of present study

1.3 Fundamental Questions and Approach

Many results have in the past been premised on the basis that the Medof panels are strictly correct. The analysis in this report shows this to be a questionable assumption as a result of possible softening of the panels. Data gathered using other instruments may form a better basis of load estimation. The following hypotheses have been proposed for consideration.

1. The Medof panels form the basis of load estimation, with other devices calibrated to them.
2. The extensometer readings form the basis of load estimation, with other devices calibrated to them.

3. The strain gauges form the basis of load estimation, with other devices calibrated to them.
4. A best estimate compromise between the three estimates form the basis of load estimation.

The fundamental question is then: given the information at hand, under which hypothesis is the data more likely to be true? A Bayesian approach would suggest that

$$\Pr(H \mid I) \propto \Pr(I \mid H) \bullet \Pr(H)$$
Equation 1-1

where *H* is the hypotheses, *I* denotes the given information, $\Pr(H \mid I)$ denotes the likelihood of *H* given *I,* $\Pr(I \mid H)$ denotes the likelihood of *I* given *H,* and $\Pr(H)$ denotes the likelihood of *H* prior to receiving the information *I.*

This means that, for a set of equally likely hypotheses (prior to receiving information *I*) (or reasonably equivalent ones), the important factor in comparing the relative likelihood of a hypothesis is the likelihood of the measurements and data which constitute *I* under the hypothesis under consideration, as compared to the likelihood for other hypotheses. The data are the whole body of evidence: Medof panel readings, extensometer readings, strain gauge readings as well as all the other information such as observations of the state of the sand core, inclinometer readings and so on.

There are ample reasons to reject Hypothesis (3), since there is great uncertainty in these measurements. Certainly based on the analysis in the present report, (1) is questionable. This would involve rejecting the extensometer readings and accepting the Medof calibration, while there are good grounds to question the accuracy of the Medof panels. With regard to (4), the weight of evidence favours (2). The Medof panel results contain excellent information, but a refined calibration constant is needed. For the present report, this is based on the extensometer results.

1.4   Velocity Effects

In interpreting the data, the mechanics of failure varies with the speed of interaction. This will have a strong influence on the distribution of load. Figure 1-5 shows the effect of velocity in medium scale indentation tests. Slow interactions result in "ductile" or "creep" failure (this is not pure creep but damage-enhanced creep illustrated in the left hand side of Figure 1-5). This kind of interaction will result in pressures that are more evenly spread out than those involving brittle fracture (illustrated in the right hand side of Figure 1-5). Much higher gradients of pressure will exist if brittle fracture takes place than in the ductile failures, and this is important in interpreting data and in future modelling.
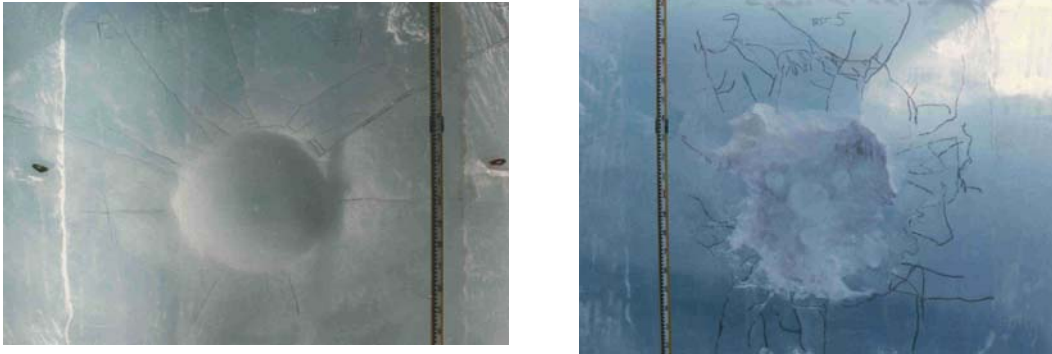
Figure 1-5: **Medium scale insitu testing with interaction area of 1.0 m^2: Left, 0.3 mm s^{-1}, ductile failure; right, 10 mm s^{-1}, brittle failure. Courtesy Dan Masterson**

1.5   Definition of an Event: Data Files

A further factor that should be borne in mind is the definition of an event. In the earlier work (Jordaan et al., 2006), an event was a major ice-structure interaction, and the data from the Molikpaq and other measurements (e.g. STRICE) result in events of different durations. Various modes of failure were included. Figure 1-7 is an example. In the present project, the events have been divided further into sub-events, in collaboration with Brian Wright, as shown for the event of Figure 1-7 in Figure 1-8 and Table **1-1**. This was extended to a set of events. These are denoted BDW data. This does represent a step forward in understanding as the different sub-events correspond to different failure modes of crushing (CR), creep (SLW), mixed mode (MM) and sliding (SLD).

Some comments need to be made. First, if the time intervals are too short, the statistics for the events are also short and will not be representative of an event of adequate duration for this purpose. The Medof panel is based on the localized areas (about 10% say), and are not necessarily representative of the whole face, and are then difficult to use in calibration or in modeling if this inadequacy is compounded by shortness of the event durations. (Here, the extensometer-deduced loads might assist.) Second, for future modeling of the kind in Figure 1-4 there are often in reality some mixed-mode aspects of the crushing failure process, and one might want to build the model on a more robust methodology that captures the essential points.

To enlarge on the point just made, an event could well include some periods of mixed-mode behaviour, and still be considered stationary. Figure 1-6 shows how such an event could be composed. Practical idealizations will doubtless included some periods of mixed-mode failure. It is also noted that averaging is appropriate even for non-stationary events. In practical modelling, it is convenient to divide the loading scenarios into series of stationary events. Too much can be made of the existence on non-stationary periods as a reason not to proceed, resulting in a slowing of progress in the development of methods of analysis.
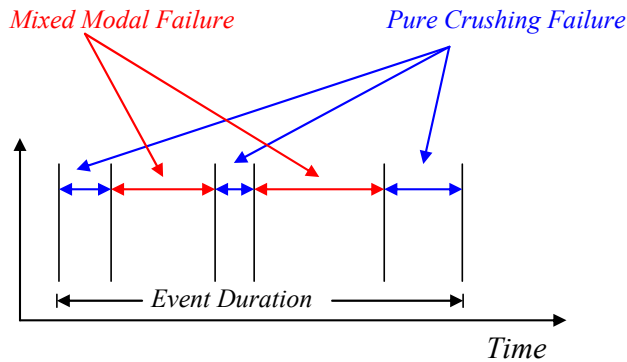
Figure 1-6:   **Illustration of potential composition of an ice loading event**

The files available for use are the following.
1. Dynamac files
2. Trimmed event files (inhouse) corrected for panels not working
3. Trimmed event files (Taylor, 2009) for comparison with STRICE and other data (Chapter 6)
4. BDW subevents—events compiled by Brian Wright
5. CHC subevents.

In the present study, the BDW events were used to estimate the correlation constants for averaging (included in the present report, Chapter 4). In the June 2008 report they were used also to calibrate the extensometer readings to the Medof panel readings, not a good procedure given the uncertainty surrounding the Medof panel calibration. The shortness of the durations makes the BDW files difficult to use effectively for calibration. The Dynamac and inhouse trimmed files were used for evaluation of events and for calibration in the present report.

Event f605120301med
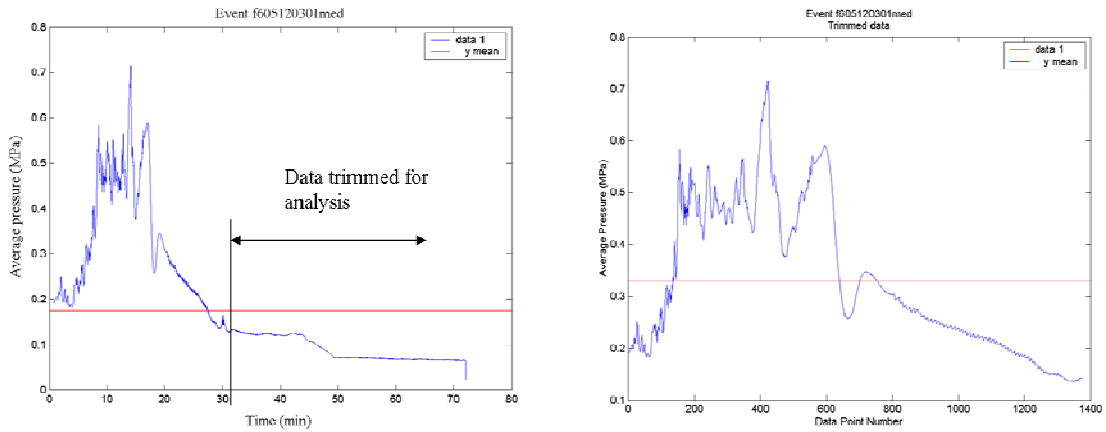
Untrimmed Data
μ= 0.1782
σ =0.1452

Trimmed Data
μ= 0.3287
σ =0.1403

Figure 1-7: Original characterization of event based on Medof panel readings (Jordaan et al., 2005)
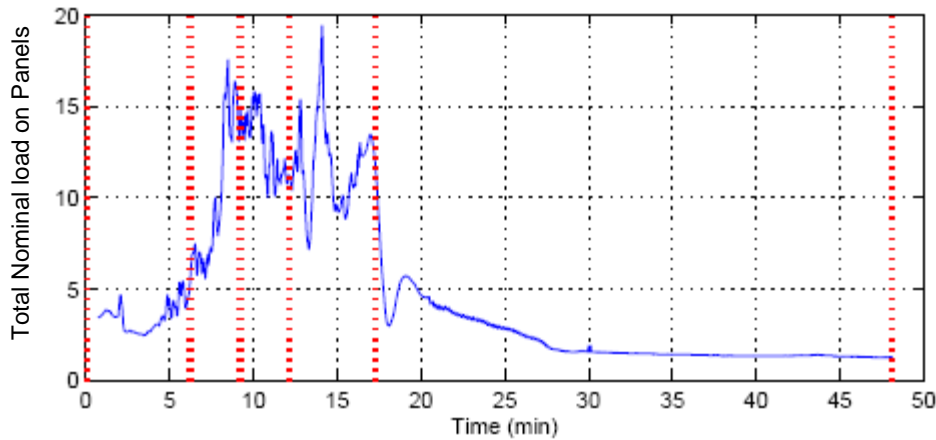
Figure 1-8: Event of Figure 1-6 with sub-events of the present study, indicated by vertical red lines

Table 1-1: Sub-events for Event of Figure 1-6

Priority	Event ID	Date	Fast file	Segment	Time period	Ice thickness (m)	Ice velocity (m/s)	Failure mode
3	0512A	12-May	F605120301	full file	03:10:16 – 03:58:24	2.5 (est.)	0.17 to creep	CR, MM & SLW
	0512A-1			1	03:10:16 – 03:16:28	2.5 (est.)	0.17	MM
	0512A-2			2	03:16:29 – 03:19:28	2.5 (est.)	<0.17	CR
	0512A-3			3	03:19:29 – 03:22:23	2.5 (est.)	<0.17	MM
	0512A-4			4	03:22:24 – 03:27:33	2.5 (est.)	<0.17	CR
	0512A-5			5	03:27:34 – 03:58:24	2.5 (est.)	creep	SLW

1.6 Geotechnical Aspects and Klohn Crippen Berger (2009)

Appendix IJA - C contains a review by C-CORE of geotechnical work done in the past on the Molikpaq response, principally focused on the April 12 events together with an addendum on the geotechnical response of the sand core. This review does not deal with the state of the sand in the core of the Molikpaq. To put this into focus, Appendix IJA - D by Kevin Hewitt has been added, in which the state of the sand core is discussed.

Subsequent to the ice loading events of 1986, a Joint Industry Project was carried out to study the events and associated measurements of the Molikpaq. This is referred to as the "1986 JIP". The recent report by Klohn Crippen Berger (2009) provides a summary of this JIP. The measurements on the Molikpaq together with the 1986 JIP and its original set of reports have in fact formed the basis of the present study. The IJA project team has concluded that the results of the 1986 JIP need reconsideration. The key aspect that should be reconsidered is the strong reliance on the original calibrations of the Medof panel in the 1986 JIP. The team is consequently in disagreement with the Klohn Crippen Berger interpretation, which is closely aligned with the 1986 JIP reports. It is considered that the arguments in the report supporting the original Medof calibration are not well-founded. It is accepted generally that hydraulically placed sand pumped through a pipeline is loose and not dilative (see Hewitt, 2009), and furthermore, prone to liquefaction. There are uncertainties in the Sandwell results, acknowledged by the present team, but these are outweighed by the far greater uncertainties in the Medof panel results. In fact, the points raised by Klohn Crippen Berger have been dealt with in our work. The ice mechanics in the report omits reference to work after the 1986 JIP in which the behaviour and failure of high-pressure zones has been discovered. The ice mechanics, as a result, are out of date. No cause to change the present approach has been found in the Klohn Crippen Berger report.

While there are disagreements as to the precise state of the sand core, the estimates based on a loose fill agree in essentials with our current estimates of load. In general terms: our advice from Ryan Phillips is that the three significant load events (March 7/8, April 12, and May 12) exceeded the "basal shear resistance" (say 140-180 MN), "but not by very much" (C-CORE Technical Memorandum, July 14, 2009). The state of the core would also be affected by the dynamic shaking during these events. Our current best estimates of load for these events based on the extensometer readings are somewhat less than 200 MN except for the April 12 event which is somewhat greater. The decelerating floe analysis suggests that the load in the May 12 event is less than 140 MN. But the geotechnical estimates are beginning to fall into the same "ballpark" as other estimates.

1.7 Face Load versus Global Loads; Pressures

Figure 1-9 shows face loading and possible global loading in idealizations. In some studies, a constant factor has been used to convert from face to global loading. The situation in reality is more complicated than this; Figure 1-10 show patterns observed in the Dynamac report (north is being used here as an arbitrary reference direction). Figure 1-11 shows idealizations of the loading situations.
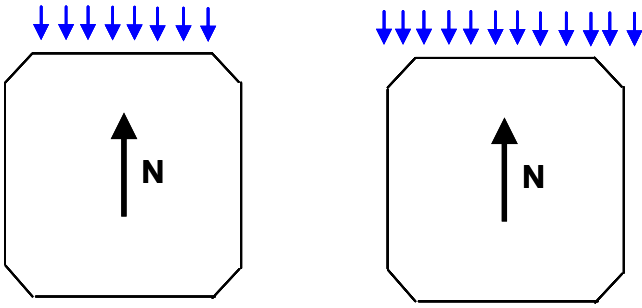
Figure 1-9   Loading scenarios; face loading (left) and global load (right)
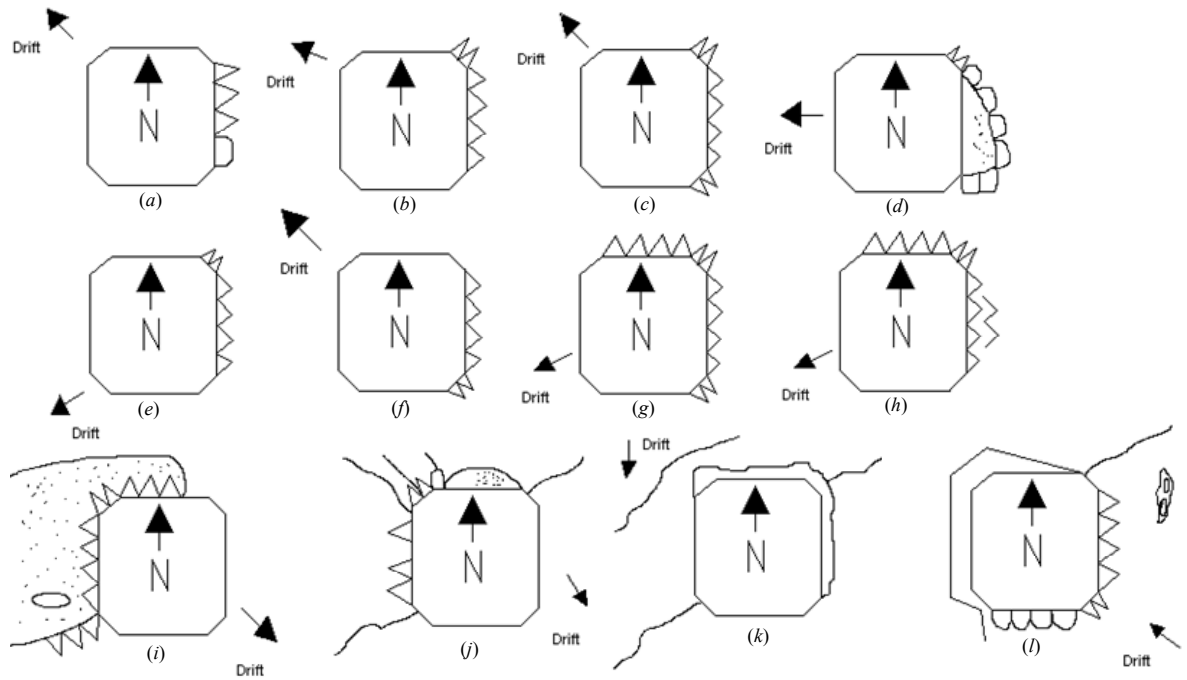
Figure 1-10   Observed loading patterns (Dynamac)

(g, h, i, l)   *(e, f, j)*   *(b, d, e, f, j)*

(Partial loading sub event)   *(Partial loading sub event)*
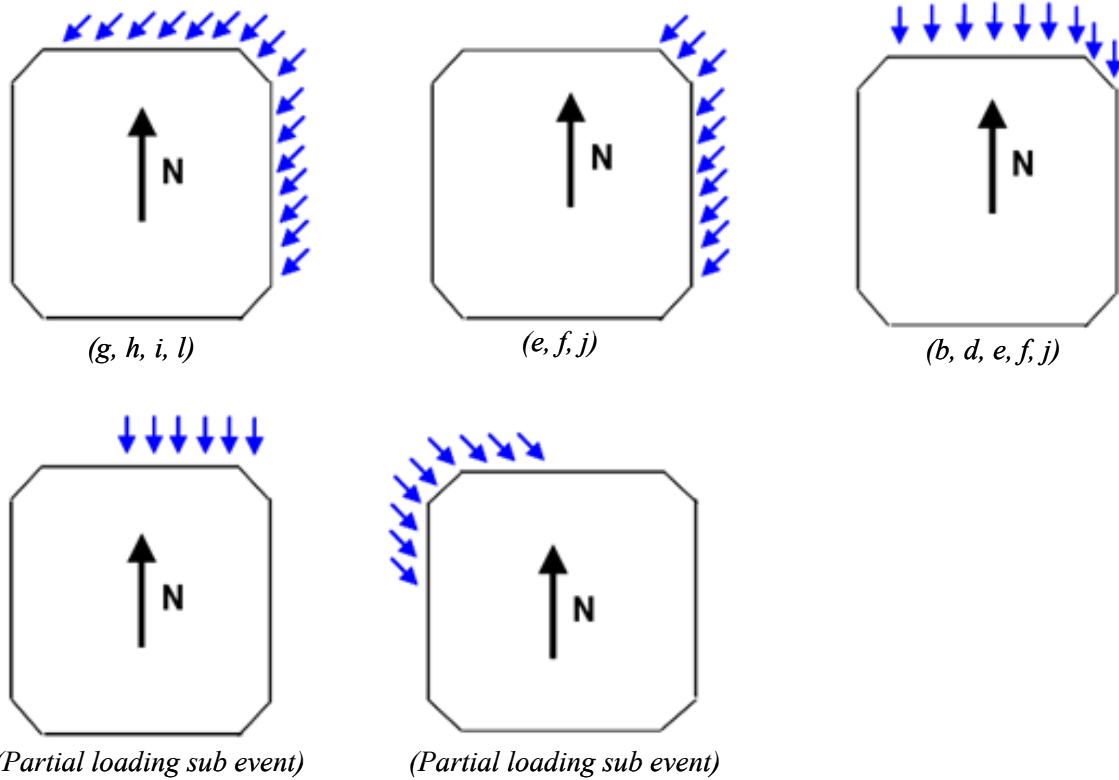
Figure 1-11   **Some idealizations of the loadings in Figure 1-10; text under each idealization refers approximately to cases in Figure 1-10.**

Figure 1-12 shows patterns that have been used in analysis; the face and the uniformly distributed load (*udl*) in our matrix method (Section 2.5) and in Sandwell (1991). The latter reference also included a "most likely" scenario with reduced loads on the corners (top right in Figure 1-12). The corner load (bottom left) was also used in the matrix method developed in the present report.

A key message is that the pattern considered should correspond as closely as possible to the observed situation in the event under consideration, with the constants for determining the load carefully assessed.
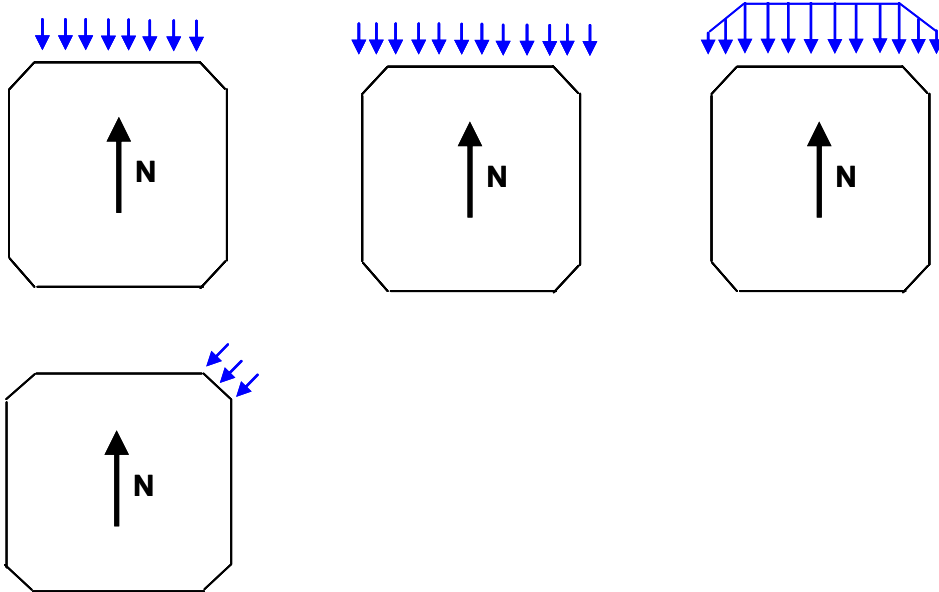
Figure 1-12 Loading patterns used in analyses; face load (top left), uniformly distributed load (top centre), "most likely" distributed load (top right), used in Sandwell (1991), and corner load (bottom left)

1.8 Organization of the Present Study

In the report, Chapter 2 includes a description of the Molikpaq structure and its response to load. This includes discussion of the Sandwell (1991) report, and the matrix method developed by the present group to account for loading on multiple faces. Chapter 3 includes a discussion of the principal load measuring devices: the extensometers, the Medof panels and the strain gauges. In Chapter 4, the technique of probabilistic averaging is discussed, with results on correlation and a comparison of linear and probabilistic averaging. Nine full events and their subevents were analyzed and these results were presented at the June 2008 project meeting in Calgary. These results are discussed briefly in Chapter 5 and given in more detail in Appendix IJA - B. The loads deduced from the Medof panels have been termed "nominal" loads because of their uncertainty. Detailed analysis of certain events is given in Chapter 5. A comparison with other data sets is given in Chapter 6 (STRICE in particular), with conclusions of the study in Chapter 7.

2 THE STRUCTURAL BEHAVIOUR OF THE MOLIKPAQ

2.1 Deformations of the Structure

Extensometers have been used to measure deformations of the main structure. The box girder deck rests upon rubber bearings which in turn rest upon the steel annulus (the main structure) (Figure 2-1). The extensometers measure the deformation between the box girder deck and this structure. The Molikpaq acts essentially as an elastic "proving ring". The use of calibrations from finite element analyses is a good way to obtain stiffnesses for global load estimates. The difficulty lies in obtaining a clear assessment of the boundary conditions imposed by the foundation and in obtaining the appropriate finite element analysis to obtain the stiffness.

Box girder deck

Extensometer

Rubber bearing
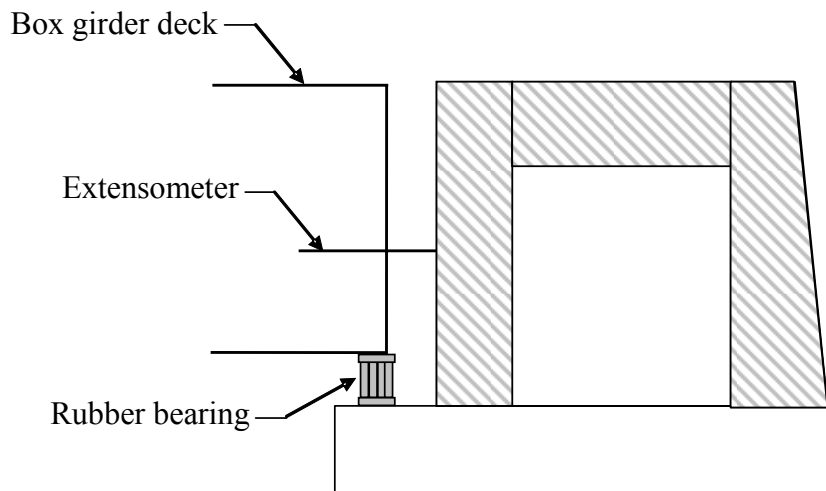
Figure 2-1   Box girder deck resting on main structure

2.2 Boundary Conditions

In calibrating the extensometers and the strain gauges, it is most important that the deformation of the caisson be determined as well as possible. Figure 2-2 shows schematically a free-body-diagram of the caisson. The division of load between the base and the core is most important. The figure is intended as a guide (schematic); we know that there is active pressure at the rear and sides. The main point to be determined here is the division between the base friction and the core. Ryan Phillips has kindly provided Figure 2-3. This suggests that the base friction is mobilized before the core resistance. Estimates of the base resistance (caisson friction) are in the range 140 to 180 MN based on the loaded weight of 380 MN (Sandwell, 1991) and a coefficient of friction of 0.364 to 0.466 (friction angle of 20º to 25º) (note that weathered steel on medium dense sand is under consideration; Hewitt, 2009). Up to the value of frictional resistance, there will be some deformation of the caisson, leading to core resistance, say 10%. Above this load, transfer of force to core will increase.
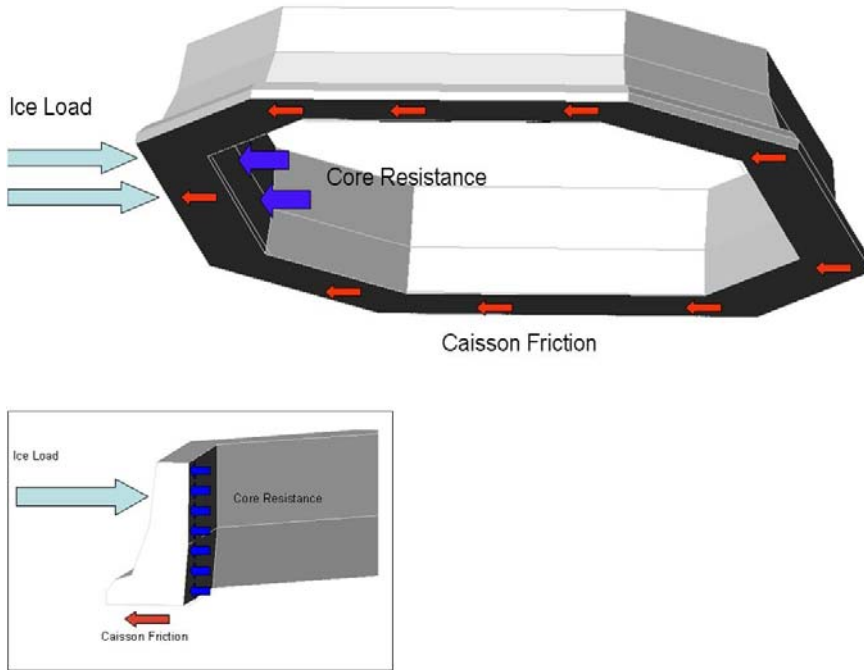
Figure 2-2: Schematic illustration of the boundary conditions imposed on the Molikpaq by the foundation. The sand core will have active resistance on the face opposite to the loaded face above.
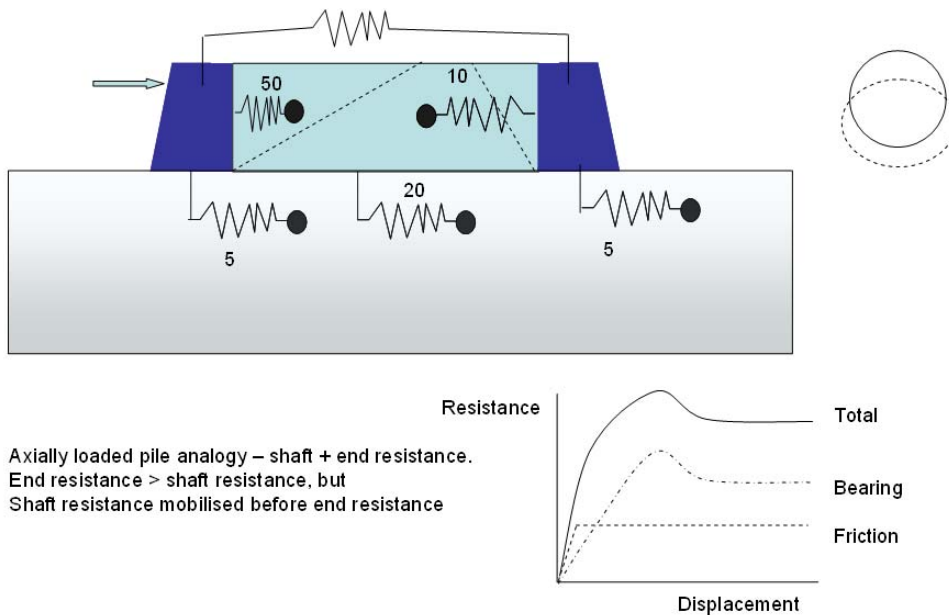
Figure 2-3: Transfer of load from the caisson to the foundation (provided by Ryan Phillips). Numbers opposite springs indicate the displacement in mm required to activate the corresponding resistance.

2.3 Finite Element Analyses

Many of the finite element studies have concentrated on soil behaviour (Jeyatharan, Sladen (EBA), Altaee and Fellenius – See Appendices IJA - C and IJA - D). In these assumptions of a rigid structure are made. The deformations given in the results are of the foundation response and are irrelevant to the structure stiffness, except in the very important sense of obtaining the correct boundary conditions in Figure 2-2. But generally, assumptions of dense sand have been made. In terms of proper structural analysis that can be used for calibration of extensometers, the report by Klohn Crippen Berger (2009) is no improvement on the other geotechnically oriented papers.

The references noted can not be used for extensometer calibration. A study that does address the ring distortion needed for calibrating the extensometer is the Sandwell (1991) report, "Extensometer Calibration for Ice Load Measurement", which was also calibrated back to the original Stardyne analysis.

2.4 Sandwell (1991) Report

The report was written as part of the 1986 JIP for Gulf Canada, and represents an analysis of the structural response, and as noted, was compared to the original Stardyne analysis, with good agreement. At the same time, reservations are expressed regarding the input assumptions. As in the report, we shall consider loading in the North-South direction as a reference for discussion. The results are expressed as "Ring Distortions" in mm and "Load Distortion Ratios" in MN mm^{-1}, which represent the calibration factors of the extensometers.

The stiffness values vary considerably (Sandwell, 1991) depending on whether one considers the loading on the centre face (i.e. the central northern face, about 58 m long) or the entire side, which was modelled as a N-S uniformly distributed loading (*udl*) of the two (NE and NW) corner faces of the octagon as well as the centre face. See Section 1.7 for a discussion of loading patterns. In summary, Sandwell (1991) considered the following:

1. uniformly distributed load (*udl*) over the centre face only,
2. uniformly distributed load (*udl*) over the entire width, and
3. the "most likely" load distribution;

see Figure 1-12.

Loading case 2 above included the same north-south distributed loading on the two corner faces as well as on the centre face. Since these loadings were in the north-south direction, other loads were applied to achieve equilibrium. These consisted of a frictional force on the side of the caisson and a lateral force; see Figure 2-4 and Sandwell (1991) for details.
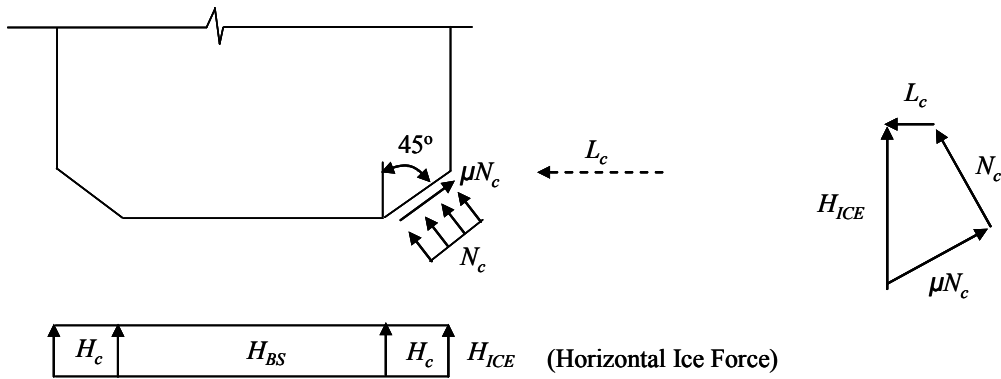
Figure 2-4   **Loading assumption used by Sandwell (1991) for *udl* over whole width**

In reality one might expect some attenuation of the *udl* towards the edges, and on the corner faces. The "most likely" load used by Sandwell consisted of a *udl* over the centre front north caisson, and a triangular load on the NW and NE sides decreasing from the *udl* value on the centre face to zero at the outside corners. This seems to be a reasonable practical interpretation of the load over a face and nearby corners. At the same time some concern is expressed that the lateral load applied at the corners might be too high, dictated by the fact that the applied loading is in the N-S direction.

In addition, the inclusion of the lateral force L_c would tend to make the structure stiffer than it is in reality. As a result, the load distortion ratios for global load would tend to be too high and exaggerate the global loads.

General Conclusions of Report
Some general conclusions from the report are as follows:

1. The stiffness (Load Distortion Ratio) was found to be in the range 2.0 to 4.2 MN mm^{-1}.
2. The interplay between loads on the 45° sides and the face are important and should be taken into account where necessary in calibration and load estimation.

Since the stiffness values quoted are about half of the prior estimates based on the Medof panels (6 MN mm^{-1}), it was surmised in the report that the results indicate that either "the actual structure and soil interaction is much stiffer than the model, or that the application of the ice load is lower or that base shear is more significant than assumed..."

Assumptions Regarding Share of Base Shear
One important assumption was that the share of the resistance offered by base friction was fixed. This was generally set at 40% although some sensitivity runs were carried out. As discussed above, it is considered that too much load is being transmitted into the core; about 80-90% might be transmitted through base friction.

Complicating factors are:

1. How was the ratio achieved? It is stated in the report that "it was assumed that strain compatibility required that the base friction be mobilized before the sand core resisted significant load". (This is consistent with the discussion in section 2.2 above). Imposition of frictional forces would result in structural deformation and consequent loading of the core.

2. A related aspect is that it was assumed that 60% of the base shear was distributed over the leading edge of the caisson and that the remaining 40% was distributed over the trailing edge of the caisson. In this context, see Figure 2-5.

On the assumption that the load is transferred to the base and by friction to the foundation, two load paths are illustrated in Figure 2-5. The results in the Sandwell report (Cases 20 and 21) suggest that the path leading to shear under the leading edge (lower part of Figure 2-5) is stiffer than the path that is more distributed across the base (upper part of Figure 2-5).
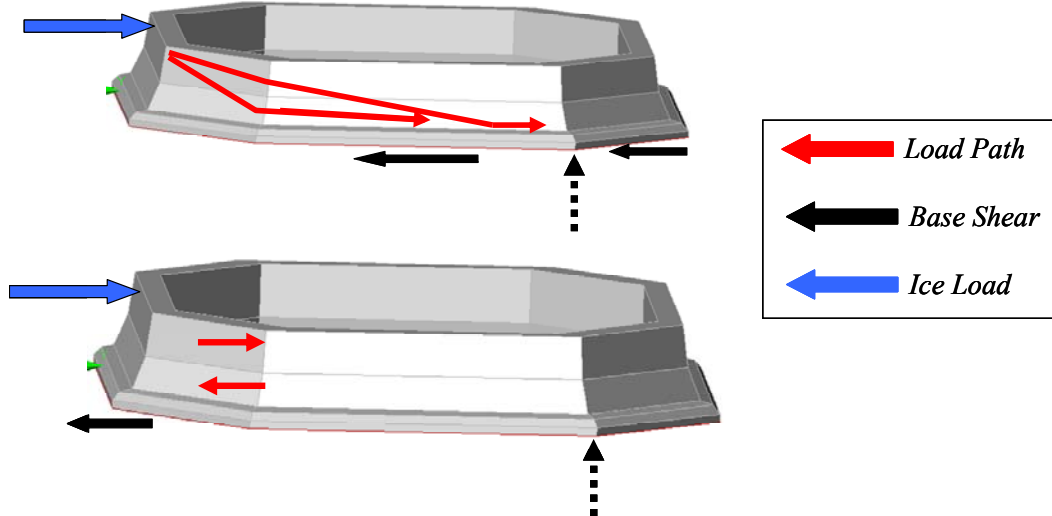
Figure 2-5:   **Illustration of possible load paths assuming load is transferred to the foundation by base friction**

Soil Stiffness

The stated assumption for the soil spring properties at the I-65 site was "dense cohesionless soil with dry density of 18 kNm^{-3} and density below water at 10 kNm^{-3}". It was also stated that a passive soil coefficient of 6.0 was assumed. The sand core as placed was actually loose. Hewitt (2009) investigated the soil spring stiffness values stated in the Sandwell report and concluded that they likely correspond to soil less dense than description given in the first two sentences of this paragraph.

Results and Sensitivities

The main results from the Sandwell 1991 study are reproduced in Table 2-1 and Table 2-2, the latter showing sensitivities to various assumptions. A "Calibration Run" (Load Case 0 in Table 2-1) was carried out (Page 2-12 of the Sandwell (1991) report). The loading is very similar to load case 18, and so are the ice thicknesses but the stiffnesses

are rather different. (4.2 versus 3.0 MN mm^{-1}). Discussion on the effect of creep on the loading (Page 3-3 of the Sandwell (1991) report) leads to the conclusion that a reduced load (i.e reported load reduced from that used in the FE analysis) was employed in the calculation of stiffness (about 110/87.9 = 1.25). If the stiffness of 4.2 MN mm^{-1} is divided by this value, a stiffness of 3.36 is obtained, closer to the Case 18 value.

In Table 2-2, various sensitivities are given. The results show that increasing the base shear increases the stiffness. This might be the consequence of the high proportion of the load transmitted to the base of the loaded face rather than to the rest of the base, with consequent increased passive resistance on the adjacent face, or simply a stiffer structural configuration.

Table 2-1: Results of Sandwell (1991) Analysis

Molikpaq Structural Ring Distortions and Load Distortion Ratios

Load Case No.	Global Load Level (MN)	North Face Load (MN)	Event	Loading Pattern	Ice Thickness	Base Shear	Loaded /Trailing	Soil Springs	N-S #468 +#472	E-W #474 +#470	NW-SE #475 +#471	NE-SW #469 +#473	Using Global Load (MN/mm)	Face Load Only (MN/mm)
0	87.9	87.9	Mar 25	Centre Face		50%	60% / 40%	Base	-20.7	8.2	-0.5	-0.3	4.2	4.2
1	125	72.3		Full UDL	1.38m	40%	60% / 40%	Base F24	-32.1	11.3	-4.0	-3.5	3.9	2.3
2	125	72.3		Full UDL	1.38m	40%	60% / 40%	Twice k	-27.1	9.2	-3.7	-3.4	4.6	2.7
3	125	72.3		Full UDL	1.38m	60%	60% / 40%	Base F24	-29.4	9.4	-4.0	-3.6	4.3	2.5
4	125	125.0		Centre Face	2.23m	40%	60% / 40%	Base F24	-46.5	17.4	-0.9	-0.4	2.7	2.7
5	125	89.4		Most Likely	1.71m	40%	60% / 40%	Base F24	-38.9	14.9	-2.5	-2.0	3.2	2.3
6	125	72.3		Full UDL +2m	1.38m	40%	60% / 40%	Base F24	-35.4	11.8	-4.6	-4.2	3.5	2.0
7	125	72.3		Full UDL -2m	1.38m	40%	60% / 40%	Base F24	-28.0	10.4	-3.2	-2.8	4.5	2.6
8	300	173.5		Full UDL	3.31m	40%	60% / 40%	Base F24	-72.8	26.0	-8.8	-7.8	4.1	2.4
9	300	300.0		Centre Face	5.35m	40%	60% / 40%	Base F24	-98.2	37.5	-1.9	-0.8	3.1	3.1
10	300	173.5		Full UDL	3.31m	60%	60% / 40%	Base F24	-67.3	22.4	-8.6	-7.8	4.5	2.6
11	300	173.5		Full UDL	3.31m	20%	60% / 40%	Base F24	-83.9	32.8	-8.9	-7.6	3.6	2.1
12	300	173.5		Full UDL	3.31m	40%	60% / 40%	Twice k	-61.0	19.6	-8.3	-7.5	4.9	2.8
13	481	286.5		Full UDL	5.31m	40%	60% / 40%	Base F24	-107.1	35.2	-13.4	-11.9	4.5	2.7
14	481	286.5		Full UDL	5.31m	60%	60% / 40%	Base F24	-96.8	28.6	-13.3	-12.1	5.0	3.0
15	481	286.5		Full UDL	5.31m	20%	60% / 40%	Twice k	-89.6	25.6	-12.7	-11.6	5.4	3.2
16	125	89.4	Apr 12PM	Most Likely	3.41m	50%	60% / 40%	Base I65	-32.1	12.2	-2.2	-1.8	3.9	2.8
17	125	89.4	Apr 12PM	Most Likely	3.41m	50%	60% / 40%	Twice k	-27.2	8.9	-2.1	-1.8	4.6	3.3
18	89.4	89.4	Apr 12PM	Centre Face	3.41m	50%	60% / 40%	Base I65	-29.4	10.7	-0.4	-0.2	3.0	3.0
19	300	214.5	May 12	Most Likely	3.41m	40%	60% / 40%	Base I65	-79.3	31.2	-5.3	-4.3	3.8	2.7
20	300	214.5	Apr 12AM	Most Likely	8.89m	40%	60% / 40%	Base I65	-68.0	26.9	-4.5	-3.6	4.4	3.2
21	300	214.5	Apr 12AM	Most Likely	8.89m	40%	10% / 90%	Base I65	-75.1	33.3	-3.6	-2.6	4.0	2.9
22	300	214.5	Apr 12AM	Most Likely	8.89m	40%	10% / 90%	kp=3	-97.5	45.6	-4.0	-2.7	3.1	2.2
23	214.5	214.5	May 12	Centre Face	3.41m	40%	60% / 40%	Base I65	-72.2	27.0	-1.1	-0.4	3.0	3.0

Table 2-2:   **Results of Sandwell (1991): Sensitivity Analysis**

Molikpaq Face Load Distortion Rate Sensitivities

From Load Case	To Load Case	Face Load (MN)	Change in Assumptions	Relative Change in Load Distortion Ratio			
				From (MN/mm)	To (MN/mm)	Change (%)	Change Ratio
1	3	72.3	40% Base Shear to 60% Base Shear	2.3	2.5	9.2	1.09
8	10	173.5	40% Base Shear to 60% Base Shear	2.4	2.6	8.2	1.08
13	14	286.5	40% Base Shear to 60% Base Shear	2.7	3.0	10.6	1.11
8	11	173.5	40% Base Shear to 20% Base Shear	2.4	2.1	-13.2	0.87
11	8	173.5	20% Base Shear to 40% Base Shear	2.1	2.4	15.2	1.15
11	10	173.5	20% Base Shear to 60% Base Shear	2.1	2.6	24.7	1.25
1	2	72.3	Core Stiffness Doubled	2.3	2.7	18.5	1.18
8	12	72.3	Core Stiffness Doubled	2.4	2.8	19.3	1.19
16	17	89.4	Core Stiffness Doubled	2.8	3.3	18.0	1.18
1	6	72.3	Load Application 2 m Higher	2.3	2.0	-9.3	0.91
1	7	72.3	Load Application 2 m Lower	2.3	2.6	14.6	1.15
1	8	72.4-173.5	Ice Thickness 1.38m to 3.31 m	2.3	2.4	5.8	1.06
4	9	125-300	Ice Thickness 2.23m to 5.35 m	2.7	3.1	13.6	1.14
8	13	173.5-286.5	Ice Thickness 3.31m to 5.31 m	2.4	2.7	12.2	1.12
19	20	214.5	Ice Thickness 3.41m to 8.89 m	2.7	3.2	16.6	1.17
11	15	173.5-286.5	Doubled Core Stiffness and Ice Thickness 3.31m to 5.31m	2.1	3.2	54.6	1.55
1	5	72.3-89.4	Face Load, "Full" UDL to Face Load, "Most Likely"	2.3	2.3	2.0	1.02
18	23	89.4-214.5	Face Load, Base Shear 50% to Base Shear 40%	3.0	3.0	-2.3	0.98
16	18	89.4	Face Load, "Most Likely" to Face Load Only	2.8	3.0	9.2	1.09
19	23	214.5	Face Load, "Most Likely" to Face Load Only	2.7	3.0	9.8	1.10
20	21	214.5	"Loaded" Part of Base Shear from 60% to 10%	3.2	2.9	-9.5	0.91
20	22	214.5	Reduce Core Stiffness to kp=3 and "Loaded" Part of Base Shear from 60% to 10%	3.2	2.2	-30.3	0.70

2.4.1 Shell International Finite Element Analysis

Staff at Shell International checked the structural stiffness of the Sakhalin Molikpaq structure as obtained from their finite element model. Note that in this model the spacer at the bottom of the caisson is included. Shell has stated that the soil stiffness in the analysis was very low and that the calibration might therefore not be reliable.

In their analysis, applying a distributed load of 400 MN on the north face of the structure, results in a displacement of 200 mm and 48 mm of the northern part of the caisson and southern part of the caisson, respectively (at the location of the extensometer). Assuming a rigid body motion of the box girder deck, the deck moves 94 mm. This suggests that the northern extensometer would measure –106 mm, while the southern extensometer would measure –46 mm. Adding these two values gives –152 mm. The extensometer calibration factor based on this FEM is therefore 2.6 MNmm^{-1} (400 MN/152 mm). This is taken as the stiffness for a face load. Note the statement from Shell in the preceding paragraph.

2.4.2 Conclusions Regarding Structure Stiffness and Extensometer Calibration for Face Loads

Whichever result for structural stiffness (load distortion ratio) is favoured in the Sandwell report, they all show values that are about half that obtained from loads based on the original calibration of the Medof panels. Uncertainties remain regarding the assumptions in the analysis. The first pertains to the soil stiffness as discussed above; it is not entirely clear what assumption was used in the analysis. Another difficulty relates to the percentage of load transferred to the base by shear. With regard to the stiffness of the core, a further complication is that the major load situations involved vibrations and large fluctuations in load generally leading to excess pore pressure and liquefaction. The pore pressure in the near-field is therefore a consideration. See for example Ashour and Norris (2003) and Gerber and Rollins (2006).

The following is a rough estimate for the load distortion ratio (structure stiffness) for face loads. First use Case 23 as a starting point, with a value of 3.0 MN mm^{-1}. Then multiply this by 1.25 to account for 90% base shear (10% increase in load distortion ratio for a 20% increase in base shear as shown by the sensitivities in the table). Then multiply by 2.2/3.2 = 0.688 using Cases 20 and 22 to account for the loose core. The stiffness of the core is less important in the present interpretation, since most of the loading is transferred through friction. At the same time it is noted that liquefaction occurred in the key events, causing considerable softening of the core. Case 23 with k_p = 3 would significantly overestimate the stiffness of the core; k_p = 1.0 might have been more appropriate.

The result of the adjustments just noted is 2.6 MN mm^{-1} for the face load distortion ratio. This value must be regarded as approximate, but is supported by the analysis of Shell noted in the preceding section, subject to the qualification expressed in the first paragraph of Section 2.4.1, and also in general terms by the decelerating floe analysis of Chapter 5.

2.5 Matrix Solution for Biaxial Loading

In most cases of ice interaction with the Molikpaq, the loading was from two directions. A matrix solution to relate the effect of ice loads on multiple faces of the Molikpaq to the caisson response, as defined by ring distortions, was developed. These correspond to deflections at positions measured by extensometers. The notation for the loads and ring distortions are as indicated in Figure 2-6. Loads on the NE, N, NW and E face are considered; the method can be extended for loads from other directions. The loads are assumed to act normal to the structure faces, i.e. frictional effects are assumed to be small. The ring distortions for each direction represent the sum of the extensometer readings on the corresponding opposing sides of the deck.
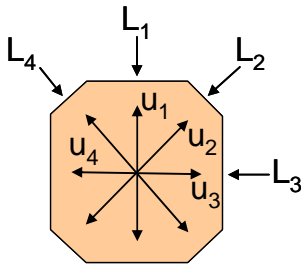
Figure 2-6:   Notation for face loads and deflections at extensometer positions

It is assumed that the extensions u_i vary linearly with the loads L, which is certainly reasonable for the steel structure and any proportional loading. Then the response can be described in terms of the matrix

$$\begin{bmatrix} u_1 \\ u_2 \\ u_3 \\ u_4 \end{bmatrix} = \begin{bmatrix} M_{1,1} & M_{1,2} & M_{1,3} & M_{1,4} \\ M_{2,1} & M_{2,2} & M_{2,3} & M_{2,4} \\ M_{3,1} & M_{3,2} & M_{3,3} & M_{3,4} \\ M_{4,1} & M_{4,2} & M_{4,3} & M_{4,4} \end{bmatrix} \begin{bmatrix} l_1 \\ l_2 \\ l_3 \\ l_4 \end{bmatrix}$$

Assuming symmetry (note that the structure is not perfectly symmetrical), one can deduce that

$$M_{1,1} = M_{3,3} \ (= R_1 \text{ say})$$
$$M_{2,2} = M_{4,4}$$
$$M_{4,2} = M_{2,4}$$
$$M_{1,3} = M_{3,1} \ (= R_3 \text{ say})$$
$$M_{1,2} = M_{3,2} = M_{1,4} = M_{3,4}$$
$$M_{2,1} = M_{4,1} = M_{2,3} = M_{4,3} \ (= R_{24} \text{ say})$$

From the Sandwell (1991) report, ring distortions u_1, u_2, u_3 and u_4 and corresponding loads have been chosen for load cases of the types shown in Figure 2-7, where a single prime denotes a full *udl* load case and no prime indicates a face load case.
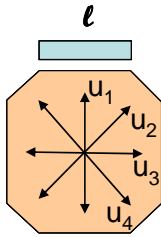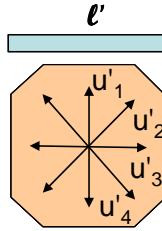
Figure 2-7: **Face load and full load cases**

The elements $M_{1,1}$, $M_{3,1}$, and $M_{2,1}$ have been determined from the face load cases as the average ratios of ring distortion to face load over all of the corresponding cases (i.e. u_1/l, u_3/l and u_2/l and u_4/l respectively) in Sandwell (1991).

The deduced corner loads and resulting ring distortions are denoted with a double prime (Figure 2-8).
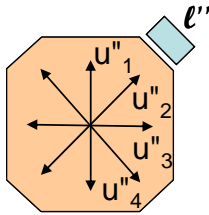
Figure 2-8: **Corner load cases (not modelled in Sandwell, 1991)**

The effect of loads on the corner faces has been estimated from the full UDL and face load cases. Sandwell (1991) models the corner load as

$$N_C = \frac{H_C}{\sin(\pi/4) + 0.15\cos(\pi/4)}$$

Equation 2-1

where 0.15 is the friction coefficient. Given a full load ℓ', the load ℓ'' acting on each corner is

$$\ell'' = \frac{\ell' \cdot (15.606/88.863)}{\sin(\pi/4) + 0.15\cos(\pi/4)}$$

Equation 2-2

and the center load is

$$\ell = \ell' \cdot (57.653/88.863)$$

Equation 2-3

Given the assumed linear response, the ring distortion associated with the full UDL load can be written in terms of the ring distortions associated with the face and corner loads as

$$u_i{}' = \left[\frac{u_i}{l}\right] \cdot l + 2 \cdot \left[\frac{u_i{}''}{l''}\right] \cdot l''$$

Equation 2-4

where $\left[\dfrac{u_i}{l}\right]$ and $\left[\dfrac{u_i{}''}{l''}\right]$ are the stiffnesses for ring distortion i for the center and corner loads respectively. Reworking the equation gives

$$\left[\frac{u_i{}''}{l''}\right] = \frac{\left(u_i{}' - \left[\frac{u_i}{l}\right] \cdot l\right)}{2l''}$$

Equation 2-5

The elements $M_{2,2}$ and $M_{2,4}$ etc. are estimated as follows. There is not enough information to differentiate $M_{2,2}$ and $M_{2,4}$ from the available data given that both corners are always loaded at the same time. It was initially assumed that the ratio $K = M_{2,4} / M_{2,2}$ was the same as the average ratio $M_{1,3} / M_{1,1}$ (determined as -0.374). This was subsequently modified to $K = -0.187$ as the lower value gives a better fit for the full width interactions.

For the ring distortions $u_2{}'$ and $u_4{}'$ in the NE and NW directions, one then has

$$u_2{}' = \left[\frac{u_2}{l}\right] \cdot l + \left[\frac{u_2{}''}{l_2{}''}\right] \cdot l_2{}'' + \left[\frac{u_2{}''}{l_4{}''}\right] \cdot l_4{}''$$

Equation 2-6
and

$$u_4{}' = \left[\frac{u_4}{l}\right] \cdot l + \left[\frac{u_4{}''}{l_2{}''}\right] \cdot l_2{}'' + \left[\frac{u_4{}''}{l_4{}''}\right] \cdot l_4{}''$$

Equation 2-7

The first equation becomes:

$$u_2{}' = R_{24} \cdot l + \left[\frac{u_2{}''}{l_2{}''}\right] \cdot l_2{}'' + K \cdot \left[\frac{u_2{}''}{l_2{}''}\right]$$

Equation 2-8

from which

$$\left[\frac{u_2{}''}{l_2{}''}\right] = \frac{u_2{}' - R_{24} \cdot l}{l_2{}'' + K}$$

Equation 2-9

and similarly

$$\left[\frac{u_4{}''}{l_4{}''}\right] = \frac{u_4{}' - R_{24} \cdot l}{l_4{}'' + K}$$

Equation 2-10

From the data in Table 2-1 (using only cases with full *udl* loads and cases with soil springs equal to either Base F24 or Base I65), one obtains

$$M = \begin{bmatrix} -0.3861 & 0.0097 & 0.1442 & 0.0097 \\ -0.0047 & -0.1096 & -0.0047 & 0.0123 \\ 0.1442 & 0.0097 & -0.3861 & 0.0097 \\ -0.0047 & 0.0123 & -0.0047 & -0.1096 \end{bmatrix}$$

The stiffness values $M_{i,j}$ have been determined from the data in Table 2-1 of the Sandwell (1991) report. All face load stiffnesses were normalized to 2.6 MNmm^{-1} and the ring distortions were modified accordingly for each load case. For development of the model, load cases with the full uniformly distributed load (Figure 2-7b) were used with soil spring constants based on either F24 or I65. Nine load cases from Table 2-1 met this requirement consisting of Cases 1, 3, 6, 7, 8, 10, 11, 13 and 14.

The results are shown in Figure 2-9 through Figure 2-12. There is good agreement between the two results.
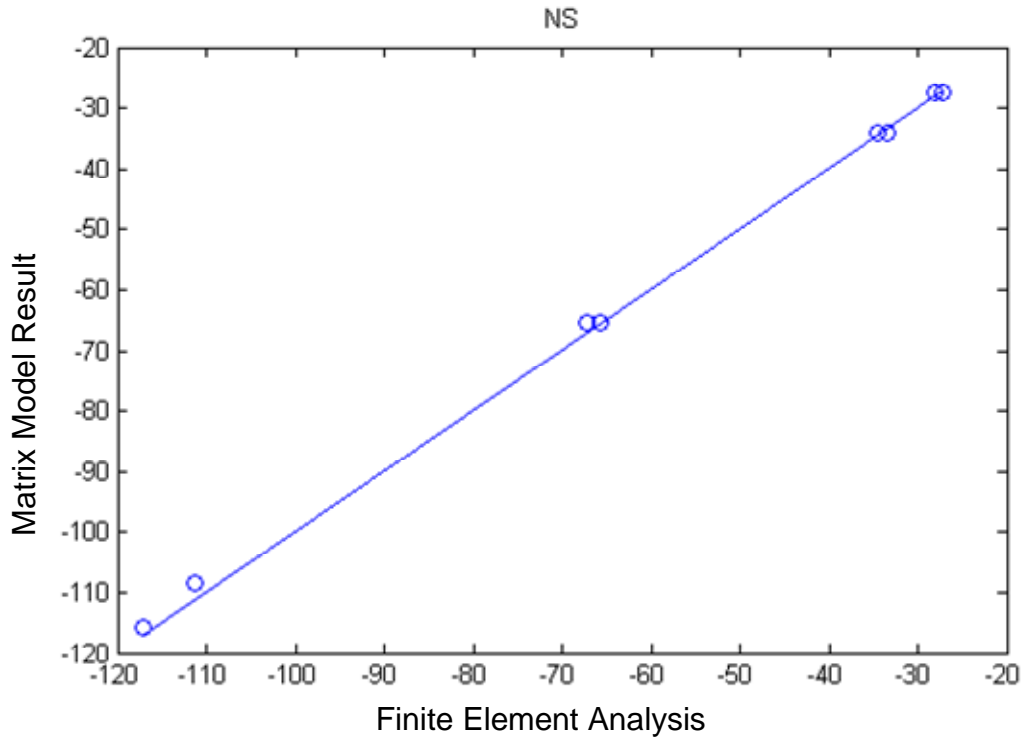
Figure 2-9: **Comparison of NS ring distortions based on matrix and FEA Models**
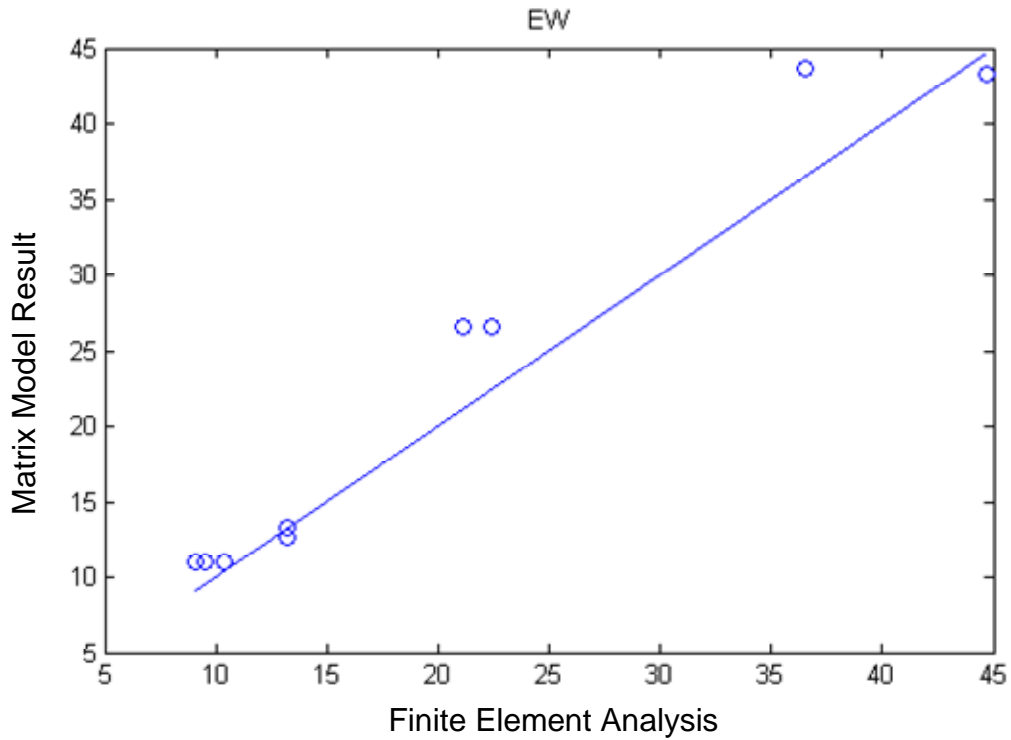
Figure 2-10: **Comparison of EW ring distortions based on matrix and FEA models**
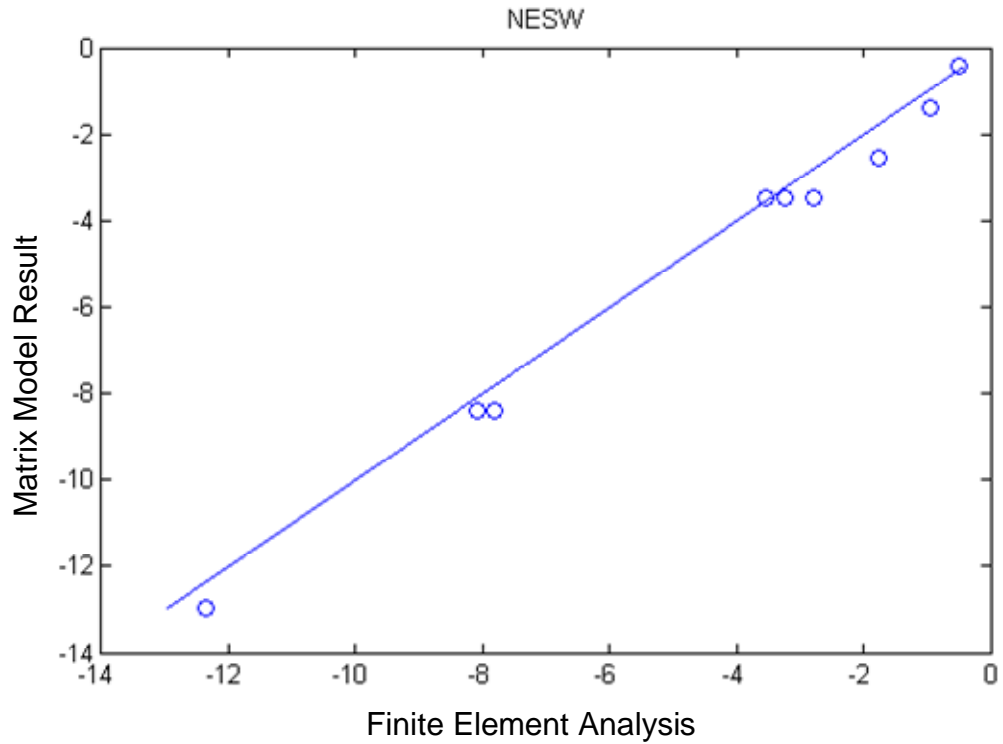
Figure 2-11: Comparison of NE-SW ring distortions based on matrix and FEA models
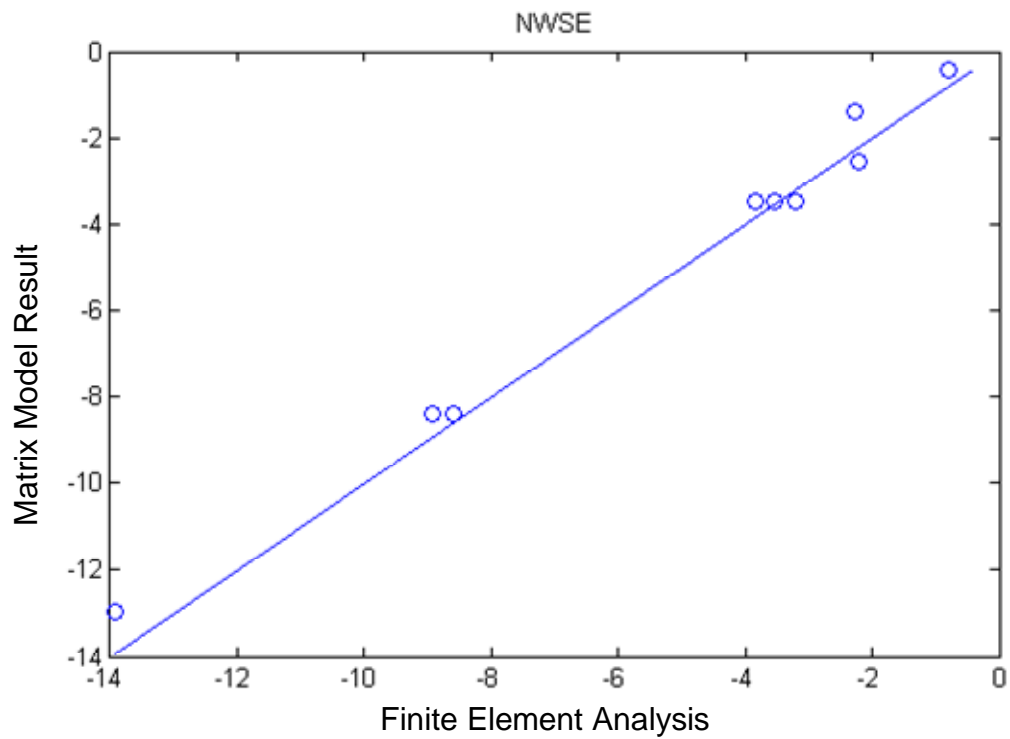
Figure 2-12: Comparison of NW-SE ring distortions based on matrix and FE models

2.6   Conclusions

The main factors affecting the choice of stiffness are:

1. core stiffness, and
2. proportion and distribution of load on the base and the consequent load path.

It is difficult to obtain a definitive estimate of the structure stiffness from the Sandwell report for use with the extensometer readings. In our calibration work, the values of stiffness (Load Distortion Ratio) equal to 2.2, 2.6 and 3.0 MNmm^{-1} have been chosen. Our best estimate is of the order of 2.6 MNmm^{-1} but the surrounding uncertainty must be taken into account as these values are for face loads.

The loading pattern in the loading case under consideration must be carefully considered in choosing the appropriate factor. A methodology based on matrix methods for dealing with biaxial loading and superposition on multiple faces has been developed successfully, but does suffer from difficulties in the calibration based on the Sandwell report.

A new finite element analysis with well chosen boundary conditions would be most useful.

3   INSTRUMENTATION

3.1   Introduction

This chapter provides a detailed review of the primary load measuring devices with which the Molikpaq was equipped: the extensometers, the Medof panels and the strain gauges. In Phase 1 of the project, the ice loads were analyzed using the Medof panels, with some attention to the extensometers, and some discussion of possible softening of the Medof panels. In the current phase of the project, the extensometers have been used to determine ice loads acting on the Molikpaq. For this reason the extensometers and Medof panels have been discussed in the greatest detail in the following.

3.2   Extensometers

The extensometers consisted of an extension rod with a range of displacement of ± 250 mm which monitored the displacement of the caisson and deck, and also between the deck and the 42" conductor casing. A cable around a guide pulley was connected to a position transmitter; please see Figure 2-1. In the Gulf Report Phase 1A, Vol. III, the following is stated: "The overall system accuracy is maintained as a result of the amplification of the extension rod movement through the pulley assembly. Measurement accuracy of better than ± 2 mm is realized."

There were in total 10 extensometers with 8 located along the face of the structure as illustrated in Figure 3-1 which measured displacement relative to the deck, and 2 extensometers located in the core portion of the structure which measured absolute movement of the core relative to the deck. To determine loads on the structure, the ring distortion was obtained by summing the deflection measured on opposite faces. For example the load on the north face was determined by summing the deflection of both the north and south faces.

NS Ring Distortion $= N+S$
EW Ring Distortion $= E+W$
$NE\text{-}SW$ Ring Distortion $= NE+SW$
$NW\text{-}SE$ Ring Distortion $= NW+SE$
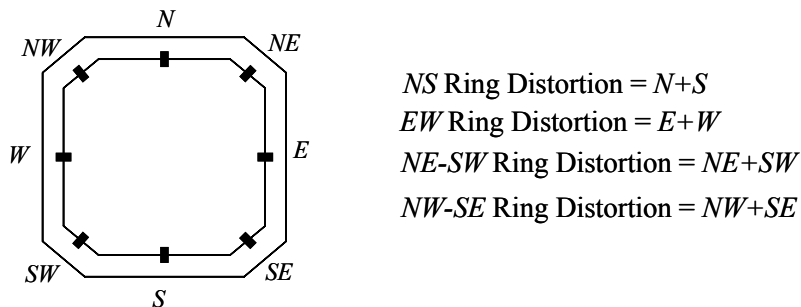
Figure 3-1:   **Approximate extensometer locations which were used to obtain the structural ring distortion of the Molikpaq.**

Calibration of the Load Distortion Ratio using finite element analysis has been dealt with in Chapter 2.

3.3 Medof Panels

3.3.1 Introduction

The Medof panels have formed the basis of almost all past analysis, with the other measurements calibrated against them. Therefore special attention is paid to these panels.

The Tarsiut Island was the first caisson type structure to be used in the Arctic and was operated by Gulf Canada Resources Ltd. During 1981 and 1982 drilling of the Tarsiut N44 well was carried out. During the winter season of 1982-3 the drilling had ceased and the caisson was left on site to be used as a test platform to study full scale ice-structure interactions. This project was referred to as the Tarsiut Island Research Program. Twenty one Medof panels were placed around the structure (Figure 3-2). The Medof panels used at the Tarsiut Island location were 1.1m wide and 1.75m high.
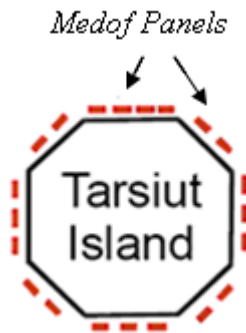
Figure 3-2   **Arrangement of 21 Medof panels situated around Tarsiut Island (1982-1983)**

The Mobile Arctic Caisson, later known as the the Molikpaq structure, was used at a number of Arctic locations in the 1980's. The Molikpaq structure was outfitted with 31 Medof panels which were 1.135 wide by 2.715 m high, with a capacity of 20 MN. The Medof panels were placed on the North, North East and East faces of the structure (Figure 3-3) in groups of 4 or 5. The Molikpaq structure was deployed at Tarsiut P-45 during the 1984-5 winter season where it experienced 18 recorded ice crushing events. During the 1985-6 winter season, the Molikpaq was deployed at Amauligak I-65 where it experienced 167 recorded ice events, of which 10 were with multi-year ice.
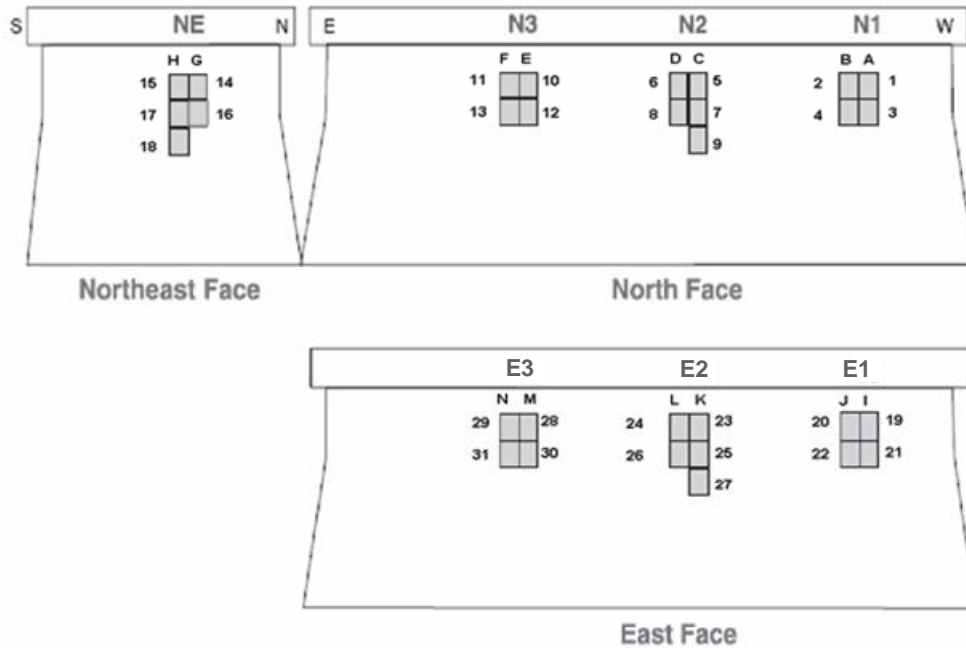
Figure 3-3: **Arrangement of 31 Medof panels situated on the North, North East and East faces of the Molikpaq. (1984-1985 and 1985-1986)**

3.3.2 Medof Panel Construction for Installation on the Molikpaq

The details of the construction of the Medof panels have been reported by Fenco (1983a). The panels were composed of two parallel steel plates with Adiprene L100 urethane buttons sandwiched between the plates. The outside plate had a thickness of 12.5 mm (1/2") while the Adiprene L100 buttons had a thickness of 2.54mm (1/10") with a diameter of 9.5 mm (3/8"). The back plate had a thickness of 4.5mm (0.179in) and was attached to the plating of the Molikpaq structure. The polyurethane buttons were closely spaced at 12.7 mm (1/2") centre to centre (Figure 3-4). Adiprene L100 is a polyether urethane-based rubber which is formed by reacting an isocyanate group with a polyamine group. The Adiprene L100 buttons have a density of 1060 kg/m^3. The remaining space between the steel plates was filled with the liquid $CaCl_2$. The response of each Medof panel to loading was measured in terms of the height of the $CaCl_2$ in a measuring tube.
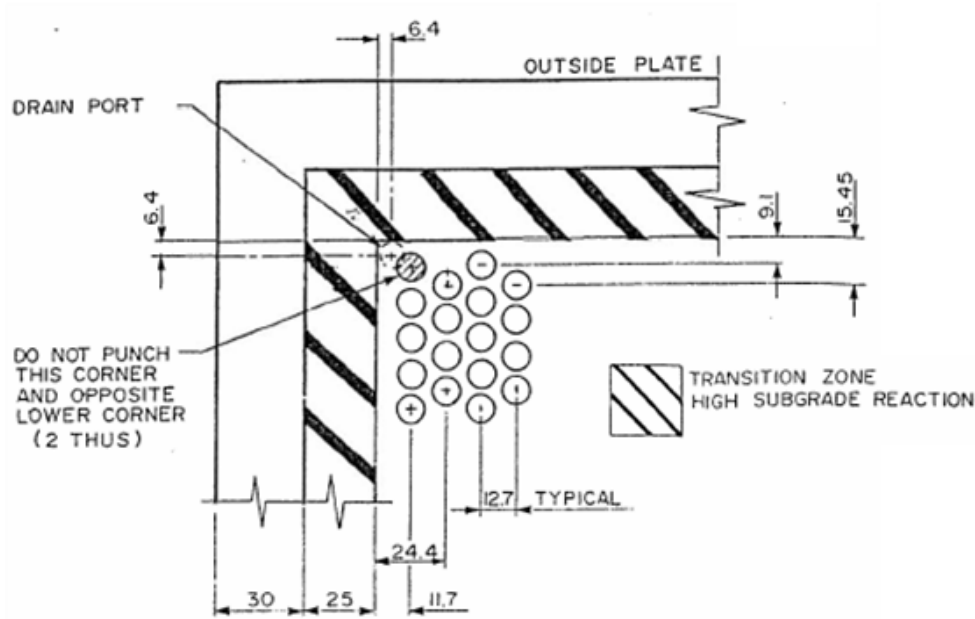
Figure 3-4:   **Arrangement of Adiprene L100 urethane buttons (Fenco, 1983a)**
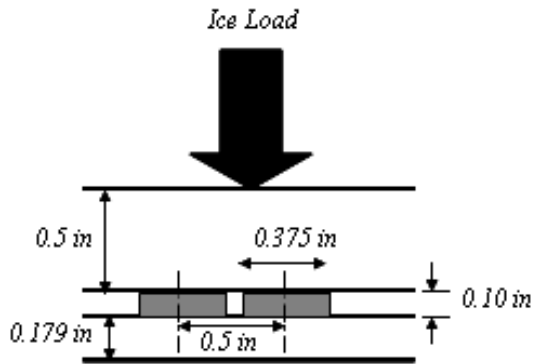
Figure 3-5:   **Medof Panel cross sectional view.**

If one considers a uniformly applied load over a 0.5" thick plate simply supported on four sides with the dimensions equal to that of the Medof panels at 1.135 m wide and 2.715 m high, a calculation of plate deflection can be made. Considering an applied load of 2.5 MN, similar in magnitude to those seen on the Medof panels, the maximum deflection of the plate is calculated to be 0.36m. This deflection of the plate shows that most of the load is being taken by the Adiprene L100 buttons.

3.3.3 Medof Panel Calibration

Calibration results are available for Medof panels from the Tarsiut P-45 (1982-3 season, associated with the Tarsuit structure) and before the deployment of the Molikpaq at the Tarsuit P-45 (1984-5) site and at the Amauligak I-65 site (1985-6). Recalibration results are available for 10 Medof panels from the Tarsiut P-45 location (1982-3 season after being removed from the ice surrounding the Tarsiut Island). There are no recalibration results for the Medof panels which were used at the Amauligak I-65 location. The original calibration results for the Tarsiut P-45 Medof panels are also available from the recalibration report prepared by Fenco (1983b).

Amauligak I-65

Similarly to the Tarsiut Medof panels, the calibration tests for the Amauligak Medof panels conducted by Fenco involved a stress-strain calibration at temperatures ranging from 0 to -25°C, a 24 hour creep test, and a pressure versus fluid output test at 0, -10 and -20°C up to a pressure of 1.86 MPa for each of the 31 panels. One of the panels was subjected to repeated loading for 6 cycles of load.

The present team has conducted an independent check of the original calibration slopes produced by Fenco (Figure 3-6). Table 3-1 shows the resulting values (at -10°C) in the third and fourth columns (renumbering according to Fenco, 1983 has been done). The values agree well with those in the report by Smyth and Spencer (1987). These have in turn been checked against the Channel Description File for April 12 (by R. Frederking) and again good agreement has been found. Table 3-1 also shows the 24-hour creep values, with some values of creep over 50% in 24 hours with a mean of over 33%.
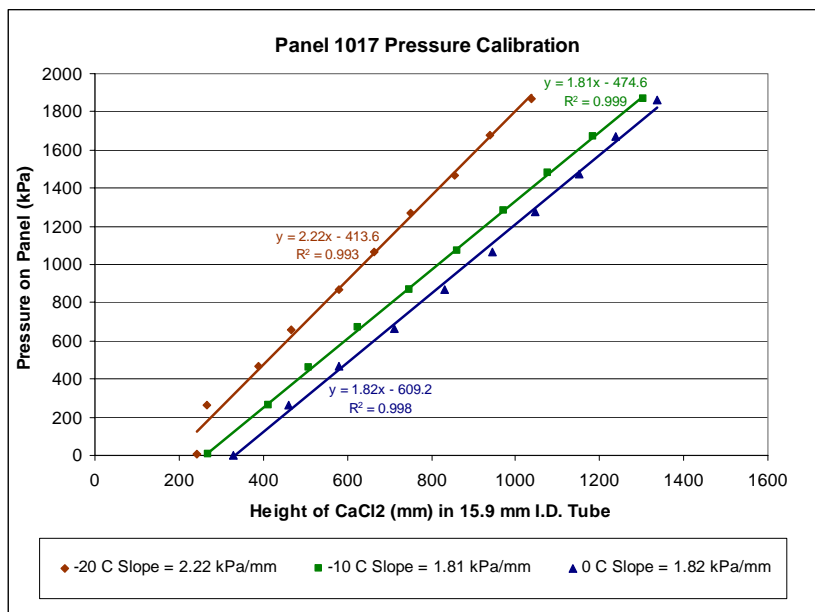
Figure 3-6: **Effect of temperature on the calibration factor for the Amauligak Medof Panels**

Table 3-1: Calibration Results for Amauligak Medof Panels

Corrected Panel Numbers	Diameter (mm)	Slope (kPa/mm) (-10°C)	Slopes (kPa/mm) equivalent to 19.1 mm diameter	Creep % (24 hour)
1001	15.9	1.24	1.80	51
1002	15.9	1.58	2.28	37
1003	12.7	1.23	2.79	39
1004	15.9	1.77	2.55	37
1006	15.9	1.35	1.95	25.5
1007	15.9	1.29	1.86	19
1008	15.9	1.26	1.82	23
1009	19.1	1.38	1.38	25
1010	25.4	1.43	0.808	17.5
1011	15.9	1.28	1.85	22
1012	15.9	1.79	2.58	43.5
1013	12.7	1.84	4.16	39
1014	19.1	1.36	1.36	32
1016	15.9	2.08	3.00	26.5
1017	15.9	1.81	2.61	30
1018	15.9	1.56	2.25	29
1019	15.9	1.53	2.21	35
1020	15.9	1.44	2.08	31
1021	15.9	1.15	1.66	34
1022	15.9	1.16	1.67	35
1023	15.9	1.43	2.06	37
1024	15.9	1.80	2.59	32
1026	12.7	1.38	3.13	42
1027	15.9	1.30	1.87	35
1028	15.9	1.14	1.64	36
1029	19.1	1.47	1.47	30
1030	15.9	1.32	1.90	30
1031	15.9	1.53	2.21	39
1032	19.1	1.48	1.48	36
1033	15.9	1.43	2.07	57
1034	19.1	1.65	1.65	39
		Mean = 1.47	Mean = 2.09	Mean = 33.7

There was minor variation in the individual calibration factors from the 0 to −10°C tests but a more significant change was observed by decreasing the temperature from −10 to −20°C. In the original Fenco report, the results showed that a stiffening effect occurred for the −20°C calibration. This result was questioned in the original report itself, but the

variation in the calibration factor with decreasing temperature was confirmed in the subsequent report by Smyth and Spencer (1987). Even though the air temperature was −20°C or lower during some ice structure interaction events at Amauligak, with the water temperature at approximately −2°C it is considered that the −10°C calibration is adequate since the temperature gradient between air and water would average at about −10°C.

Review of the creep tests shows that creep develops very quickly. The results have been analyzed using Kelvin viscoelastic elements by Smyth and Spencer (1987) who give a good practical assessment. Some values of creep are over 50% in 24 hours with a mean of over 33% (Table 3-1). These assessments are largely based on single loading and recovery curves, and are as a result inappropriate calibrations given that the Medof panels would have undergone very many load and unload cycles.

A prototype panel (Panel 1002, later renumbered 1010) was subjected to 6 cycles of loading which showed some variation in the slopes of the regression lines. Table 3-2 shows the calibration factor obtained for each cycle. For a single panel the coefficient of variation is about 12%. Note that there are indications of softening of the panel on the 5th and 6th loading even though the loads are far lower those that are encountered during a crushing event.

Table 3-2:   Repeated Loading of Prototype Panel 1010

	Slope (kPa/mm) (-10°C)	Slopes (kPa/mm) equivalent to 19.1 mm diameter
1st Loading	0.617	0.890
2nd Loading	0.599	0.864
3rd Loading	0.766	1.106
4th Loading	0.649	0.937
5th Loading	0.559	0.807
6th Loading	0.564	0.813
	Mean = 0.626	Mean = 0.903
	Standard Deviation = 0.077	Standard Deviation = 0.111

Tarsiut Island Research Project

It should be noted first that the ice conditions were relatively mild in this deployment, with no recorded crushing against the panels. The 10 Tarsiut Medof panels were subjected to a stress-strain calibration at temperatures ranging from 0 to -25°C, a 24 hour creep test, and a pressure versus fluid output test at 0 and -10°C up to a pressure of 1.5MPa. A comparison of the original calibration constants for the Tarsiut Medof panels with the recalibration constants was carried out during June 2009. Figure 3-7 shows the original calibration and recalibration curves for panel M16. This work involved reproducing plots developed by Fenco (1983b) to determine the calibration constants.

Panel M16 Pressure Calibration

$y = 1.474x - 189.7$
$R^2 = 0.999$

$y = 1.188x + 20.5$
$R^2 = 0.994$

$y = 1.646x - 798.5$
$R^2 = 0.989$

◆ -10C Original Calibration ■ -10C Recalibration (0% Air) ▲ 0C Recalibration (0% Air)
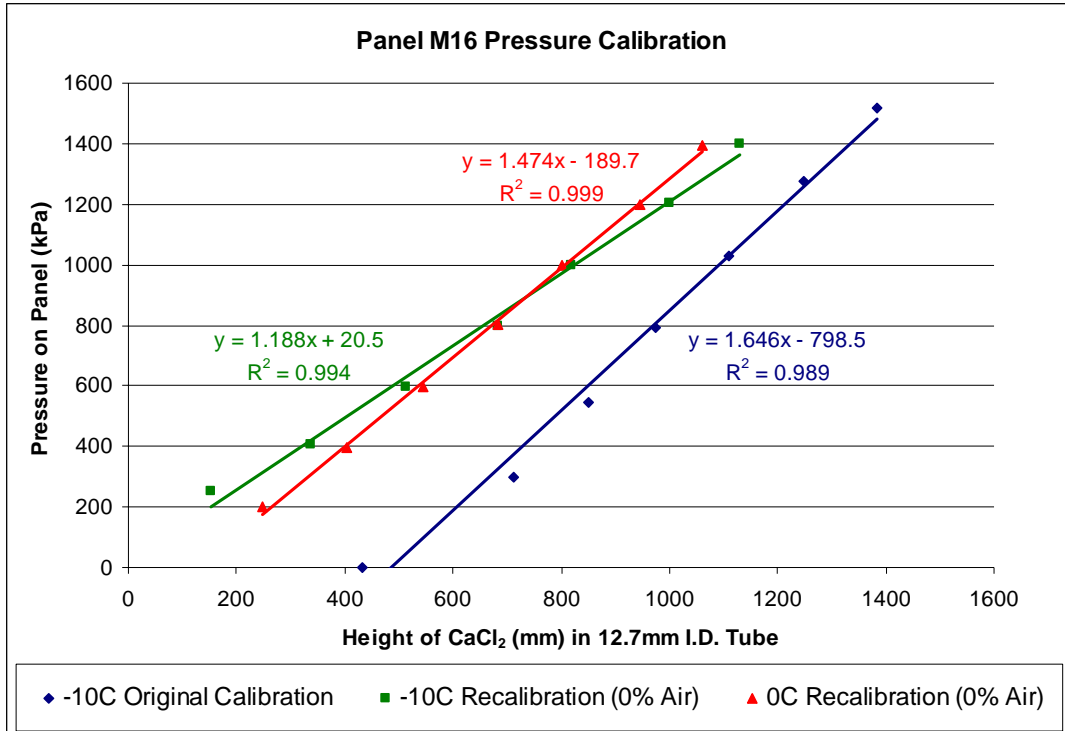
Figure 3-7: Comparison of the original calibration vs. the recalibration for panel M16. One can see that the recalibration factor is 28% softer than its original calibration factor.

Table 3-3 shows the results for all 10 panels of a comparison between the original calibration factors with the recalibration factors. The panels are on average 16% softer during the recalibration, with a maximum of 31% occurring in panel P19. The significance and the potential causes of this softening of the Medof panels will be discussed in the following.

Spencer (1988) conducted laboratory tests on Medof panels and identified a nonlinearity in the elastic response, and obtained also the creep response. A comparison was made between the calibration constants for panels P17 and M16. The results confirm the result for M16—panel softened. For panel P17, a hardening was also found, but not as much as in Table 3-3. Note that this was the only panel in Table 3-3 not to show softening, and illustrates the variability of panel response. But the main conclusion from Table 3-3 remains that there is quite widespread softening, even for these panels that did not see ice-crushing loads. We would question the conclusion in the report to the effect that "… the original M16 data may have been in error and the characteristics of the panels have not greatly changed over the intervening period." Analysis of the recalibrations discussed above show this not to be the case.

Finally, the report deals with one-time loading only.

Table 3-3: Recalibration Results for Tarsiut Medof Panels

Panel Numbers	Diameter (mm)	Original Calibration Slope (kPa/mm)	-10°C Zero Percent Air Slopes (kPa/mm)	Ratio between Original and -10°C Slopes	Temperature of Original Calibration (°C)
M16	12.7	1.65	1.19	1.39	-10
P2	12.7	1.26	1.02	1.24	-10
P6	12.7	1.27	0.95	1.34	-8.5
P10	12.7	1.53	1.19	1.29	-8.5
P11	12.7	1.03	0.92	1.12	-2
P12	12.7	1.02	0.93	1.1	-8.5
P16	12.7	1.26	1.02	1.24	-10
P17	12.7	1.1	1.78	0.62	-8.5
P18	12.7	1.66	1.34	1.24	-8.5
P19	12.7	1.27	0.87	1.46	-21
		Mean = 1.31	Mean = 1.12	Mean = 1.20	

3.3.4 Analysis of Panel Deformation and Problems in Past Calibrations and Analyses

Stress Level and Deformation

The aim of this section is to develop an understanding of the level of stress applied to the Medof panel buttons and the resulting strain. The Medof panel calibration results provide one with the maximum pressure applied over the entire panel and the corresponding fluid height in the sight tubes of known diameter. For the purpose of this analysis, 3 panels have been considered. These are Panels 1013, 1010, and 1033 which represent the stiffest, softest and average stiffness respectively of the 31 panels calibrated.

The panels can be conceived as being beams (the outside ½" plate) on an elastic foundation, the latter consisting of the buttons, the stiffness of which is spread uniformly across the plate. The assumption of elasticity of the buttons can be questioned, and linear elasticity in particular, but the method outlined here will give the essential features of the panel behaviour. A natural way to analyze the plate is to consider it initially as a beam spanning the short distance (1.135 m) as in Figure 3-8 (a). A unit width is considered as shown. A key parameter is the characteristic of the system, λ:

$$\lambda = \sqrt[4]{\frac{k}{4EI}} \text{ in m}^{-1},$$

Equation 3-1

where k is the modulus of the supporting medium in Nm^{-3}, E is the elastic modulus of the beam (Nm^{-2}) and I the second moment of area of the beam (m^4). The value $1/\lambda$ is the characteristic length in metres.

To calculate k, we use the result of the calculation below of displaced volume and Equation 3-2. The result is that the pressure of 1.86 MPa results in a deflection of 0.174 mm; hence $k = 1.07 \times 10^{10}$ Pa m^{-1}, and we note that $E = 200$ GPa, $I = 1.71 \times 10^{-7}$ m^4. Then $\lambda = 16.7$ m^{-1} and the characteristic length is 6 cm. Considering a fixed support, the deflection, slope, bending moment and shear diminish to zero at the following distances from the support, respectively, expressed as multipliers of the characteristic length: $3\pi/4$, π, $\pi/4$, and $\pi/2$.

This result (characteristic length of 6 cm) shows that the plate bends sharply under applied loading. A concentrated load on the panel would not spread far from the area of concentration. The result is that high pressures tend to be transmitted directly into the polyurethane buttons.

Because of the construction of the panels, there is an edge effect which restricts the downward motion of the front plate along the edges of the panel framing. To account for this effect in determining the potential volumetric displacement of the panel, a finite beam on an elastic foundation which is fixed at both ends with a uniformly distributed loading has been considered (note that the panels were welded onto the structure). The deflection of the beam is given by the equation shown below:

$$y = \frac{q}{k}\left[1 - \frac{1}{\sinh(\lambda l) + \sin(\lambda l)}\left\{\begin{array}{l}\sinh(\lambda x)\cos(\lambda x') + \sin(\lambda x)\cosh(\lambda x') + \sinh(\lambda x')\cos(\lambda x) \\ + \sin(\lambda x')\cosh(\lambda x)\end{array}\right\}\right]$$

Equation 3-2

where y is the vertical beam deformation, q is the uniformly distributed load per unit width, k is the foundation stiffness, and λ is the characteristic of the system as described above. If a pressure of 1.86 MPa is applied to the beam the resulting deflection of the beam is shown in Figure 3-8.
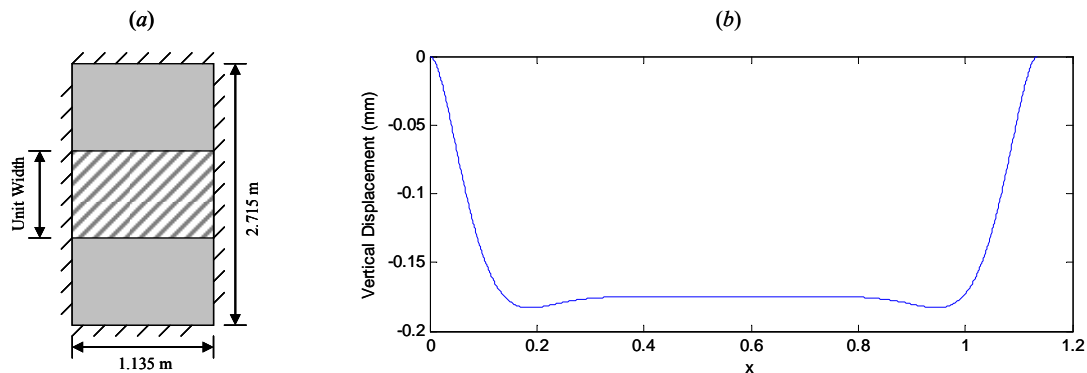
Figure 3-8   **Beam-on-elastic-foundation analysis. (a) Unit width analyzed in two dimensions; (b) Estimated vertical deflection of Medof panel plating during calibration**

From this it was concluded that 0.0575m on each side of the panel is a reasonable distance to exclude in calculating the volumetric displacement of the panel. Note that the plate bends rapidly to achieve an equilibrium deflection of about 0.175 mm in the central zone, corresponding to the pressure of 1.86 MPa being supported entirely on the buttons (checked by multiplying the 0.175 mm deflection by the k value above).

To obtain the deflection of the beam, the volume change of the panel is needed. From the calculation below, the effective area for calculation of volumetric displacement of the panel is 2.60 m $\times$ 1.02 m = 2.65 m^2; a distance of 0.0575 m has been subtracted from the edges, as justified above. The volume of the interior of the Medof panels was then 2.65m^2 $\times$ 0.00254m = 6.73 $\times$ 10^{-3} m^3. The volume of fluid within the panel is estimated to be 3.76 $\times$ 10^{-3} m^3 based on Figure 3-9. The change in volume within the panel can be determined by knowing the change in fluid height in the sight tube and that the diameter of the three tubes was 19.1mm. The calibration slope gives the fluid height given that the maximum applied pressure was 1.86 MPa. The strain in the Medof panel buttons can be found by taking the change in volume discussed above divided by the volume of fluid within the panels. For the three panels selected, 1013 (stiffest), 1033 (average stiffness) and 1010 (softest) the strains were found to be 0.033, 0.066, and 0.169 respectively.

While there was a pressure of 1.86 MPa applied to the Medof panels during the calibration, the pressure in the buttons is higher as the fluid between buttons does not support any of the loading. The factor of 2.26 which can be applied to the pressure on the Medof panels to determine the pressure in the buttons is calculated in Figure 3-9. The resulting stress in the buttons for a 1.86 MPa uniformly applied panel pressure is 4.20 MPa. The formation of high pressure zones during ice interaction with the panels will result in much larger stresses in individual buttons during the interaction.

$Area_1$=12.7 mm x 25.4 mm

$Area_2$=2 x $Area_{Button}$

$Area_{Button} = \dfrac{\pi}{4}(9.52mm)^2$

$\dfrac{Area_1}{Area_2} = 2.26$
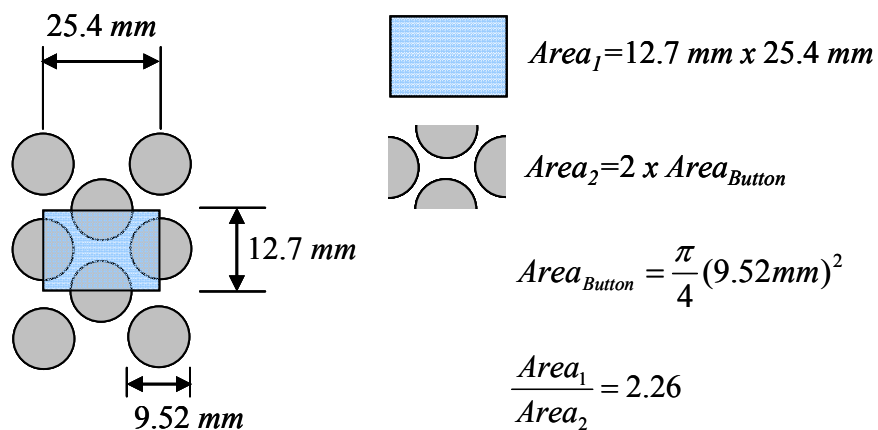
Figure 3-9   **Computation of stress magnification factor for Medof panel buttons.**

High-pressure Zones

In this section, we account for the presence of high-pressure zones (*hpz*s) in the ice. This factor was not included in the original calibration and analyses. It is noted that much has been learnt of these entities during the last two decades (Jordaan, 2001)..

Frederking (2009) prepared an estimate of the largest average pressures on the Medof panels (Figure 3-10). From this work it was concluded that "for an area of 1m^2 these pressures would be doubled using A$^{-0.7}$ to adjust the pressures." The present group reconsidered this in the light of the formation of high pressure zones.
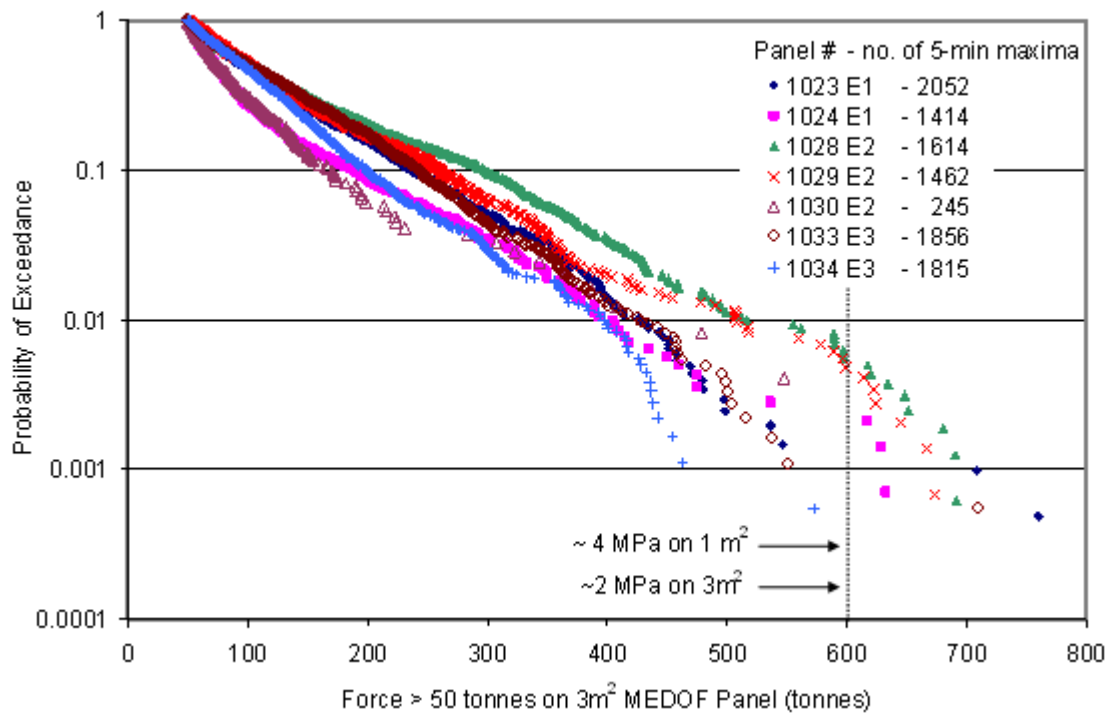
Figure 3-10   **Largest average pressures on the Medof panels (Frederking, 2009).**

During an ice interaction with a given Medof panel, a high-pressure zone may well be of the size 0.1 m^2, or smaller. Under these conditions, the stresses on the buttons would be greatly increased. Given that there could be 2 MPa acting on 3m^2 (area of the panel shown in Figure 3-10 above then there could be up to 20 MPa acting on 0.1 m^2 using the relationship $P = cA^{-0.7}$, where the constant c can be determined knowing 2 MPa acts on 3 m^2. The stress on individual Medof panel buttons can then be obtained using the factor determined in Figure 3-9. Thus it is likely that individual buttons could be exposed to pressures up to 45 MPa under high pressure zones.

This is one way to consider the problem. In reality, *hpz*s can occur in a variety of sizes. Our experience based on experimental evidence is that, for ice at –10ºC, the central part of the *hpz* experiences pressures of the order of 70 MPa routinely.

Consideration of Loading Condition

While the pressures the panels were exposed to during the calibration were far too low, there were also problems with the loading conditions under which the panels were calibrated.

Review of the 24 hour creep tests showed that creep developed very quickly with creep values exceeding 50% in one case with a mean of 33%. These were for single loadings only. If these tests were repeated the panel may well have softened, leading to strains exceeding those observed in Table 3-1. The panels were largely subjected to a single static loading, with the exception of one panel which underwent 6 cycles of loading but at low stress levels. For the single panel tested the coefficient of variation was about 12% with indications of softening occurring after only 4 cycles. The Medof panels would have been subjected to many load and unload cycles during their deployment at the Amauligak I-65 location. This effect was only studied in a limited way on 1 of the 31 Medof panels. No consideration was given to dynamic effects which occur during the high frequency loading associated with ice crushing.

3.3.5 *Uncertainties Resulting From Medof Panel Construction*

There are several reasons for the variability in the response of the Medof panels. These reasons all relate to the construction of the Medof panels; namely the material choice of Adiprene L100 buttons and the adhesive used to apply them to the steel plates. The following section includes a discussion of all of the factors that might possibly cause the panels to change their calibration with time, or other circumstances that lead to uncertainty in the calibration.

The behaviour of the panels has already been summarized, and the question of high-pressure zones has been raised. Further aspects related to the construction will now be discussed.

A summary of the main conclusions and an assessment of the relative importance of the various uncertainties are given in Section 3.3.6.

Bonding of the Buttons within the Medof Panels

Khan and Lopez-Pamies (2002) conducted a study of the compressive uniaxial mechanical response of Adiprene L100. During this work they have confirmed that Adiprene L100 has a Poisson's Ratio of 0.49, meaning that it undergoes negligible volume contraction during compression. Figure 3-11 is an illustration of an Adiprene L100 button in compression. The specimen is triaxially constrained due to the adhesive

which bonds the Adiprene L100 to the steel plates. This triaxial constraint increases the stress required to cause deflection of the button. Smyth and Spencer (1987) state that the adhesive bonding the Adiprene L100 to the steel plates was hand-applied. Hand-applied adhesive introduces the potential for the Adiprene L100 buttons to become unbonded. If this is the case the stress required to deflect the buttons will be greatly reduced as can be seen in Figure 3-12 after Canatec (1991).
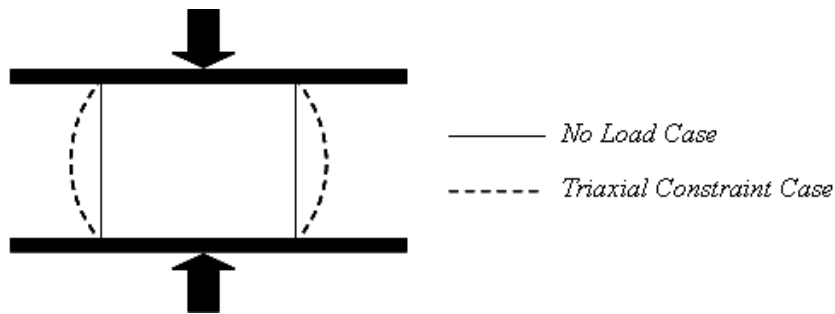
Figure 3-11:   Adiprene L100 button undergoing triaxially constrained compression.
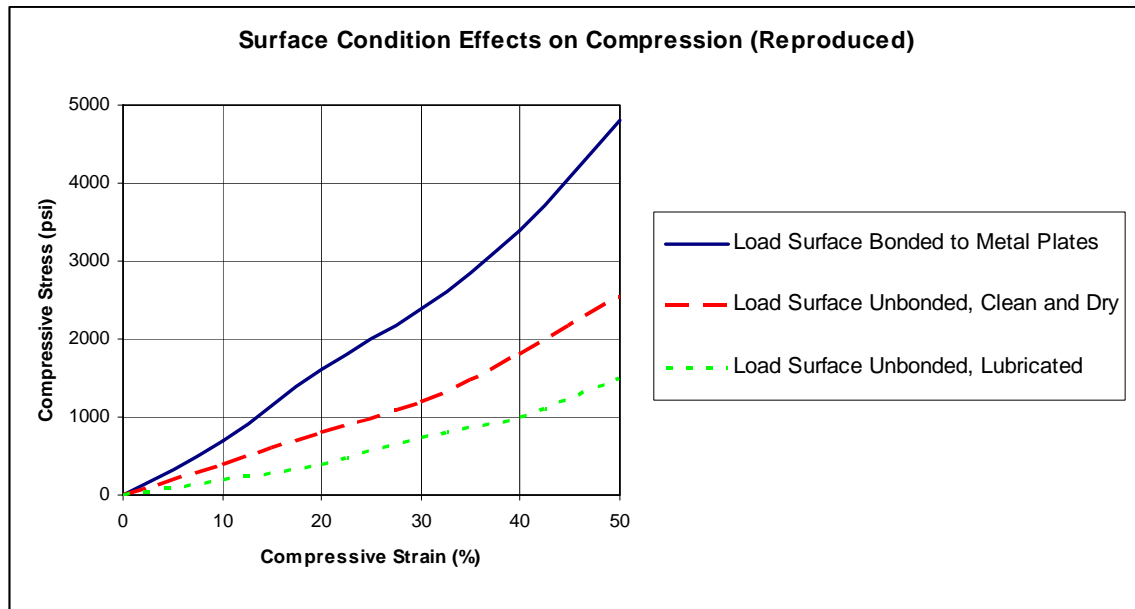
Figure 3-12:   The effect of the surface condition of Adiprene L100 buttons for bonded and unbonded loading conditions (After CANATEC, 1991).

Nonlinearity of Polyurethane Stress-strain Behaviour

Stress and strain results derived for the buttons from the calibration results are plotted in Figure 3-13 together with a stress-strain curve at low stresses for a similar polyurethane material tested by Qi and Boyce (2005) If well bonded, the buttons would be triaxially constrained. Figure 3-12 shows that if the Medof panel buttons were not triaxially constrained, the resulting strains would be increased by a factor of two. This has been

reflected in Figure 3-14 ("adjusted" lines). The overall agreement between the stress-strain curves deduced from the calibrations and the experimental results of Qi and Boyce is satisfactory.

Stresses and strains in the Medof panel buttons of the magnitude suggested in Section 3.3.4 could be up to an order of magnitude greater than those obtained in the calibration of the panels. The result of Qi and Boyce (2005) in Figure 3-13 and Figure 3-16 shows that the material is non-linear and becomes significantly softer with increased strain, suggesting that the calibration factors of the Medof panels are likely to be too stiff, possibly by a factor of 2 or more for higher stresses.
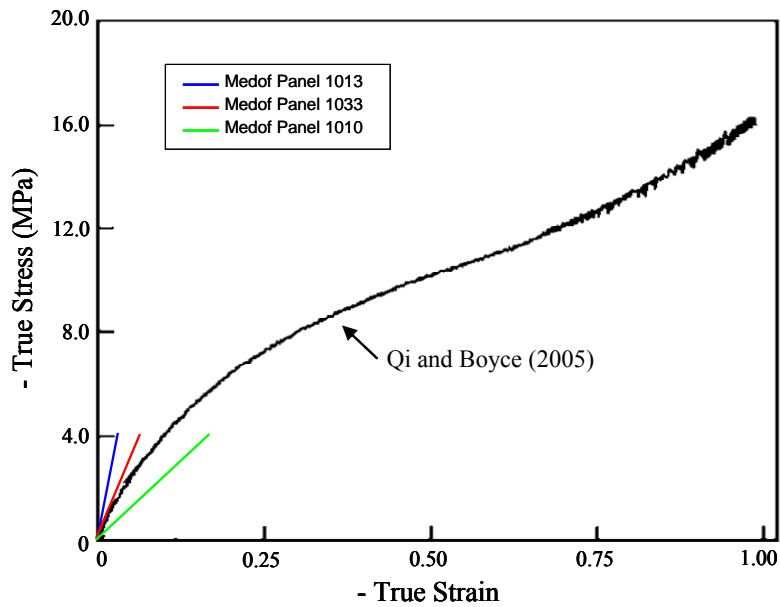
Figure 3-13 **Black line is true stress- true strain curve obtained experimentally by Qi and Boyce (2005) for polyurethane. Also shown are superimposed stress strain curves which are derived for the buttons contained within Medof panels 1016, 1020, and 1028 during the initial calibration.**
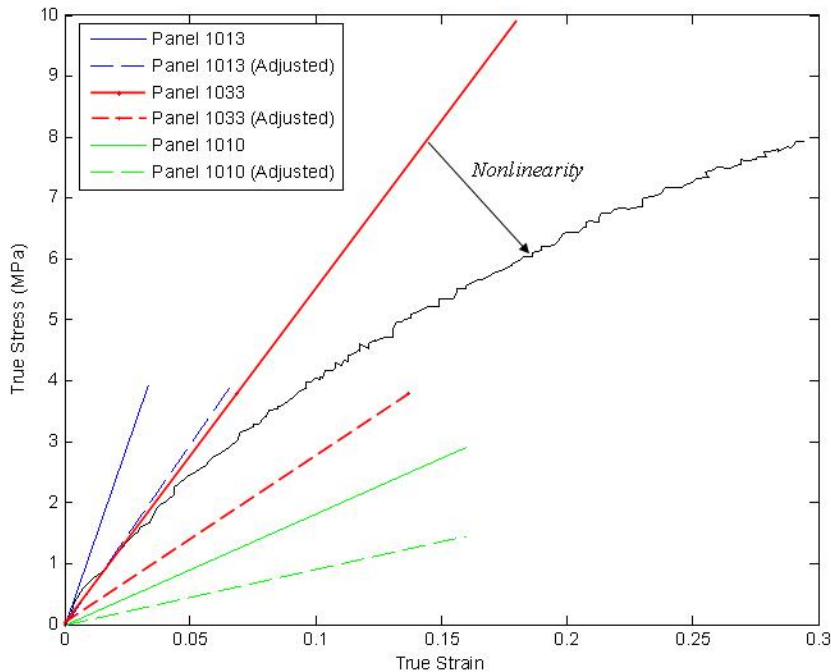
Figure 3-14   Black line is from experimental results of Qi and Boyce (2005). Strains have been increased by a factor of two (adjusted values) to compare with the uniaxially supported specimen tested by Qi and Boyce (2005).

The Mullins Effect

One of the most likely causes of the softening of the Medof panels is the Mullins effect. This is a softening of the stress-strain relationship which is dependent on the maximum loading previously encountered. The softening begins after only a small number of cycles (Qi and Boyce, 2005). The individual Medof panel buttons would have undergone very many load and unload cycles. The softening of the material appears for deformations lower or equal to the maximum deformation (or stress) previously applied. When the deformation exceeds this level, the material stress–strain response returns to the same path as that of the stress–strain initially obtained. This result can be seen in the test on a polyurethane sample published by Qi and Boyce (2005) in Figure 3-15. The softening is related to an irreversible effect (damage) within the material which increases with increasing strain (or stress).

At times when the loading is less than the prior maximum, nonlinear elastic behaviour prevails with a much lower stiffness level than that of the original sample. In the case of the Medof panels, the presence of high pressure zones discussed in Section 3.3.4 would result in significant softening of the panels due to very large pressures occurring on individual buttons within the panel. This effect could lead to over-estimation of ice loads by a factor of 2 or more, as suggested by the result in Figure 3-15.
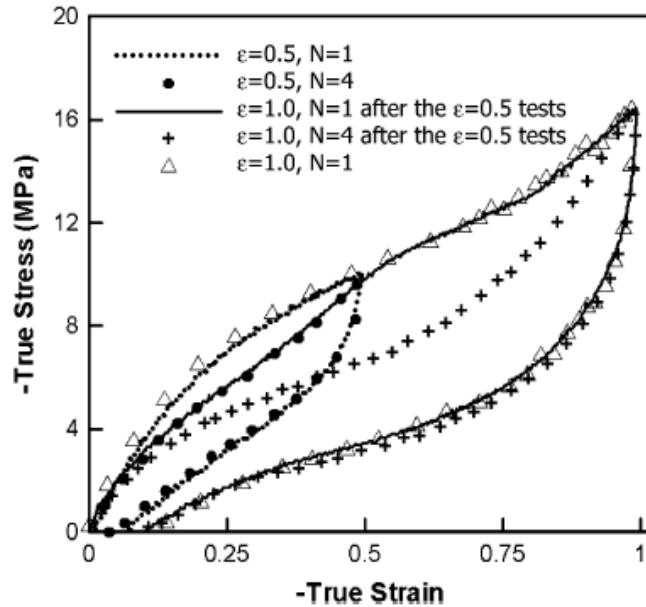
Figure 3-15   Stress-strain curve showing the Mullins Effect (Qi and Boyce, 2005).

Cyclic Loading of Medof Panels

There has been considerable research dedicated to studying the effects of combined static and cyclic loading on the creep deformation response of polymers and other materials, compared to their static creep response. "It has been consistently observed that under cyclic loading conditions, deformation rates of polymers tend to increase" (Vinogradov et al., 2000). This phenomenon has been termed vibrocreep which involves maintaining a mean stress and cycling the load about the mean at various frequencies (Figure 3-6). Durham and Thomas (1977) have reported that the natural rubber (SMR 5) characterized as a linearly viscoelastic material under static loading has exhibited highly nonlinear time-dependent effects under low frequency load-unload cycles. These effects were found to lead to considerably accelerated creep rates, up to 10 times higher than that of the static load cases. The accelerated creep rate is a result of damage accumulation.

Microstructural damage to the Adiprene L100 buttons due to the vibrocreep experienced during ice loading is likely to have caused the Medof panels to become softer, which would result in a higher load reading based on their original calibration.
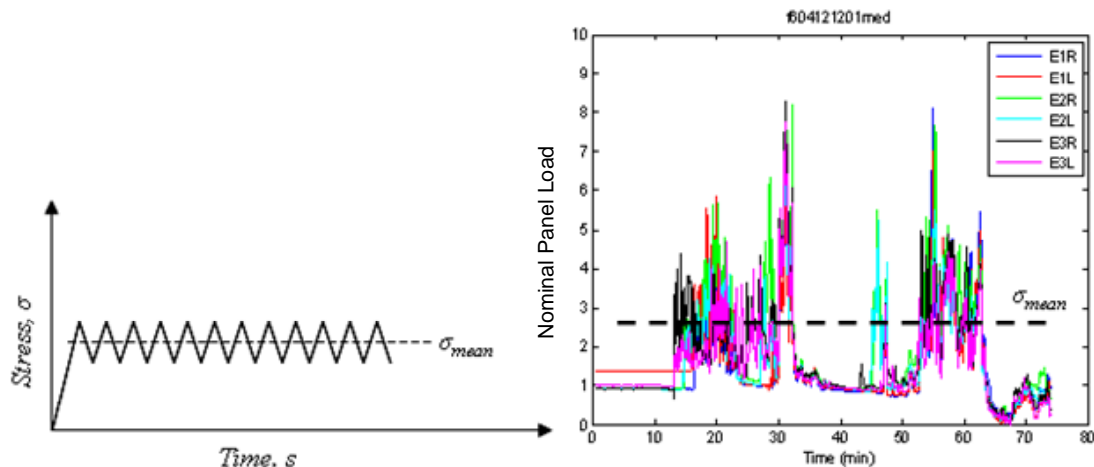
Figure 3-16: **Illustration of loading associated with vibrocreep. Left, idealized loading; right, load on Medof panel**

3.3.6 Discussion and Conclusions

Recalibration of the Medof panels used during the Tarsiut P-45 (1982-3) deployment showed an average softening of approximately 16% during that time, with a maximum of 31%. The panels were placed within the ice (rubble field) and received relatively light loading. Consequently, they did not experience the levels of stress and the repetitions of load that occur under crushing conditions. Nevertheless, softening did occur as just noted.

Before being placed at the Amauligak I-65 location, the Molikpaq spent the 1984-5 season at the Tarsuit P-45 location during the 1984/85 winter season where it experienced 18 recorded ice crushing events. There was likely considerable softening during this period.

Our understanding of the Mullins effect in polyurethanes is that most softening occurs during the first (approximately) 6 cycles but that further softening can occur with many more repetitions. The extensometer analysis shows that the loads at Amauligak were about half those measured by the Medof panels, or somewhat less. The decelerating floe analysis of May 12 (Section 5.2.2) suggested softening further that that which occurred earlier in the season. Considering the severity of the ice interactions at the Amauligak I-65 location, where much more severe loads as compared to the Tarsiut P-45 deployment were obtained, the softening effect might have increased.

The analysis above leads to the strong conclusion that there is uncertainty regarding the Medof panel loads much beyond that suggested by the work of Smyth and Spencer (1987). It is our conclusion that the Medof panels may have been over-reading by the order of 100% or more at the Amauligak location. The Medof panels are not seen as a convincing basis for calibrating other devices.

## 3.4	Strain Gauges

Strain gauges can provide valuable information if corrected for drift and if the strains obtained are high enough to ensure reliability in the results (i.e. large enough to overshadow natural variations). It is true to say that the strain gauges are often "correlated" to the Medof panel results. But one can have a high correlation with various factors relating the two; the correlation will not depend on this relationship.

Obtaining loads is complicated considerably, and much uncertainty added, by the fact that the gauges used were in locations of high strain and stress gradient. Further, the position of the load (and high-pressure zones) will have a very significant effect on the readings. A large number of possible values of loads and of positions thereof could give the same reading on a strain gauge. Figure 3-17 and Figure 3-18 show the uncertainty in strain gauge factors.

There were many strain gauges applied to the Molikpaq and these could possibly be used together to provide a better estimate of loads.
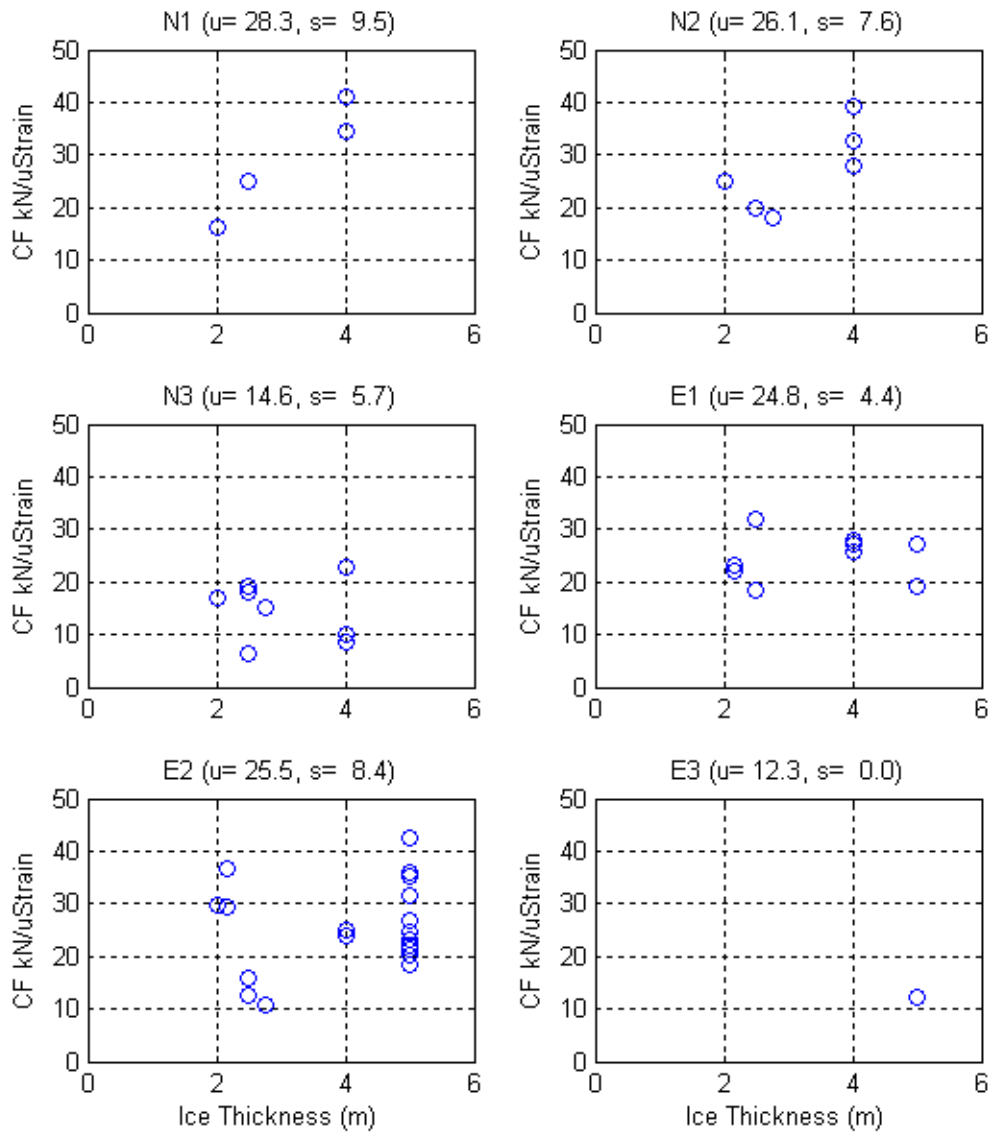
Figure 3-17: **SG09 Strain Gauge Calibration Factors by Column and Ice Thickness**
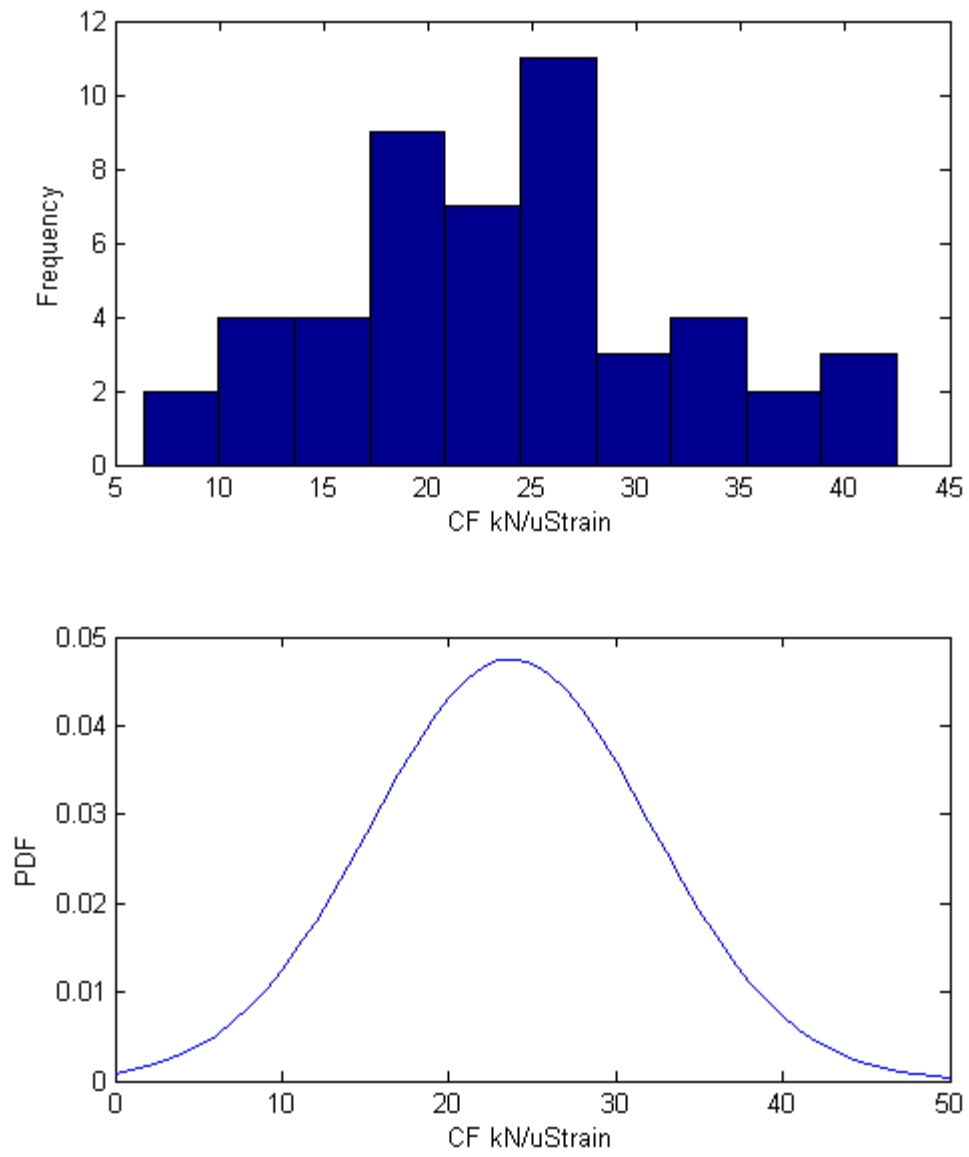
Figure 3-18: Histogram and probability density function (PDF) of S09 strain gauge calibration factors (mean = 23.7, std = 8.4, COV = 0.35)

4   PROBABILISTIC AVERAGING

4.1   Introduction

When attempting to extrapolate to obtain global loads from local measurements, for instance those from the Medof panels, the question arises as to the appropriate measure of standard deviation. To take a simple example, consider first two adjacent panels. If the readings are fully correlated, then if one panel reads high, so does the other. If one reads low, so also does the other. In obtaining loads, one would not assume that one panel read high while the other reads low. The implication is that the mean and the standard deviation of readings for the average of the combined panels would be the same as for individual panels. In this case, simple (linear) extrapolation of the pressures to obtain the global load, i.e. multiplying the Medof reading by the structure width divided by the panel width, seems reasonable.

Now consider two distant panels: if they are uncorrelated, then there is no reason to assume that a high reading on one would imply a high reading on the other. The mean values, under similar loading conditions, would be the same, but averaging the two readings reduces the standard deviation. In fact, analysis shows that the standard deviation of the average is the standard deviation of an individual panel divided by $\sqrt{2}$. This will now be explained.

By considering a linear function of random quantities, it is possible to calculate the standard deviation of pressure distribution for a group of two panels or columns, whether they are correlated or not. If $Y = aX_1 + bX_2$, where X_1 and X_2 have a joint probability distribution, the variance is

$$\sigma_Y^2 = E\left(aX_1 + bX_2 - a\mu_{X_1} - b\mu_{X_2}\right)^2,$$
Equation 4-1

where $E(\cdot)$ denotes expected value and the μ's denote mean values.

As a result,

$$\sigma_Y^2 = a^2\sigma_{X_1}^2 + \sigma_{X_2}^2 + 2ab\sigma_{X_1,X_2},$$
Equation 4-2

where σ_{X1}^2 and σ_{X2}^2 are variances and $\sigma_{X1,X2}$ the covariance.

If $Y = (X_1 + X_2)/2$, then, assuming equal variances σ and using Equation 4-2

$$\sigma_Y^2 = \frac{1}{4}\left(\sigma^2 + \sigma^2\right) + \frac{1}{2}\sigma^2 \cdot \rho,$$

$$= \frac{1}{2} \cdot \sigma^2\left(1 + \rho\right),$$

in which ρ is the correlation coefficient.

As a result

$$\sigma_Y = \sigma \sqrt{\frac{1}{2}(1+\rho)}.$$

Equation 4-3

We see that if $\rho = 1$ (high correlation), $\sigma_Y = \sigma$ whereas if $\rho = 0$, $\sigma_Y = \sigma/\sqrt{2}$, as stated above.

If we consider eight panels, with means and individual standard deviations all equal to μ and σ respectively, knowing also that the pressures are stochastically independent, then the average pressure over eight panels will have a mean of μ with a standard deviation of $\sigma/\sqrt{8} = \sigma/2.83$. This shows that the standard deviation of an averaged load can be considerably less than the local standard deviation, and a much larger reduction can be expected for a wide face of the order of 90m. This example was based on the assumption of independence between panels, and it is important to consider correlation between adjacent panels.

To illustrate application of the method, an interaction involving mainly crushing is considered (Figure 4-1). The nominal interaction area represents the contact area that would occur without spalling of ice. The actual interaction area represents the area of contact with intact ice (after spalling). The high pressure zones represent areas of high pressure which are observed during crushing events. These high pressure zones can reach pressures up to the order of 70 MPa over smaller areas. Given the nature of the pressure distribution during crushing events, one expects the average pressure over a wide structure (shown in red) will have significantly less variance than the pressure measured over a single panel (shown in black).
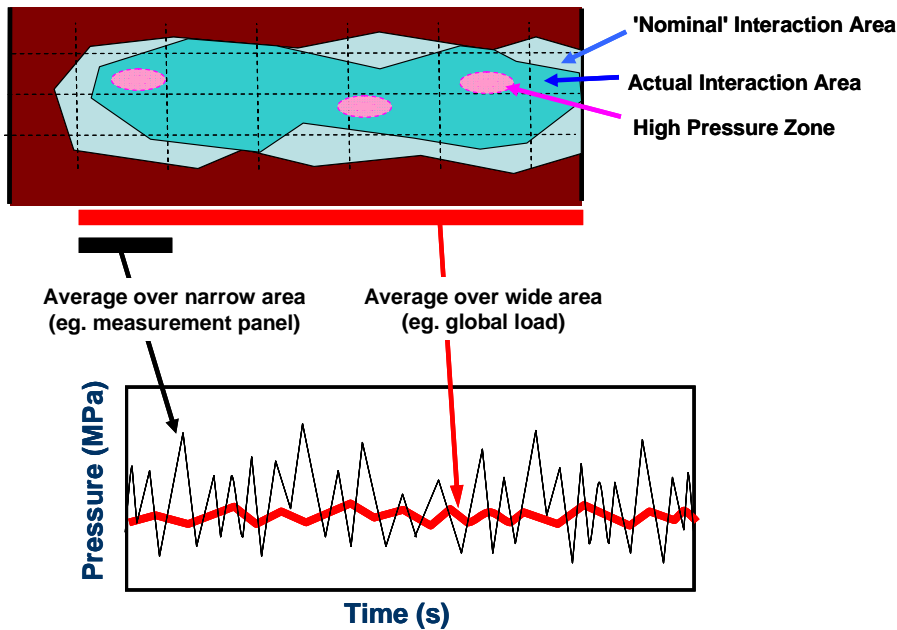
Figure 4-1: **Pressure Averaging for Crushing Failure Model**

4.2   Histograms for Individual Medof Columns

To provide background on the analysis to follow and to respond to client request, the histograms for selected individual Medof columns are provided. The trimmed event files (inhouse), corrected for panels not working, were used for this exercise. The three representative sample events given in Table 4-1 have been selected for further analysis.

Table 4-1: **Events selected for analysis of column load distributions.**

Event No.	fastfile	Ice Thickness Lower Estimate (m)	Ice Thickness Upper Estimate (m)	Velocity (m/s)	Ice Type	Loaded Face
01	f511121901	0.8	0.8	0.57	FY	N
23	f605120301	1.5	3.5	0.17	FY/MY	N
58	f603081731	4.3	4.3	0.04	MY	N

For each of the above events, histograms of loads acting on each column of the North face were generated and distributions were fitted to these data. Results of this analysis are shown in Figure 4-2, Figure 4-3 and Figure 4-4 for events 01, 23 and 58, respectively. The local column loads show a skewed and non-normal distribution. In the figures the data have been fitted to lognormal distributions, although other distributions such as Weibull or gamma may also be considered. Column to column variation in the load distributions are observed for all events. This likely results from local variations in ice thickness, physical properties, as well as from randomness of the failure processes.
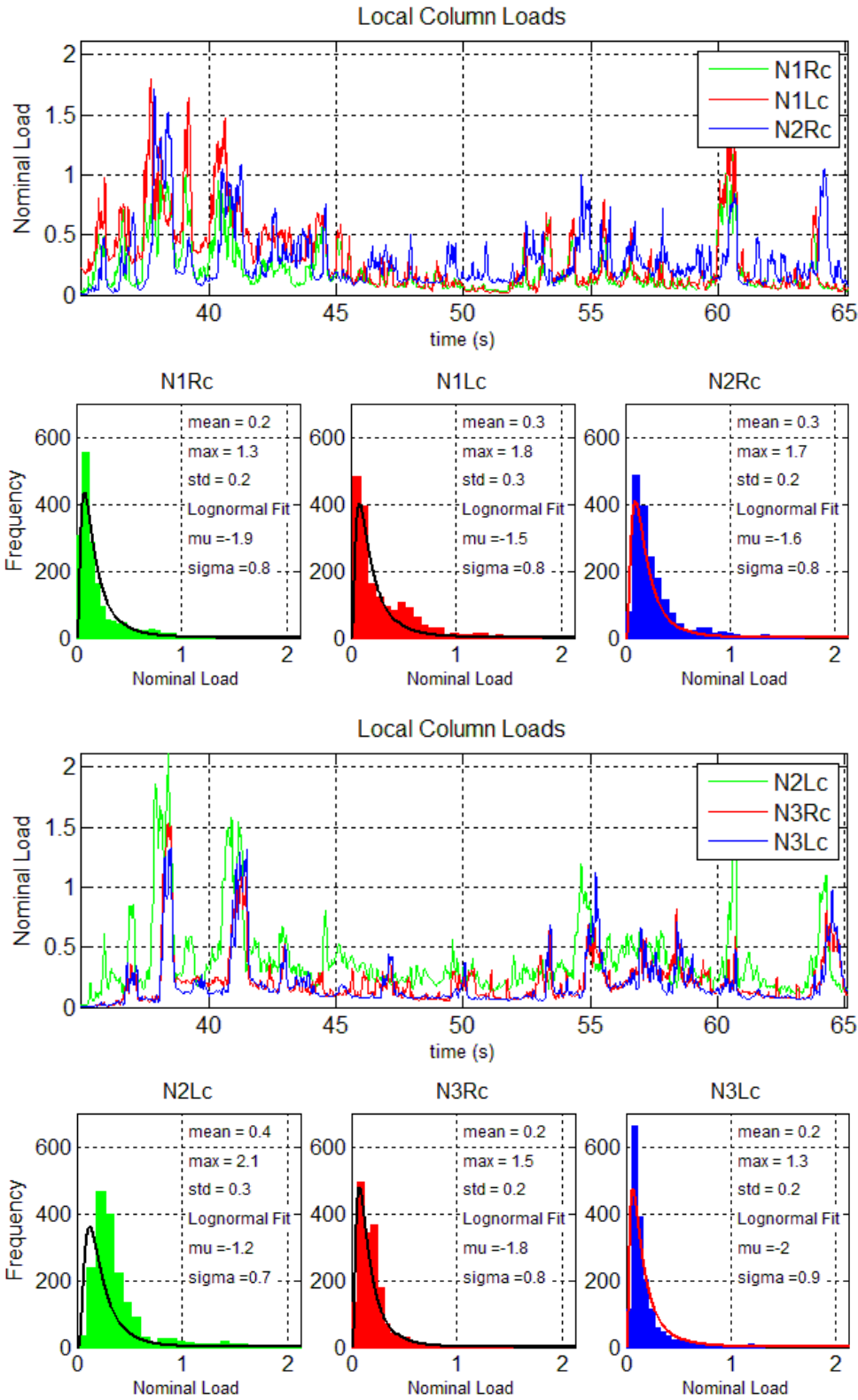
Figure 4-2   **Histograms of nominal loads of columns for the North face during event 01**
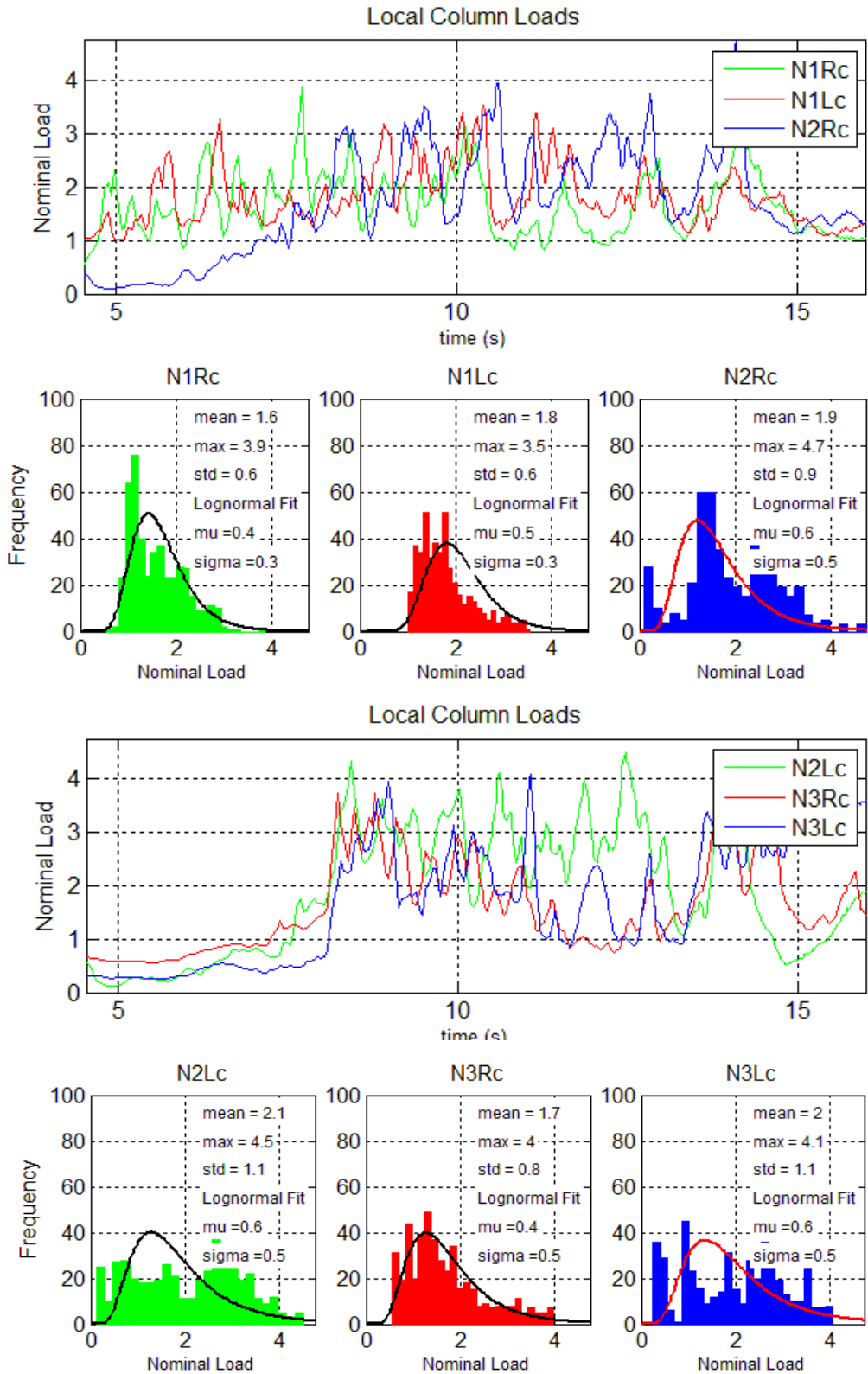
Figure 4-3 **Histograms of nominal loads of columns for the North face during event 23**
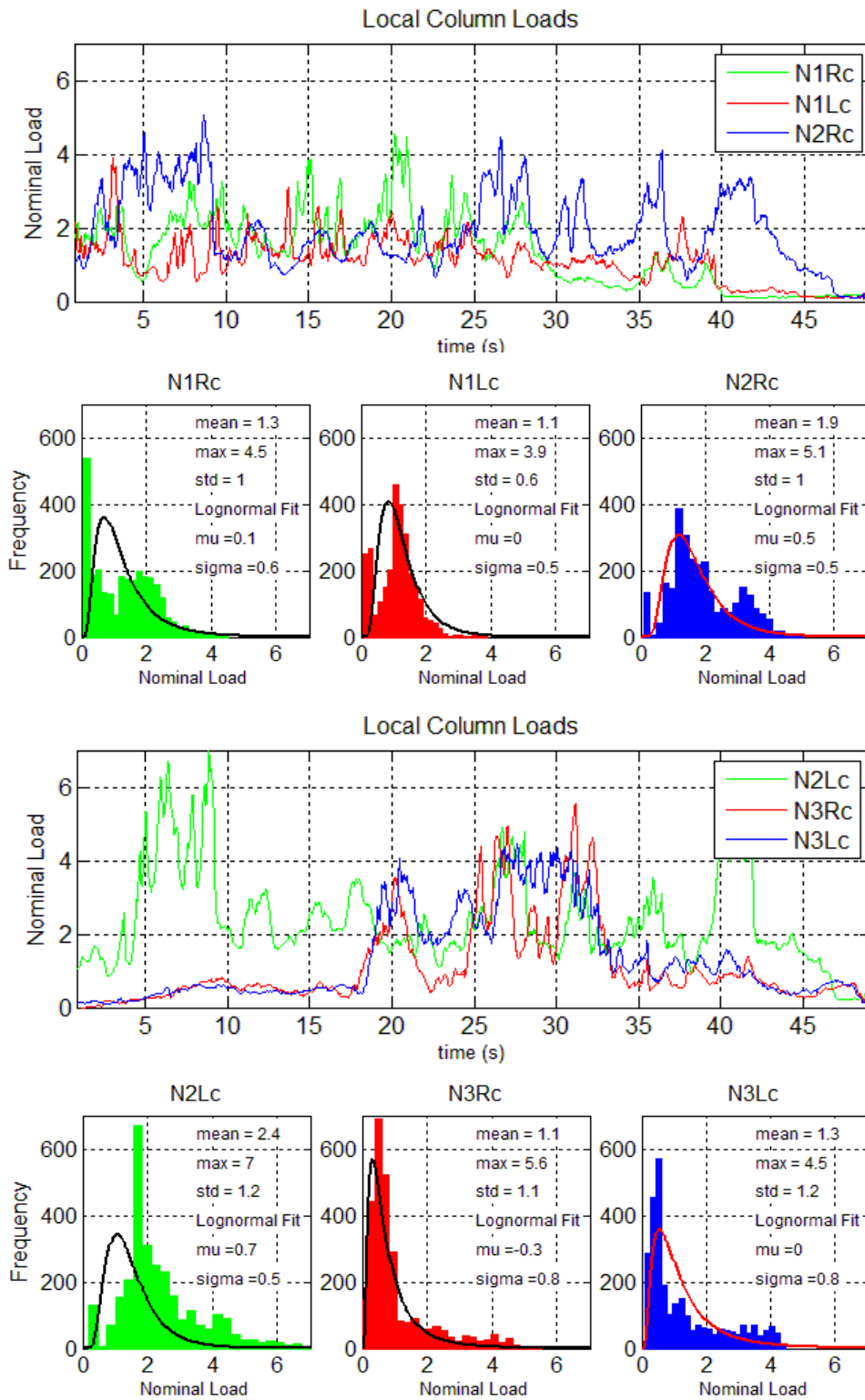
Figure 4-4　　　**Histograms of nominal loads of columns for the North face during event 58**

As can be seen, the ice force (or pressure) is not normally distributed. For large areas, a normal (or Gaussian) distribution follows as a result of the Central Limit Theorem (see Jordaan, 2005). If one adds together or averages many random quantities, one obtains a random quantity that approaches the normal distribution, regardless of the underlying distribution. In the case of ice loads acting on a structure, the global loads may be considered the sum of local loads across the structure width. The idea behind the Central Limit Theorem is illustrated in Figure 4-5. This notion is central in modeling global pressures as a random averaging process with a normal distribution defined by a mean and standard deviation.
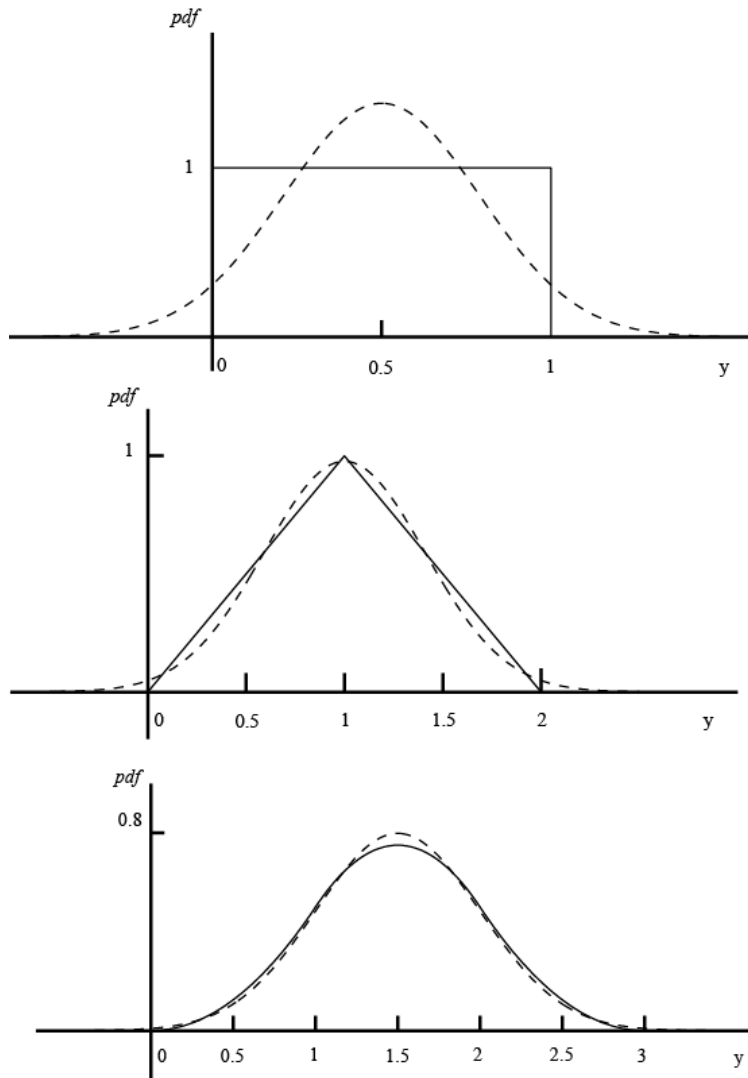
Figure 7.14 Addition of uniformly distributed random quantities (dotted line is normal distribution)

Figure 4-5   Addition of uniformly distributed random quantities; dotted line is normal distribution (Jordaan, 2005).

4.3 Autoregressive Method

Average ice failure pressures over wide structures can be estimated from measured load or pressure data over panels covering only part of the structure, using a "probabilistic averaging" method. A practical method needed to be developed to account for the fact that certain pairs of columns were adjacent while the pairs were also separated as noted in Figure 3-3.

The method that is proposed is based on a first-order autoregressive process (Vanmarcke, 1988). This is based on the Markov assumption. In a process in time, an event of a Markov process depends on the previous one and not those earlier in the process ("knowledge of the present makes the future independent of the past"). The correlation is directional because time moves forward only. The value at time t depends on the value at time $(t-1)$ plus an uncorrelated time series (usually white noise).

A process in space (such as ice pressure over a contact face) is distinct from a process in time since there is no preference of directionality. The following event correlates to both the preceding one and the following one (in a spatial sense). This can be expressed by the second-order difference equation:

$$X(t) = a[X(t-1) + X(t+1)] + U(t),$$
Equation 4-4

where $X(t)$ is the random series and the a is a constant and $U(t)$ is an uncorrelated random series. If the process has a correlation function $\rho(\tau)$ where τ is the lag distance, which is the distance between two points noting that space rather than time is the key variable, then the associated covariance function is (Vanmarcke, 1988):

$$B_X(\tau) = \sigma_X^2 \rho(\tau),$$

where σ_X^2 is the variance at a given location. This will be denoted simply as σ^2 in the following. The variance σ_T^2 over an interval of length T after averaging of a one-dimensional random process with variance σ^2 is

$$\sigma_T^2 = \gamma(T)\sigma^2,$$
Equation 4-5

where the variance function $\gamma(T)$ is obtained as (Vanmarke, 1983):

$$\gamma(T) = \frac{2}{T}\int_0^T (1 - \frac{\tau}{T})\rho(\tau)d\tau.$$
Equation 4-6

The square root of the variance function, $[\gamma(T)]^{1/2}$ is the "reduction factor" to be applied to the point standard deviation σ in order to obtain the variance for the structure as a whole. The quantities ρ and σ are to be obtained from the data (measured quantities).

Appropriate values of γ can be determined for both panel widths and structure widths; it is possible to estimate the variance in average pressure over the structure face given the variance in load over measurement panels. Since the panels were in separate groups, an alternative to Equation 1-4 has been used when considering the Medof panels, as described later on though the general principle still applies).

In their analysis of loads on the Molikpaq at Amauligak I-65, Jordaan et al. (2005) considered an exponential correlation function of the form

$$\rho(\tau) = \left[1 + \frac{|\tau|}{c}\right] e^{-|\tau|/c}$$

Equation 4-7

to represent the correlation between pressures at separation distances τ, where c is a characteristic spacing which can be calibrated based on measured loads at different separation spacings c. The pressures considered were average pressures over the contact height. Based on analysis of a number of load events, Jordaan et al. (2005) recommended values of c in the range 0.82 to 1.37, corresponding to correlations of 0.6 to 0.8 between Medof panels at a spacing of 1.135 m.
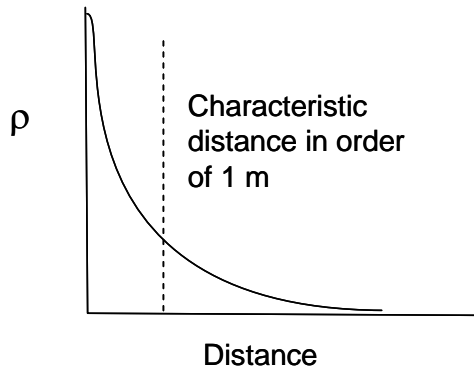
Figure 4-6: **Illustration of exponential correlation function**

Given the above exponential correlation function, the reduction function (Equation 4-6) for the process variance can be reduced to

$$\gamma(T) = 2\frac{c}{T}\left(2 + e^{-T/c} - 3\frac{c}{T}(1 - e^{-\frac{T}{c}})\right)$$

Equation 4-8

This equation is used in determining the variance in load over the structure face, given the variance at a fixed point.

4.4 Direct Method

In determining the variance of a column load from that of a group, a direct method was used in the Jordaan et al. (2005) study exploiting the fact that the panels on a given face were separated into three groups of pairs. Given the small characteristic lengths c, the loads on the three groups on a face are essentially independent, so the variance $\sigma_M{}^2$ on the three groups equal the variance $\sigma_G{}^2$ on a single group, divided by the number of groups ($N_G = 3$), i.e.

$$\sigma_M{}^2 = \frac{\sigma_G{}^2}{N_G}$$

Equation 4-9

The column loads are correlated since they are only 1.135 m apart. The variance $\sigma_G{}^2$ for a group of two adjacent columns is determined from the variance $\sigma_C{}^2$ of the column loads as follows. Defining the group load L_G as the average of the column loads L_{C1} and L_{C2}, Equation 4-3 may be used.

$$\sigma_G{}^2 = \sigma_C{}^2 \left[\frac{1}{2}(1+\rho) \right]$$

Equation 4-10

Then, using Equation 4-9,

$$\sigma_M{}^2 = \sigma_C{}^2 \left[\frac{1}{2}(1+\rho) \right] / N_G.$$

Equation 4-11

Using $\sigma_S^2 = \sigma_C^2 \cdot \gamma$ and Equation 4-11 above, one can estimate the variance $\sigma_S{}^2$ on the structure of width W_S from the variance $\sigma_M{}^2$ on the measured load as

$$\sigma_S{}^2 = \sigma_M{}^2 \cdot \frac{\gamma(W_S)}{\left[\frac{1}{2}(1+\rho) \right] / N_G}.$$

Equation 4-12

4.5 New Method for Project using Bi-functional Correlation Relationships

In the Jordaan et al. (2005) work, effort was concentrated on crushing type failures as it was assumed that these result in the highest loads. In order to make the method more general for the purposes of comparing loads estimates based on the different measurement devices (Medof panels, strain gauges and extensometers), and for different failure modes, it was extended as described in the following.

The exponential correlation function of Equation 4-7 does not provide the flexibility to model all the different failure events. To model more complex events, a bi-functional correlation function consisting of the weighted sum of two exponential correlation functions was found to provide better results.

$$\rho(\tau, q_1, c_1, c_2) = q_1 \cdot \left[1 + \frac{|\tau|}{c_1}\right] e^{\frac{-|\tau|}{c_1}} + (1 - q_1) \cdot \left[1 + \frac{|\tau|}{c_2}\right] e^{\frac{-|\tau|}{c_2}}$$

Equation 4-13

The corresponding reduction function for the process variance is

$$\gamma(T) = q_1 \cdot \left[2\frac{c_1}{T}\left(2 + e^{-\frac{T}{c_1}} - 3\frac{c_1}{T}(1 - e^{-\frac{T}{c_1}})\right)\right] + (1 - q_1) \cdot \left[2\frac{c_2}{T}\left(2 + e^{-\frac{T}{c_2}} - 3\frac{c_2}{T}(1 - e^{-\frac{T}{c_2}})\right)\right]$$

Equation 4-14

In determining line loads from the measured loads, the work of section 4.3 was extended for the case where the loads on the different panel groups are not independent. The variance σ_M^2 for the three groups of panels on a face can be determined from the variance σ_G^2 of the group loads as follows. Defining the measured load L_M as the average of the group loads L_{G1}, L_{G2}, and L_{G3},

$L_M = (L_{G1} + L_{G2} + L_{G3})/3$,
Equation 4-15

The variance σ_M^2 is determined in a manner similar to Equation 4-1 and the following above; as a result

$$\sigma_M^2 = \left[\sigma_{G1}^2 + \sigma_{G2}^2 + \sigma_{G3}^2 + 2\sigma_{G1,G2} + 2\sigma_{G1,G3} + 2\sigma_{G2,G3}\right]/9$$

or

$$\sigma_M^2 = \sigma_G^2\left[\frac{1}{3}\left(1 + \frac{2}{3}\rho_{1,2} + \frac{2}{3}\rho_{1,3} + \frac{2}{3}\rho_{2,3}\right)\right]$$

Equation 4-16

This can be approximated as,
$$\sigma_M^2 \approx \sigma_G^2\left[\frac{1}{3}\left(1 + \frac{4}{3}\rho(18.5) + \frac{2}{3}\rho(37)\right)\right],$$

Equation 4-17

where the distance between groups is approximately 18.5m. Using $\sigma_S^2 = \sigma_C^2 \cdot \gamma$, Equation 4-10 and Equation 4-17, one can estimate the variance $\sigma_S{}^2$ on the structure from the variance $\sigma_M{}^2$ on the measured load as

$$\sigma_S{}^2 = \sigma_M{}^2 \cdot \frac{\gamma(W_S)}{\left[\frac{1}{2}\left(1 + \rho(1.135)\right)\right] \cdot \left[\frac{1}{3}\left(1 + \frac{4}{3}\rho(18.5) + \frac{2}{3}\rho(37)\right)\right]}$$

Equation 4-18

4.6 Determination of Model Parameters and Calibration

To evaluate and compare the different load related measures for the Molikpaq ice interaction events (Medof loads, extensometer readings, and strain gauge readings), analyses were conducted for the events and sub-events agreed upon at the May 2008 meeting and summarized in Table 4-2 and Table 4-3 (BDW classification). Only sub-events involving predominantly creep and crushing failure modes were considered.

In this preliminary work, the Medof panel results were used to determine correlations. Since the calibration coefficients are not known, and the values of loads consequently uncertain, the values are designated as "Nominal".

Table 4-2: Events considered for calibrations

Event	Faces Loaded		Event Duration	Ice Thickness		Sail Heights	Est. Contact Area	Load Obs. on Lower Panel
	Medof	No Medof		Min.	Max.	mean/max		
			min.	m	m	m	m2	Y/N
Mar-25-N-1	N, NE, E	NW	130	2.5	3.0		18.7	N
Apr-12-E-1	E	SE, S	73	4.0	6.0		22.8	Y
Apr-12-E-2	E	SE, S	61	4.0	6.0		22.8	Y
Apr-12-E-3	E	SE, S	16	4.0	6.0		22.8	Y
May-12-N-1	N, NE, E		48	1.7	2.0	1.5,2.5	17.0	Y
May-22-N-1	N, NE, E		71	2.0	3.0		17.0	Y
May-22-N-2	N, NE, E		73	3.0	4.0	1,2	17.0	Y
Jun-02-E-1	E		74	1.8	2.5		14.6	Y
Jun-02-E-2	E		68	1.8	2.5		14.6	Y

Event	Fast File	CHC Calibration Number	BW Event Number	Ice Type	Max nominal load	Modes (*Definitions found in Section 1)
Mar-25-N-1	f603251302	2	N/A	SY/MY ?	11.90	SLW
Apr-12-E-1	f604121101	9	14	MY	19.46	CC,CR,MM,SLW
Apr-12-E-2	f604121201	11	15A	MY	43.23	CR,M,SLD
Apr-12-E-3	f60412140A	10	15B	MY	10.63	CR,MM
May-12-N-1	f605120301	8	16	FY (MY inclusions)	47.57	CR, MM, SLW
May-22-N-1	f605220801	3	17	MY	16.19	SLW, MM
May-22-N-2	f605221301	5	18	MY	24.68	CR, SLD, SLW
Jun-02-E-1	f606021301	6	19	FY (MY inclusions)	14.89	CR, MM, SLW, SLD
Jun-02-E-2	f606022001	7	20	FY (MY inclusions)	10.06	SLW, CR, MM

Table 4-3: **Sub-events Events Considered for Calibrations**

Event	Subevent	Failure Mode	Subevent Duration	Load Obs. on Lower Panel	Max Nominal Load	Avg Nominal Load	No. Groups Loaded	Max. Extens- ometer Reading	Max. Summed Strain
			min.	(Y/N)				mm	uStrain
Mar-25-N-1	1	Creep	130.14	N	11.9	5.5	3	-0.8	370
Apr-12-E-1	3	Crushing	4.39	N	13.3	8.5	1	-2.0	403
Apr-12-E-2	1	Crushing	1.42	Y	10.6	8.2	1	-0.2	110
	2	Crushing	1.64	Y	12.8	11.0	2	-2.2	206
	3	Crushing	5.57	Y	22.9	15.8	3	-5.6	514
	4	Crushing	1.93	Y	17.3	12.4	2	0.3	427
	5	Crushing	4.21	Y	13.7	9.3	1	0.7	338
	6	Crushing	4.45	Y	43.2	20.0	2	-6.0	589
	8	Crushing	7.73	Y	27.7	17.9	2	-7.6	631
Apr-12-E-3	1	Crushing	1.5	Y	9.9	7.5	2	-6.1	393
May-12-N-1	2	Crushing	2.98	Y	30.1	23.0	3	-7.0	687
	4	Crushing	5.15	Y	47.6	32.7	3	-21.7	1232
	5	Creep	30.83	Y	43.3	15.3	3	-13.5	753
May-22-N-1	1	Creep	37.55	Y	16.2	13.4	3	-7.7	588
May-22-N-2	1	Crushing	2.95	Y	3.6	1.5	1	-1.2	94
	2	Crushing	5.63	Y	17.7	8.9	3	-2.7	505
	4	Crushing	2.05	Y	2.8	1.0	3	1.6	68
	5	Crushing	5.05	Y	11.7	5.8	3	1.4	390
	6	Creep	9.55	Y	24.7	19.7	3	-6.6	544
Jun-02-E-1	1	Creep	9.07	Y	6.4	5.2	1	-2.2	406
	2	Crushing	20.57	Y	14.9	7.1	2	-4.0	415
	4	Crushing	10.73	Y	11.4	9.0	3	-6.5	406
	5	Crushing	3.25	Y	7.6	6.8	2	-6.6	400
	7	Crushing	12.18	Y	14.6	8.3	2	-3.4	406
	8	Crushing	6.47	Y	9.9	5.5	1	-6.2	350
Jun-02-E-2	1	Creep	23.4	Y	6.4	5.4	3	-5.2	351
	2	Crushing	3.55	Y	10.1	5.9	3	-2.1	350

* Loads shown are measured loads on six MEDOF panel columns, calculated using the uniform method for missing lower panels.

The analysis steps carried out are summarized below and explained in more detail in the relevant subsections which follow.

Analysis Steps:

➢ Development of Correlation Functions
- Correlations between column loads were determined based on the sum of the middle and top panel loads (i.e. loads associated with the lower panel on the middle right column were not included into order to maintain consistency).
- Bi-functional correlation functions were developed separately for creep and crushing type sub-events. First the average (over all sub-events) correlations at specified panel separations were determined, and then bi-functional correlation functions were chosen which fit the data.

➢ Estimation of North and East Face Nominal Loads based on MEDOF Panels
- Estimates of face loads were made for each sub-event, based on both linear and probabilistic averaging. Two models for treating thick ice cases were considered, as there is some uncertainty regarding loads below the middle row of panels (as there is only one lower panel).

➢ Calibration of Medof Panels
- Because there is considerable uncertainty regarding MEDOF panel loads, as an alternative approach, MEDOF panel adjustment factors were determined based on

the assumption that extensometer readings in conjunction with a structure stiffness of 3 MNmm^{-1} based on FEA results give correct loads.

4.7   Development of Correlation Functions

4.7.1   Comments on Load Distributions

The method implemented for probabilistic averaging is based on the assumption that certain statistical properties for the process being modeled, such as values of the mean, standard deviation and correlations are constant for the event under consideration. This is a reasonable assumption for events of reasonable duration. One aspect is whether the load is uniform across the contact face in the case of creep loads, as past experience has shown that loads might tend to be larger towards the outer edges of the contact face. These variations would not affect correlations but could affect the interpretation of results and resulting face load calculations.

To determine if there are variations in the load across the face, the mean load for each group has been determined for each MEDOF panel group. The results are summarized in Table 4-4. In 4 of 6 creep events, representing 201 of 241 minutes, the load on the middle group was smaller than the load on the outside groups. The most significant difference was for the 130 minute March 25, 1986 event.

Table 4-4: Variation in Nominal Panel Load with Location on Face

Event	Subevent	Failure Mode	Average Load		
			N1/E1	N2/E2	N3/E3
			(Nominal)	(Nominal)	(Nominal)
Mar-25-N-1	1	Creep	2.47	0.83	2.18
Apr-12-E-1	3	Crushing	0.00	6.16	2.32
Apr-12-E-2	1	Crushing	2.29	1.82	4.10
	2	Crushing	2.29	3.79	4.96
	3	Crushing	5.14	6.13	4.52
	4	Crushing	3.43	4.82	4.17
	5	Crushing	2.07	2.81	4.43
	6	Crushing	5.06	7.62	7.28
	8	Crushing	6.13	6.21	5.61
Apr-12-E-3	1	Crushing	3.84	2.33	1.31
May-12-N-1	2	Crushing	8.20	7.46	7.37
	4	Crushing	10.19	10.91	11.65
	5	Creep	4.91	4.97	5.41
May-22-N-1	1	Creep	4.22	3.17	5.98
May-22-N-2	1	Crushing	0.13	0.07	1.33
	2	Crushing	0.39	3.59	4.92
	4	Crushing	0.05	0.12	0.86
	5	Crushing	0.29	2.38	3.12
	6	Creep	4.19	8.25	7.26
Jun-02-E-1	1	Creep	0.03	0.24	4.89
	2	Crushing	0.26	3.40	3.42
	4	Crushing	3.24	2.72	3.06
	5	Crushing	3.62	1.98	1.17
	7	Crushing	0.91	4.30	3.12
	8	Crushing	0.37	0.97	4.16
Jun-02-E-2	1	Creep	2.25	1.44	1.70
	2	Crushing	0.47	3.01	2.40
Average		Creep	3.01	3.15	4.57
		Crushing	2.78	3.93	4.06

4.7.2 Correlation between Columns based on Middle and Top Panel Loads

For each of the selected sub-events, the correlation coefficient was calculated for each pair of columns. Example plots of correlation coefficient versus separation are shown in Figure 4-7a for a crushing type interaction and Figure 4-7b for a creep type interaction (the blue points indicate data). As a rule, for crushing type interactions the correlations fall off quite rapidly with separation distance, while for creep type interactions the correlations remain relatively high even at a 40 m spacing. It is of note that the correlations coefficients can be negative as the events are of limited duration.

It was considered that the methodology should be improved to provide better fits to the data. Accordingly, a method that is based on bi-functional functions for correlations has been applied.

(a)
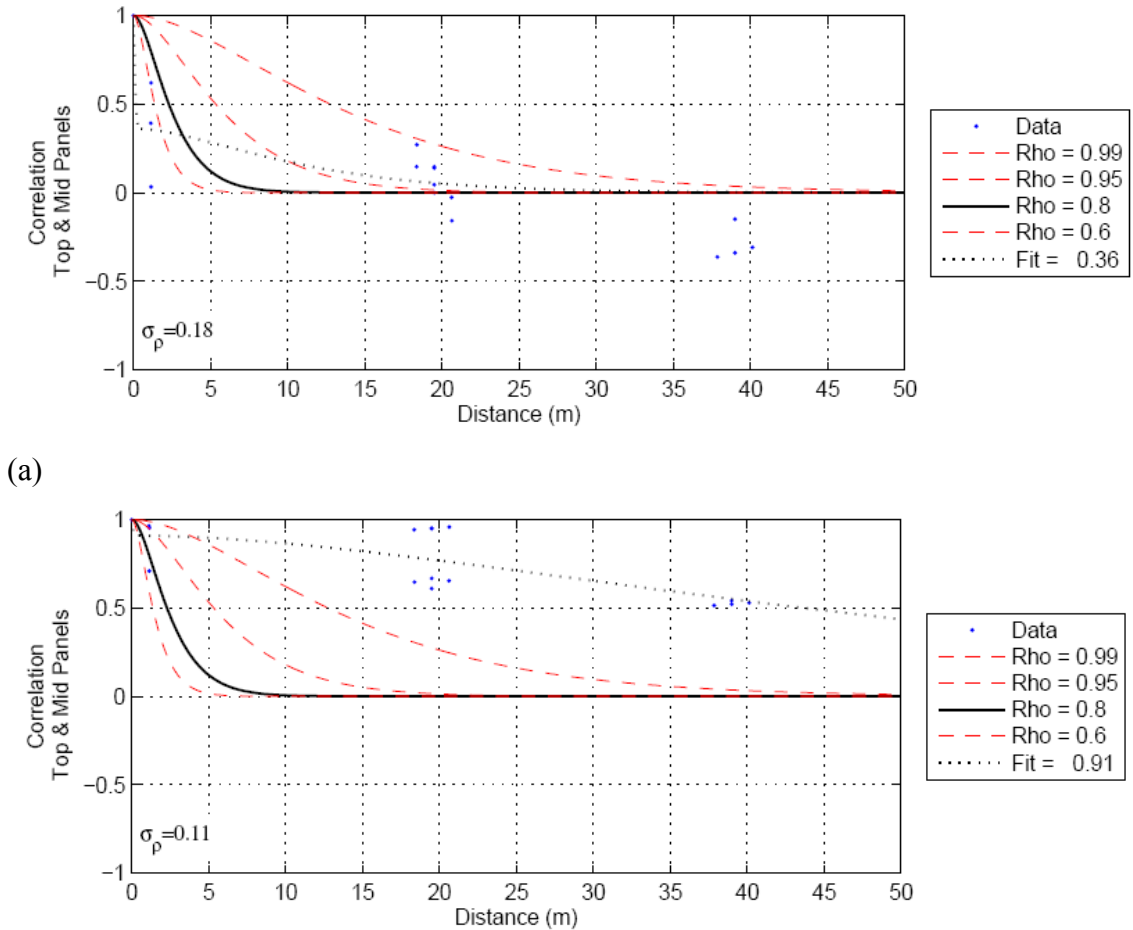
Figure 4-7: **Examples of correlation coefficients as a function of separation for a) crushing and b) creep**

4.7.3 Development of Bi-functional Correlation Functions for Creep and Crushing

The correlations at specified panel separations for duration-averaged crushing and creep events are shown in Figure 4-8 (a) and Figure 4-8 (b). The bi-functional correlation model described in Section 2 was then manually adjusted to give reasonable fits to the data (by adjusting the coefficients q_1, c_1 and c_2). The resulting fits are included in Figure 4-8 (a) and Figure 4-8 (b) and the associated coefficients are shown in

Table 4-5.

It is seen that much improved fit has been obtained.
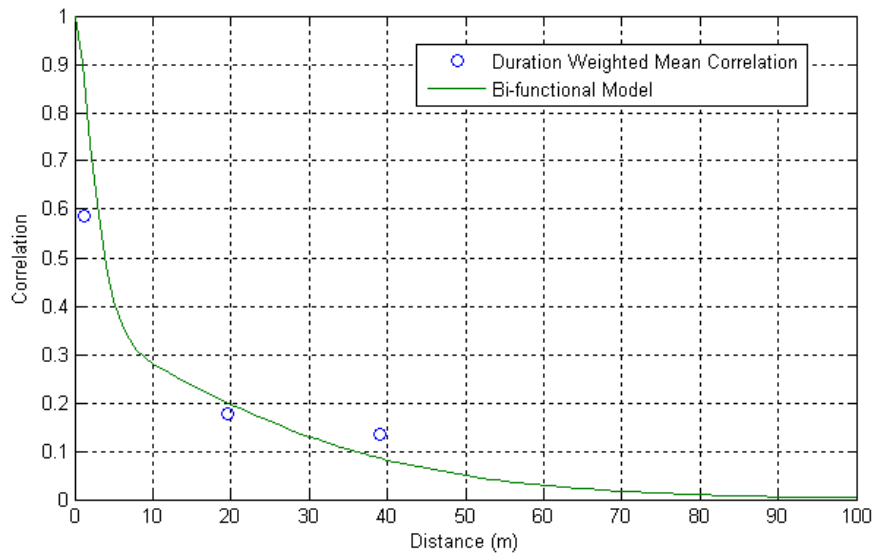
(a)
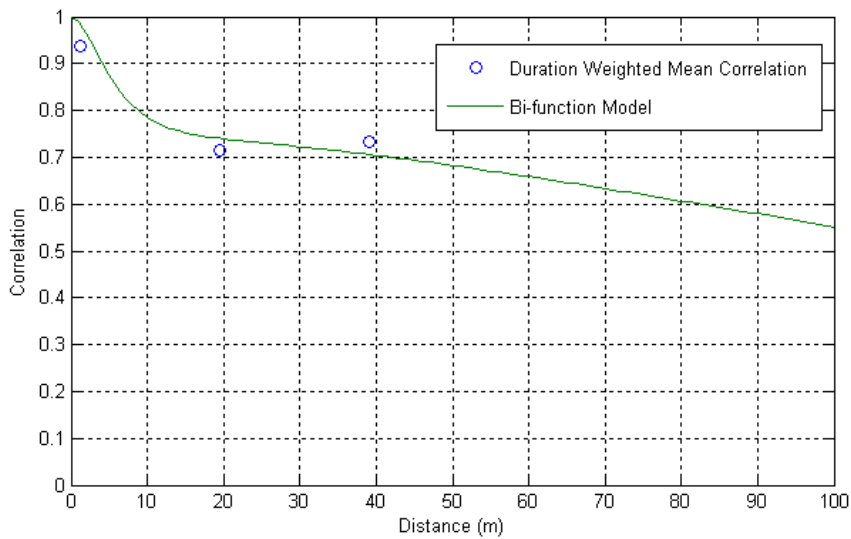
(b)

Figure 4-8:   Bi-functional correlation models chosen for a) crushing type events and b) creep type events

Table 4-5:   Coefficients for bi-functional correlation models

Failure Mode	q_1	c_1	c_2
		m	m
Crushing	0.68	1.5	15
Creep	0.25	3	100

4.8 Linear vs Probabilistic Estimation of North and East Face Loads based on Nominal Medof Loads

4.8.1 Treatment of Bottom Panel Loads for Thick Ice

Except for the right column in the middle panel groups, the MEDOF panels reached depths of 2.915 m. The right column in the middle panel group on the north and east faces covered ice interactions to a depth of 5.63 m. In considering the relationship between actual loads and the loads measured on the MEDOF panels, consideration should be given to the possibility of ice thicker than the 2.915 and 5.63 m limits. Also there could be significant loading below these limits due to either rubble or intact ice pushed below the rubble.

Where loads were observed on the bottom panel of the middle right column on the east or north faces (Figure 4-9), the loads time traces columns without bottom panels were increased to include estimated bottom panel loads. The possibility of loads below the bottom panels was not considered and is unlikely given the quoted ice thickness values.
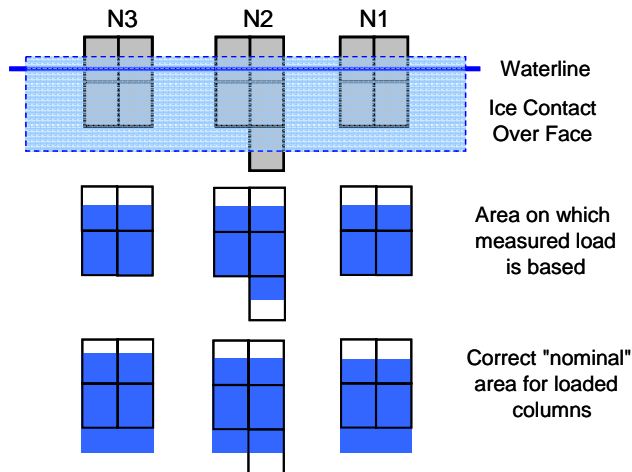
Figure 4-9:   "Nominal" Contact Area for Columns given Uniform Thick Ice

Two assumptions have been implemented regarding loads on the bottom panels:

i)   For each column, assume the bottom panel has the same load as the bottom panel for the right column in the center group of the face, irrespective of the top and middle panel loads ("Uniform" Method for Bottom Panel Loads)

4-19

ii) For each column, assume the same ratio of total column load to the load on the top and middle panels as for the right column in the center group of the face ("Ratio" Method for Bottom Panel Loads).

Neither of these methods is satisfactory, particularly for ice crushing. The ice failure process in a crushing failure consists of high-pressure zones generally concentrated near the centre of the ice sheet, with occasional excursions towards the edges. Both methods fail to recognize this. Figure 4-10 illustrates the potential problems regarding bottom panel loads. The left and right columns of group N1 show significant middle panel loads at 40 minutes, whereas the middle group columns show moderate to small middle panel loads. At the same time, the lower panel of the middle right column shows a significant bottom panel load. Using the Ratio method can result in very large assumed loads on the N1 columns at 40 minutes.
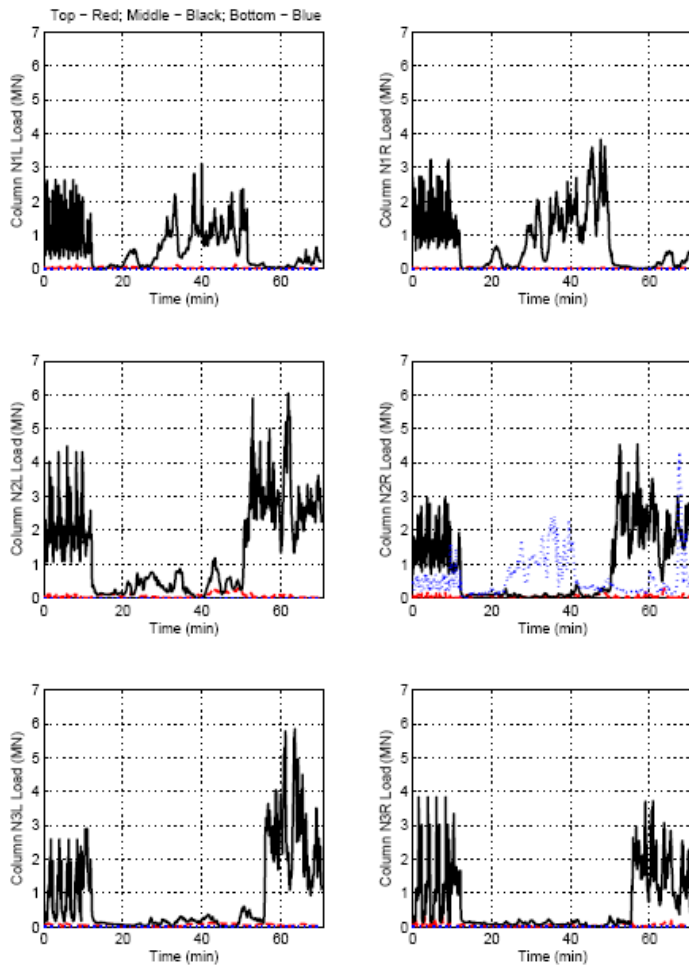
Figure 4-10:   **Illustration of effect of bottom areas with no panels**

4.8.2 Linear vs Probabilistic Averaging

Two methods were used for estimated time traces of face loads for the selected sub-events.

With "Linear Averaging", the load $L_C(t)$ over the contact width W_C is determined as

$$L_C = L_1 \cdot \frac{W_C}{W_1}$$
4-19

where $L_1(t)$ is the average column load at each point of time t, W_C is the contact width (generally 59 m), and W_1 is the column width (1.135 m).

With "Probabilistic Averaging" the load $L_C(t)$ over the contact width W_C is determined as

$$L_C(t) = \frac{W_C}{W_1} \cdot \left[u + \Delta(t) \cdot \sqrt{\frac{\gamma(W_S)}{\left[\frac{1}{2}\left(1 + \rho(1.135)\right)\right] \cdot \left[\frac{1}{3}\left(1 + \frac{4}{3}\rho(18.5) + \frac{2}{3}\rho(37)\right)\right]}} \right]$$

Equation 4-20

where u is the average (over time) of the mean column load and $\Delta(t)$ is the deviation $L(t) - u$ of the mean column load $L(t)$ from the mean u at each point of time,

4.8.3 Results for Linear and Pressure Averaging

The above methods were applied for the selected sub-events. The maximum face loads for each event are summarized in Table 4-6. The largest load (375 MN) using the uniform bottom method occurs for the April 12th East face crushing event. Results are expressed in nominal Medof loads. Table 4-7 gives some earlier calibration results for the extensometers based on Medof panel nominal loads. This has been added to illustrate the extreme variety of results that are found if very short-duration events are used to calibrate.

Table 4-6   Linear and pressure averaging loads

Event	Failure Mode	Maximum Nominal Load		Maximum Nominal Load	
		LA	LA	PA	PA
		No Bottom	Uniform	No Bottom	Uniform
Mar-25-N-1	Creep	103	103	102	102
Apr-12-E-1	Crushing	169	169	139	139
Apr-12-E-2	Crushing	188	375	158	320
Apr-12-E-3	Crushing	84	92	73	82
May-12-N-1	Crushing	168	344	141	296
May-22-N-1	Creep	108	140	107	139
May-22-N-2	Crushing	123	214	103	180
Jun-02-E-1	Crushing	128	129	114	116
Jun-02-E-2	Creep	86	87	85	86

Table 4-7:   **Extensometer calibration results based on nominal Medof loads.**

SUB EVENTS

Event	Subevent	Failure Mode	LA (Excluding Bottom Panel)	PA (Excluding Bottom Panel)
Mar-25-N-1	1	Creep	-5.52	-5.40
Apr-12-E-1	3	Crushing	-6.65	-5.37
Apr-12-E-2	1	Crushing	-7.82	-6.31
	2	Crushing	-4.25	-3.43
	3	Crushing	-8.26	-6.67
	4	Crushing	-4.42	-3.57
	5	Crushing	-3.23	-2.61
	6	Crushing	-3.64	-2.94
	8	Crushing	-4.68	-3.78
Apr-12-E-3	1	Crushing	4.19	3.39
May-12-N-1	2	Crushing	-6.55	-5.29
	4	Crushing	-0.96	-0.78
	5	Creep	-3.21	-3.14
May-22-N-1	1	Creep	-7.43	-7.26
May-22-N-2	1	Crushing	-13.89	-11.22
	2	Crushing	-8.16	-6.59
	4	Crushing	3.81	3.07
	5	Crushing	-2.62	-2.12
	6	Creep	-2.40	-2.34
Jun-02-E-1	1	Creep	-3.70	-3.62
	2	Crushing	-11.71	-9.46
	4	Crushing	-34.98	-28.26
	5	Crushing	10.84	8.76
	7	Crushing	-11.21	-9.06
	8	Crushing	-17.01	-13.74
Jun-02-E-2	1	Creep	-2.88	-2.82
	2	Crushing	-9.59	-9.38

FULL EVENTS

Event	Failure Mode	PA (Excluding Bottom Panel)	PA (Including Bottom Panel) Method 1	PA (Including Bottom Panel) Method 2
Mar-25-N-1	Creep	-5.40	-5.40	-5.40
Apr-12-E-1	Crushing	-6.41	-6.41	-6.41
Apr-12-E-2	Crushing	-3.27	-5.58	-6.76
Apr-12-E-3	Crushing	-6.22	-3.81	-8.88
May-12-N-1	Crushing	-2.60	-8.55	-10.41
May-22-N-1	Creep	-4.27	-5.48	-6.70
May-22-N-2	Crushing	-3.20	-8.40	-5.86
Jun-02-E-1	Crushing	-6.36	-5.83	-6.80
Jun-02-E-2	Creep	-5.28	-5.64	-6.35

4.9   Other Failure Modes and Factors

While the above method is reasonable for interactions which are predominantly crushing, other interaction and failure modes occur which involve correlations over different distance and time scales. At the same time, it should be noted that creep and crushing failures result in the greatest loads. A brief comparison is given below of the characteristics of the different modes:

Crushing:
Crushing events are characterized by random load traces on different panels that generally are uncorrelated as shown in Figure 4-11.
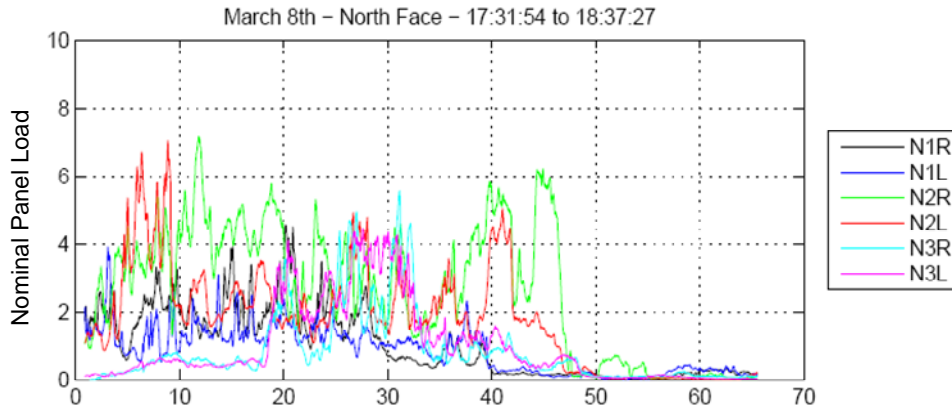
Figure 4-11: Example Crushing Event

Creep failure

Creep failure occurs at low velocities and shows highly correlated variations in pressure at different locations as can be seen in Figure 4-12. The characteristic distance in such cases can be as large as the structure width.
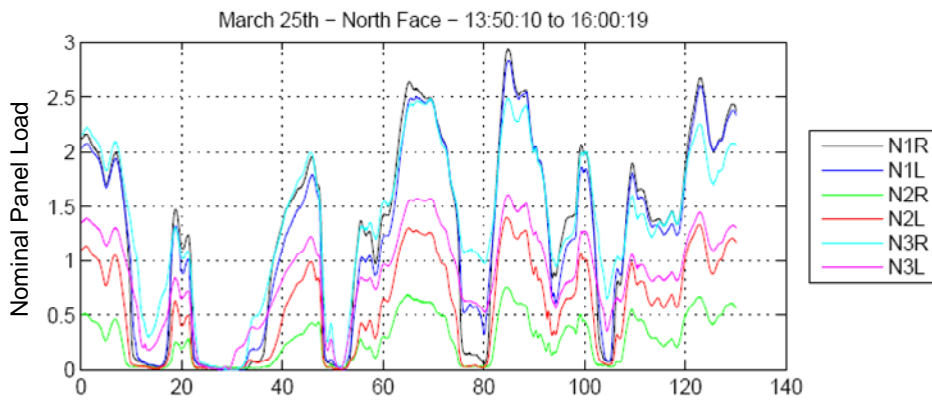
Figure 4-12: Example Creep Event

Flexural failure

Repeating flexural failures can result from buckling of the advancing ice or failure due to buildup and submersion of rubble and can occur across the width of the structure or locally (Figure 4-13).
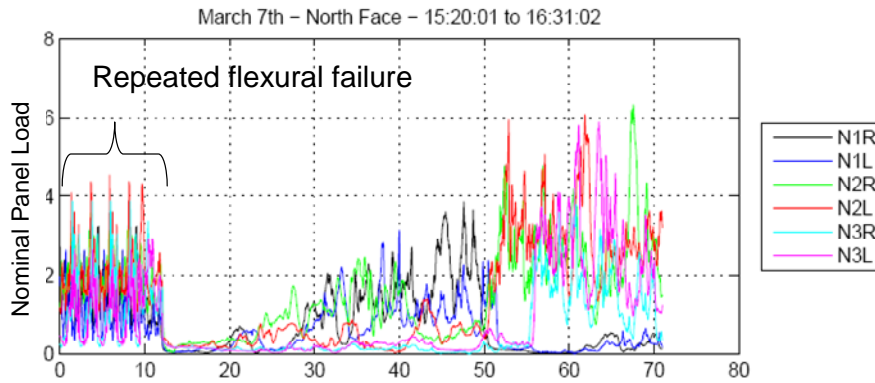
Figure 4-13:   Example Flexure Event

Variation in thickness

Variations in the thickness of ice encountered can occur as a result of interaction with a multi-year ridge or embedded features (eg. second year or multi-year inclusions) as illustrated in Figure 4-14. These could appear as correlated variations in pressure across the structure face or part of the face if the thickness variation is not taken into account or if the strength of the new feature is different.
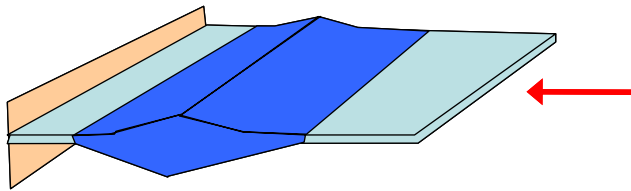
Figure 4-14:   Variation in Contact Thickness

Variation in contact width

As a feature impacts the contact width will increase, enveloping additional panels (Figure 4-15). This can appear as negative or positive correlation in the load on different panels.
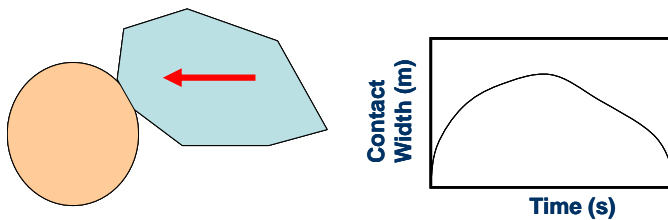
Figure 4-15:   Variation in Contact Width

Splitting and spalling

Splitting and spalling events can cause a sudden change in actual contact area. Actual pressures could rise on the remaining ice, but nominal pressures might drop. These events may not be visually apparent to an observer, and could appear on panels, as positively or negatively correlated pressure changes on panels over durations considerably longer than those associated with the development of high pressure zones during crushing.

Additional factors

Examination of actual load time traces shows that the measured data can vary in a complicated manner when all of the above factors play a part. Different failure modes can occur at different locations at the same time, and areas of higher pressure can be seen to move across the contact face if the feature is moving at an angle to the face. At the same time, an ice-structure interaction event can be idealized as a random averaging process, and the assumption made that the process is stationary.

As noted, the data has many fluctuations, due to fractures, splits, and variations in ice thickness and other dimensions. If all of these aspects were measured, for instance if local variations in ice thickness were measured, one could develop a model to account for these effects. In the context of the present observations, the causes of the load fluctuations are considered as background random events within a stationary process, contributing to the variance. The process is therefore treated as stationary for a given time interval. This is considered to be a reasonable engineering approach. At the same time, caution should be exercised in using events that are of very short duration to estimate the statistical parameters of the process.

5   DETAILED ANALYSIS OF MOLIKPAQ EVENTS

5.1   Introduction

As noted in Section 1.7, when reviewing individual events, it is important to take into account the type of loading that is imposed on the structure. In interpreting the loads, for comparison to the Medof panel and strain gauge loads, the calibration factors should be chosen to give face loads. If total global loads on the structure are sought, then the factor to give this value must be chosen carefully. In either case, the factors must be chosen to correspond as closely as possible to the actual field loading conditions.

In Phase 1 of the project, events were analyzed according to the BDW classification (see section 1.5). The results are given in Appendix IJA - B as they are potentially useful; loads from the original Medof calibration are termed "nominal loads". During the project meeting in June of 2008 following the completion of Phase 1, it was decided to analyze each ice structure interaction event individually, based on an order of priority which was determined at that time. The work presented in the following is a detailed analysis of the five ice-structure interaction events listed below:

> Event 0325A – March 25th, 1986 – Starting at 08:30
> Event 0325B – March 25th, 1986 – Starting at 13:50
> Event 0512A – May 12th, 1986 – Starting at 03:10
> Event 0307A – March 7th, 1986 – Starting at 15:20
> Event 0307B – March 7th, 1986 – Starting at 16:38

An analysis of a decelerating floe which impacted the Molikpaq structure on May 12, 1986 has been conducted. This approach serves as an independent check of the global ice loads and the stiffness of the Molikpaq structure, which can be compared with the finite element analysis conducted by Sandwell (1991).

In Section 3.3.5 significant uncertainties were raised regarding the accuracy of the Medof panels which had previously been used to determine the ice loads acting on the Molikpaq. In this chapter the approach was to consider the extensometers to be the primary estimate of the magnitude of the ice loads acting on the structure. Section 2.4 provided a review of the extensometers and the finite element work done by Sandwell to determine a best estimate of the stiffness of the structure. The analysis that follows has been carried out using Ring Distortion Ratios for face loads of 2.2, 2.6 and 3.0 $MNmm^{-1}$. The value of 2.6 $MNmm^{-1}$ is our best estimate of the Ring Distortion Ratio. These values are also in the range of that determined independently using the decelerating floe analysis. Strictly speaking, there are small differences in the Ring Distortion Ratio for face loads depending on whether the loading is on the centre face or the entire face. This is not included here but could be, with more detailed finite element analysis.

The extensometers have been used to estimate a factor for which the Medof panel load estimates should be multiplied by to account for their likely overestimation of the applied ice load. The strain gauges have then been calibrated to the newly factored Medof panel

ice loads. Loads determined by the original Medof panel calibration are termed "nominal loads" without units. The values are very useful in determining which faces and sides were loaded; also with regard to the bottom panel loading.

Because of its importance, the "Decelerating Floe" analysis is given first.

5.2   Decelerating Floe: Event 0512A - May 12, 1986 – f605120301

Event ID – 16
Crushing
Ice Thickness: 2.5m
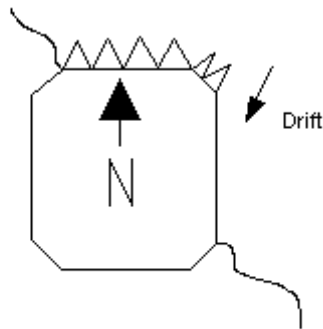
5.2.1 Dynamac Event Description

A large floe (4 nm x 8 nm) of thick first year ice (with large multi-year inclusions) impacted the Molikpaq. Initial contact was made on the east corner of the north face and the north east face. As its speed reduced, vibrations increased. The frequency decreased and the amplitude increased as the drift speed dropped. The initial floe velocity was reported to be 0.18 m/s and the floe was observed to stop after 27 minutes (Timco et al., 2005).

Figure 5-2 shows the magnitude of loading occurring on the North, North East and East faces during the event as measured by the Medof panels. Each colour represents a nominal Medof column load. At approximately 16 minutes into the ice loading event, the sight tubes of Medof panel 1010 began to overflow with fluid[1], resulting in a loss of data. For this reason, the Medof panel data have been trimmed at 16 minutes. Extensometer data are available for the full ice loading event. Inspection of the figure shows that the loads on the NE and E faces are relatively small as a first approximation (taking into account the fact that the global load is a vector sum) and there appears to have been a wedge crack occurring near the west face based on the rubble map shown in Figure 5-1.

---

[1] Possibly related to panel softening
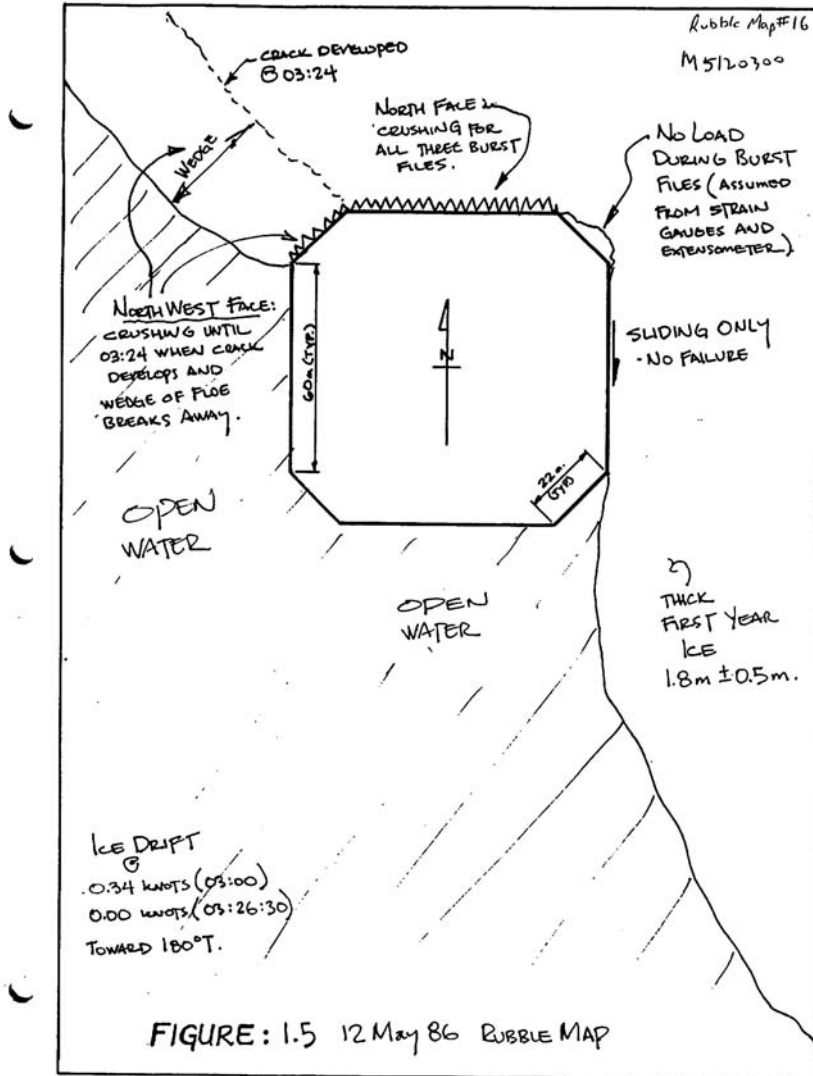
Figure 5-1   Rubble map showing floe impact occurring on May 12, 1986
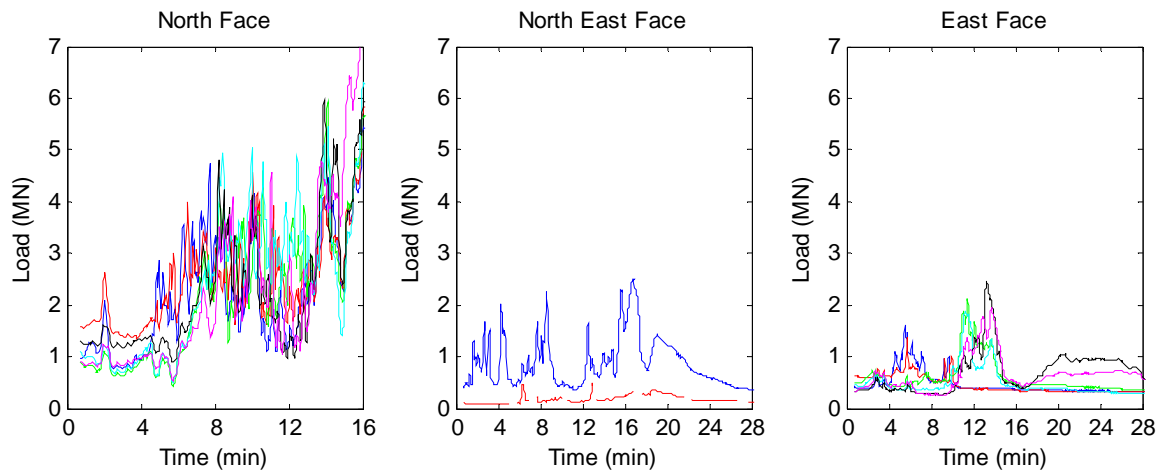
Figure 5-2   Loadings on North, North East and East Medof panels.
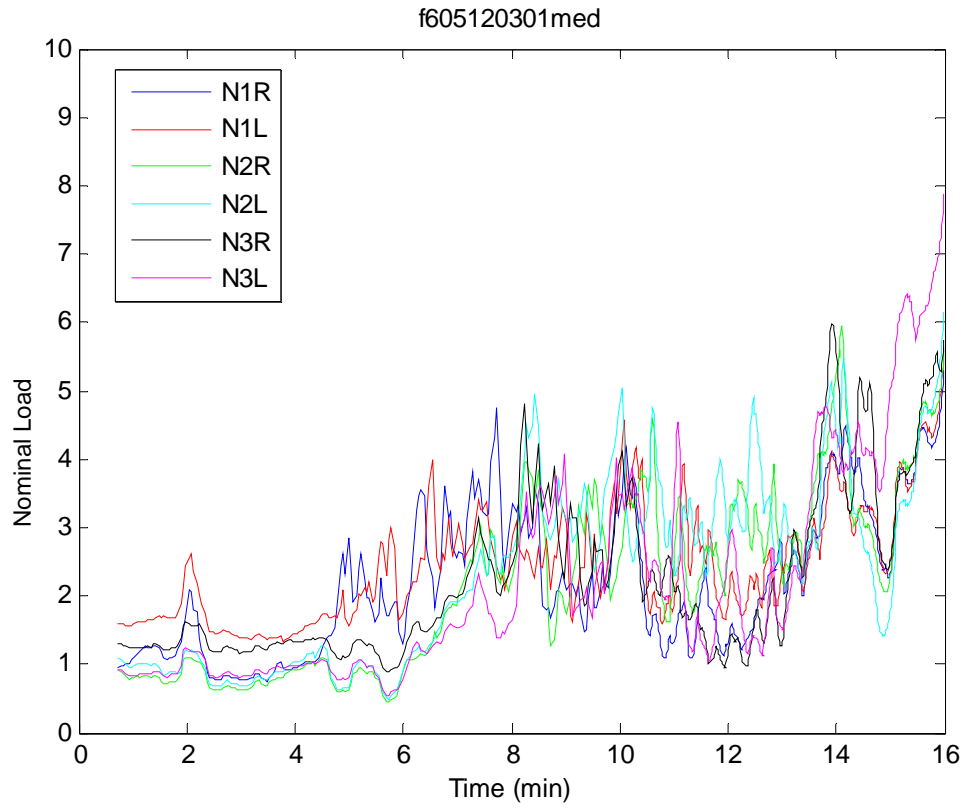
Figure 5-3   **Nominal Medof column loads acting on the North face.**
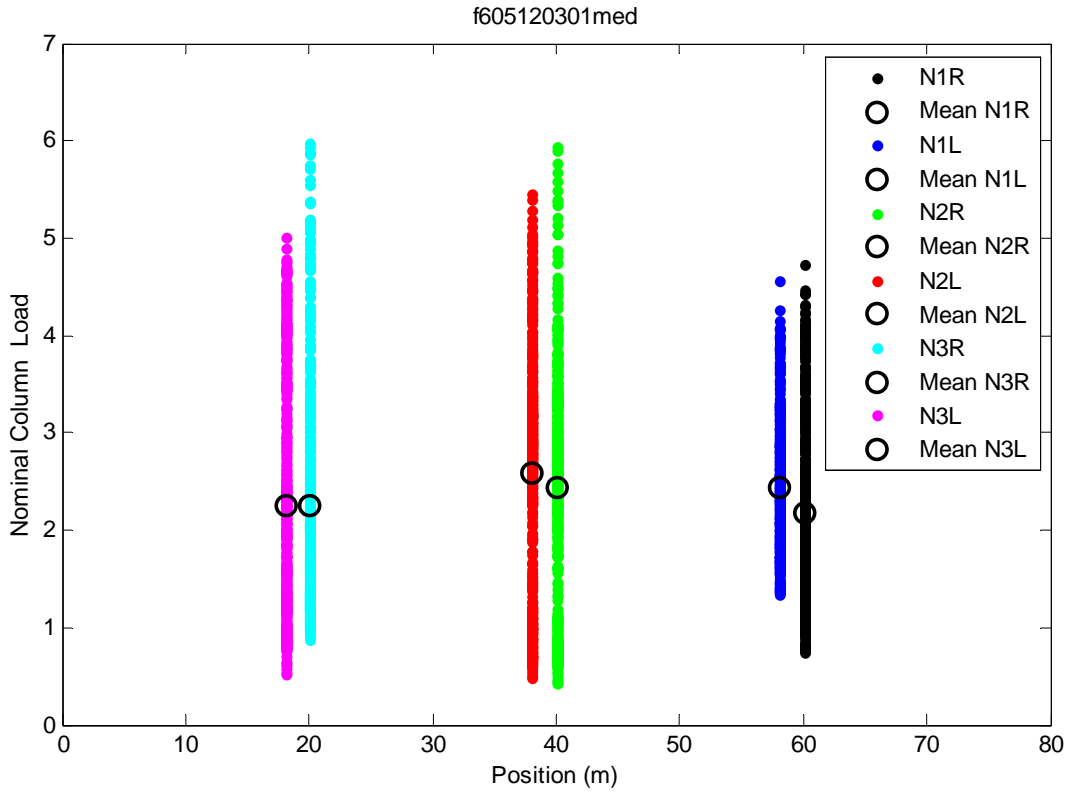
Figure 5-4: Distribution of Nominal Medof ice loading on the North face of the structure
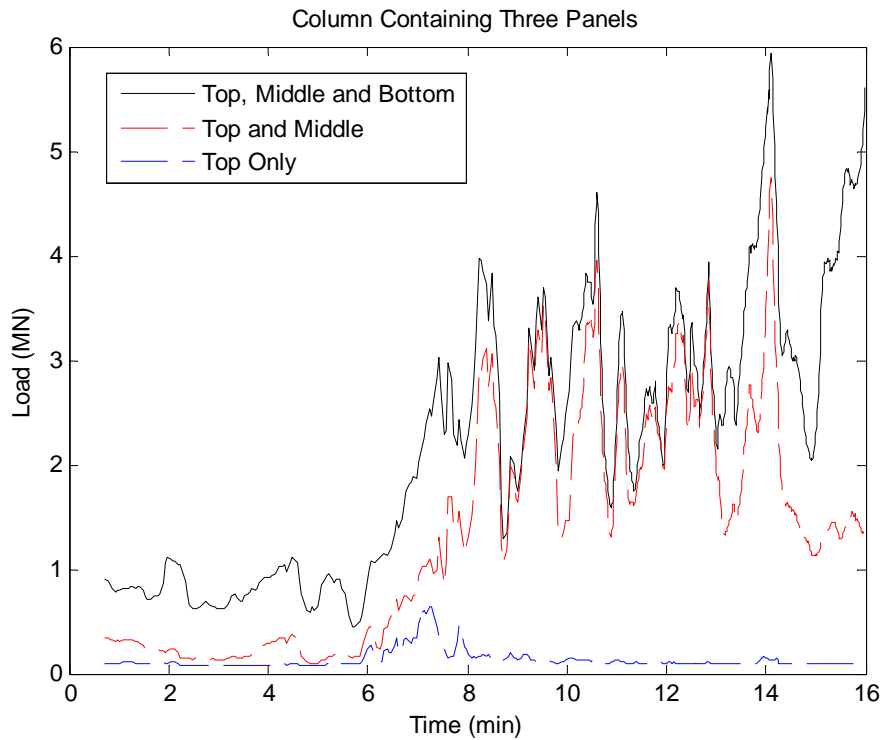
Figure 5-5: Loading on top, middle and bottom panels in column N2R.
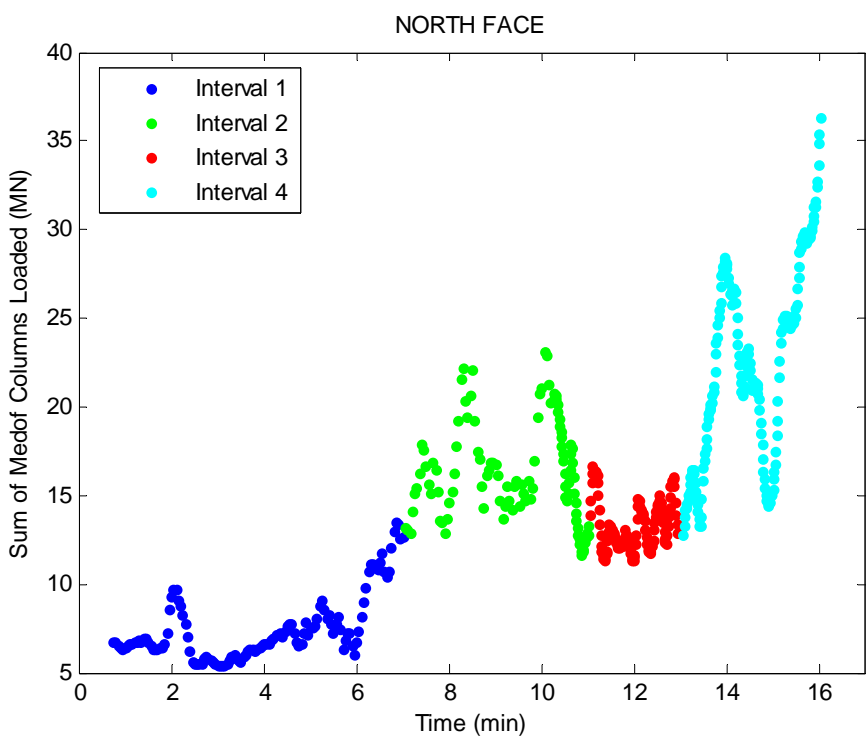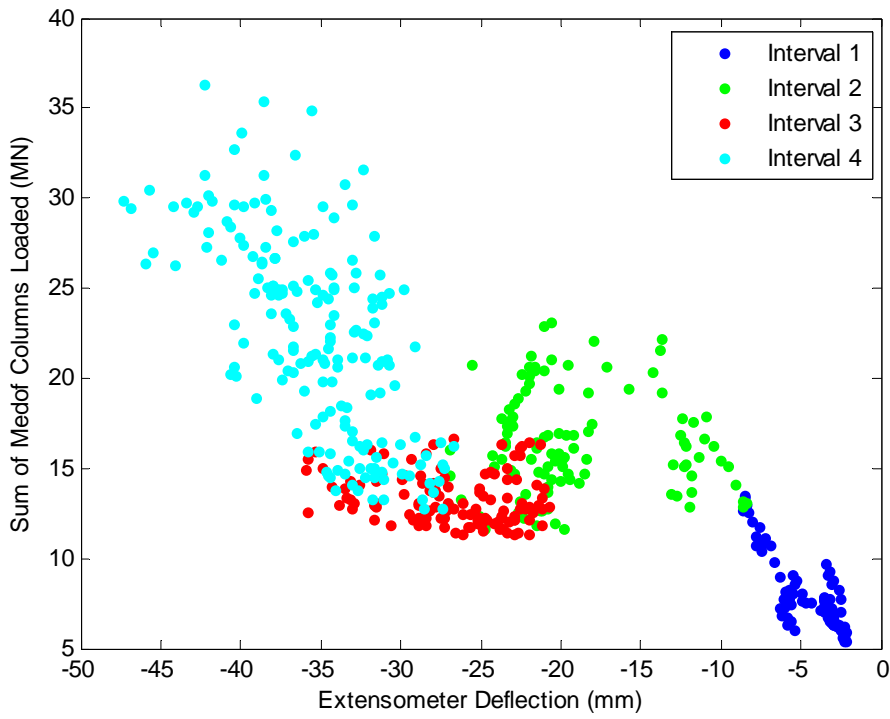
Figure 5-6: Colours represent selected intervals of interest within the data.

5.2.2 Maximum Force Based on Floe Deceleration and Ring Deformation

Approach

The maximum force during the May 12 event was calculated based on the floe deceleration, assuming that an accurate time trace of the relative force can be obtained from the extensometer readings. The floe velocity $v(t)$ at any time t is

$$v(t) = v(0) - \int_0^t a(t)\, dt$$

Equation 5-1

where $v(0)$ is the initial velocity and $a(t)$ is the acceleration at time t. At $t = t_{end}$ the floe is stopped so

$$0 = v(t_{end}) = v(0) - \int_0^{t_{end}} \frac{F(t)}{M_T}\, dt$$

Equation 5-2

where $F(t)$ is the interaction force and M_T is the mass of the floe, including added mass. Assuming that the Molikpaq ring distortion is linearly related to the interaction force, i.e.

$$F(t) = K\Delta(t)$$

Equation 5-3

where $\Delta(t)$ is the distortion at time t and K is the corresponding stiffness, one obtains

$$\int_0^{t_{end}} \frac{K\Delta(t)}{M}\, dt = v(0)$$

Equation 5-4

or

$$K = \frac{M \cdot v(0)}{\displaystyle\int_0^{t_{end}} \Delta(t)\, dt}$$

Equation 5-5

Calculations

It is necessary to determine the appropriate combination of extensometer readings to represent the variation in load. The stiffness is determined by calibration such that the resulting load causes the floe to stop in the observed time.

Following Timco et al. (2005), the mass of the floe is estimated assuming a rectangular floe with length 15000 m, width 7000 m, average thickness 2.5 m, and density of ice equal to 1000 kgm^{-3} as 260 million tonnes. The initial floe velocity was taken as 0.18 m/s and that the floe was observed to stop after 27 minutes.

The effect of added mass has been taken into account using the relationship:

$$M_T = \left(1 + \frac{h_s}{2W_D - h_s}\right)M$$

Equation 5-6

from Marcellus and Morrison (1982), where h_s is the floe draft; W_D is the water depth and M is the mass of the floe. A value of 5 m was used for the floe draft, giving an added mass of 8.8%.

Day file data that covers the period immediately before and through the first 9 minutes of the impact were also considered. The combined day file and fast file data up to the end of the impact are shown in Figure 5-7. The day file data consist of the average, maximum and minimum values over the 5 minutes preceding each record. It appears that there could have been some loading before 3:01 a.m. on May 12th but we have used 3:01 a.m. as the impact start time in further analysis.

Dynamics of Interaction

The interaction was characterized by dynamic action induced by the ice compressive failure at the loaded face. The variation of load, as expressed by the extensometer readings (appropriately scaled) has been taken into account in the analysis. Local fluctuations in displacement will take place at the contact zone, as the load rises and rapidly falls after each pulverization event. In the analysis, the situation further back into the floe was accounted for, where the movement would be steady. The dynamic action does not involve movements of the structure as a whole; it is confined to movements of the structure wall and a small amount of liquefied soil behind. The inertial mass involved in the vibration is therefore relatively small.

Further analysis of the dynamic situation would be useful and interesting, but is beyond the scope of the present work. We do not consider that a significant change to the present estimates of load would result.
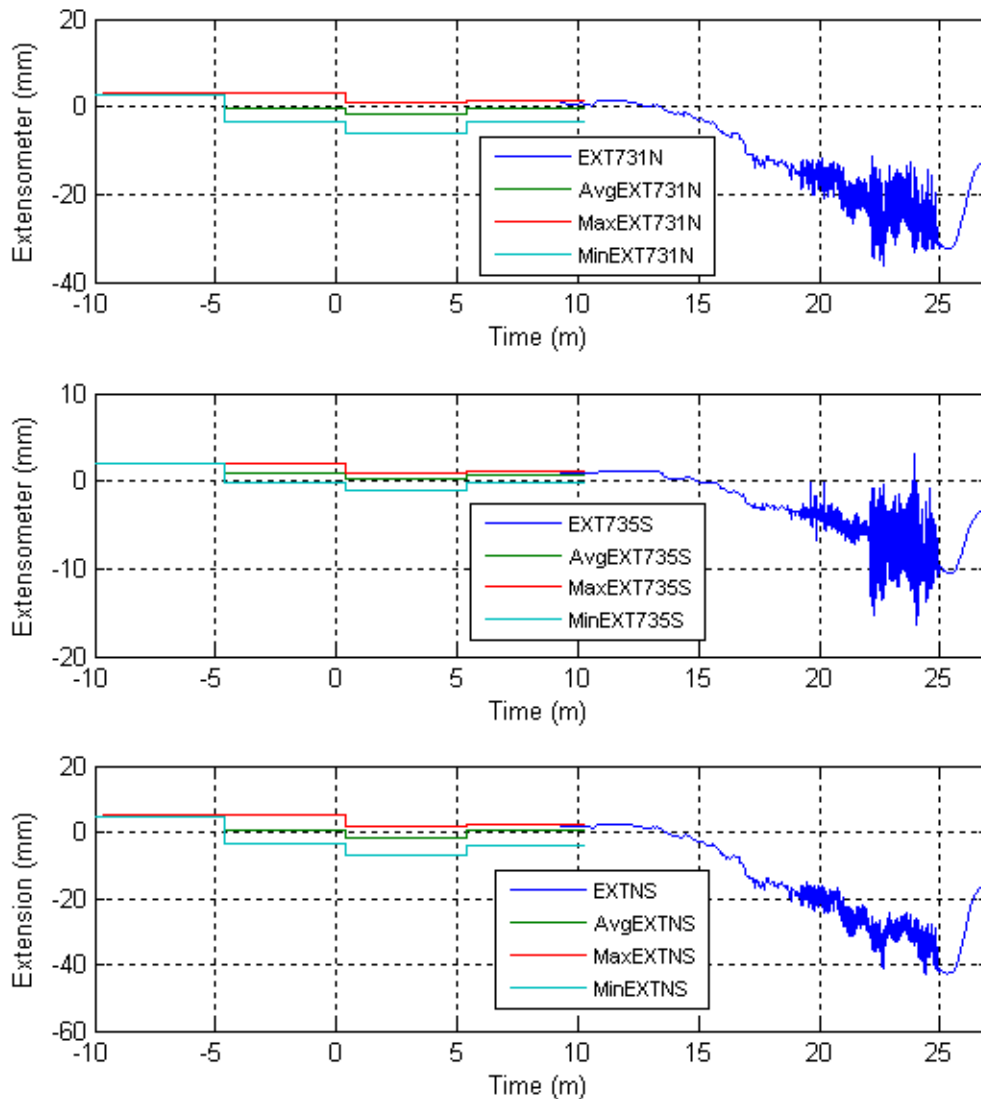
Figure 5-7: Combined Day File and Fast File Information for May 12th Impact

The method previously documented has been used to determine the load trace necessary to stop the floe in 27 minutes, assuming that the load is proportional to the North-South ring distortion. Figure 5-8 shows a time trace of the North-South distortion, corrected for the initial offsets shown at time -10 minutes in Figure 5-7, and shows the load trace required to stop the floe in 27 minutes. The necessary global stiffness was 2.19 MNmm^{-1} and the maximum load was 105 MN. It is possible but not certain that the floe underwent some rotation during the event; this would have the effect of reducing the kinetic energy involved in failure of the ice. The effect is considered to be relatively small, based on our experience in energy transfers of this kind.
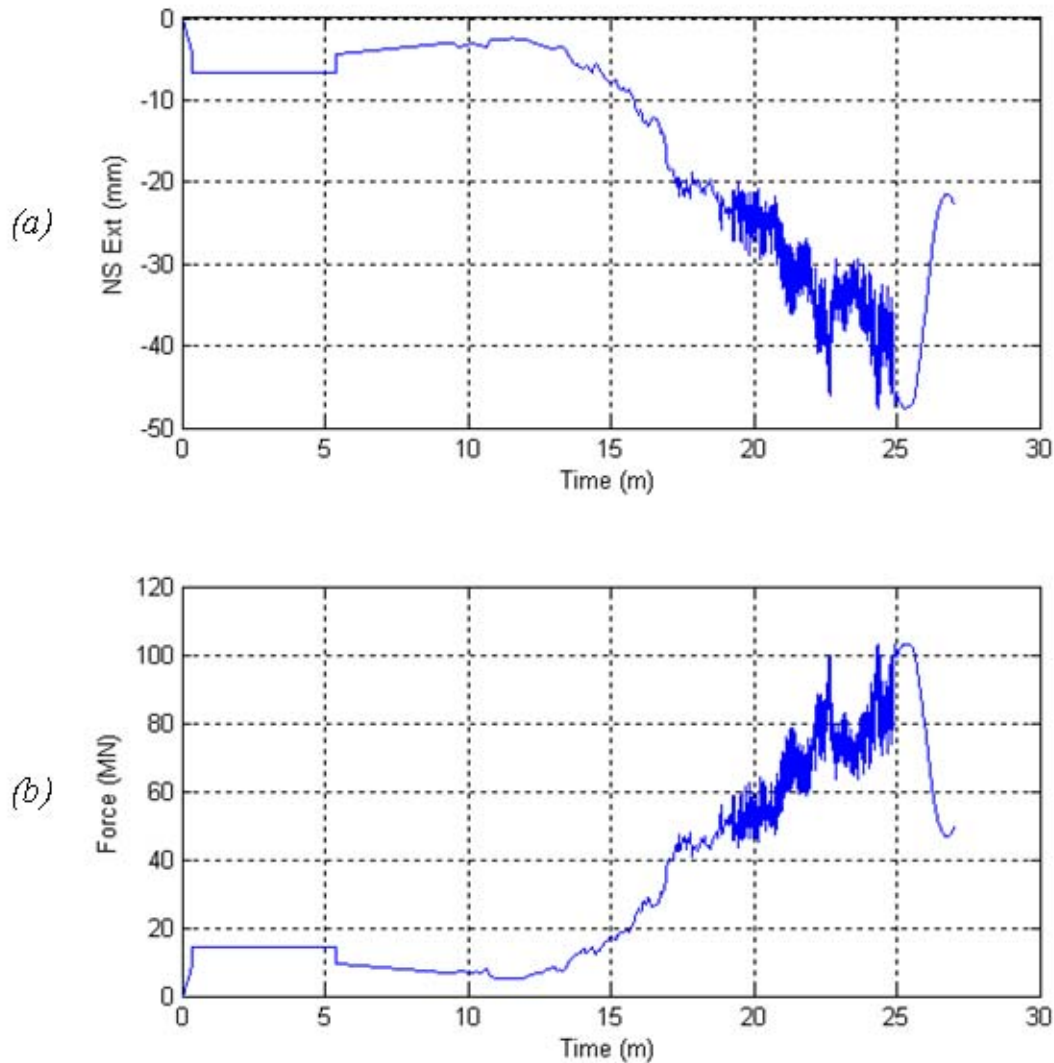
Figure 5-8: **(a) North-South distortion, corrected for initial extensometer offsets and. (b) corresponding load trace required to stop the floe in 27 minutes.**

A sensitivity analysis relating to uncertainty in the time during which the floe deceleration proper occurred has been carried out. To reflect this, the first 12 minutes of the impact have been removed. The contribution for the first 12 minutes corresponds to small loads, based on the extensometer ring distortion. The results of this approach can be seen in Figure 5-9 which leads to an increased global stiffness and maximum global load required to stop the floe in 15 minutes as opposed to the 27 minute approach described previously. A structural stiffness of 2.89 MNmm^{-1} with a maximum global load of 130 MN is the result of this.
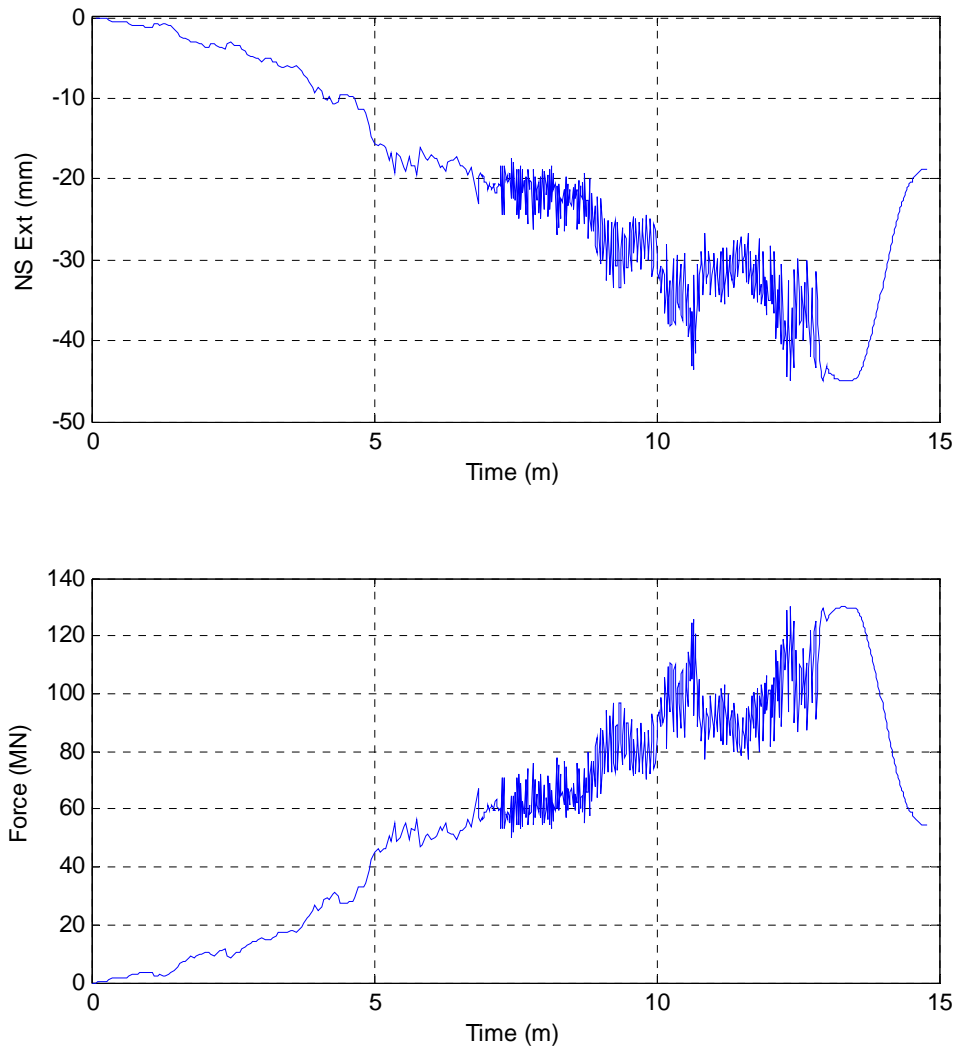
Figure 5-9 **(a) North-South distortion, adjusted such that 12 minute segment with low loading is removed. (b) corresponding load trace required to stop the floe in 15 minutes (as opposed to 27 minutes).**

5.2.3 Analysis of Face Loads Acting on the Structure

At approximately 16 minutes into the ice loading event, the sight tubes of Medof panel 1010 began to overflow. For this reason the event has been truncated such that the Medof panel analysis included the time leading up to the point of overflow only.

In Phase 1 of the project, the Medof panels were used to develop face loads acting on the structure. To achieve this, a probabilistic averaging technique was used. In the present phase of the project the extensometers have been used to calculate the ice loads acting on the face of the structure. Here we wish to compare the results generated by both

approaches. The face loads calculated using the Medof panels are systematically higher than those calculated using the extensometers with stiffness values chosen based on both the Sandwell (1991) finite element analysis and the floe deceleration event described above. Figure 5-10 shows the probabilistically averaged face load calculated from Phase 1 using the Medof panels, which has been factored to produce a best fit slope equal to 1.0 when plotted against the face loads generated by the extensometers for a structural stiffness taken to be 2.6 MNmm^{-1}. This result indicates the magnitude of softening which would have occurred in the Medof panels and requires that the face load determined based on the Medof panel data be multiplied by a factor of 0.52. Table 5-1 shows the appropriate factor which would be required to adjust the probabilistically averaged Medof panel load for various structural stiffness values, along with the associated maximum face load.
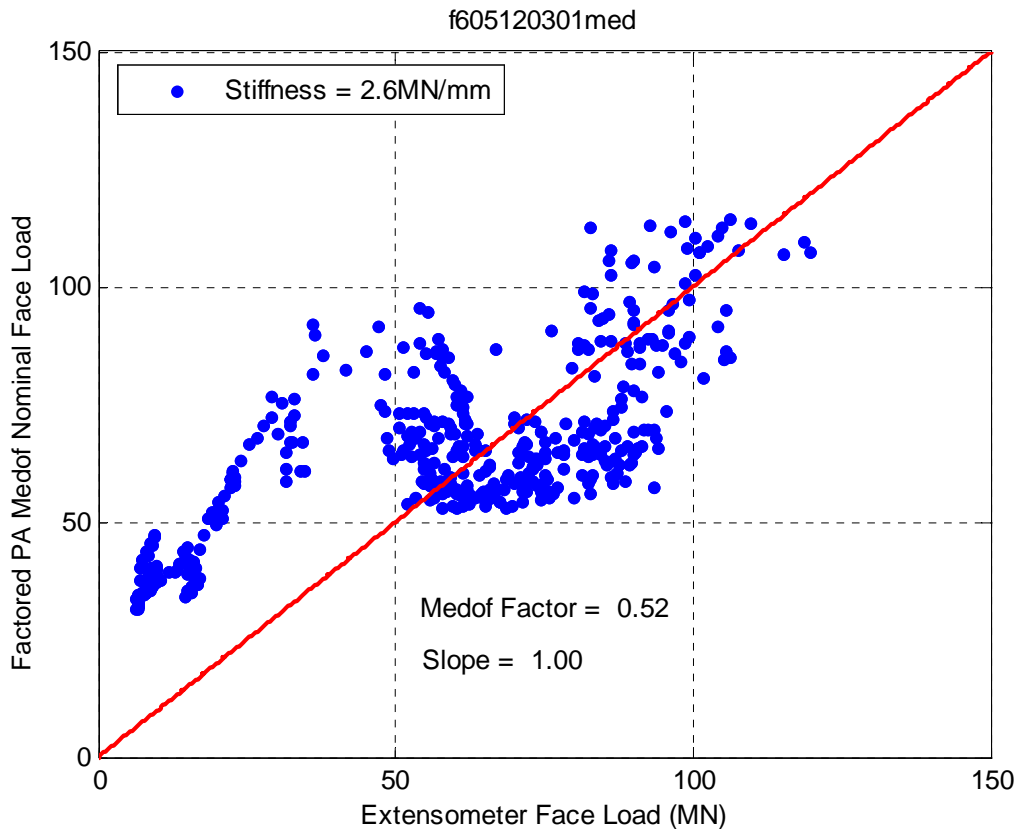
Figure 5-10: **Extensometer face load versus a factored Medof face load which has undergone probabilistic averaging.**

Table 5-1: **Medof panel load factors and associated maximum face loads**

Structural Stiffness (MN/mm)	Medof Factor	Max Face Load (MN)
2.2	0.44	104.4
2.6	0.52	123.4
3.0	0.60	142.3

As the strain gauges are located in the same approximate locations as a group of Medof panels (i.e. strain gauge N1 is located behind the N1 group of Medof panels) it is reasonable to calibrate the two together. As was discussed above, the Medof panels

should be factored to account for the softening which they had likely undergone. Figure 5-11 shows strain gauge SG09 data plotted against the factored Medof group load (assuming a structural stiffness of 2.6 MNmm^{-1}) for positions N1, N2 and N3. The factor used is the same factor which was required to achieve a slope of 1.0 in the calibration of Medof panels to extensometer data. Table 5-2 shows the calibration results assuming various structural stiffness values.
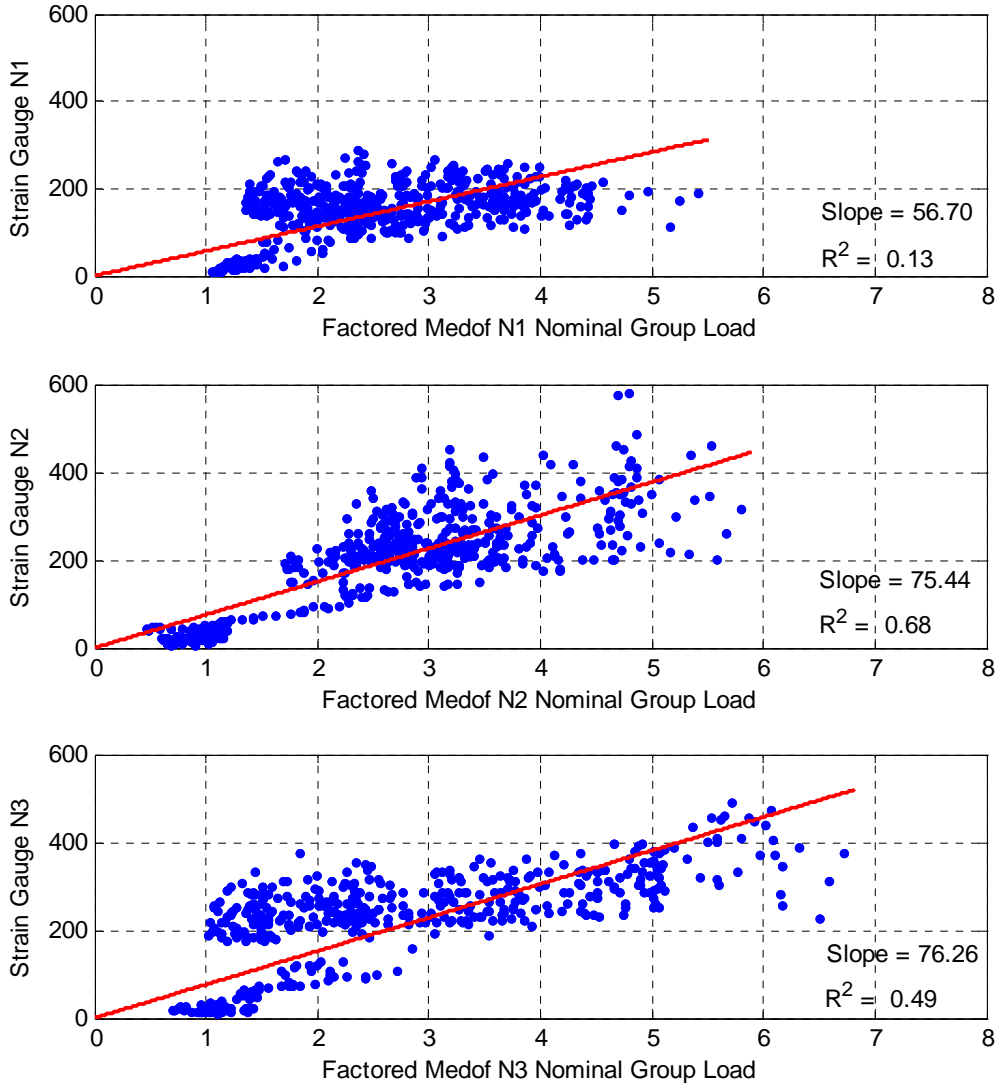
Figure 5-11:   **Strain gauge data has been calibrated to Medof panel group loads. Medof panel loads have been factored based on the discrepancy between them and the extensometer values.**

Table 5-2: **Strain gauge calibration results with factored Medof panels**

Structural Stiffness (MN/mm)	Strain Gauge N1	Strain Gauge N2	Strain Gauge N3
2.2	67.0	89.1	90.1
2.6	56.7	75.4	76.3
3.0	49.1	65.4	66.1

5.2.4 Maximum Global Force Based on Matrix Model

The stiffness matrix developed based on the Sandwell (1991) report was applied to estimate the loads during the May 12, 1986 event from the extensometer values. The ring distortions are plotted in Figure 5-12 (a) and the loads calculated using the matrix solution are plotted in Figure 5-12 (b). Figure 5-12 (c) shows the north and east global load components as well as the total load. The maximum total load is 125 MN.

The method has been shown to be very sensitive to any drift in the extensometer values, though for the May 12th event the correction for drift should be reasonable as it is known that there was zero load prior to impact with the floe. Other possible inaccuracies associated with the treatment of corner loads in developing the method have been described. The global loads are shown in Figure 5-12 (c); the maximum values are as follows:

     Maximum Global Load - North Component 126 MN
     Maximum Global Load - East Component   28 MN
     Maximum Global Load - Total   126 MN

Overall, this is a good result indicating mainly north face loading.
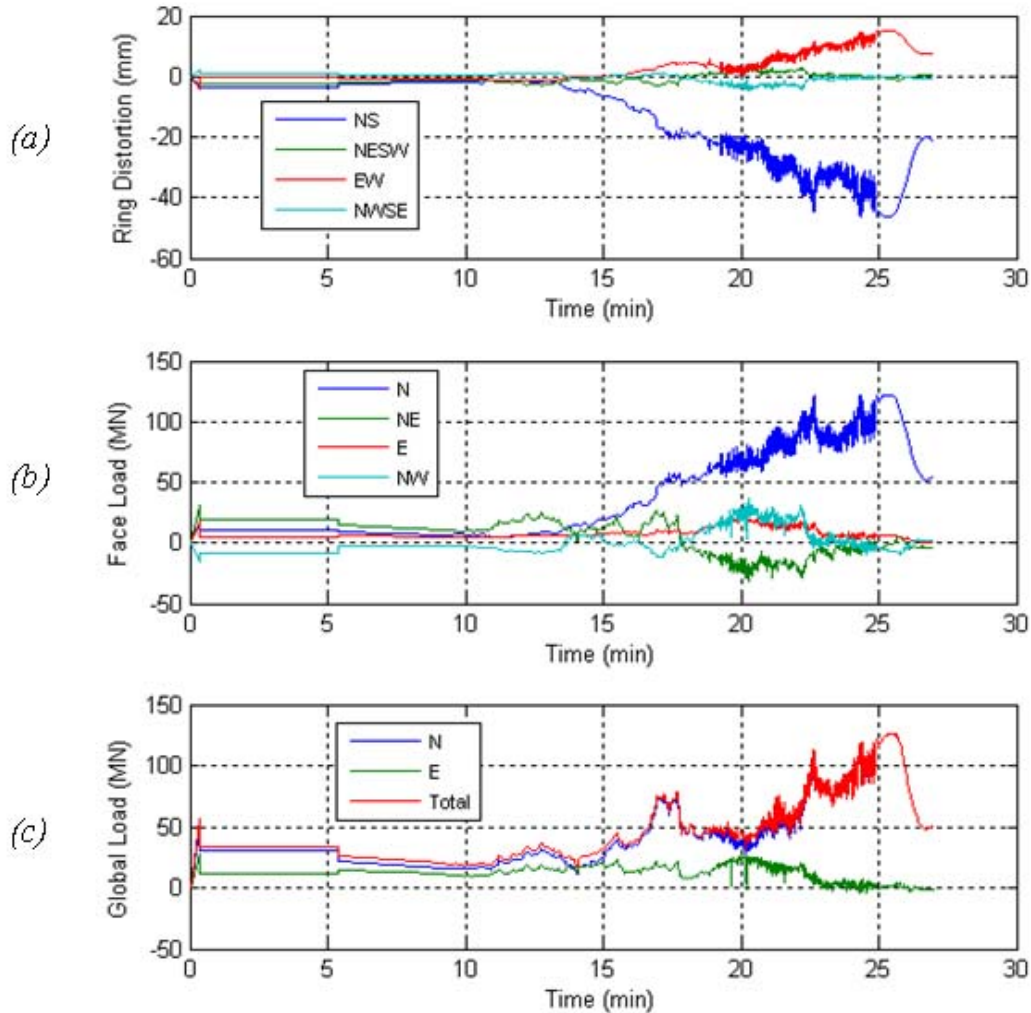
Figure 5-12: **Application of matrix method to May 12, 1986 event**

5.2.5 Concluding Remarks for May 12, 1986 Event

An analysis of a decelerating floe which impacted the Molikpaq structure based on mechanics, was conducted in Section 5.2.2. This method of analysis provides a measure of the stiffness of the structure which is independent of the finite element analysis which was conducted by Sandwell (1991). The peak load associated with this event is 105 MN. On the assumption of a shorter duration of the impact, a load of 130 MN is obtained. The ring distortion ratio of 2.6 MNmm^{-1} gives a load of 123 MN.

The matrix model has also been applied to the May 12, 1986 data set. Using this approach a global load of 126 MN is estimated. This result includes the predominant loading on the North face in addition to small loading occurring on the North East and East faces.

5.3   Event 0325A - March 25, 1986 – f603250801

Event ID – 0325A
Creep Event
Ice Thickness: 3.5m
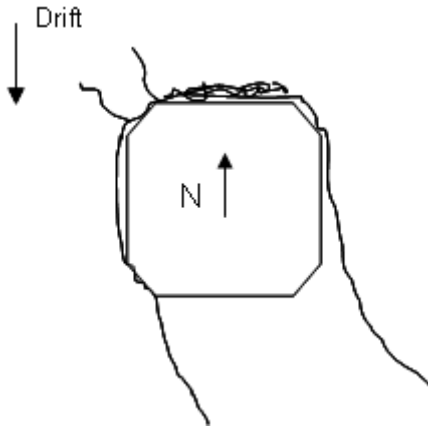
5.3.1 Dynamac Event Description

After three weeks of being stationary, the multiyear ice in the vicinity of the Molikpaq began to slowly creep towards the south, thereby simultaneously loading the N, NW & NE faces. The ice drift speed was estimated at less than 1 m/hr. The figures below are intended to provide summary information about the event.

The March 25th event involved the predominant loading of the North face with some loading occurring on the North West and North East faces (see also Figure 5-13). This event represents a good case for analyzing the face loads estimated by the extensometers, with calibration of Medof panels to the extensometer load. The analysis of the extensometers has brought the Phase 1 Medof panel face load estimate of approximately 98 MN down to 34 MN using a load distortion ratio of 2.6 MNmm^{-1}. In order to estimate the global load, an adjustment must be made to account for the loading occurring on the North West and North East faces of the structure.

North Face

North East Face
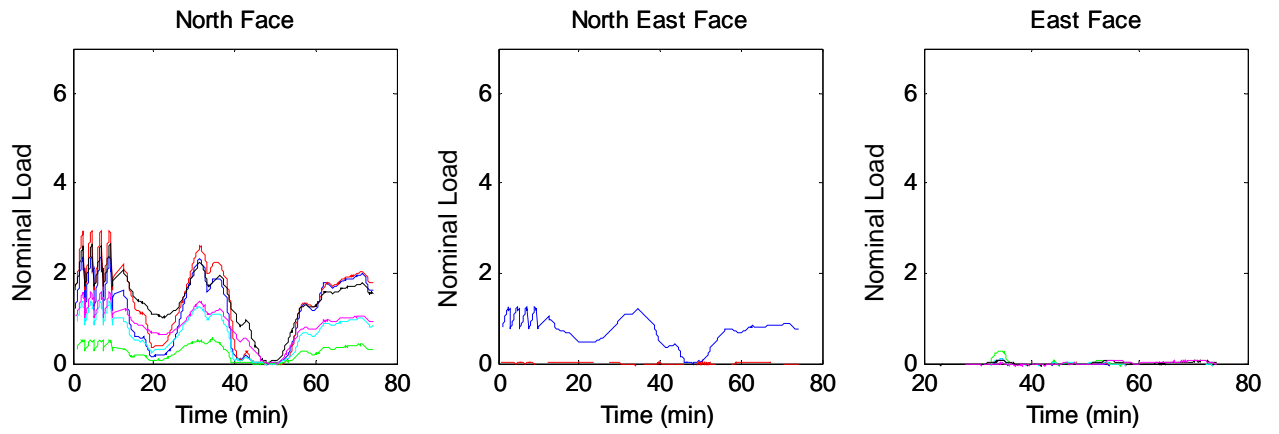
East Face

Figure 5-13   **Nominal Medof column loads acting on the North, North East and East faces**

f603250801med
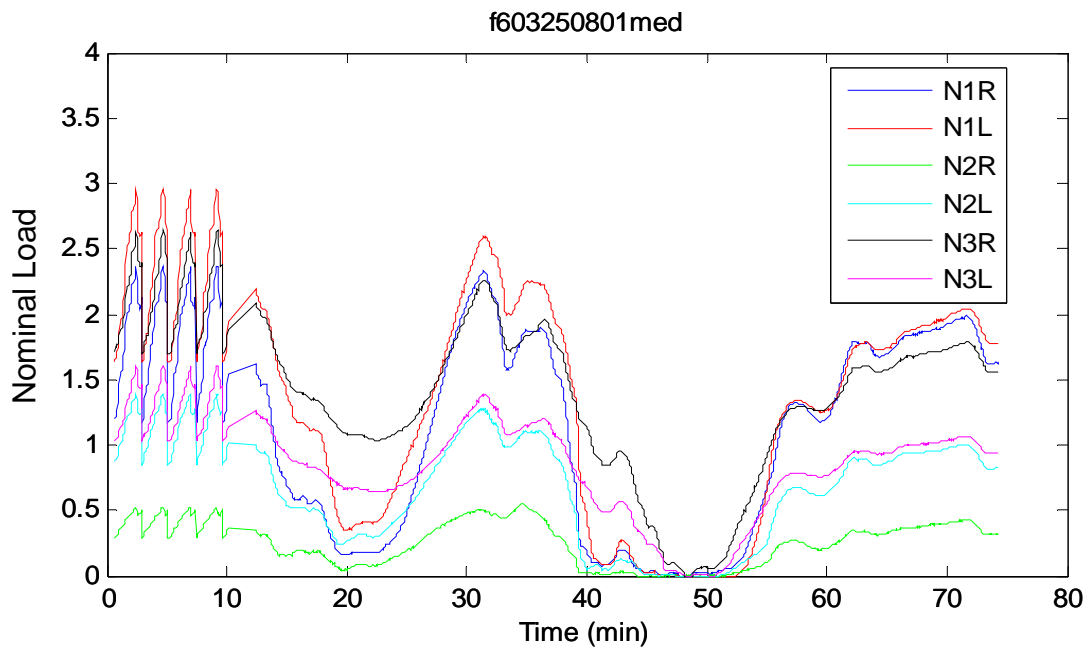
Figure 5-14   **Nominal Medof column loads acting on the North face of the Molikpaq structure**
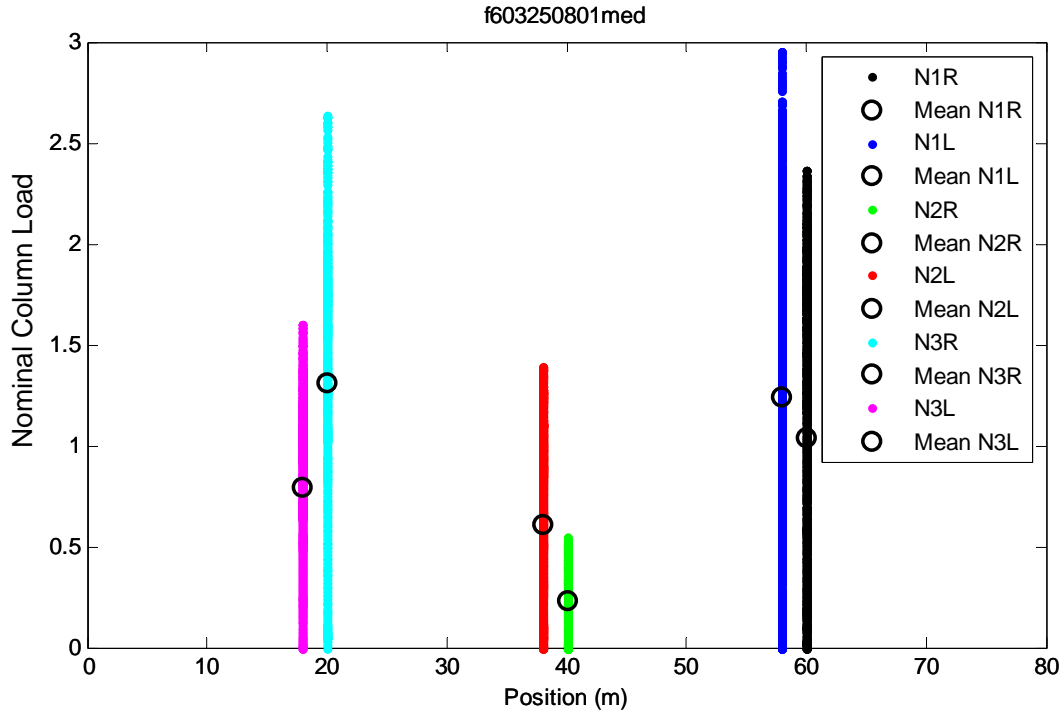
Figure 5-15: Distribution of Medof column nominal ice loading on the face of the structure
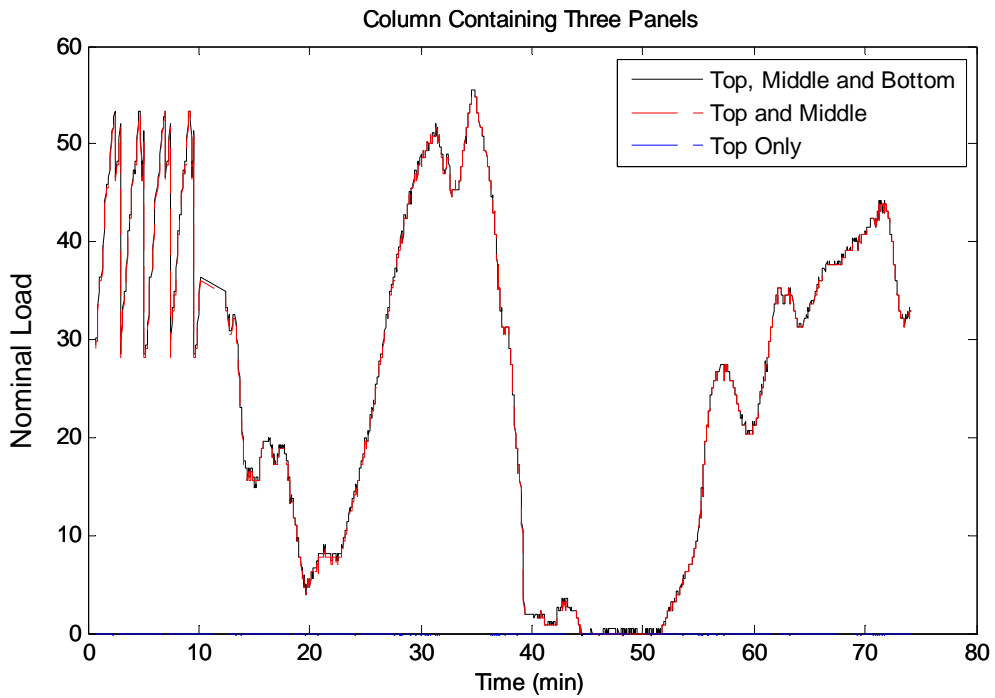
Figure 5-16: Loading on top, middle and bottom panels in column N2R.
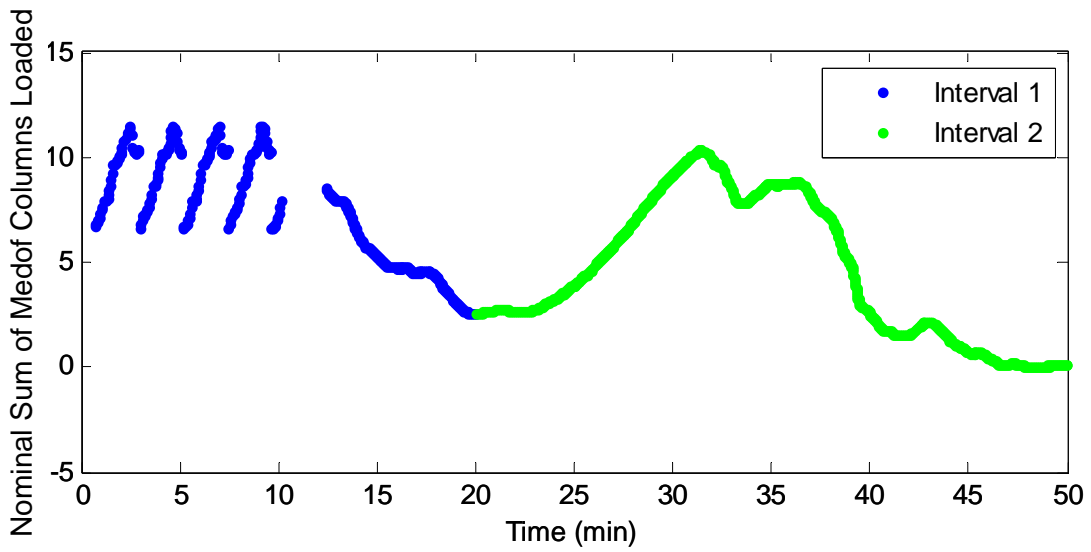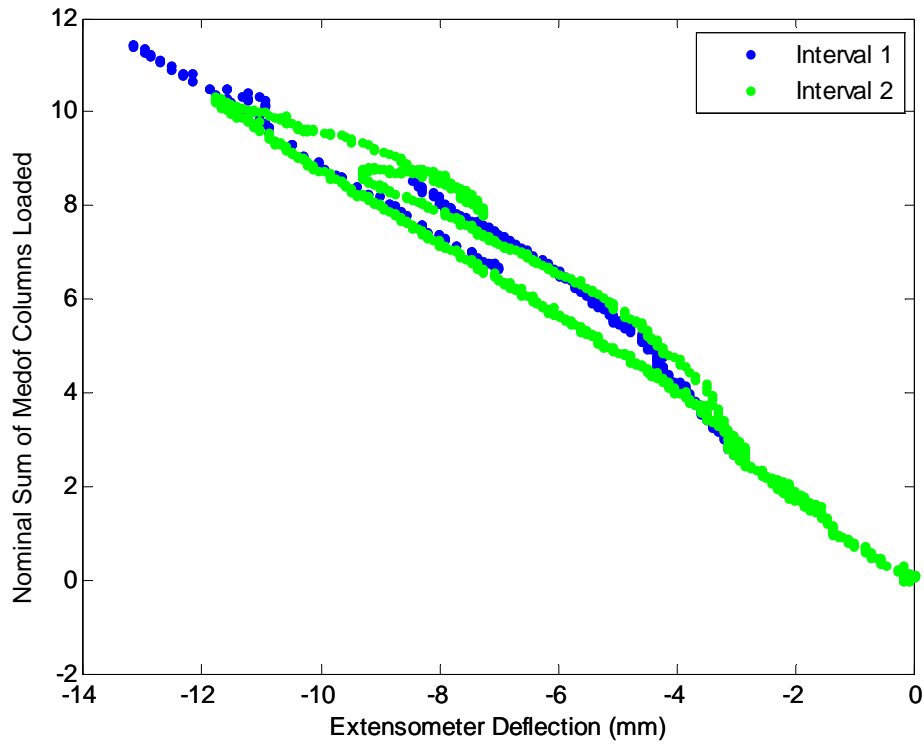
Figure 5-17: The colors represent selected intervals of interest within the data.

5.3.2 Analysis of Face Loads Acting on the Structure

The extensometers have been used to calculate the ice loads acting on the north face of the Molikpaq structure. Figure 5-18 shows the probabilistically averaged face load calculated from phase 1 using the Medof panels which has been factored to produce a best fit slope equal to 1.0 when plotted against the face loads generated by the extensometers. This result indicates the general magnitude of softening which would have occurred in the Medof panels

Below, a ring distortion ratio of 2.6 MNmm^{-1} was used to determine the face load based on the extensometer ring deformation. This result required that the face load determined based on the Medof panel data be multiplied by a factor of 0.32. Table 5-3 shows the appropriate factor which would be required to adjust the probabilistically averaged Medof panel load for various structural stiffness values, along with the associated maximum face load.
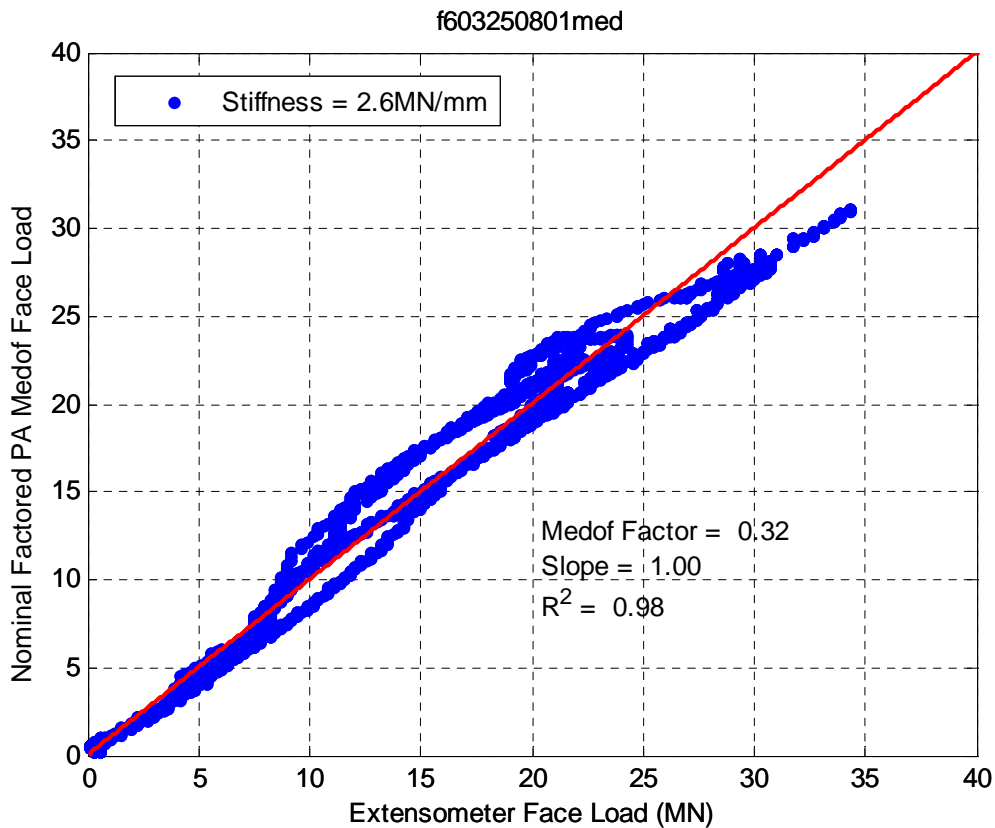
Figure 5-18:   **Extensometer face load versus a factored Medof face load which has undergone probabilistic averaging.**

Table 5-3:   **Medof panel load factors and associated maximum face loads**

Structural Stiffness (MN/mm)	Medof Factor	Max Face Load (MN)
2.2	0.27	28.9
2.6	0.32	34.2
3.0	0.37	39.5

As the strain gauges are located in the same approximate locations as a group of Medof panels (e.g. strain gauge N1 is located behind the N1 group of Medof panels) it is reasonable to calibrate the two. However, as was discussed above, the Medof panels should be factored to account for the softening which they had undergone. Figure 5-19 shows strain gauge SG09 data plotted against the factored Medof group load for positions N1, N2 and N3 (as the loading was primarily on the North face). The factor used is the same factor which was required to achieve a slope of 1.0 in the calibration of Medof panels to extensometer data. Table 5-4 shows the calibration results assuming various structural stiffness values.
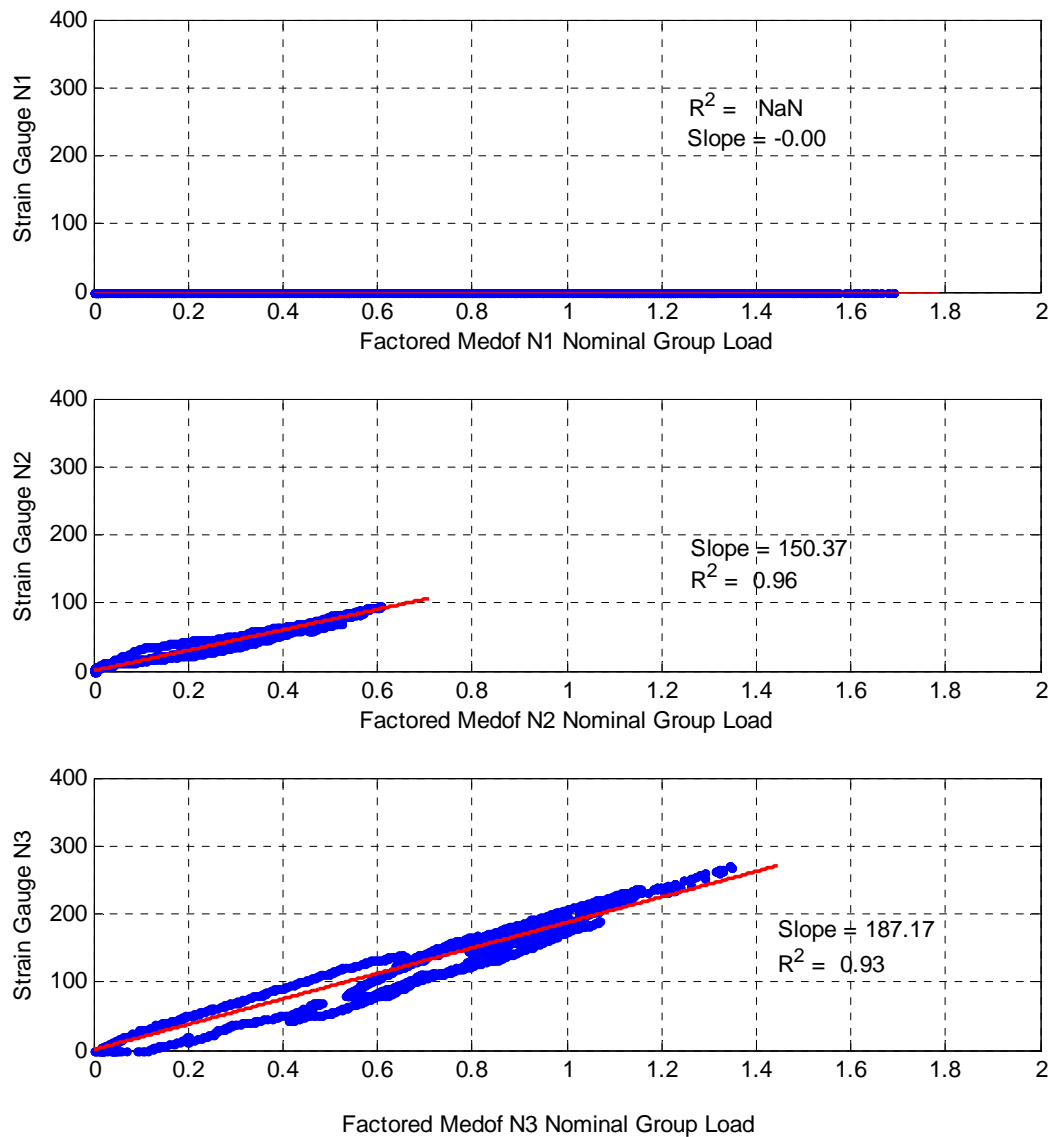
Figure 5-19: **Strain gauge data has been calibrated to Medof panel group loads. Medof panel loads have been factored based on the discrepancy between them and the extensometer values.**

Table 5-4: **Strain gauge calibration results with factored Medof panels**

Structural Stiffness (MN/mm)	Strain Gauge N1	Strain Gauge N2	Strain Gauge N3
2.2	n/a	177.7	221.2
2.6	n/a	150.4	187.2
3.0	n/a	130.3	162.2

5.3.3 Concluding Remarks for March 25 (A), 1986 Event

The March 25th, 1986 event was a creep loading event which involved the predominant loading of the North face with some loading occurring on the North West and North East faces. This event represents a good case for analyzing the face loads estimated by extensometers, with calibration of Medof panels to the extensometer load. The analysis of the extensometers has brought the Phase 1 Medof panel face load estimate of approximately 98 MN down to 34 MN using a face load ring distortion ratio of 2.6 MNmm^{-1}.

5.4   Event 0325B - March 25, 1986 – f603251302

Event ID – 0325B
Creep Event
Ice Thickness: 3.5m
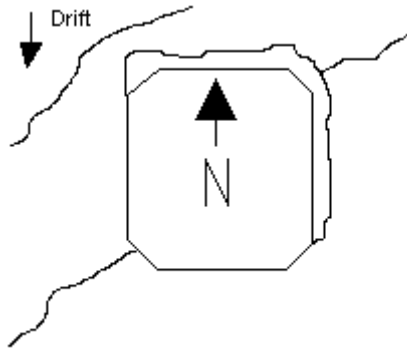
5.4.1 Dynamac Event Description

After three weeks of stationary conditions, the multi-year ice in the vicinity of the Molikpaq began to slowly creep towards the south, thereby simultaneously loading the north, north west & north east faces. The ice drift speed was estimated at less than 1 m/hr. The figure below is intended to show the magnitude of loading occurring on the North, North East and East faces during the event. Each colour represents a Medof nominal column load.

The March 25th event involved the predominant loading of the North face with some loading occurring on the North West and North East faces, with very small loading occurring on the East face due to minor rotation of the ice (see also Figure 5-20). This event represents a good case for analyzing the face loads estimated by the extensometers, with calibration of Medof panels to the extensometer load.
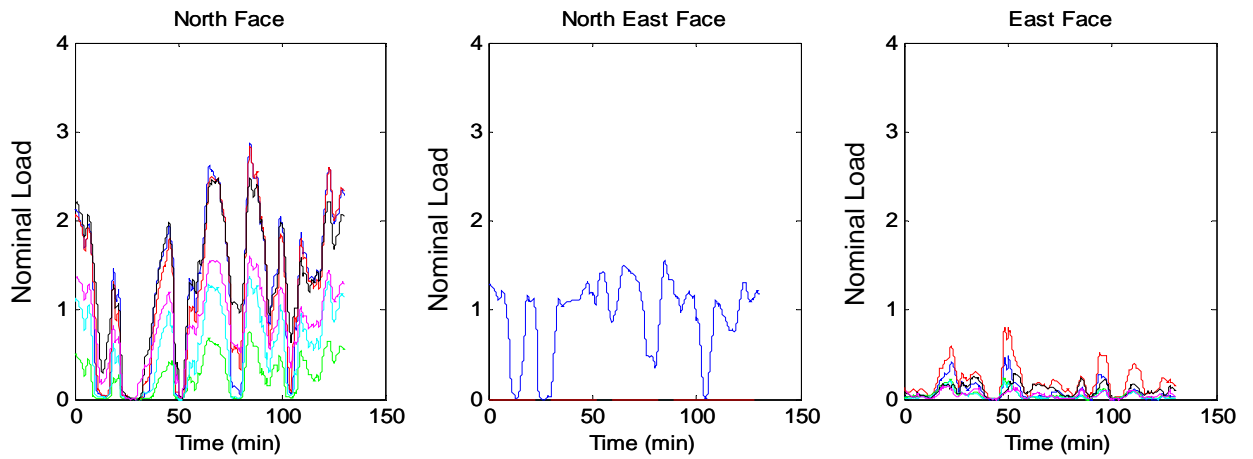
**Figure 5-20   Nominal Medof column loads acting on North, North East and East faces**
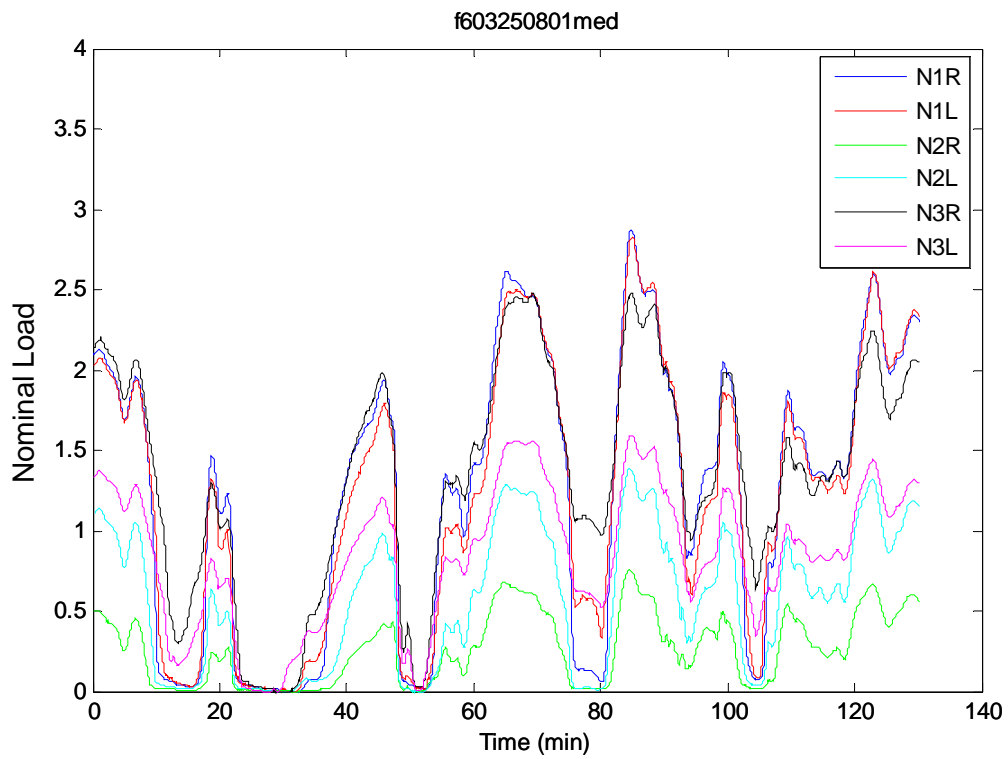
**Figure 5-21   Nominal Medof column loads acting on the North face of the structure**
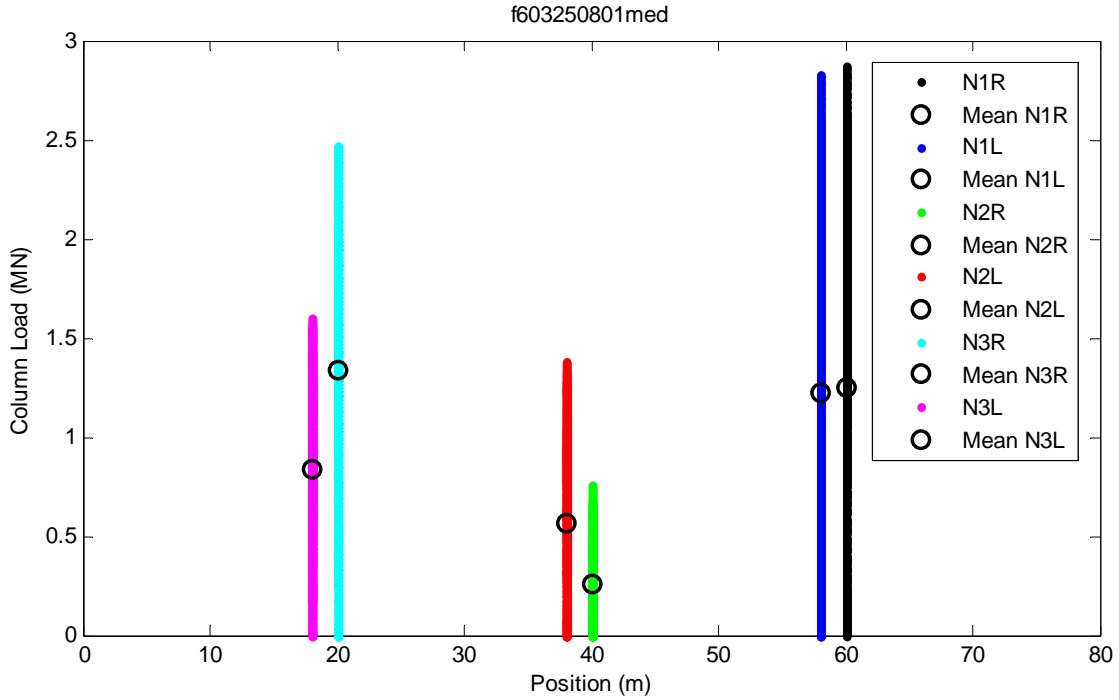
Figure 5-22: **Distribution of Medof nominal column ice loading on the face of the structure**
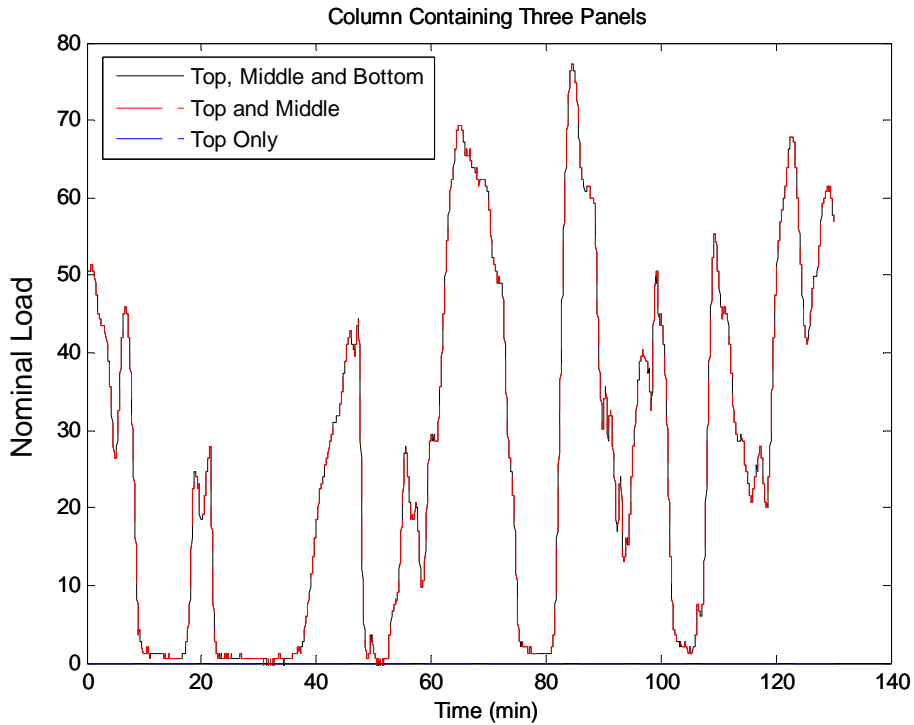

**Figure 5-23:** **Loading on top, middle and bottom panels in column N2R.**
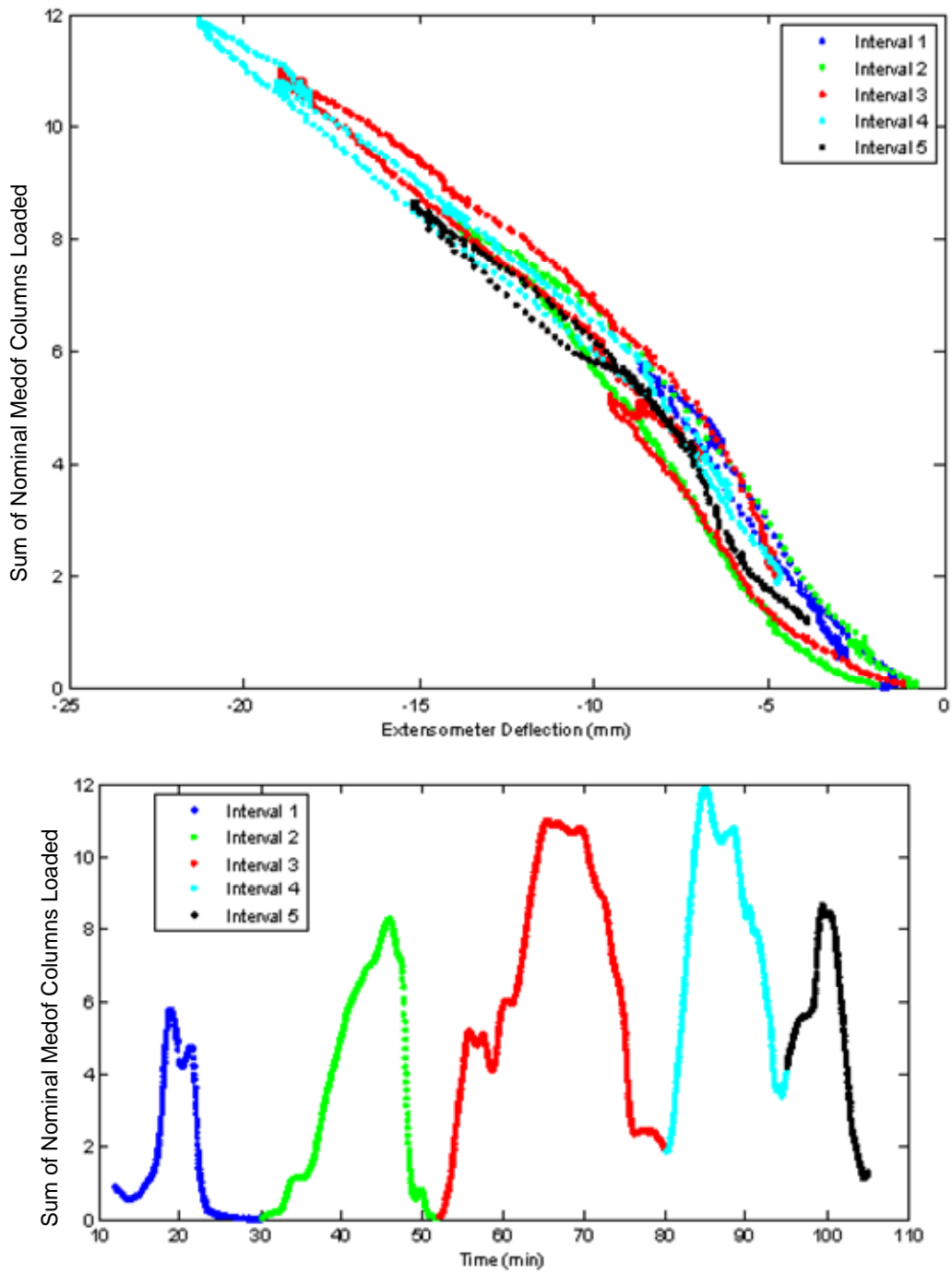
Figure 5-24: The colours represent selected intervals of interest within the data.

5.4.2 Analysis of Face Loads Acting on the Structure

The extensometers have been used to calculate the ice loads acting on the north face of the Molikpaq structure. Figure 5-25 shows the probabilistically averaged face load calculated from Phase 1 of the project based on the Medof panels which has been factored to produce a best fit slope equal to 1.0 when plotted against the face loads generated by the extensometers. This result indicates the general magnitude of softening which would have occurred in the Medof panels. A ring distortion ratio of 2.6 MNmm^{-1} was used to obtain the face load based on the extensometer ring deformation. This result required that the face load determined based on the Medof panel data be multiplied by a factor of 0.52. Table 5-5 shows the appropriate factor which would be required to adjust the probabilistically averaged Medof panel load for various structural stiffness values, along with the associated maximum face load.
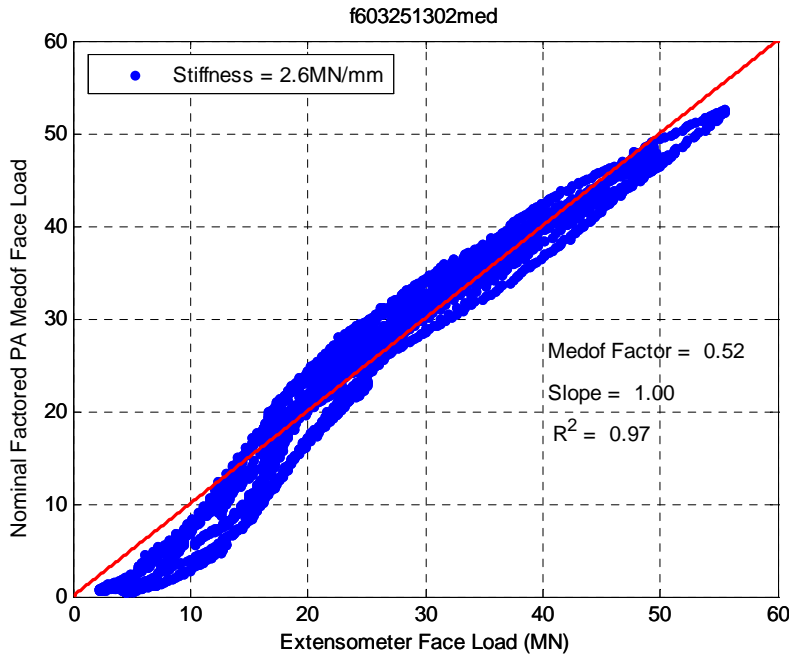

Figure 5-25:   **Extensometer face load versus a factored Medof face load which has undergone probabilistic averaging.**

Table 5-5:   **Medof panel load factors and associated maximum face loads**

Structural Stiffness (MN/mm)	Medof Factor	Max Face Load (MN)
2.2	0.44	46.8
2.6	0.52	55.3
3.0	0.60	63.8

As the strain gauges are located in the same approximate locations as a group of Medof panels (e.g. strain gauge N1 is located behind the N1 group of Medof panels) it is reasonable to calibrate the two. As was discussed above, the Medof panels should be factored to account for the softening which they had undergone. Figure 5-26 shows strain gauge SG09 data plotted against the factored Medof group load for positions N1, N2 and N3 (as the loading was primarily on the North face). The factor used is the same

factor which was required to achieve a slope of 1.0 in the calibration of Medof panels to extensometer data. Table 5-6 shows the calibration results assuming various structural stiffness values.
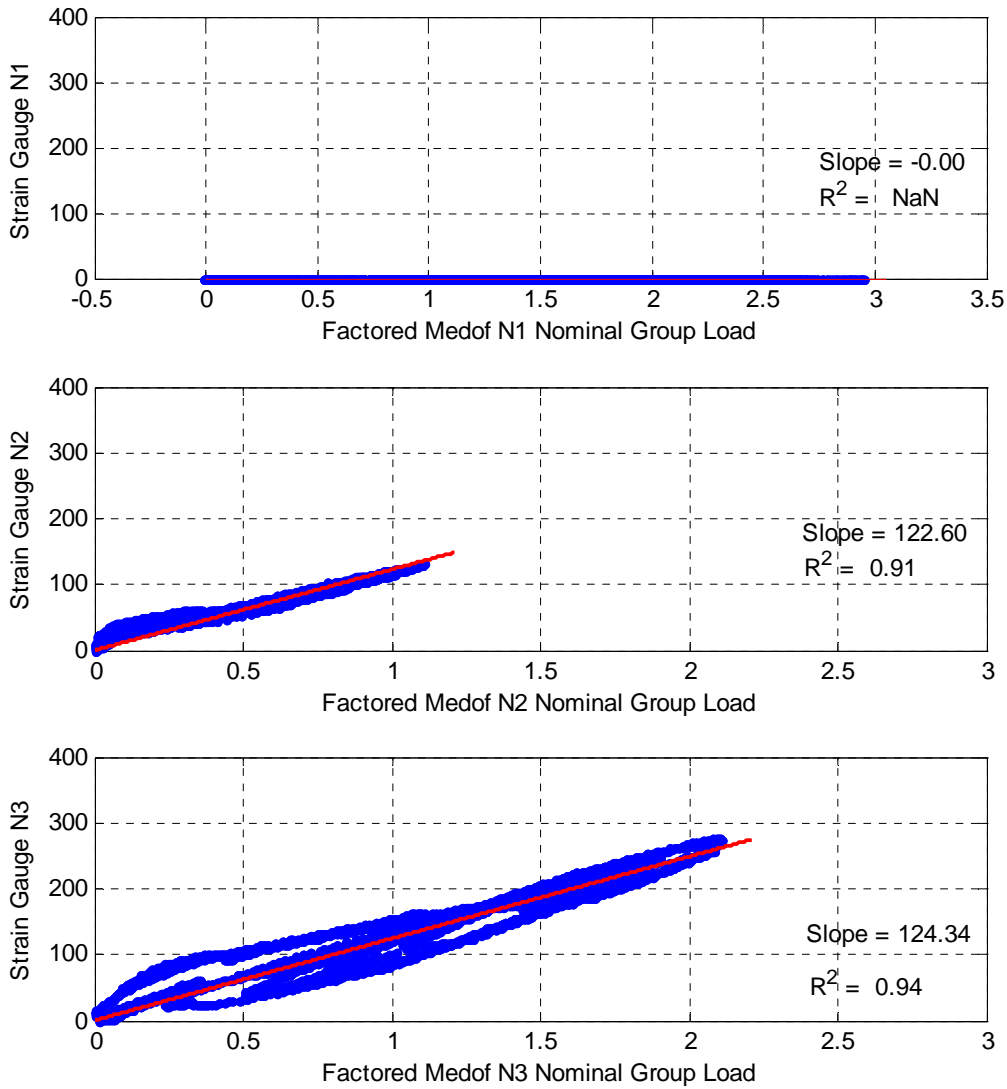

Figure 5-26: **Strain gauge data has been calibrated to Medof panel group loads. Medof panel loads have been factored based on the discrepancy between them and the extensometer values.**

Table 5-6: **Strain gauge calibration results with factored Medof panels**

Structural Stiffness (MN/mm)	Strain Gauge N1	Strain Gauge N2	Strain Gauge N3
2.2	n/a	144.9	146.9
2.6	n/a	122.6	124.3
3.0	n/a	106.2	107.8

5.4.3 Ring Distortion, Medof Load and SG09 Strain Comparison

Figure 5-27 shows a comparison of the ring distortion, Medof loads and SG09 strains as a function of time and orientation. The ice was moving toward somewhere between 200 and 220 degrees from true north. The Medof loads on the north face are much larger than those on the east or north-east face, though the number of panels on the north-east face was limited. The east-west ring distortion tends to move in the opposite direction to the north-south distortion, indicating that the effect of the north-face load in distorting the ring shape was significant. The north-east to south west ring distortion tended to move in the same direction as the north-south distortion, while the north-west to south-east ring distortion acted in the opposite direction. The strain gauges showed strains on the north east face almost as large as the sum of the strains on the north face and may indicate that the face loads were significantly larger than indicated by the middle and bottom layer Medof panels.

Figure 5-28 shows the breakdown of ring distortions into near and far extensometer readings. The top figure shows that the extension on the north face is much larger than that on the south face, as expected. Distortions in other directions are generally small.

Figure 5-29 shows the sum of panel loads for the three Medof groups on the north face. The highest loads are on the west (N1) side and the lowest loads are in the middle. Figure 5-30 and Figure 5-31 show the sum of panel loads for the Medof groups on the north-east and east faces. Figure 5-32 shows the sum of loads on top, middle and bottom rows of panels of different faces. The loads on the north and east face are on the middle row only (based on single lower panels) while there is a small load on the bottom panel of the north-east face.

Figure 5-33 shows the strain gauge readings for the different faces. There were two strain gauges on the north face and one each on the north-east and east faces.
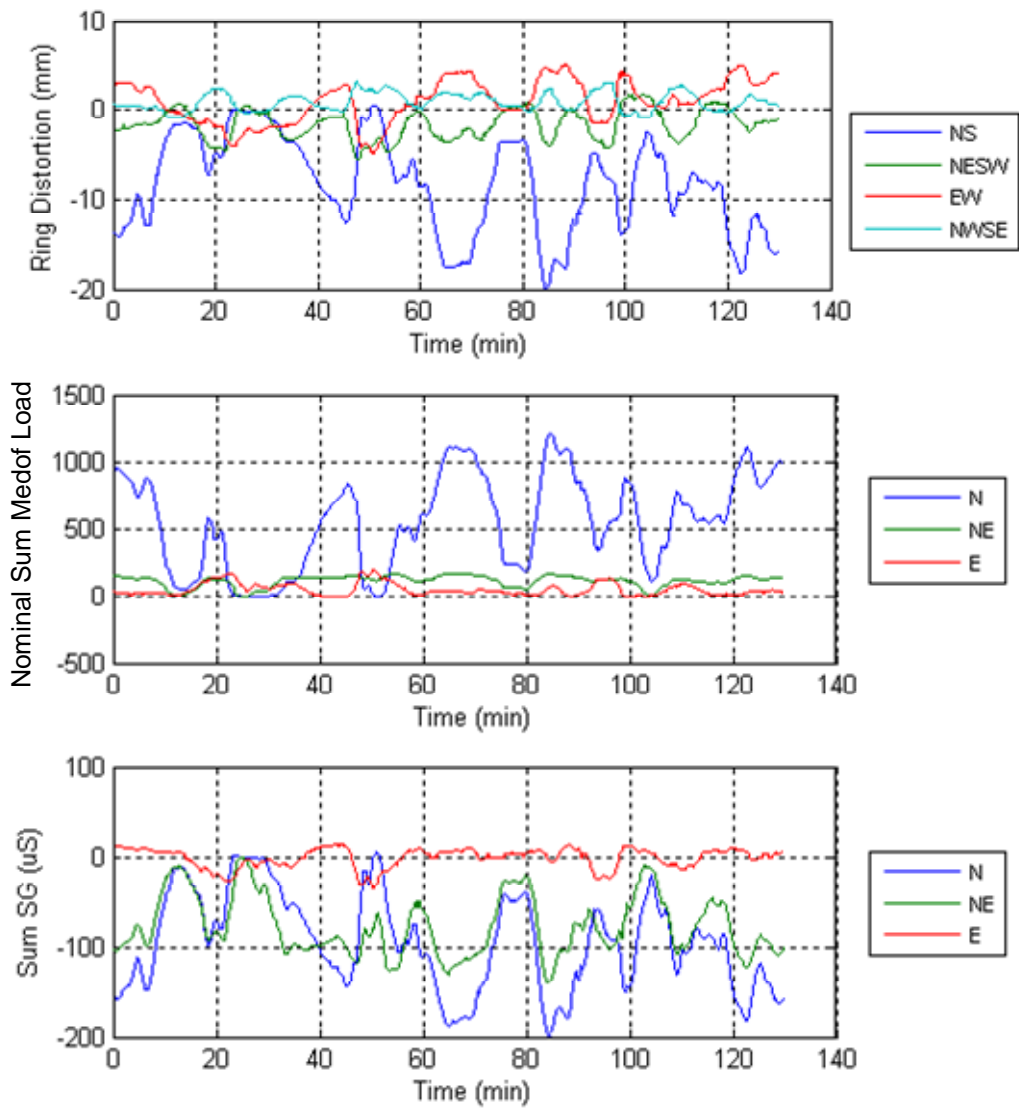
Figure 5-27: Comparison of ring distortion, Medof load and SG09 strain as a function of time and orientation
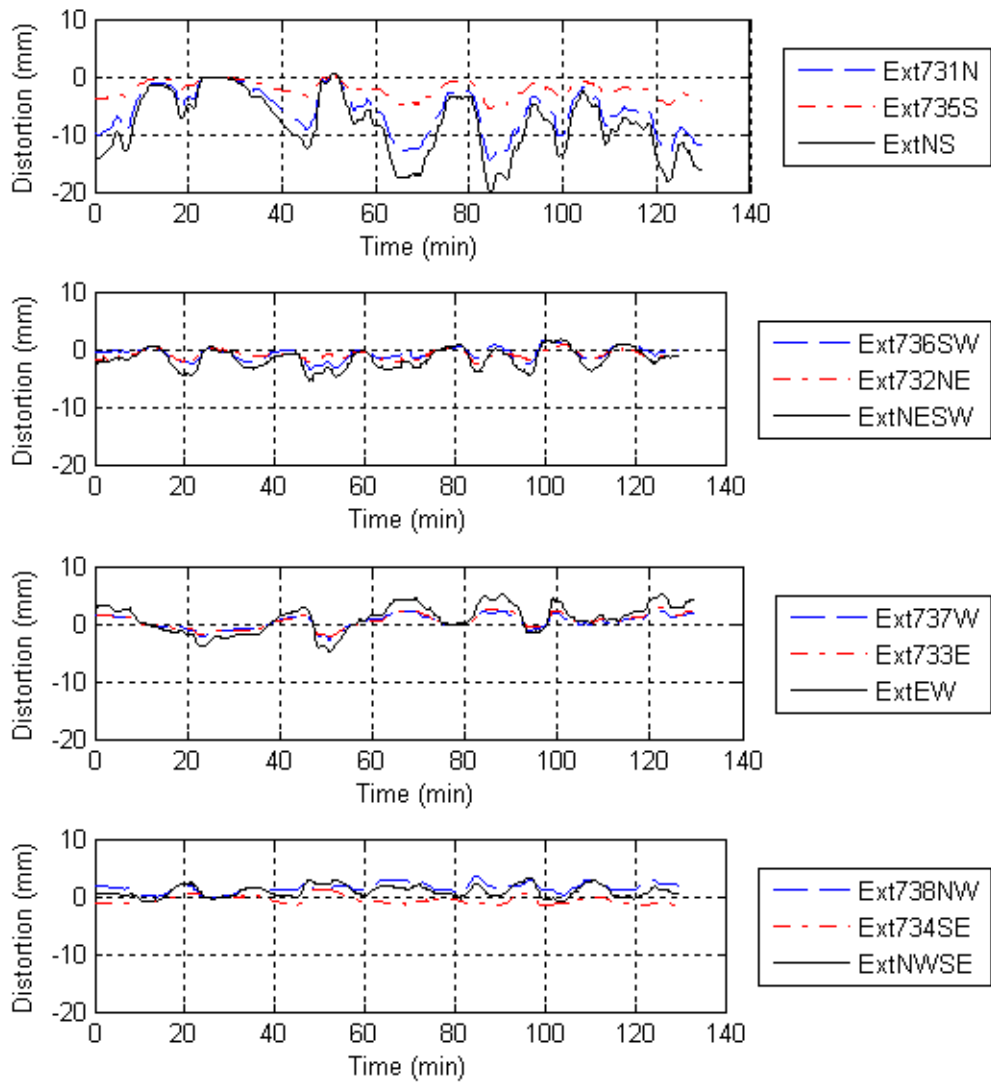
Figure 5-28   **Ring distortion and corresponding extensometer readings.**
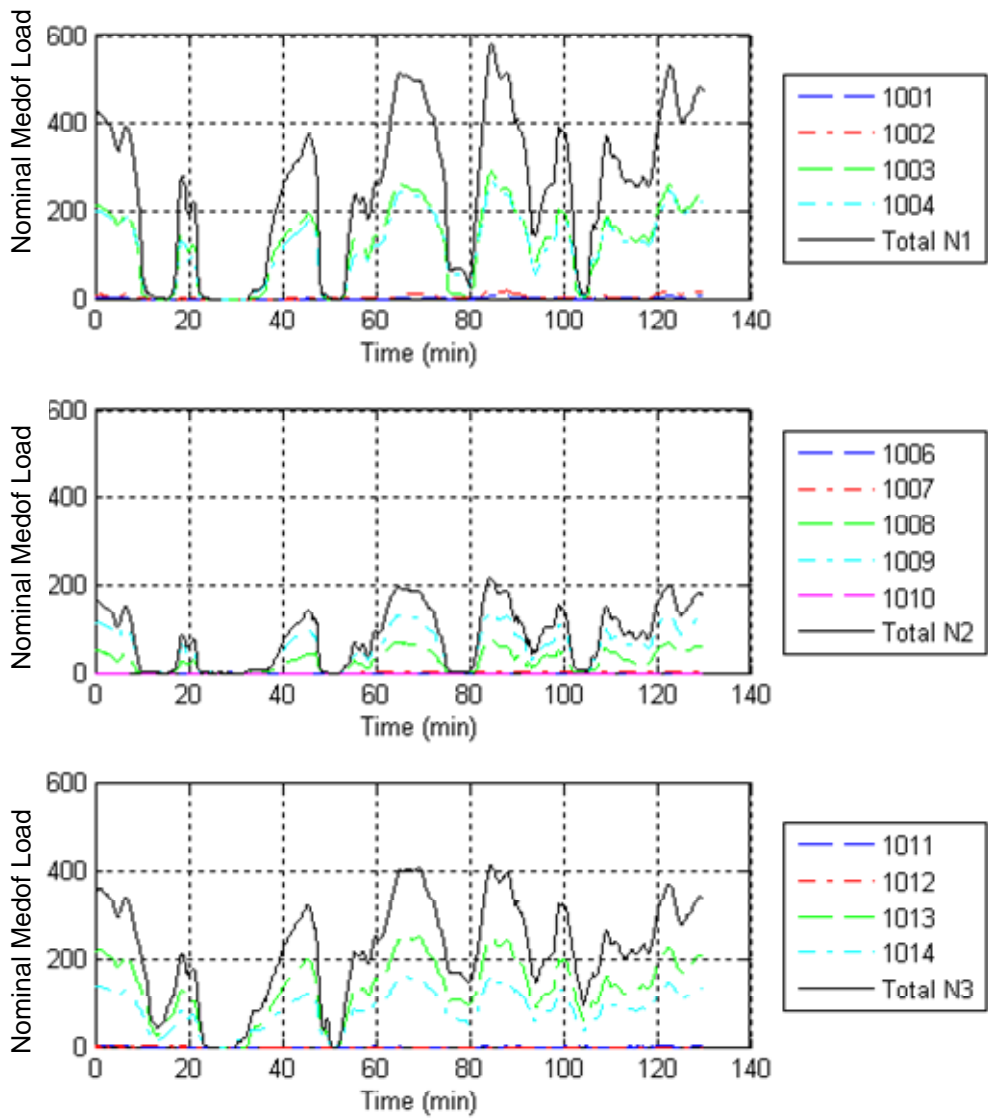
Figure 5-29   Sum of Panel Loads for Different Medof Groups on the North Face
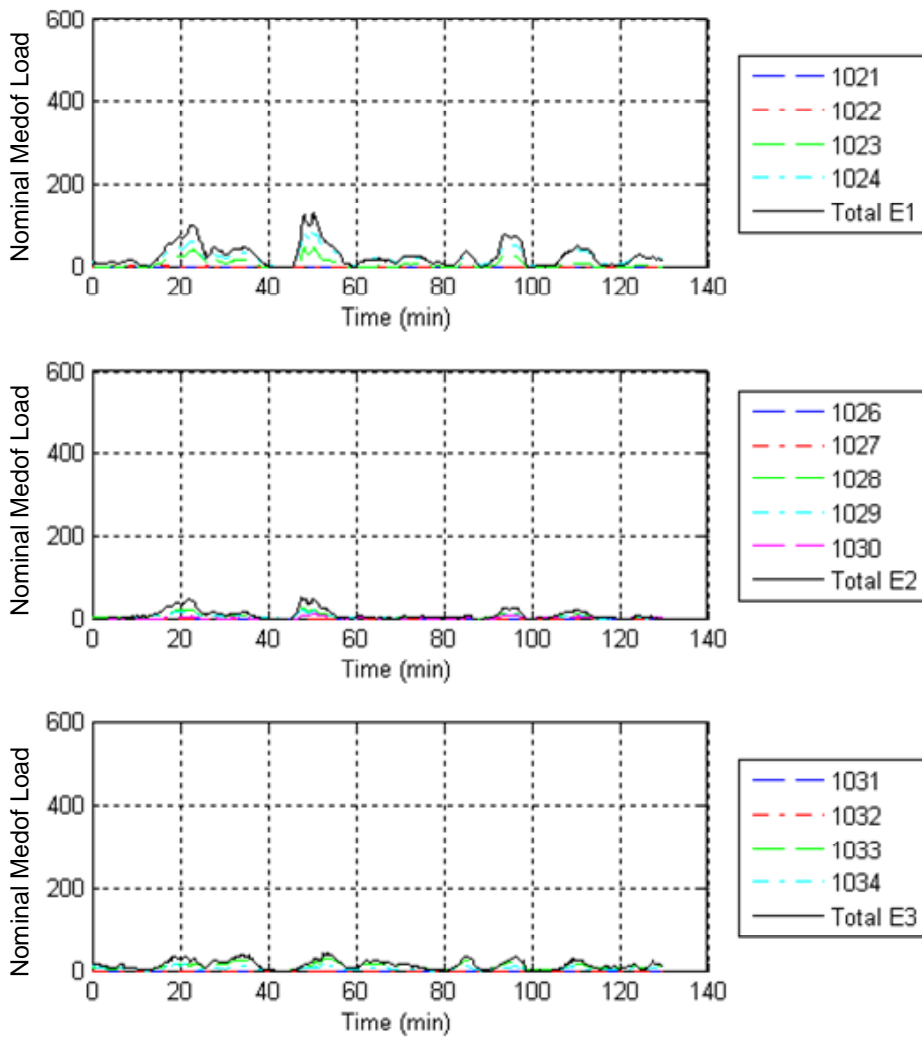
Figure 5-30   Sum of Panel Loads for Different Medof Groups on the East Face
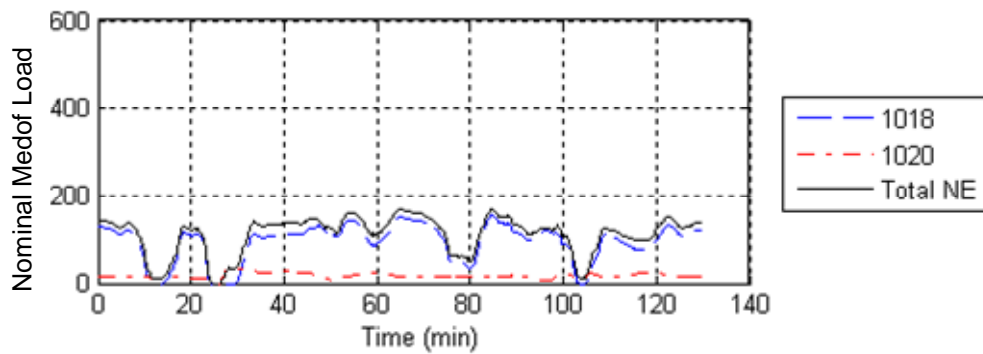
Figure 5-31   Sum of Panel Loads for Medof Group on the North-East Face
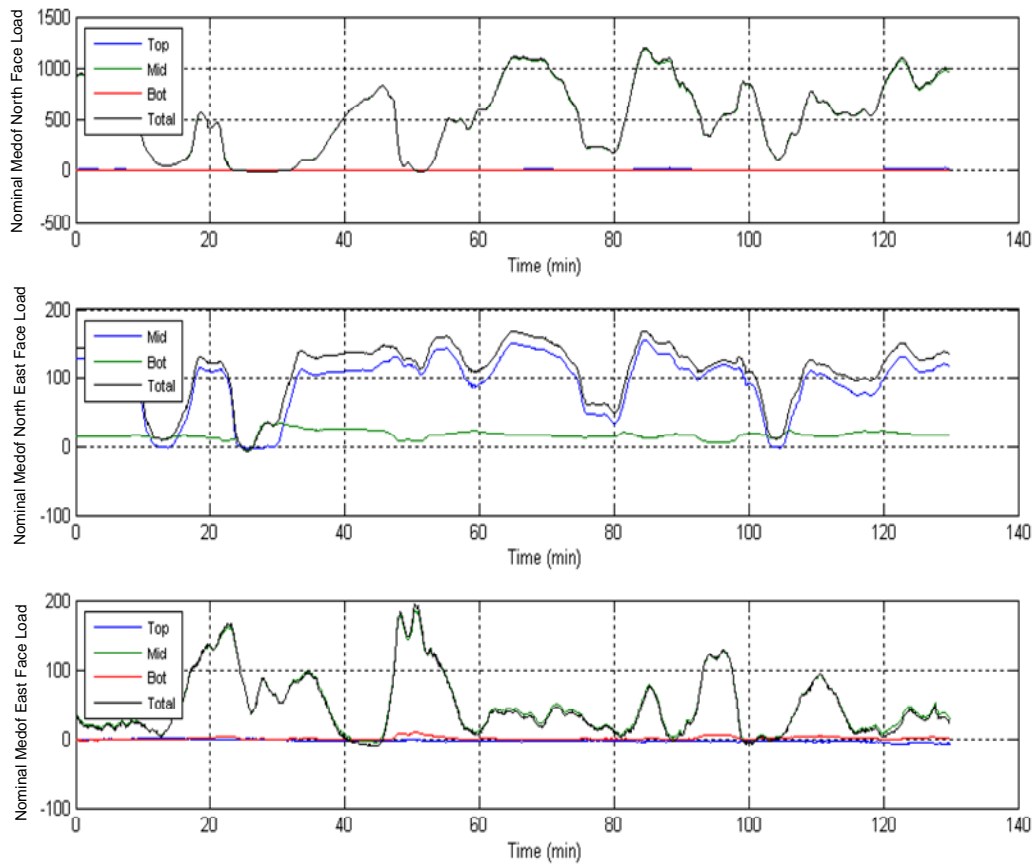
Figure 5-32   Sum of Loads on Top, Middle and Bottom Rows of Panels on Different Faces
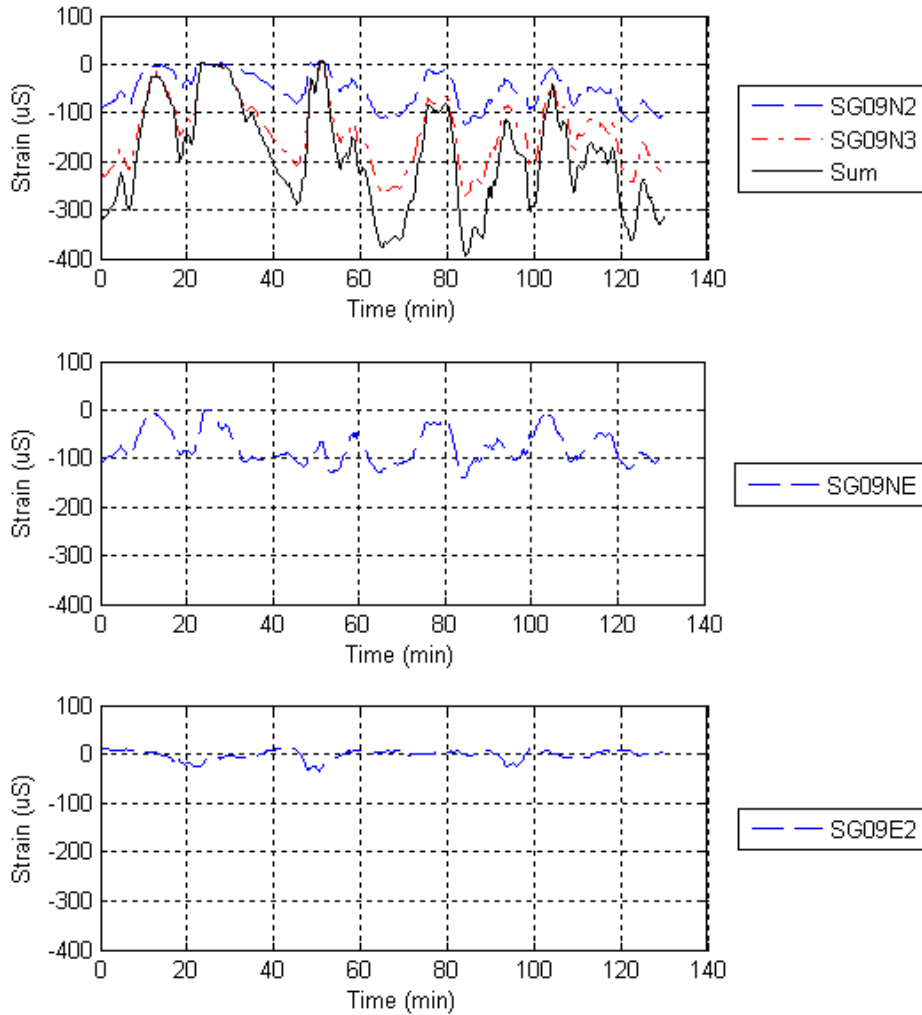
Figure 5-33   Strain Gauge Readings for Different Faces.

5.4.4 Loads Inferred From Extensometer Readings Using Matrix Approach

Figure 5-34 shows face loads inferred from ring distortions using the matrix method and a ring distortion ratio of 2.6 MNmm^{-1}. The top figure shows the ring distortions, the middle figure shows the corresponding estimated loads on the different faces, and the bottom figure shows the global loads in the north and south directions. Loads on the north face slightly over 50 MN are estimated, in agreement with the result based just on the ring distortions. Global loads of approximately 90 MN are estimated. The small negative loads on the north-west face are likely related to problems with zeroing data or to small inaccuracies in the stiffness matrix.
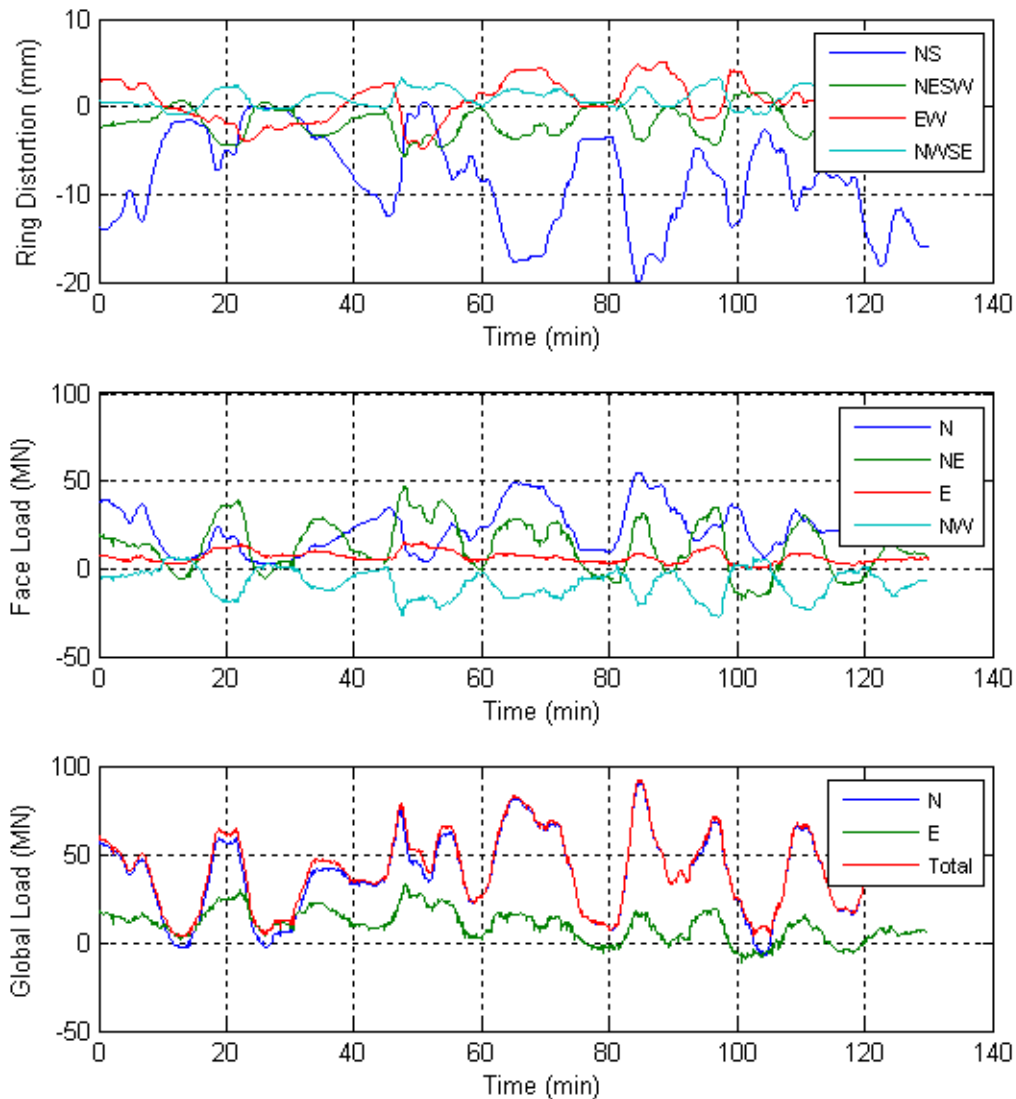
Figure 5-34   Face Loads Inferred from Ring Distortions Using Matrix Method

5.4.5 Analysis of Medof Loads on North Face

This section presents an analysis of the relationship between the loads on different Medof columns on the north face and the N-S ring deformation. By considering the different columns in isolation, it is possible to gain insight into how the face loads develops and to explain the bilinear nature of the plots of extensometer versus Medof panel loads.

Figure 5-35 and Figure 5-36 show the loads on different north face columns versus north-south ring distortion. The load increases on the east side of the north face first, then the west side and finally the middle. When the loads are combined and plotted against ring distortion, one observes a change in slope. In our opinion the effect may be due to two

possible causes. The first is uneven loading and the second is nonlinearity of the polyurethane stress strain curve as well as the Mullins effect.

Figure 5-37 through Figure 5-50 show the loads on different north face columns versus north-south ring distortion for specific time intervals (cycle loading and unloading). This makes it easier to see the sequence of loading across the face. For example, during the unloading in Figure 5-37, the middle (N2) columns unload first, followed by the columns on the west side of the face (N1), then the columns (N3) on the east side of the face. The overall effect appears to be a bilinear fit (average load shown in black), whereas this might result from loadings at different times and magnitude across the face.

Figure 3-15 illustrates another possible cause which relates to the Mullins effect. This is a result of the stress strain non-linearity of the Medof panel polyurethane buttons.

The N2 and N3 pairs of Medof columns show significant difference in magnitude between the adjacent columns as seen in the figure (and for other time intervals in subsequent figures as well). The loads on the adjacent columns could of course be different (note also that there is not significant bottom panel load); but they could also be a result of differences in the Medof panel calibration constants.

Further analysis of the intercepts for the different load cycles may be of interest. Columns that load early will take more of the total load and should have positive intercepts. Columns that load later will take less of the total load and should have negative intercepts.

The curves for loading and unloading differ. Figure 5-51 through Figure 5-56 show the loading and unloading portions of cycles 2 through 7 together on the same plots. There is a hysteresis effect when the average Medof panel loads (treated as strain) give lower values corresponding to a given ring distortion (treated as load) during the loading phase than the unloading phase. Figure 5-57 through Figure 5-61 show north face strain gauge response versus ring distortion for the same cycles for comparison.
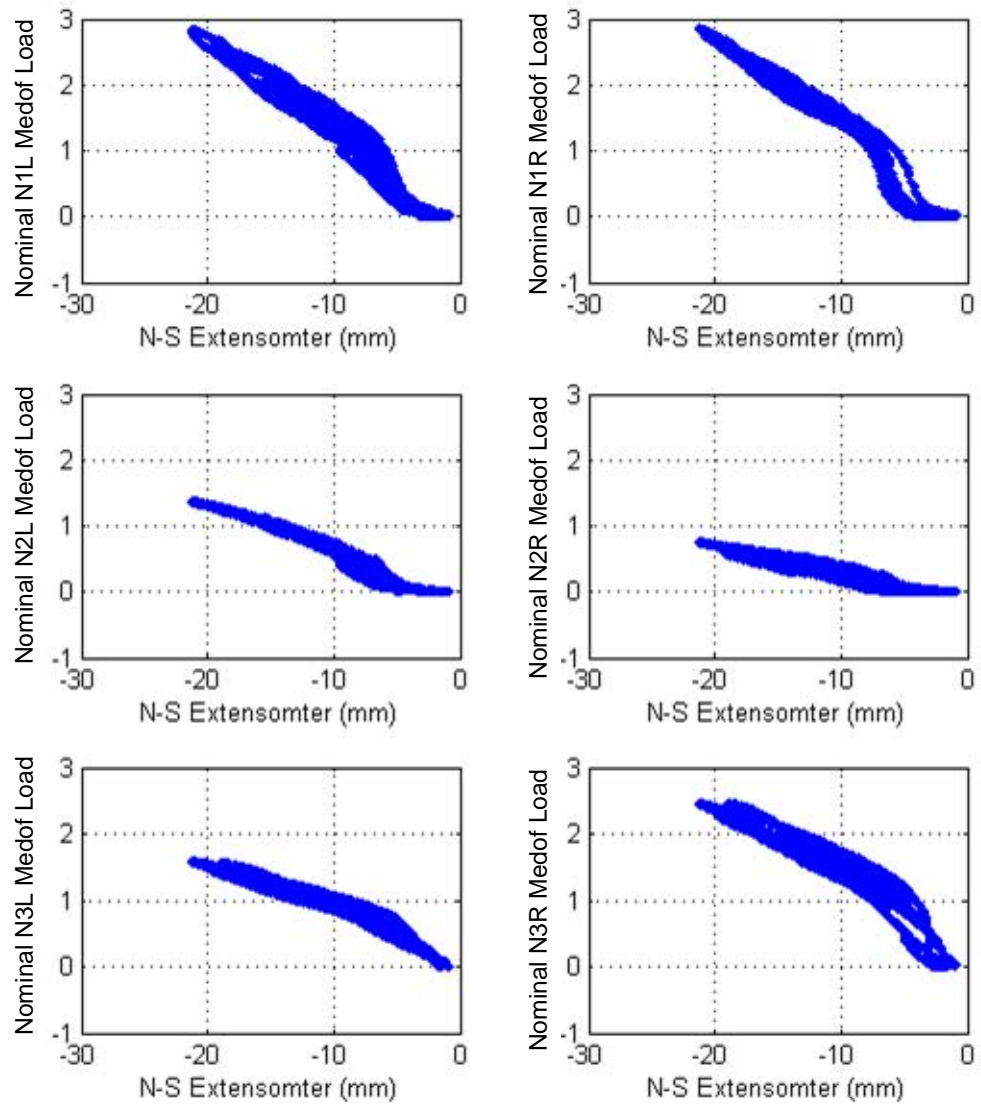
Figure 5-35   **Loads on Different North Face Columns versus North-South Ring Distortion**
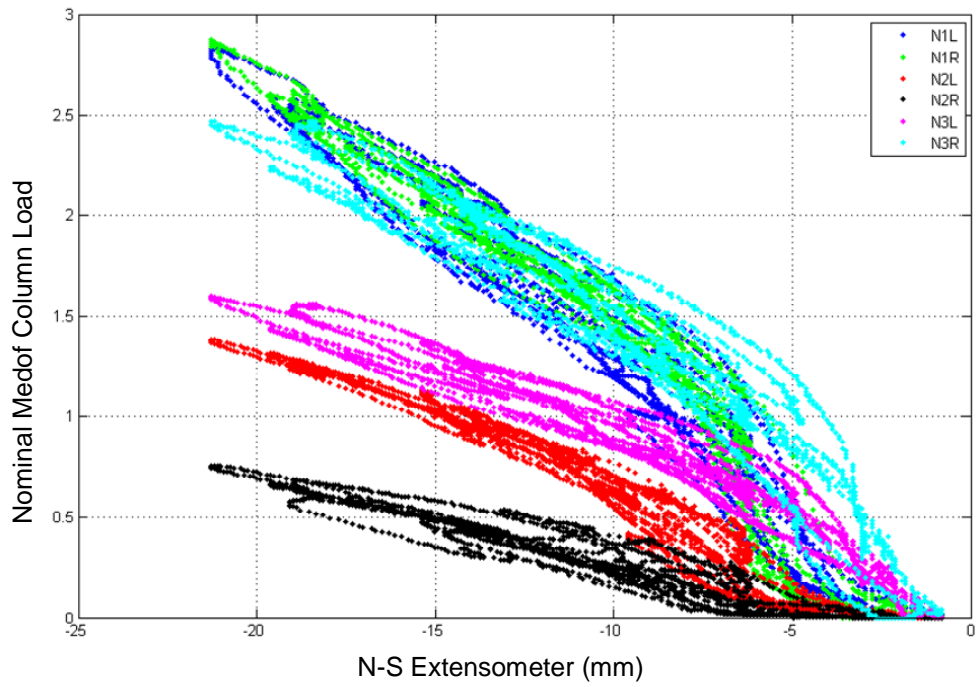
Figure 5-36   Loads on Different North Face Columns versus North-South Ring Distortion (Combined in one Plot)
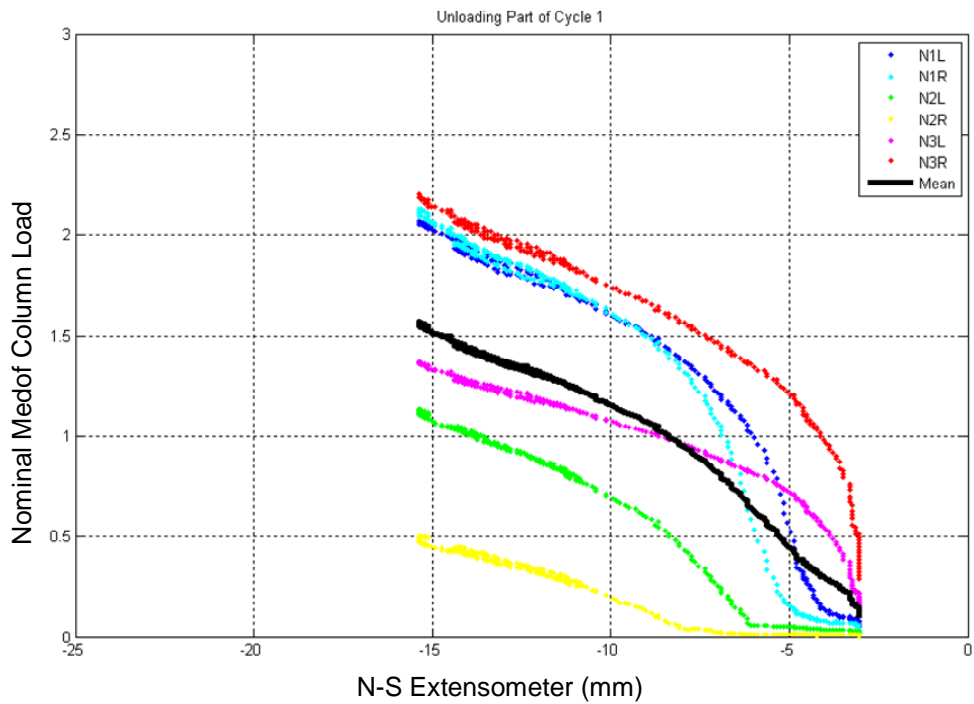
Figure 5-37   Medof Column Loads versus North-South Distortion for Unloading Part of First Cycle (only unloading part available)
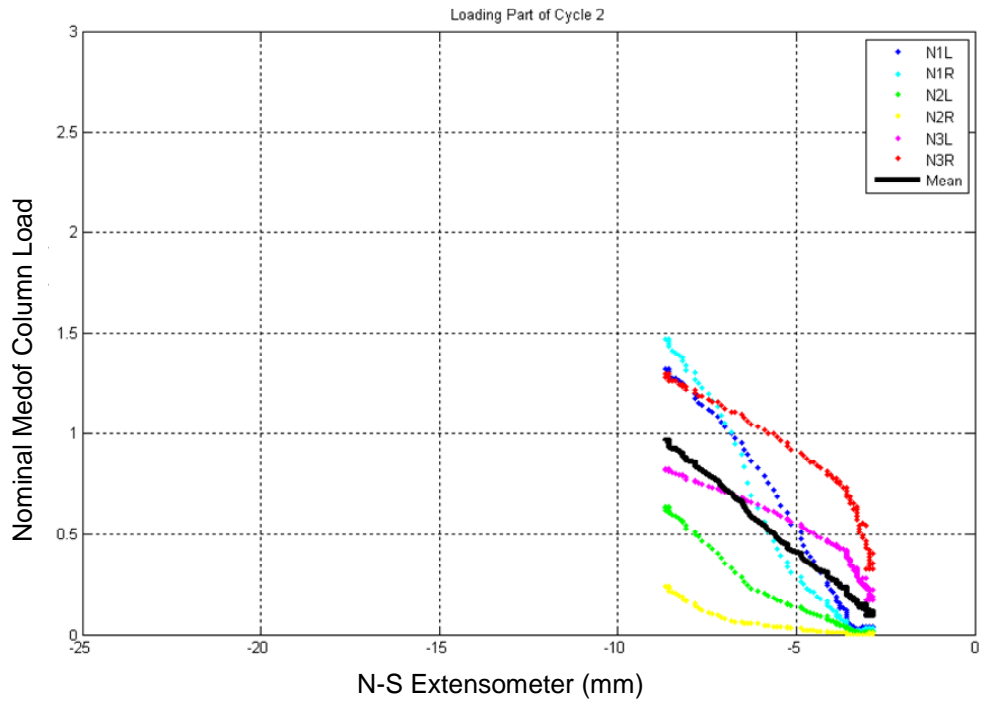
Figure 5-38   Medof Column Loads versus North-South Distortion for Loading Part of Second Cycle
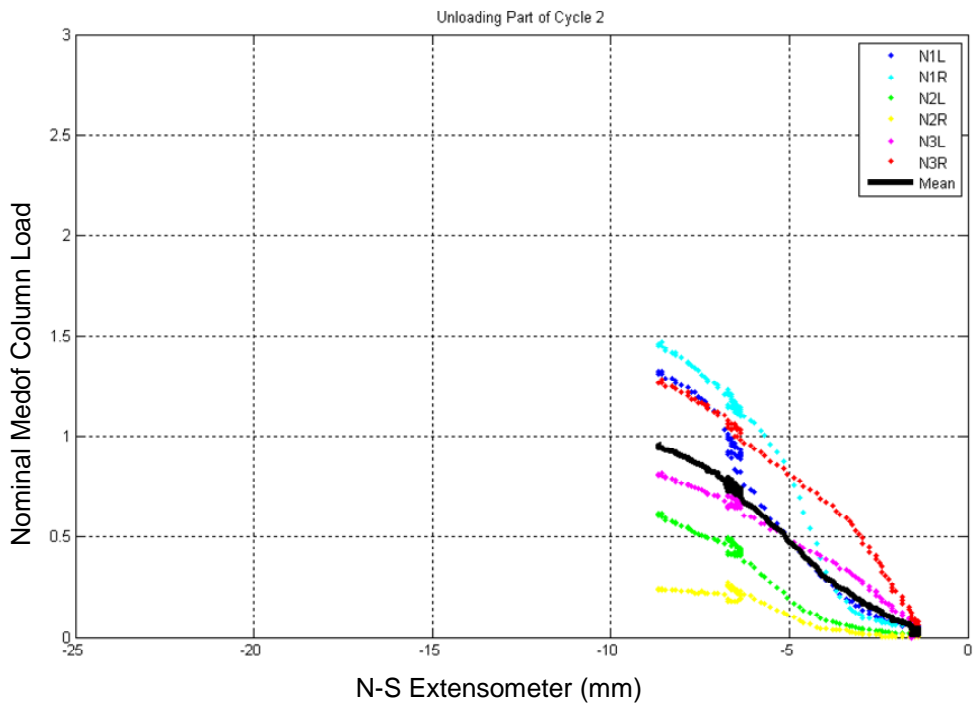
Figure 5-39   Medof Column Loads versus North-South Distortion for Unloading Part of Second Cycle
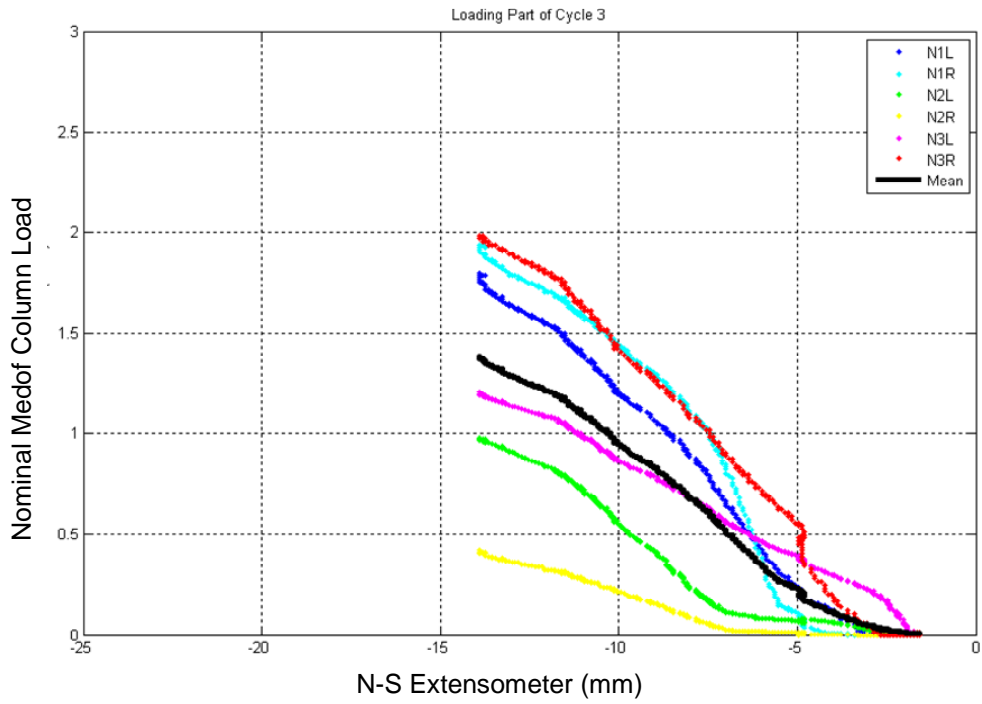
Figure 5-40 **Medof Column Loads versus North-South Distortion for Loading Part of Third Cycle**
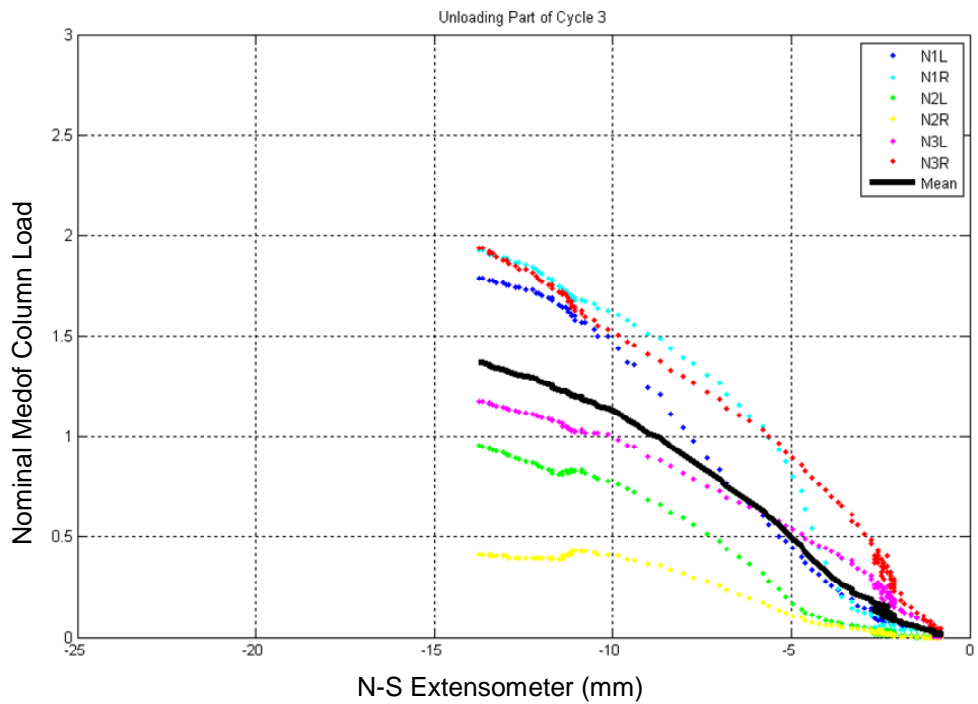
Figure 5-41 **Medof Column Loads versus North-South Distortion for Unloading Part of Third Cycle**
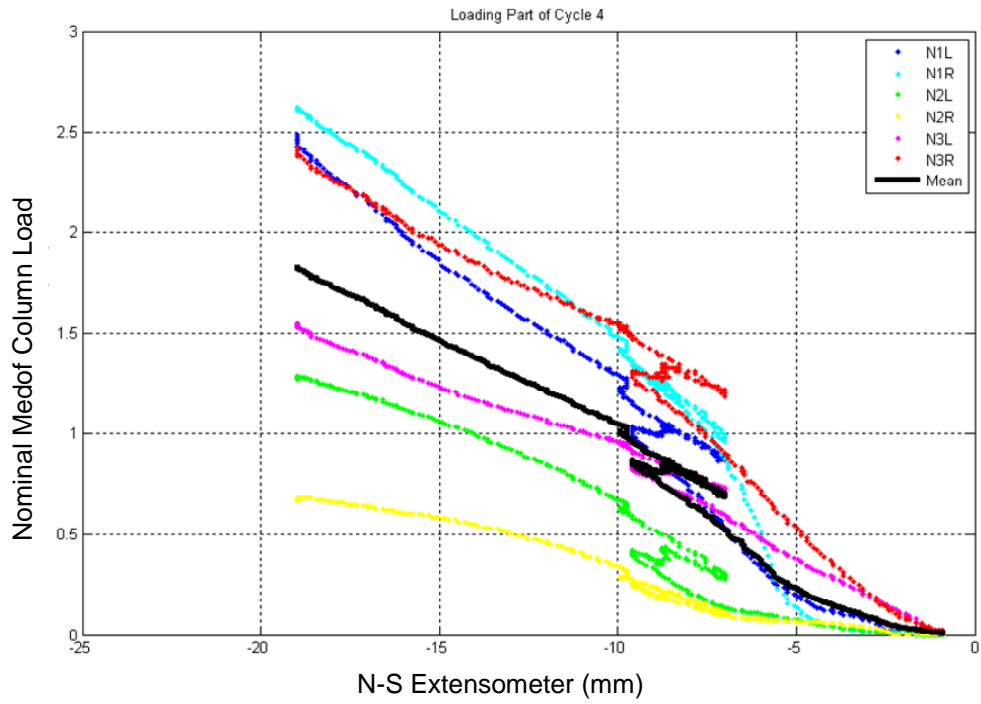
Figure 5-42   Medof Column Loads versus North-South Distortion for Loading Part of Fourth Cycle
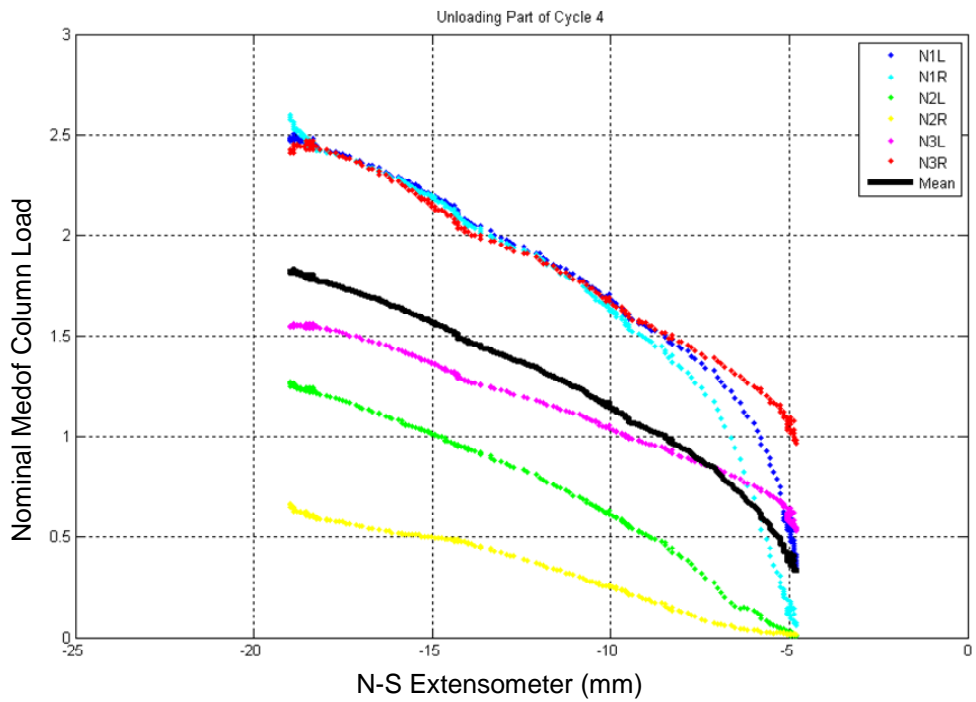
Figure 5-43   Medof Column Loads versus North-South Distortion for Unloading Part of Fourth Cycle
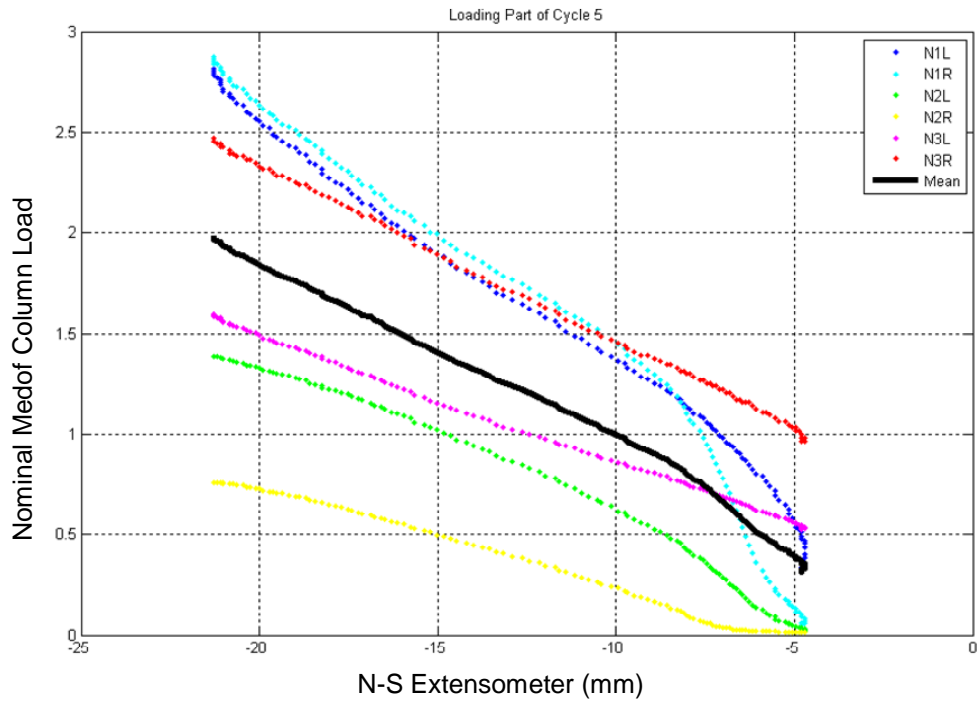
Figure 5-44   Medof Column Loads versus North-South Distortion for Loading Part of Fifth Cycle
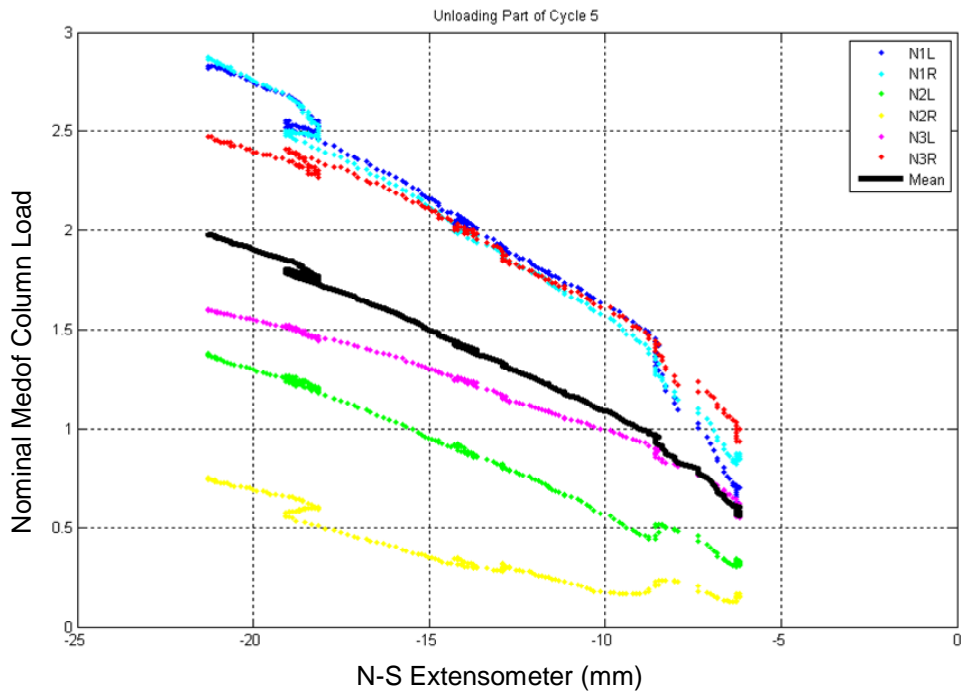
Figure 5-45   Medof Column Loads versus North-South Distortion for Unloading Part of Fifth Cycle
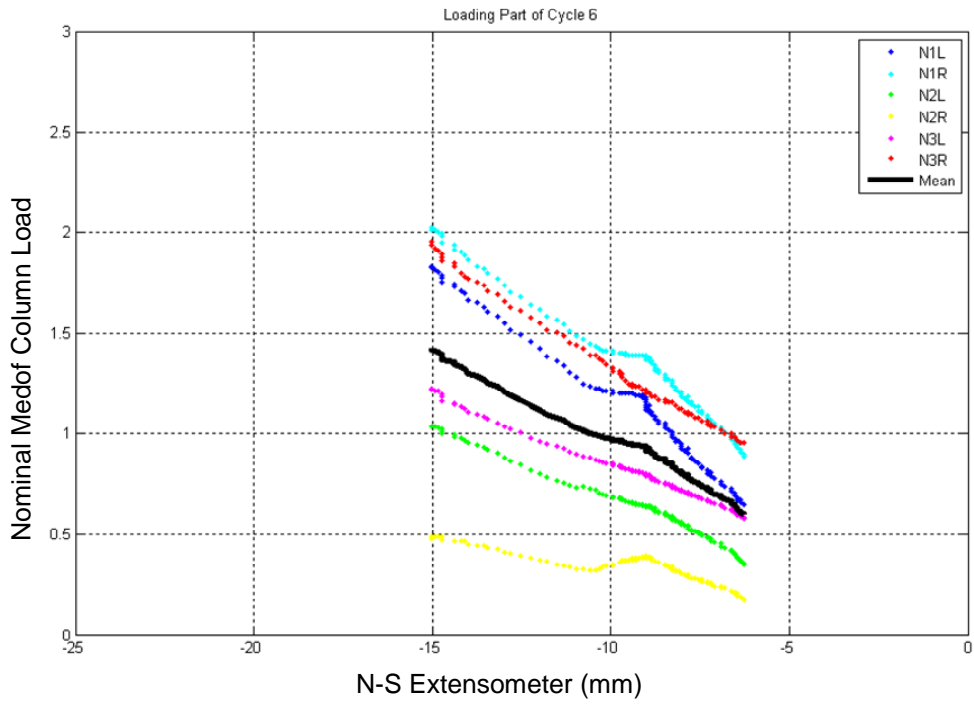
Figure 5-46   **Medof Column Loads versus North-South Distortion for Loading Part of Sixth Cycle**
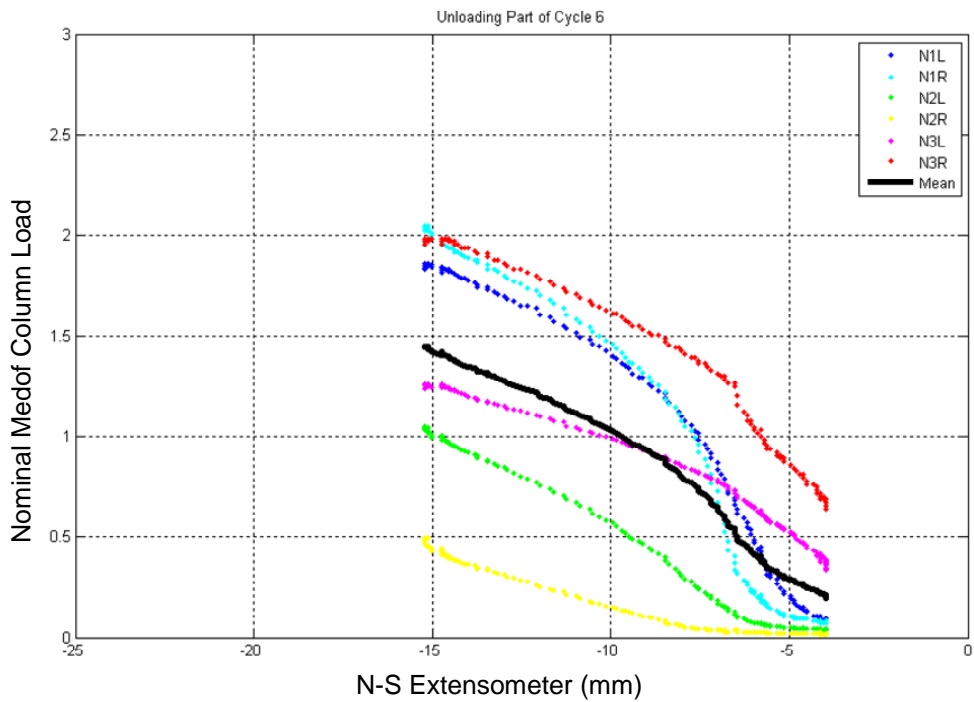
Figure 5-47   **Medof Column Loads versus North-South Distortion for Unloading Part of Sixth Cycle**
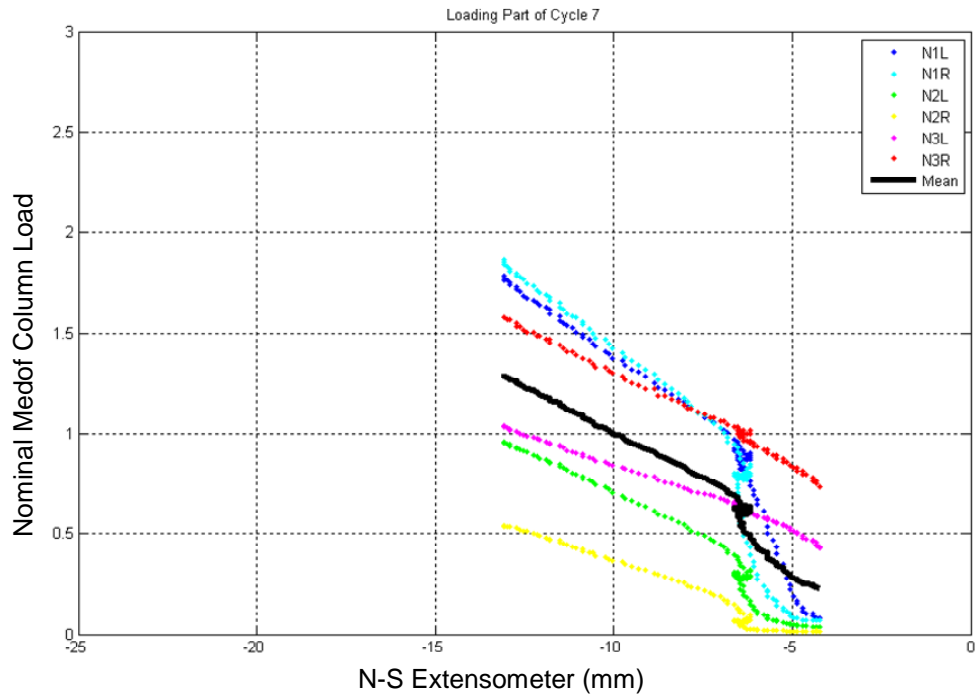
Figure 5-48   **Medof Column Loads versus North-South Distortion for Loading Part of Seventh Cycle**
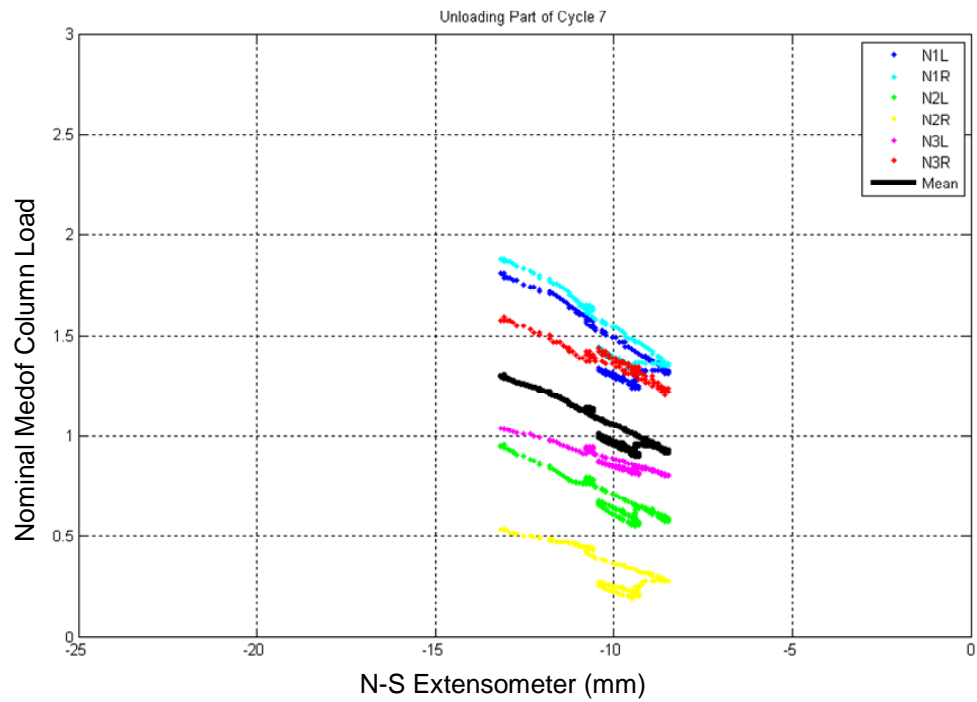
Figure 5-49   **Medof Column Loads versus North-South Distortion for Unloading Part of Seventh Cycle**
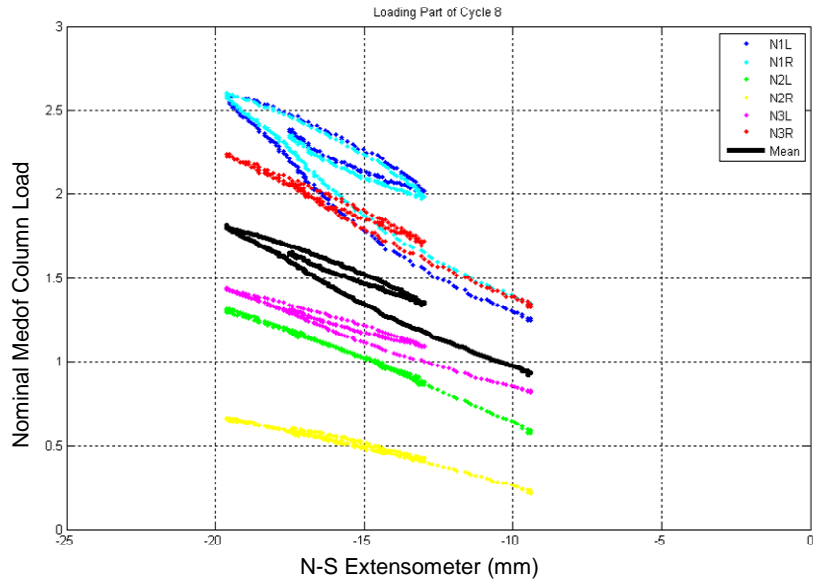
Figure 5-50 **Medof Column Loads versus North-South Distortion for Loading Part of Eigth Cycle (only loading part available)**
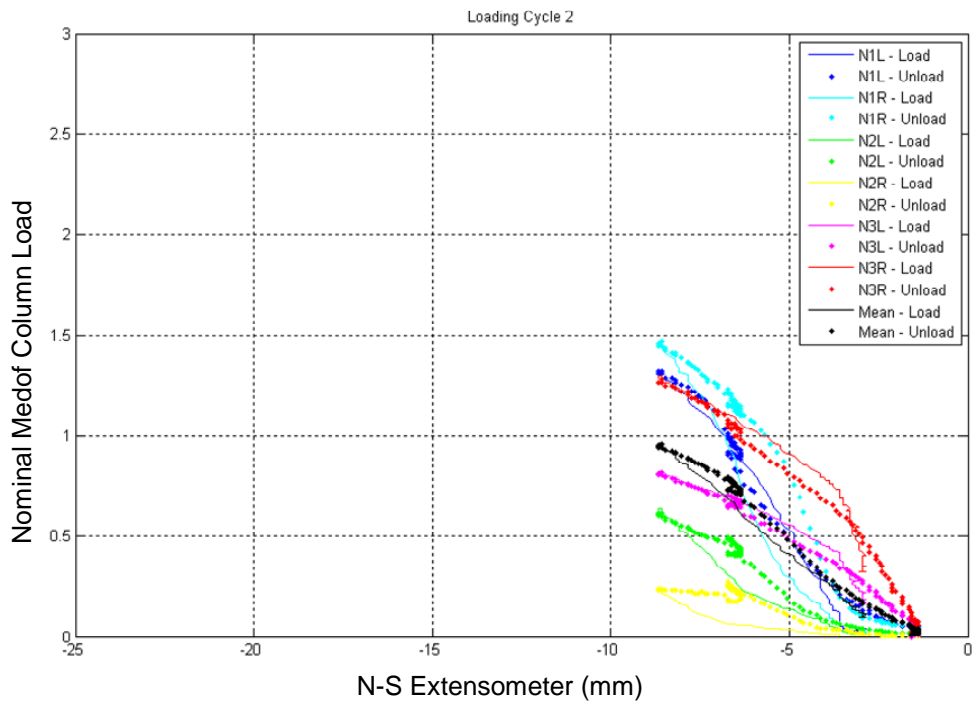
Figure 5-51 **Medof Column Loads versus North-South Distortion – Loading and Unloading During Cycle Two**
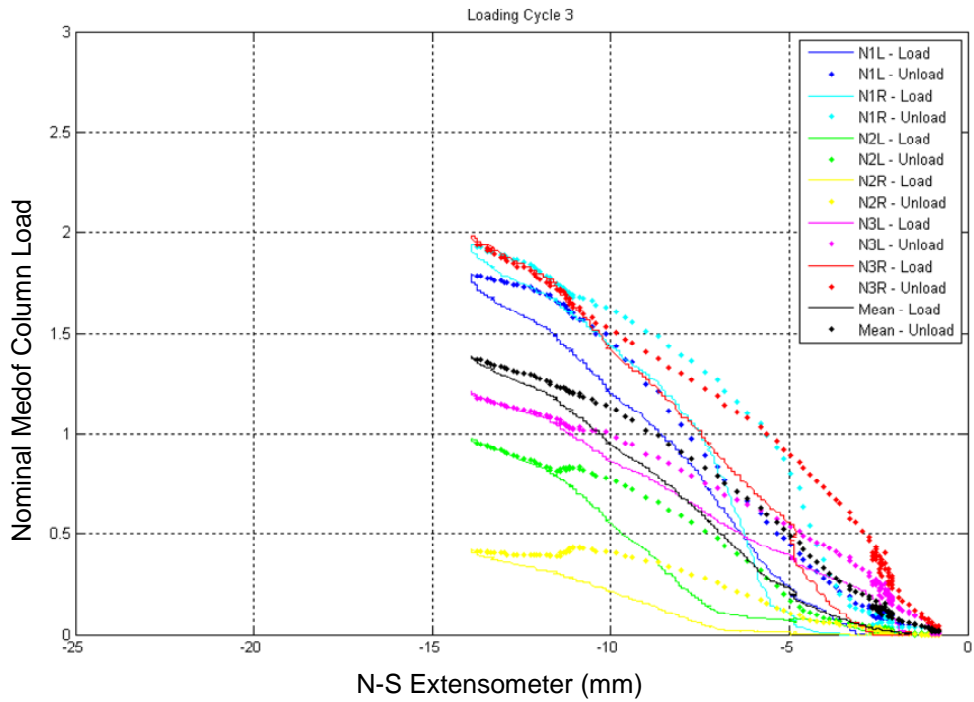
Figure 5-52   **Medof Column Loads versus North-South Distortion – Loading and Unloading During Cycle Three**
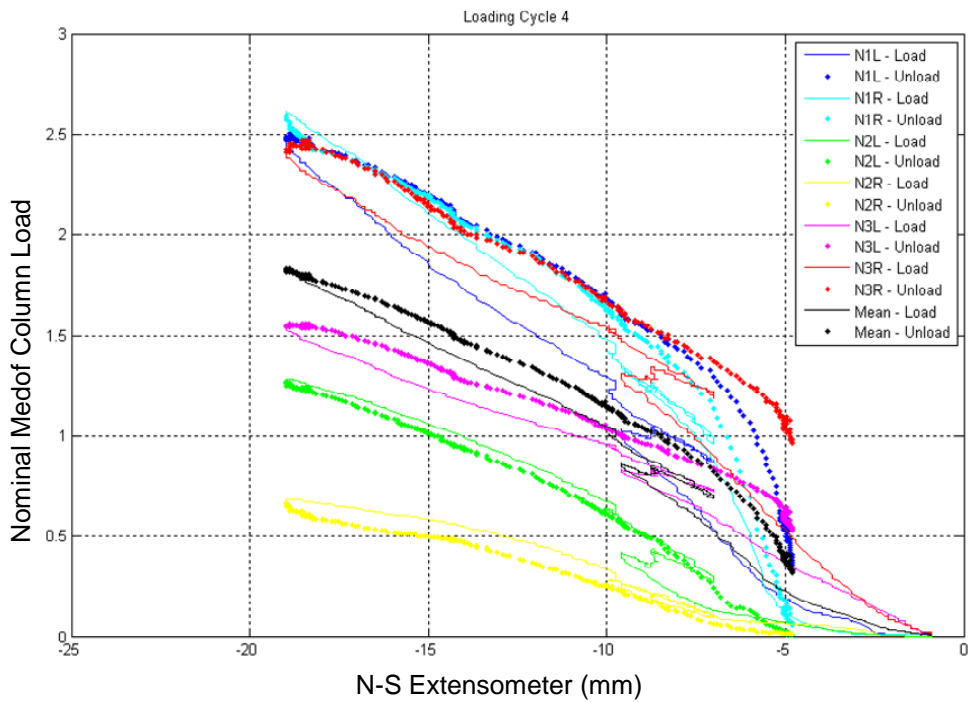
Figure 5-53   **Medof Column Loads versus North-South Distortion – Loading and Unloading During Cycle Four**
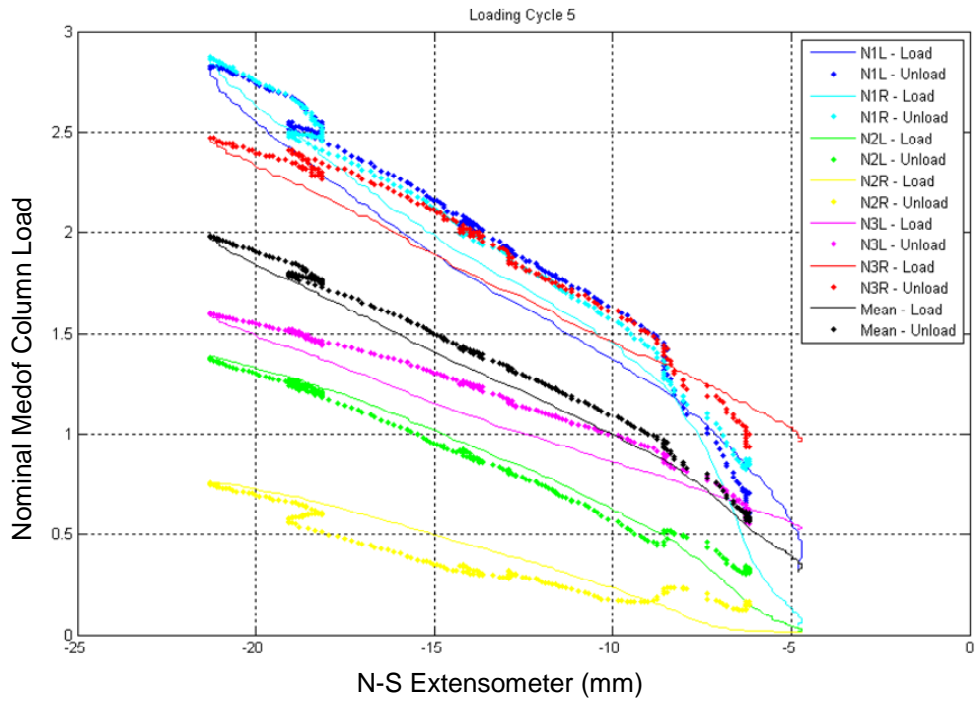
Figure 5-54   **Medof Column Loads versus North-South Distortion – Loading and Unloading During Cycle Five**
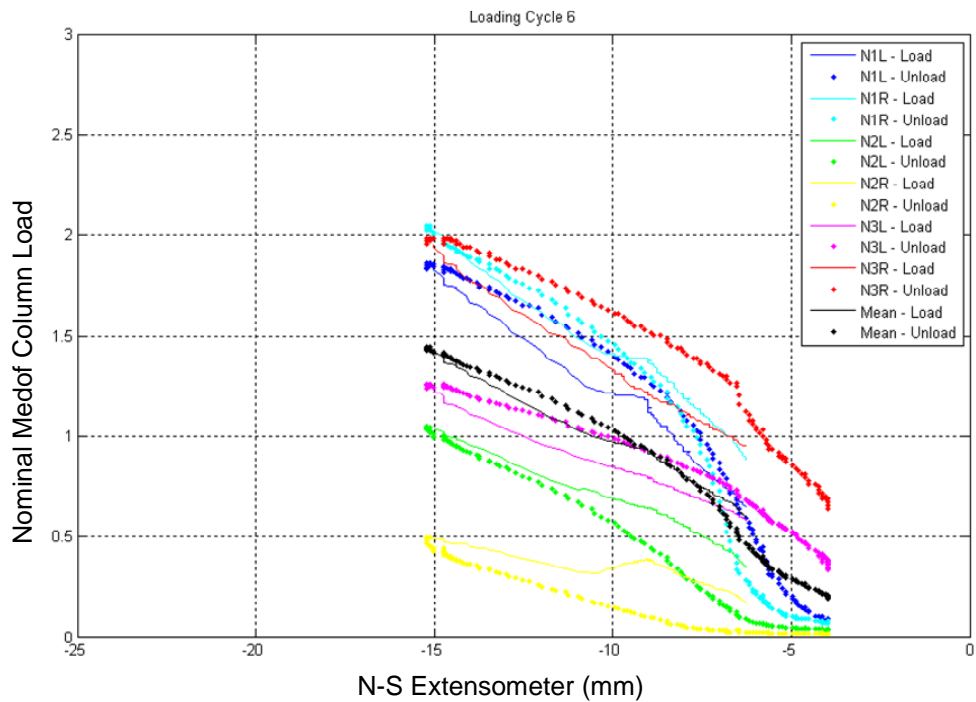
Figure 5-55   **Medof Column Loads versus North-South Distortion – Loading and Unloading During Cycle Six**
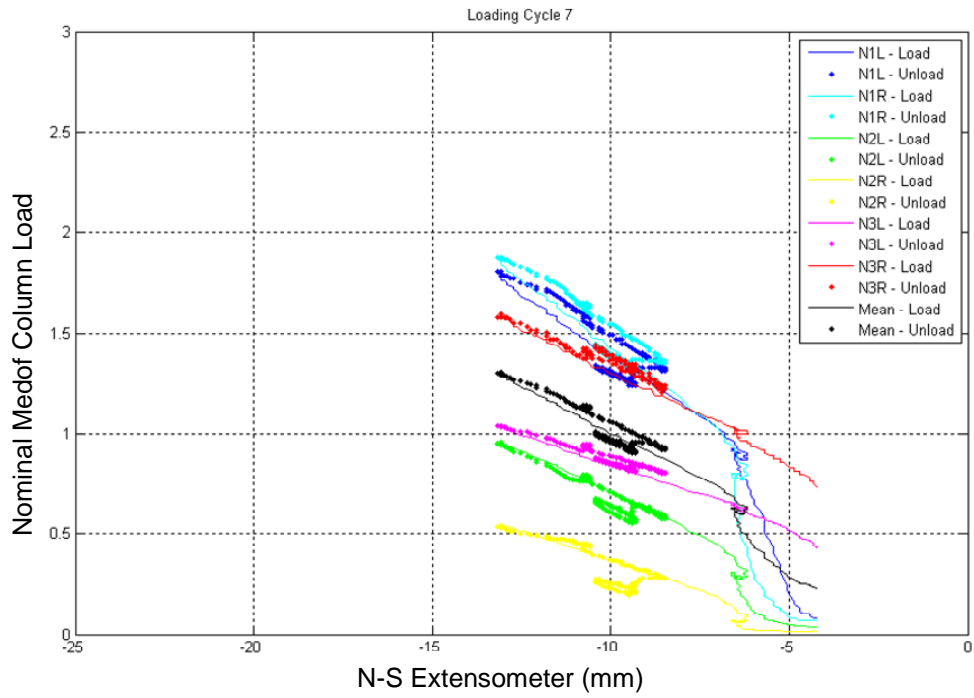
Figure 5-56   Medof Column Loads versus North-South Distortion – Loading and Unloading During Cycle Seven
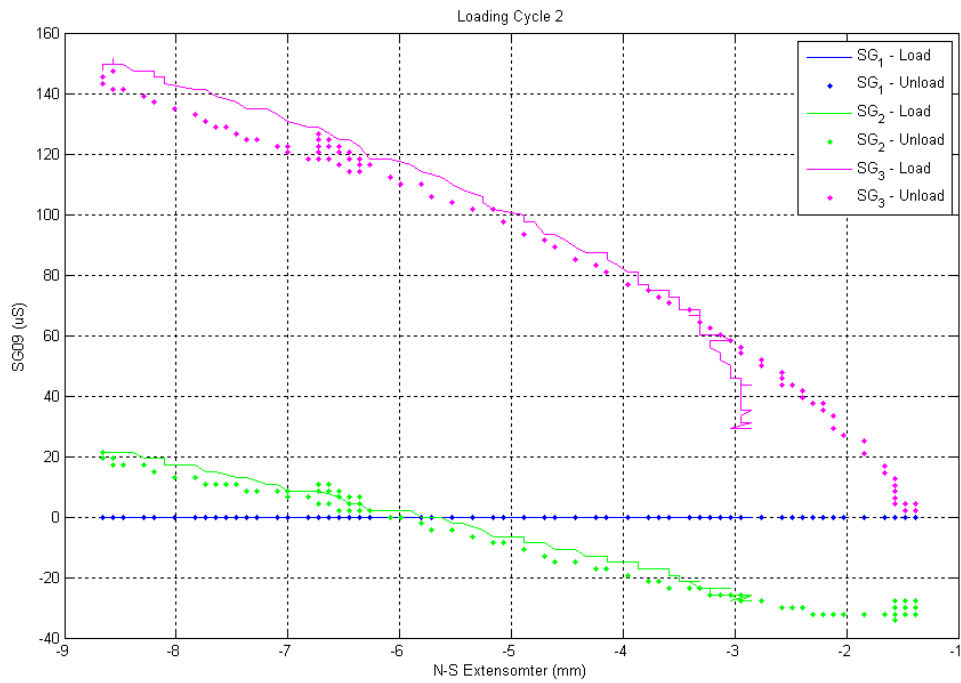
Figure 5-57   Strain Gauge 1 versus North-South Distortion – Loading and Unloading during Cycle Two
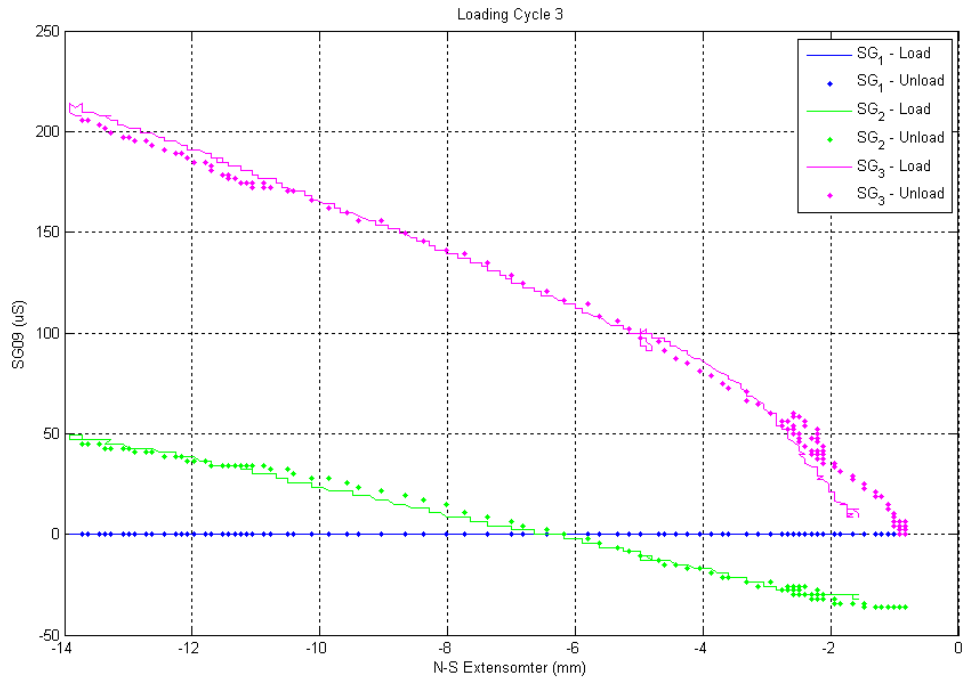
Figure 5-58   Strain Gauge 1 versus North-South Distortion – Loading and Unloading during Cycle Three
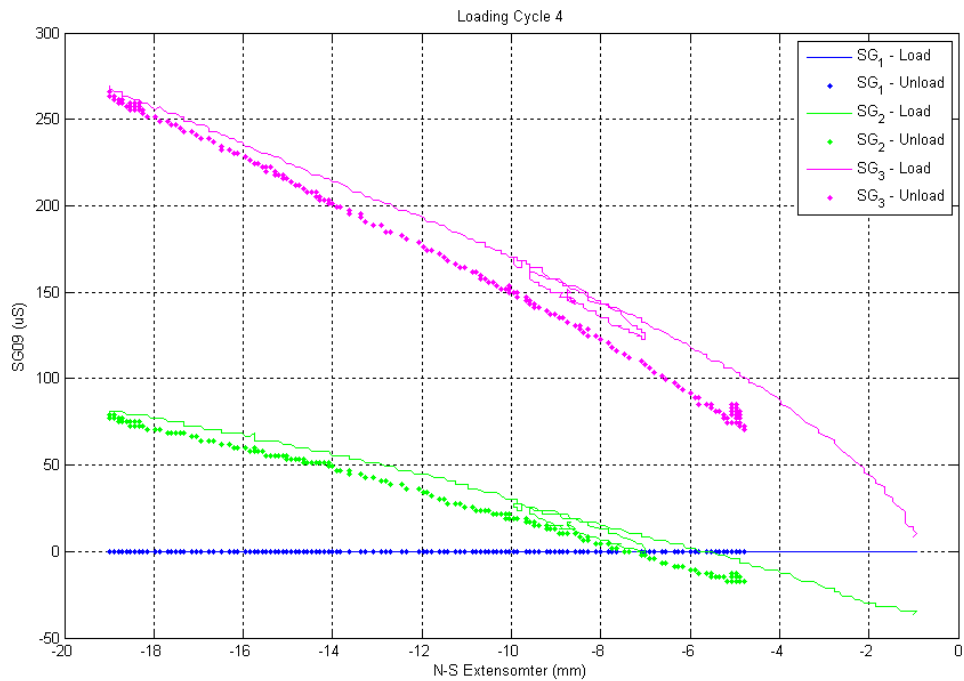
Figure 5-59   Strain Gauge 1 versus North-South Distortion – Loading and Unloading during Cycle Four
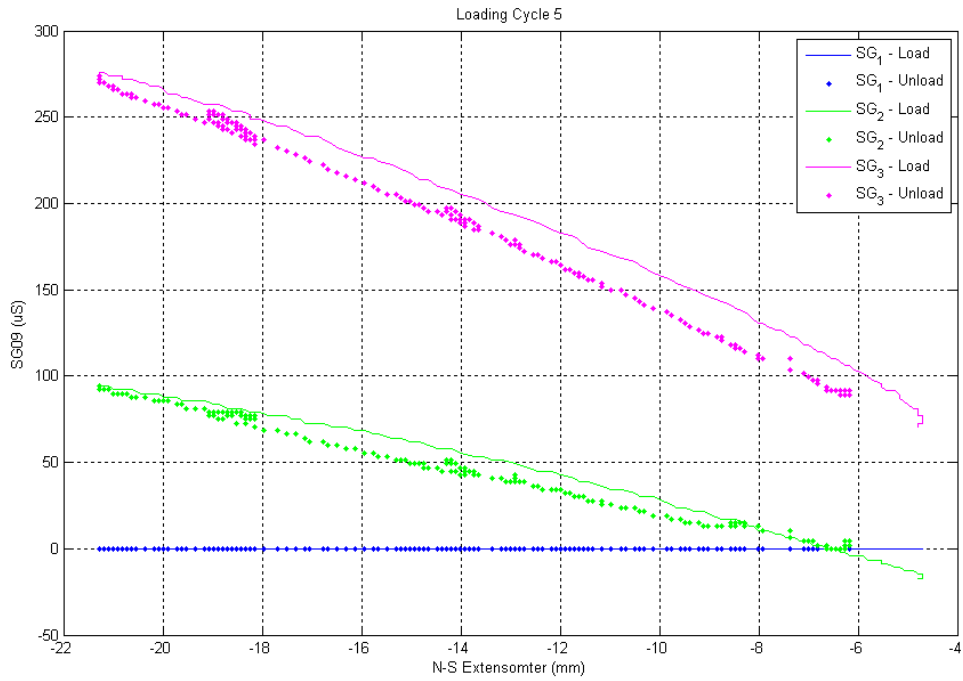
Figure 5-60   Strain Gauge 1 versus North-South Distortion – Loading and Unloading during Cycle Five
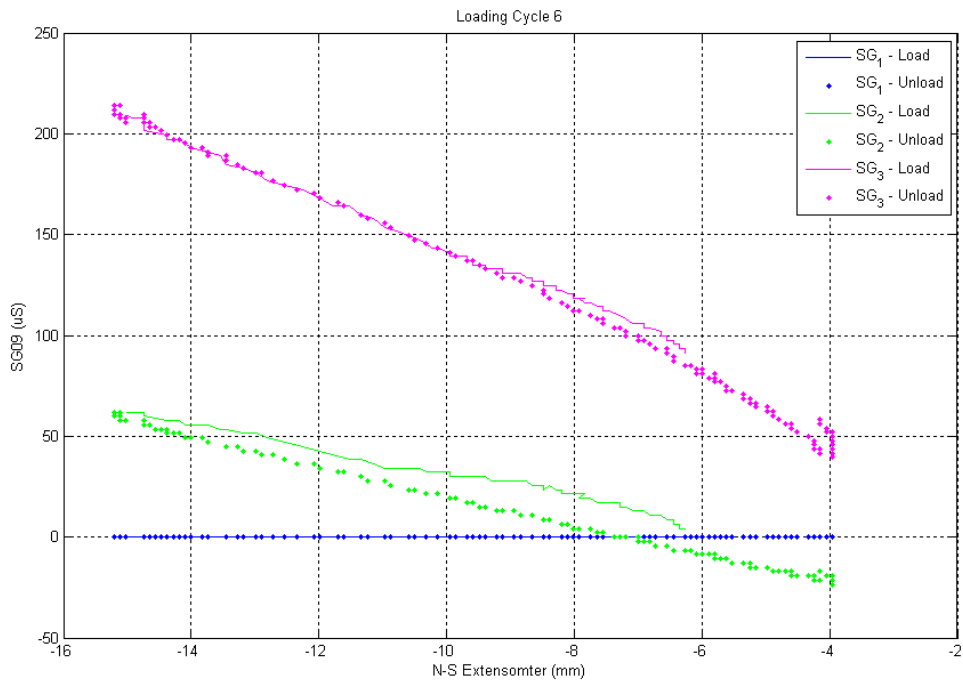
Figure 5-61   Strain Gauge 1 versus North-South Distortion – Loading and Unloading during Cycle Six
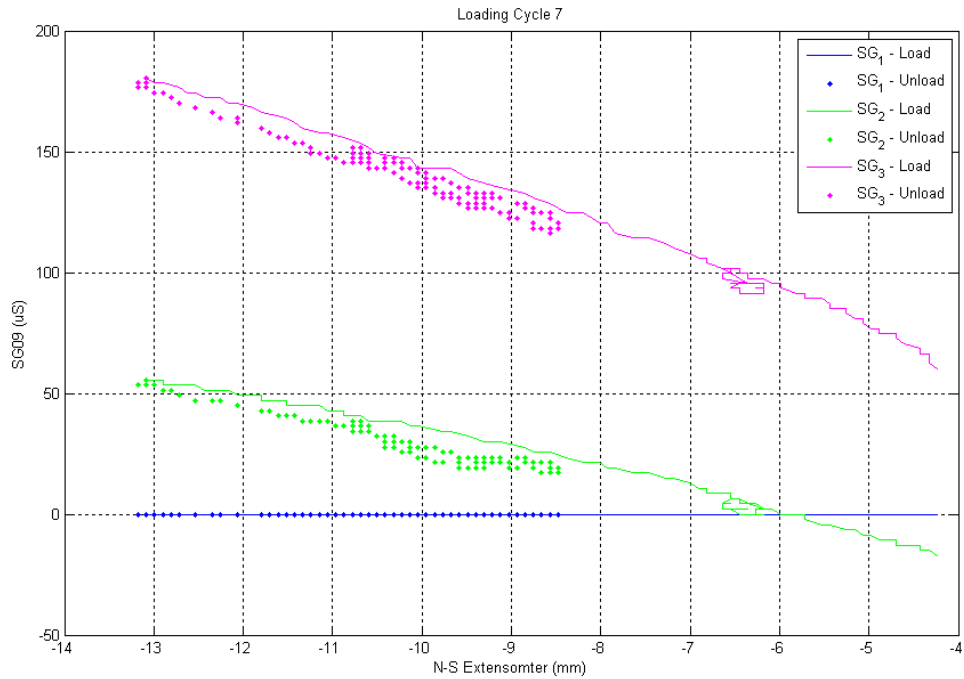
Figure 5-62   Strain Gauge 1 versus North-South Distortion – Loading and Unloading during Cycle Seven

5.4.6 Concluding Remarks for March 25 (B), 1986 Event

The March 25th, 1986 event was a creep loading event which involved the predominant loading of the North face with some loading occurring on the North West and North East faces. This event represents a good case for analyzing the face loads estimated by extensometers, with calibration of Medof panels to the extensometer load. The analysis of the extensometers has brought the Phase 1 Medof panel face load estimate of approximately 102 MN down to 55 MN using a face load ring distortion ratio of 2.6 MNmm[-1].

5.5   Event 0307A - March 7, 1986 – f603071520

Event ID – 0307A
Crushing Event
Ice Thickness: 3.5 to 10m
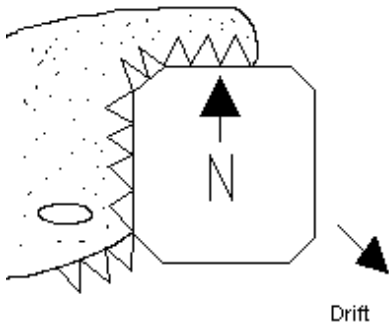
5.5.1 Dynamac Event Description

On March 7th, the Molikpaq penetrated a multi-year floe. Cracks formed early in the event (1545) but did not widen significantly until the end of the event (1700). Dynamic load began when a 50 m long 2 m high hummock came into contact with the west face at a speed of 0.05 m/s. The hummock was crushed along its longitudinal axis, producing continuous crushing with frequencies of 1 Hz. The rubble cleared around the north and south sides of the caisson. At 1606 severe global confinement of the ice prevented the rubble from the west face from clearing and so this rubble became stationary and most likely grounded on the berm. At 1616 a series of radial fractures formed off the NW. The ice direction veered from 130^0 to 160^0 and most of the load was suddenly transferred to the north face. "Extrusion and Collapse" sequences continued until the ice stopped moving.

Figure 5-63 shows the magnitude of loading occurring on the North, North East and East faces during the event. Note that there was significant loading occurring on the West and North West faces of the structure which could not be captured using the Medof panels.
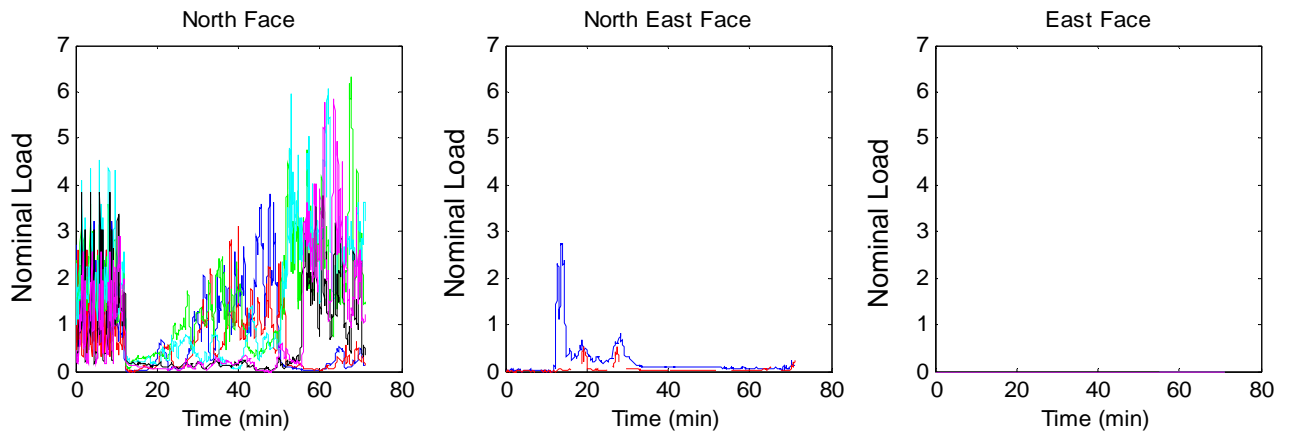
Figure 5-63   Nominal Medof column loads acting on the North, North East and East faces
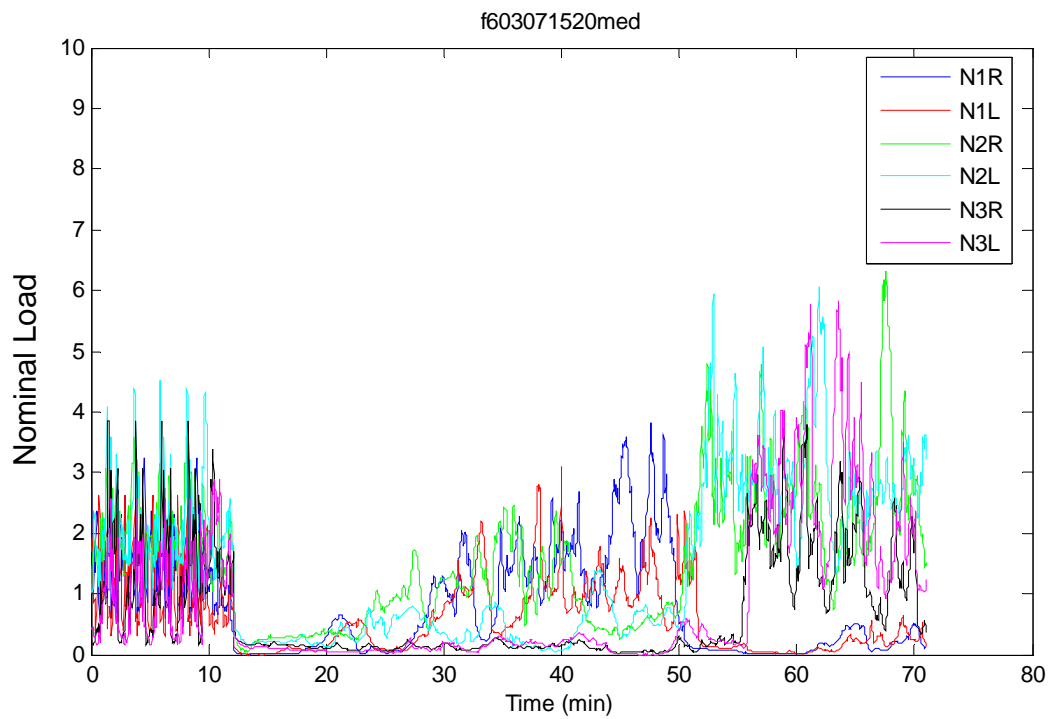
Figure 5-64   Nominal Medof column load acting on the North face of the Molikpaq structure
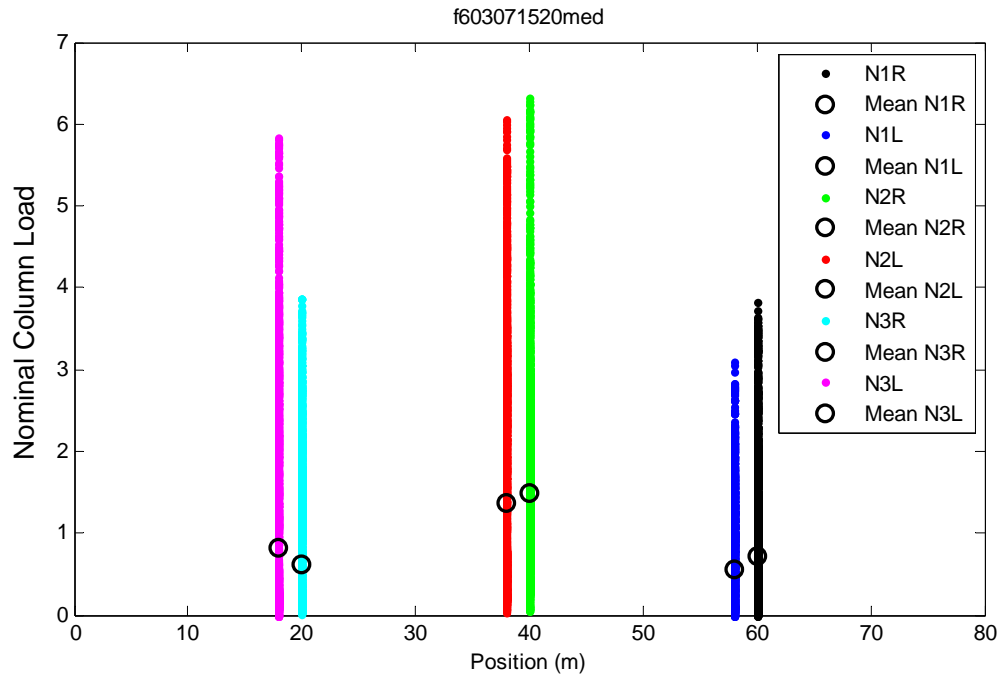
Figure 5-65: **Distribution of Medof nominal column ice loading on the face of the structure**
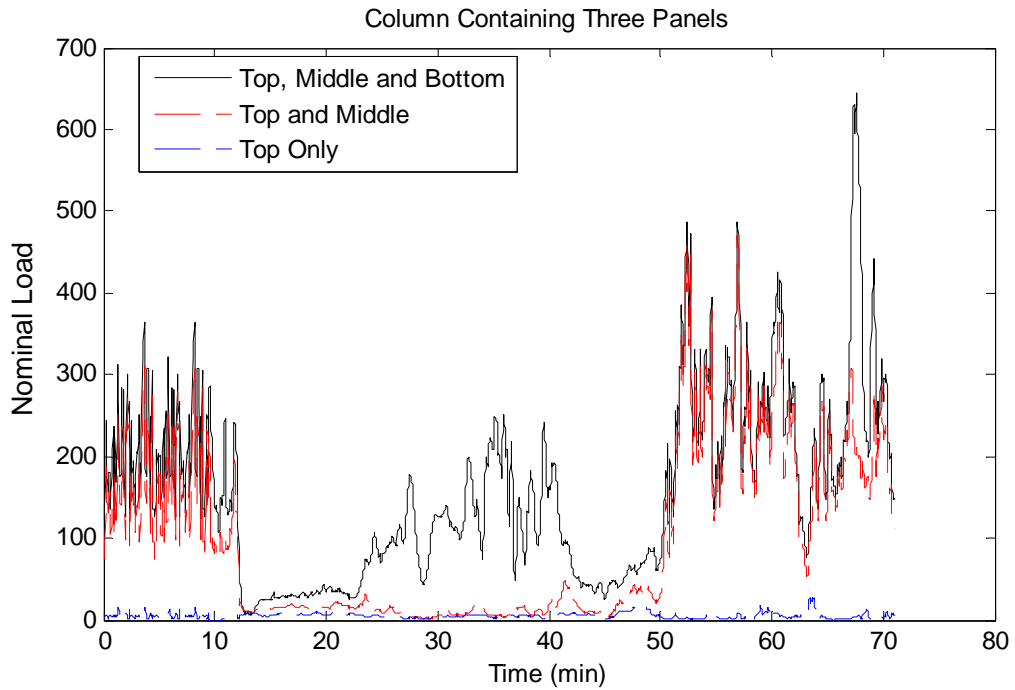
Figure 5-66: **Loading on top, middle and bottom panels in column N2R.**

5.5.2 Analysis of Face Loads Acting on the Structure

The extensometers have been used to calculate the ice loads acting on the north face of the Molikpaq structure. Figure 5-67 shows the probabilistically averaged face load calculated from phase 1 using the Medof panels which has been factored to produce a best fit slope equal to 1.0 when plotted against the face loads generated by the extensometers. This result indicates the general magnitude of softening which would have occurred in the Medof panels

Below, a structural stiffness of 2.6 MNmm^{-1} was used to determine the face load based on the ring deformation recorded by the extensometers. This result required that the face load determined based on the Medof panel data be multiplied by a factor of 0.59. This result is limited since only the north face loading measured by Medof panels can be compared to that of the extensometers. Significant loading occurred on the West and North West faces of the structure which influences the ring distortion measured on the North face. The applicability of the approach used to produce Figure 5-67 is limited to ice loading events for which a single face of the structure is loaded significantly (e.g. the North face or the East face). For this reason the matrix method was considered to be more appropriate than the result shown in Figure 5-67.
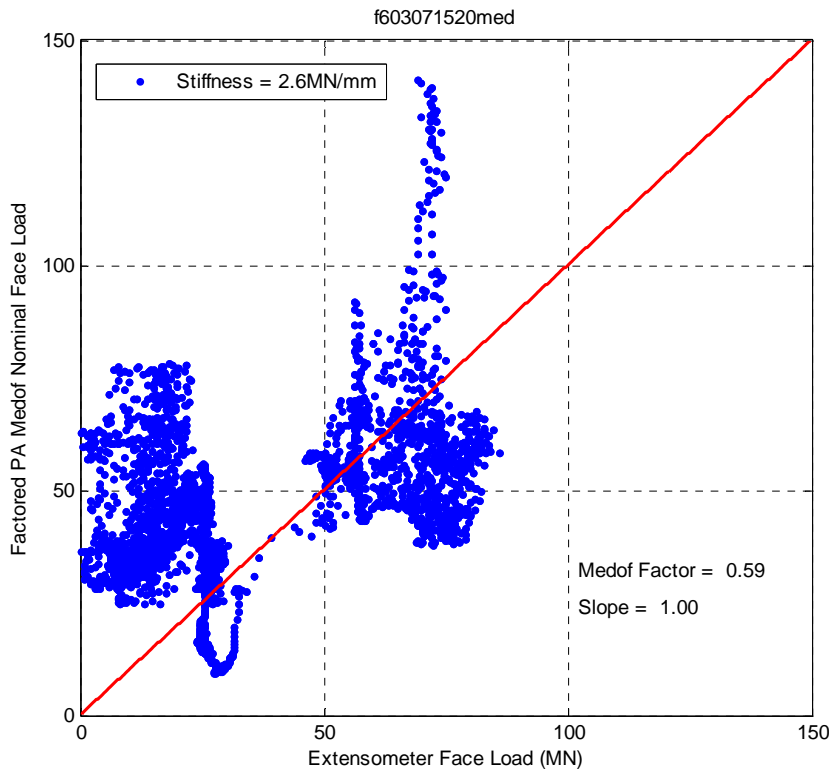
Figure 5-67:   **Extensometer face load versus a factored Medof face load which has undergone probabilistic averaging.**

An analysis of the face load acting on the North face of the structure was carried out. The face loads were estimated using the extensometers considering various structural

stiffness values. These results were used to calibrate the Medof panel loads to the extensometers. This method also served to highlight the deficiency of having panels covering only 10% of the structures loaded area. The face loads and global loads predicted based on Medof panels are highly sensitive to localized fractures and loading events. There are often significant peaks in the Medof face loads with minimal response in the extensometer face loads and vice versa. This could be the result of a localized fracture occurring around a Medof panel grouping, or partial loading across the face of the structure. Conversely, the impact of a perpendicularly orientated ridge could result in a large response from the Medof panels or no response at all, depending on the impact location. This effect is illustrated in Figure 5-68.
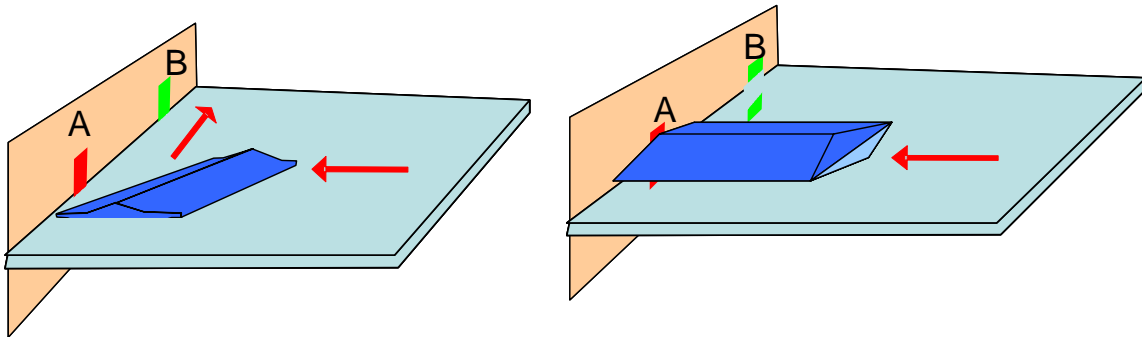
Figure 5-68 Illustration showing the effect of low panel coverage in the loaded area

5.5.3 Maximum Force Based on Matrix Solution for Stiffness

The stiffness matrix developed based on the Sandwell (1991) report was applied to estimate the loads during the March 7th, 1986 event from the extensometer values. The ring distortions for the event are plotted in Figure 5-69 (a). The loads calculated using the matrix solution are plotted in Figure 5-69 (b). Figure 5-69 (c) shows the North and West global load components as well as the total load. The maximum total global load is estimated to be 165 MN. The analysis would benefit from a more detailed analysis of zeroing.
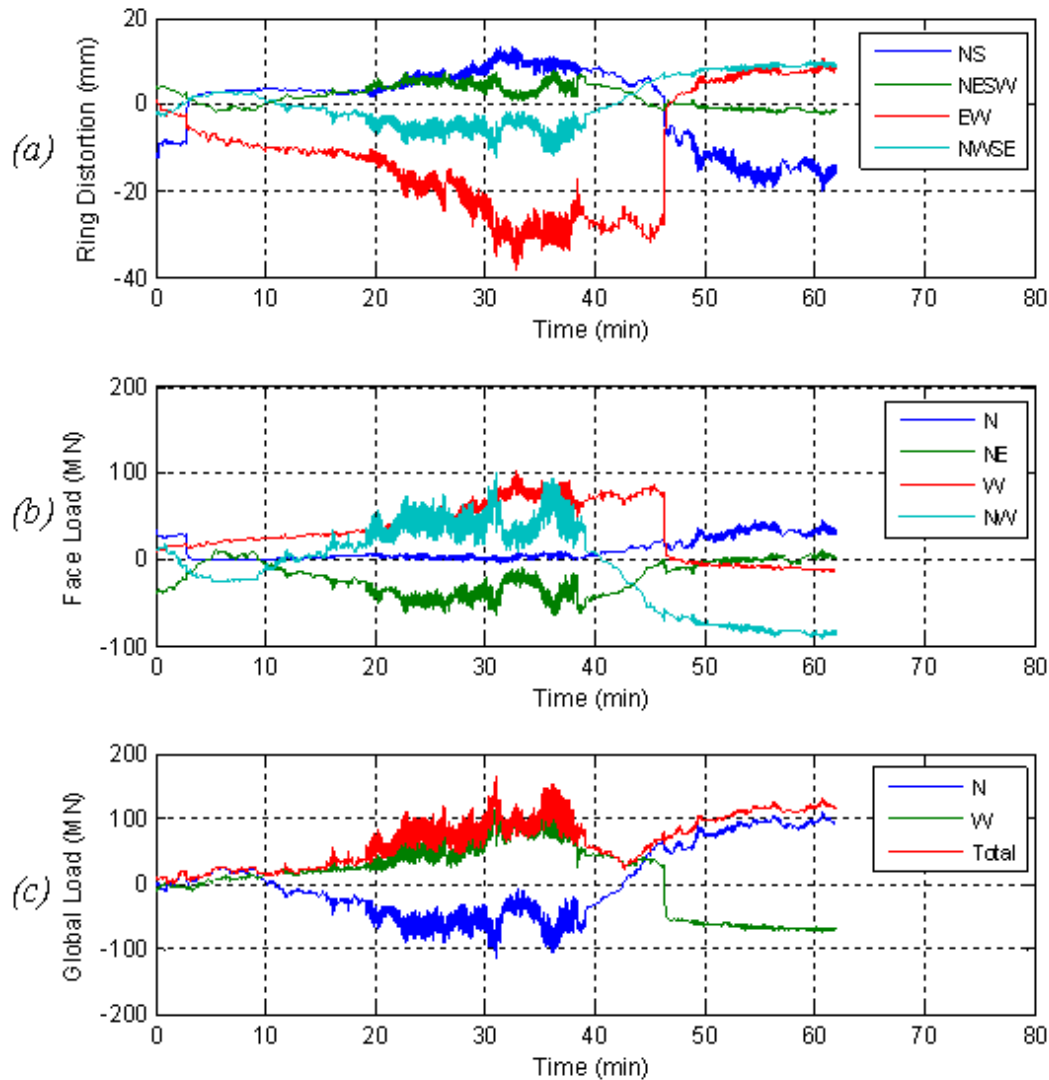
Figure 5-69:   Application of matrix method to March 7th, 1986 event.

5.5.4 Concluding Remarks for March 7 (A), 1986 Event

The March 7h, 1986 event involved multiyear ice crushing on the North, North West and West faces. The matrix method has been applied to determine the global loads acting on the structure. The maximum total global load estimated for this event is 165 MN. There is some uncertainty regarding this result. The interaction between the different faces has not been perfectly captured. It is noted that the matrix model is sensitive to zeroing. Data are often difficult to provide zeroing with complete confidence. The load estimates on the corners of the structure could also be improved. These are a function of the assumptions in the finite element analysis conducted by Sandwell (1991).

5.6   Event 0307B - March 7, 1986 – f603071603

Event ID – 0307B
Crushing Event
Ice Thickness: 3.5 to 10m

Drift
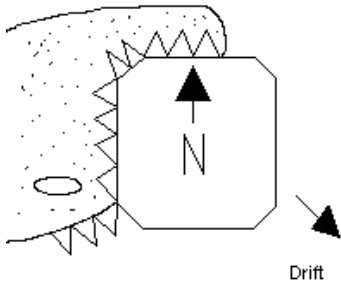
5.6.1 Dynamac Event Description

On March 7th, the Molikpaq penetrated a multi-year floe. Cracks formed early in the event (1545) but did not widen significantly until the end of the event (1700). Dynamic load began when a 50 m long 2 m high hummock came into contact with the west face at a speed of 0.05 m/s. The hummock was crushed along its longitudinal axis, producing continuous crushing with frequencies of 1 Hz. The rubble was allowed to clear around the north and south sides of the caisson. At 1606 severe global confinement of the ice prevented the rubble on the west face from clearing and so this rubble became stationary and most likely grounded on the berm. At 1616 a series of radial fractures formed off the NW. The ice direction veered from 130^0 to 160^0 and most of the load was suddenly transferred to the north face. "Extrusion and Collapse" sequences continued until the ice stopped moving.

Figure 5-70 shows the magnitude of loading occurring on the North, North East and East faces during the event. Note that there was significant loading occurring on the West and North West faces of the structure which could not be captured using the Medof panels.

Since there was multiyear ice crushing on the North, North West and West faces, the matrix method has been applied to determine the global loads acting on the structure. The maximum total global load estimated for this event is 95 MN.
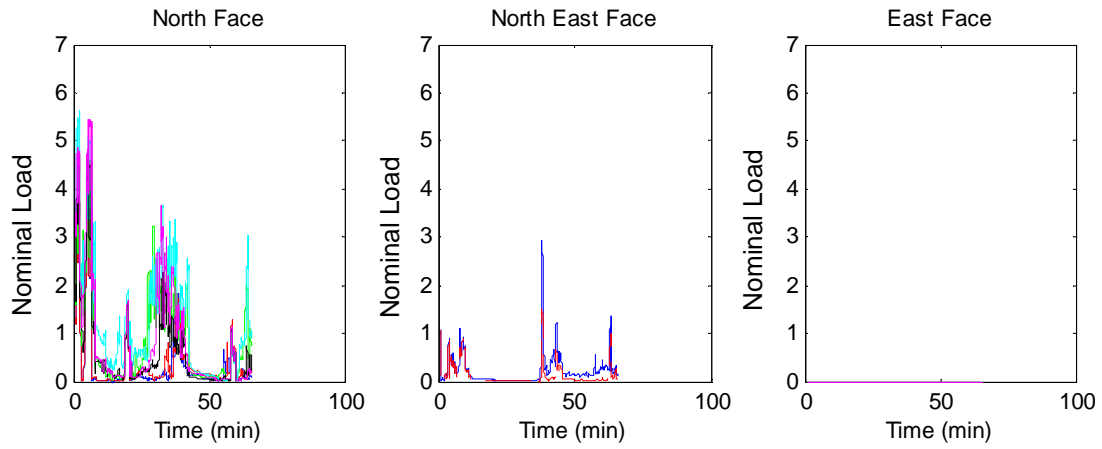
Figure 5-70   Nominal Medof column loads acting on the North, North East and East faces of the Molikpaq structure
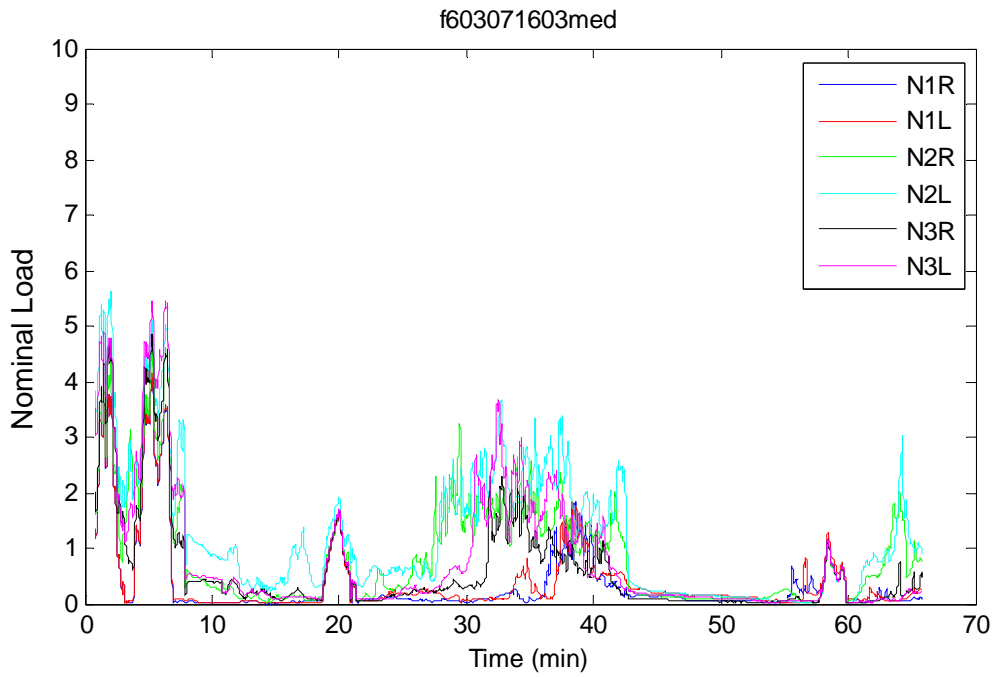
Figure 5-71   Nominal Medof column loads acting on the North face of the Molikpaq structure
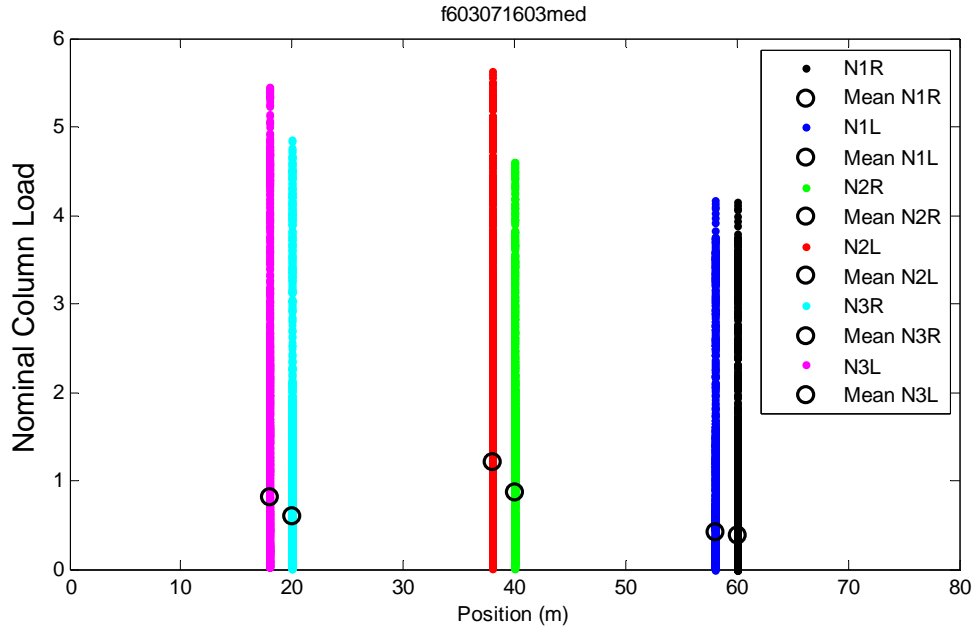
Figure 5-72: **Distribution of nominal Medof column ice loading on the face of the structure**
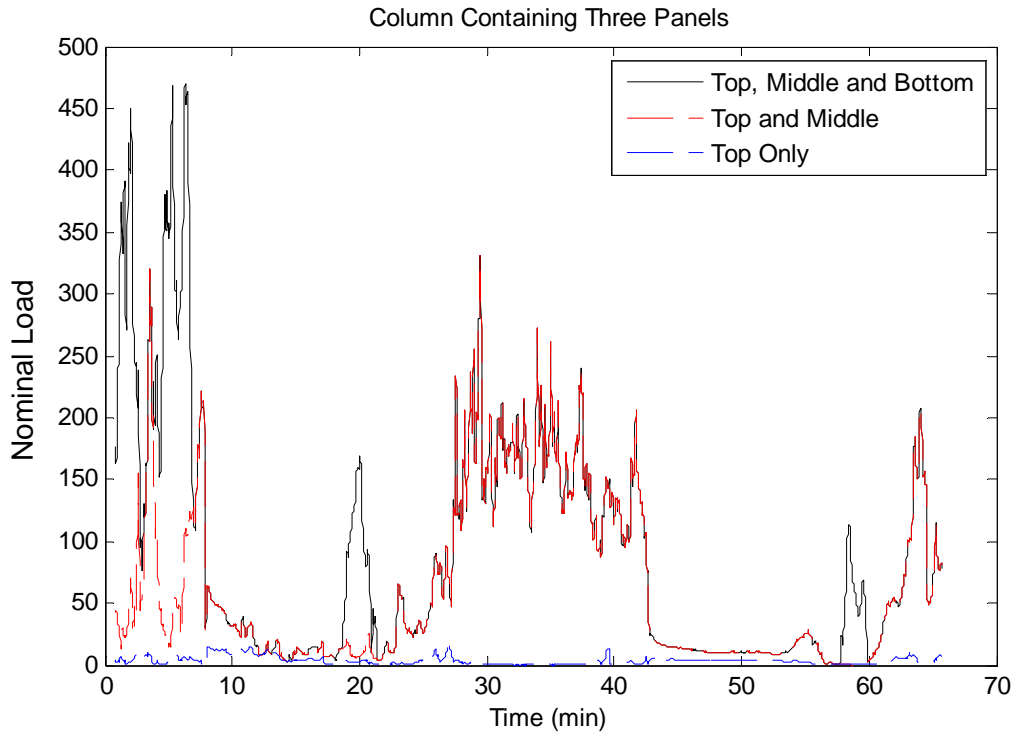
Figure 5-73: **Loading on top, middle and bottom panels in column N2R.**

5.6.2 Analysis of Face Loads Acting on the Structure

The extensometers have been used to calculate the ice loads acting on the north face of the Molikpaq structure. Figure 5-74 shows the probabilistically averaged face load calculated from Phase 1 using the Medof panels which has been factored to produce a best fit slope equal to 1.0 when plotted against the face loads generated by the extensometers. This result indicates the general magnitude of softening which would have occurred in the Medof panels. Below, a structural stiffness of 2.6 MNmm^{-1} was used to determine the face load based on the ring deformation of the extensometers. This result required that the face load determined based on the Medof panel data be multiplied by a factor of 0.48.

As can be seen in Figure 5-74, there is little agreement in the face loads calculated using the Medof panels compared to those using extensometer data. Referring to the Dynamac event description above, one can see that the loading is primarily on the North, North West and West faces. Figure 5-74 considers the North face only. Again, the applicability of the approach used to produce Figure 5-74 is limited to ice loading events for which a single face of the structure is loaded significantly (i.e. the North face or the East face). For events which have significant loading on multiple faces, the matrix approach is recommended.
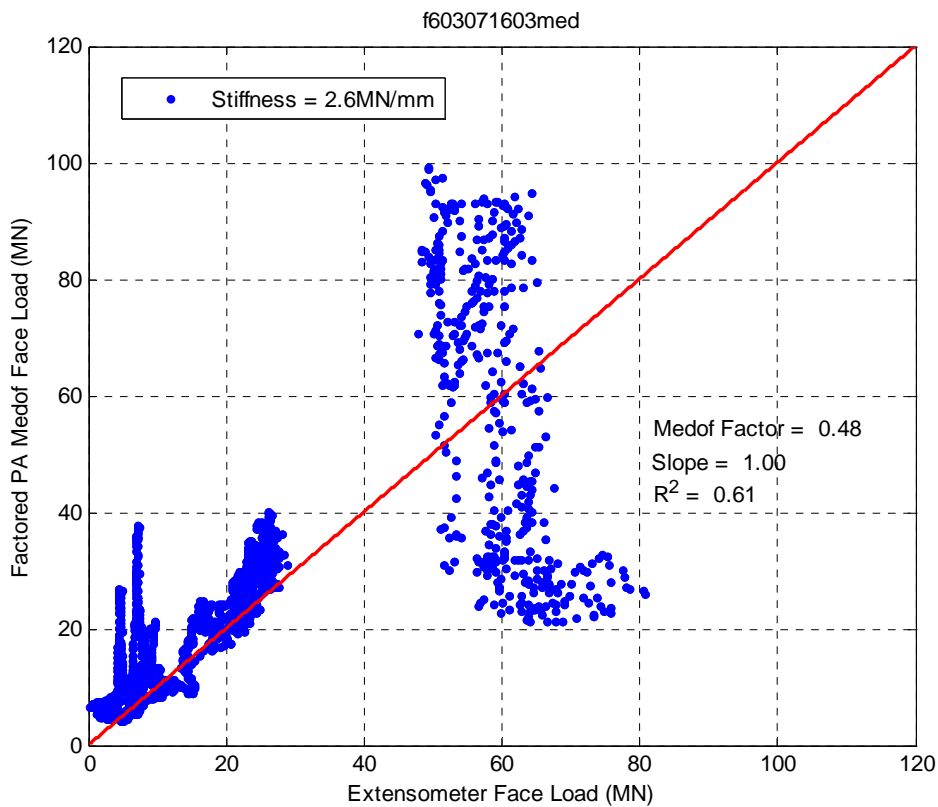
Figure 5-74: **Extensometer face load versus a factored Medof face load which has undergone probabilistic averaging.**

5.6.3 Maximum Force Based on Matrix Solution for Stiffness

The stiffness matrix developed based on the Sandwell (1991) report was applied to estimate the loads during the March 7th, 1986 event from the extensometer values. The ring distortions for the event are plotted in Figure 5-75 (a). The loads calculated using the matrix solution are plotted in Figure 5-75 (b). Figure 5-75 (c) shows the North and West global load components as well as the total load. The maximum total global load is estimated to be 95 MN. The analysis could benefit form a detailed analysis of the zeroing of the data.
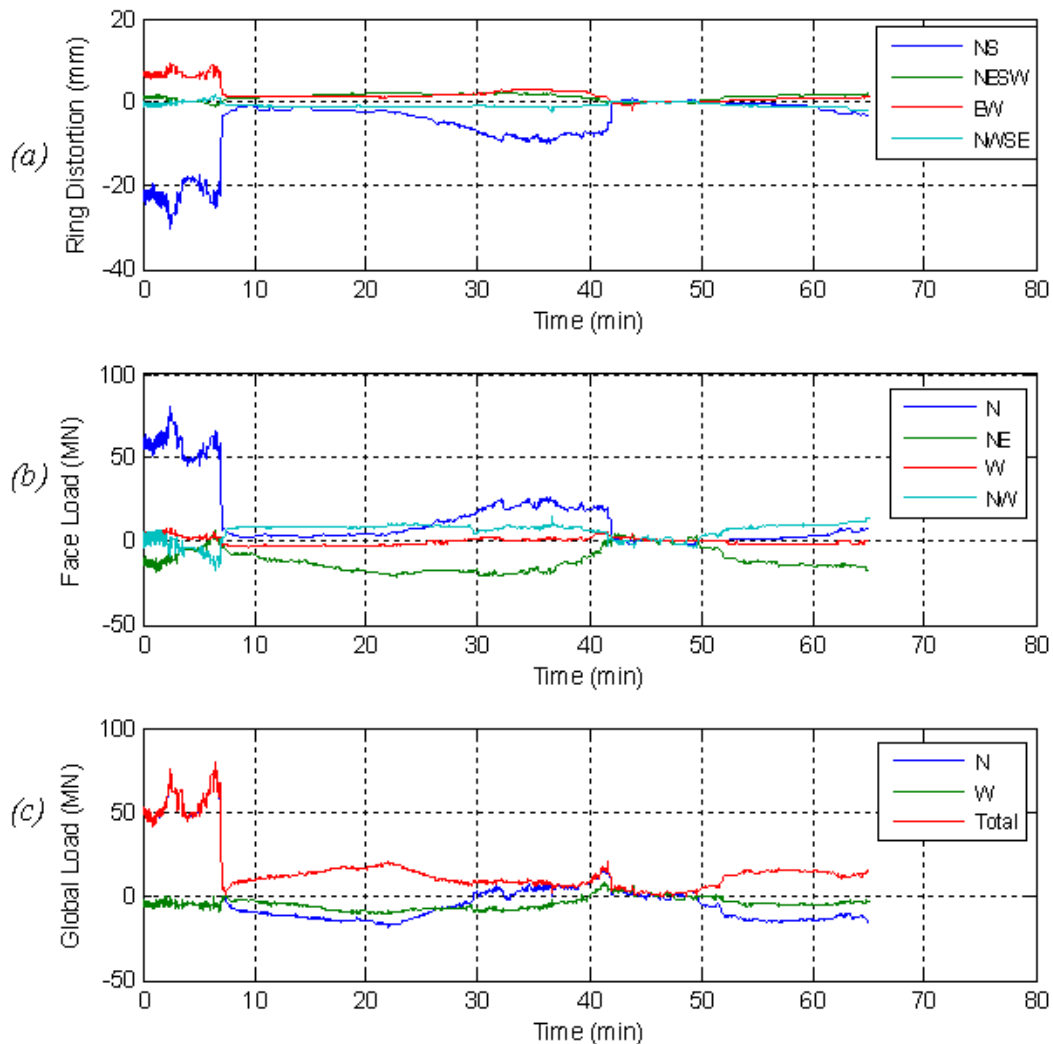
Figure 5-75:   **Application of matrix method to March 7th, 1986 event. No zeroing of data.**

The Figure 5-75 gives negative ice loads, but these are relatively small. It is believed that with further consideration the matrix method could be enhanced by improving the zeroing of the data and adjusting the stiffness matrix slightly to better estimate the corner

loadings. Figure 5-76 shows results which seem more reasonable by adjusting the stiffness matrix used in the analysis. Further consideration of this approach could yield improved results.
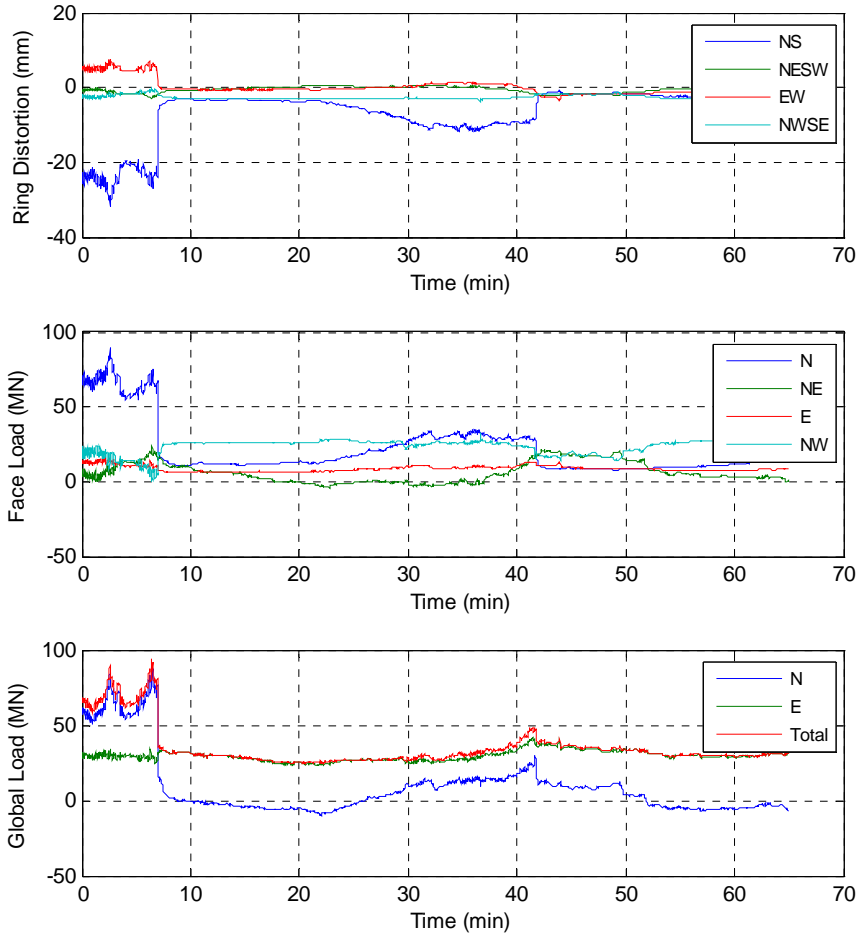
Figure 5-76: **Application of matrix method to March 7th, 1986 event. Adjusted stiffness matrix.**

5.6.4 Concluding Remarks for March 7 (B), 1986 Event

The March 7[h], 1986 event involved multiyear ice crushing on the North, North West and West faces. The matrix method has been applied to determine the global loads acting on the structure. The maximum total global load estimated for this event is 95 MN. The load estimates particularly on the corners of the structure could likely be improved with further study. These, and those on orthogonal sides are a function of the assumptions in the finite element analysis conducted by Sandwell (1991).

6   COMPARISON OF MEDOF PRESSURE WITH OTHER DATASETS [†]

6.1   Introduction

Ice does not have a simple 'failure pressure' or compressive strength value which can be used in the design of structures for ice environments (Sanderson, 1988). As shown in Figure 6-1, peak pressure data measured for a wide range of contact areas exhibits a trend of decreasing pressure for increasing area.
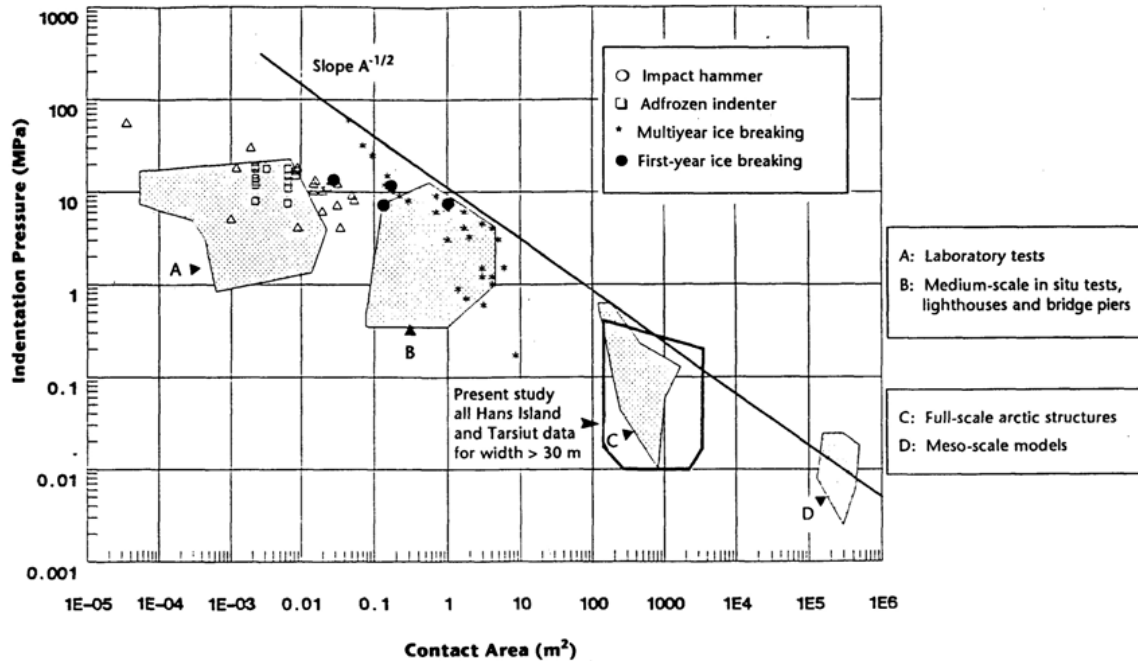
Figure 6-1   **Measured ice failure pressure versus contact area for a wide range of interaction and loading situations for various ice types, temperatures and strain rates (from Blanchet, 1990. After Sanderson, 1988).**

This scale effect has important implications for design. The selection of strengthening for full-scale structures based on laboratory-scale ice pressure data would result in highly conservative (and more expensive) designs. Another consequence of the scale effect is that local design areas (order of 1 m^2) must be designed to withstand significantly higher pressures than are required for global design (areas order of 100 m^2). As shown in Figure 6-2, for a region of an ice feature of constant width, pressure should decrease for increasing ice thickness.

[†] Chapter contributed by Rocky Taylor based on work summarized in Taylor (2010).
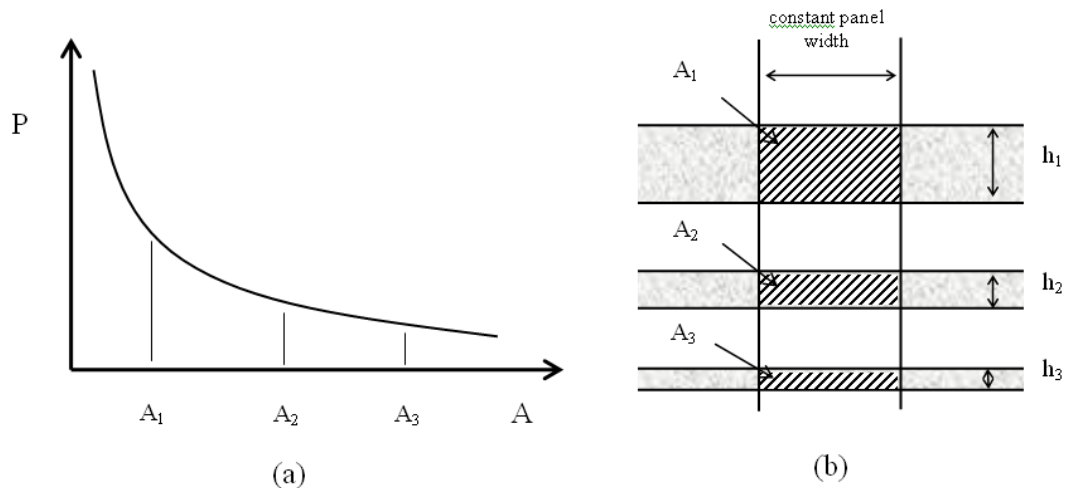
Figure 6-2   Illustration of (a) pressure-area effect; (b) increasing area for constant width panel with increasing thickness.

The following work focuses on establishing a more consistent comparison of the Molikpaq data with other available datasets. Given the differences between these datasets, as well as their associated measurement uncertainties, direct comparisons of individual events or parts of an event are not considered. There will be variation, even for a given ice thickness, from one event to another. The only meaningful option is to assess and compare the statistical parameters of each set of events.

An initial examination of mean pressure-thickness data analyzed on a per event basis is shown in Figure 6-3 (a). A trend of decreasing pressure with increasing ice thickness is evident. In Chapter 3 it was determined that softening of the Medof panels very likely occurred during the 1985/1986 deployment of the Molikpaq. Recalibration to account for this softening leads to a reduction of Molikpaq pressure estimates by a factor on the order of 50%. Accounting for this softening of the Medof panels results in greater consistency between the Molikpaq and other datasets; see Figure 6-3 (b).

The data in Figure 6-3 correspond to a variety of interaction widths. This results in some thicker ice events which have smaller interaction areas (Figure 6-3 (b), Group B) than corresponding events with thinner ice (Figure 6-3 (b), Group A). A more meaningful analysis requires a comparison of pressures for interactions acting over regions of the same width.
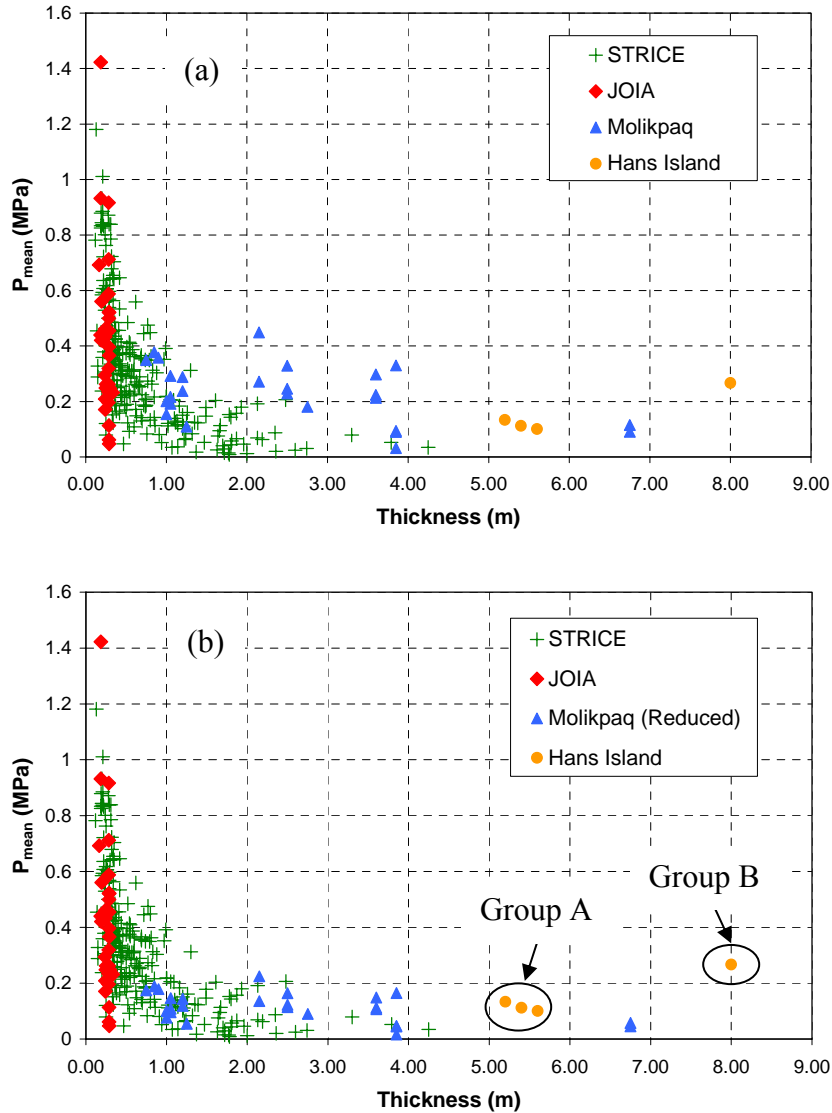
Figure 6-3   **Illustration of pressure-thickness effect based on pressure data for individual events with (a) uncorrected Molikpaq data; (b) corrected Molikpaq data.**

The following discussion is extracted from Taylor (2010), in which the scale effect of pressure with thickness is examined. Full-scale data from the Molikpaq, as well as two European Union (EU) field measurement programs, 'Validation on Low Level Ice Forces on Coastal Structures' (LOLEIF) and 'Measurements on Structures in Ice' (STRICE), have been analyzed. In the present work, data from both EU projects are collectively referred to as the STRICE dataset. Measurement data from Cook Inlet and the Japan Ocean Industries Association (JOIA) medium-scale field indentation program are included in the analysis. Discussions of event selection and the assessment of event means and standard deviations are given below.

6.2   Overview of Datasets

To allow for a comparison of pressure-thickness data, differences between the available datasets have been identified and are discussed in an attempt to establish a consistent basis for analysis. Where possible, events have been selected and processed in a way which allows for the analysis of similar types of events from each dataset. Pertinent background information, along with a description of the analysis procedures used for each dataset are given below. Additional details of the datasets may be found in Taylor (2010).

6.2.1   Molikpaq

Data available from the 1985/1986 deployment of the Molikpaq mobile arctic caisson structure at Amauligak I-65 in the Canadian Beaufort Sea are considered. Details of the structure and its deployments are available in the open literature and have been summarized in Chapters 1, 2 and 3. This dataset includes multiple interactions of a wide, vertically-sided structure with both first-year and multi-year ice. The Molikpaq was instrumented with thirty-one Medof panels to measure local ice forces, each with a capacity of 20 MN. These panels were installed on the north, northeast and east face of the caisson in groups of four or five (see Figure 6-4) and positioned with the bottom of the top panel approximately 0.2 m below the waterline.
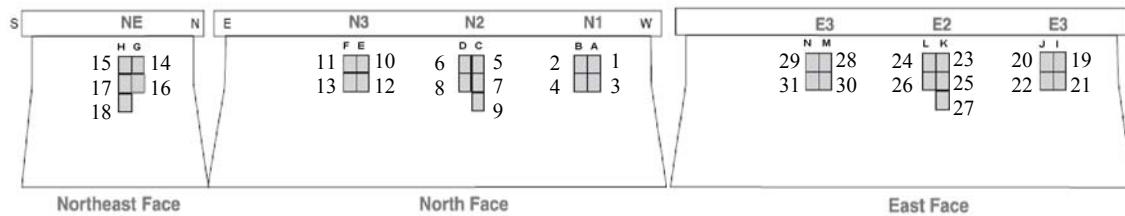
Figure 6-4   **Medof panel array numbering (letters represent columns).**

These panels were configured to measure the total force acting over the panel area (1.135 m wide by 2.715 m high). Slightly more than 10% of the length of each the north and east faces are covered with panels. During most of the interactions the Molikpaq performed well under ice loading, though on several occasions the structure experienced significant cyclic loading. During the ice loading event of April 12, 1986 liquefaction near the edge of the sand core occurred (Jefferies and Wright, 1988). Data corresponding to interactions covering a wide range of ice thicknesses, including thick multi-year ice features are available and are of interest in exploring scale effects. This dataset presents a wealth of information about full-scale behavior.

The Medof panels were configured in columns of two panels (i.e. Figure 6-4, panels 11 and 13), or in columns of three panels (i.e. Figure 6-4, panels 5, 7 and 9). As noted in Chapter 3, for two panel columns the Medof panels reached depths of 2.915 m, while the three panel columns covered ice interactions to a depth of 5.63 m. This has implications in the selection of appropriate column data for different events. As a general rule, ice loads have only been taken from columns which have instrumented panels covering the

entire thickness of the ice, to ensure loads are captured across the entire ice thickness. This is illustrated in Figure 6-5.

One exception to this rule is noted for interactions on the Northeast face. As noted by Gulf Canada Ltd. (1987), panel 17 did not function throughout the entire 1985-1986 season and panels 14 and 15 were damaged during flaring operations on December 20, 1985 and did not work after that date. To address this issue, event data from the panels on the NE face were individually examined to verify which panels were working correctly for the events of interest. Event data for malfunctioned panels were filtered out. Since panel 15 (top left) and panel 17 (middle left) both did not work, data from the entire left column of NE panels were discarded. For the right NE column, panel 14 (top right) did not work. Discarding the entire right NE column would result in the omission of all NE event data. Rather than entirely discard the data from the NE face, it was decided that the measurements from panel 16 would be taken as representative NE column loads for thin ice events.

This is seen as a reasonable assumption since spalling of the ice edge would likely result in negligible loads on the top panel, with the majority of load being transmitted through the middle panel. As with all other two panel columns, for thicker ice events, data for this column were omitted from the analysis; see Figure 6-5 (b) and (c).
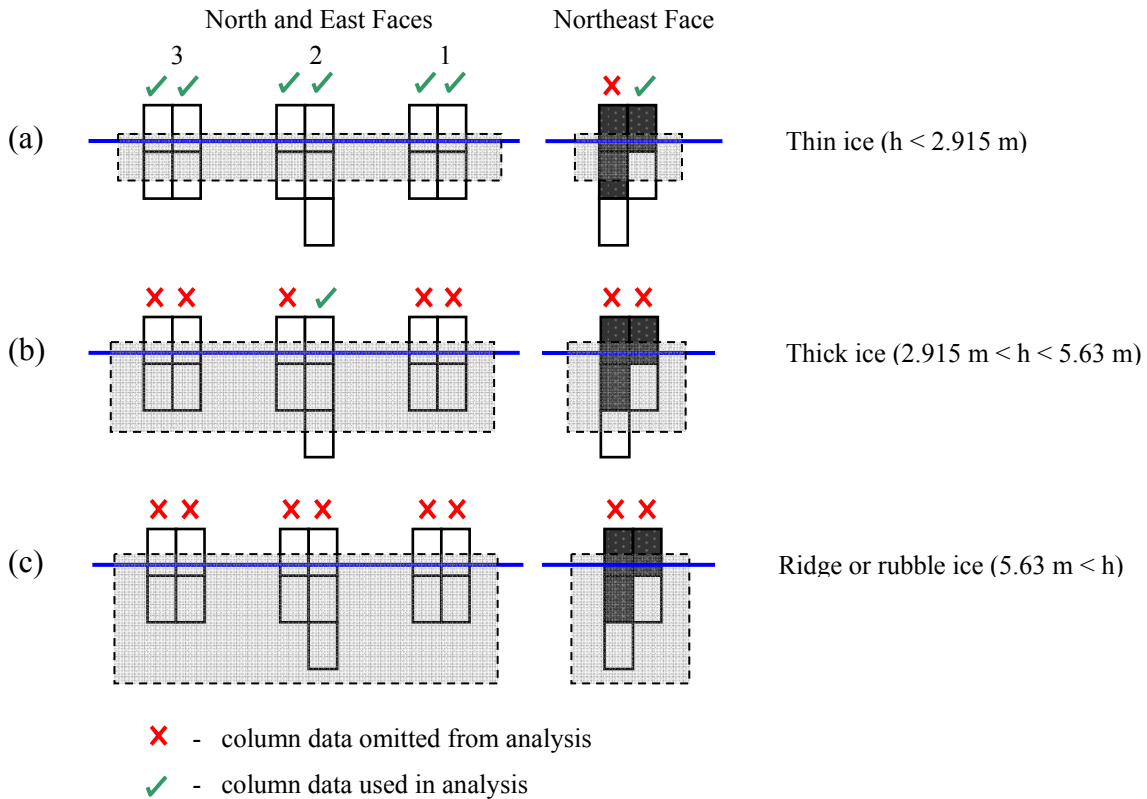
Figure 6-5   Illustration of selected columns of Medof panel data (dark panels represent broken panels) used for: (a) thin ice events; (b) thick ice events; (c) ridge/rubble events.

6-5

In reality there may be some load acting on the top panel of the NE column (i.e. panel 14), which would result in an actual pressure that is higher than those based on panel 16 only. Overall the number of events to which this applies is small, and the effects on the individual events are not expected to be significant. It has also been assumed here that the probability of loads below the bottom panels is unlikely given the quoted ice thickness values, though uncertainty associated with ice thicknesses is a likely contribution to the variation of the Molikpaq data.

In assessing the statistical characteristics of Molikpaq event data, significant effort has been placed to using an approach that is consistent with the analysis of the STRICE data. Since it was not possible to analyze directly the STRICE data (time series data are not publicly available), event means and standard deviations for STRICE have been obtained from Kärnä and Yan (2006). Based on this report it has been determined that the STRICE dataset contains only continuous crushing events, for which all panels are loaded for the entire duration of the event as stated in Kärnä and Yan (2006). A review of various event descriptions and lists (see for instance Rogers et al., 1988) resulted in the selection of relevant Molikpaq events for further analysis. Details of these events are summarized in Taylor (2010).

To provide a set of events comparable with STRICE, individual Molikpaq events were screened and processed. First all vertical groups of panels (e.g. panels 11 and 13) were combined to give column loads. Sections of the column load data files were then selected based on the global attributes of the interaction (i.e. start or stop of the event or a period of no load). In one instance, panel 9 experienced overloading for part of the event (event f605120301 on May 12, 1986); this portion of the event was filtered out. The selected data from each of the loaded columns were then linked together in series to form a single event load trace; see Figure 6-6 (a).

Next the linked time trace for each event (i.e. linked data from all loaded columns) was examined in detail. These data were then trimmed to remove periods of low local loads corresponding to clearing, sliding or other processes acting locally on the given columns of panels. This produced time traces for 'continuous' crushing events with an 'effective' duration; see Figure 6-6 (b). For thick ice events where the bottom of the ice is below the bottom of the middle panels, only the columns with three panels per column were analyzed to ensure ice loads were measured for the entire thickness. This process was repeated for all events in the analysis set. Details of the trim points used for each event are provided in Taylor (2010).
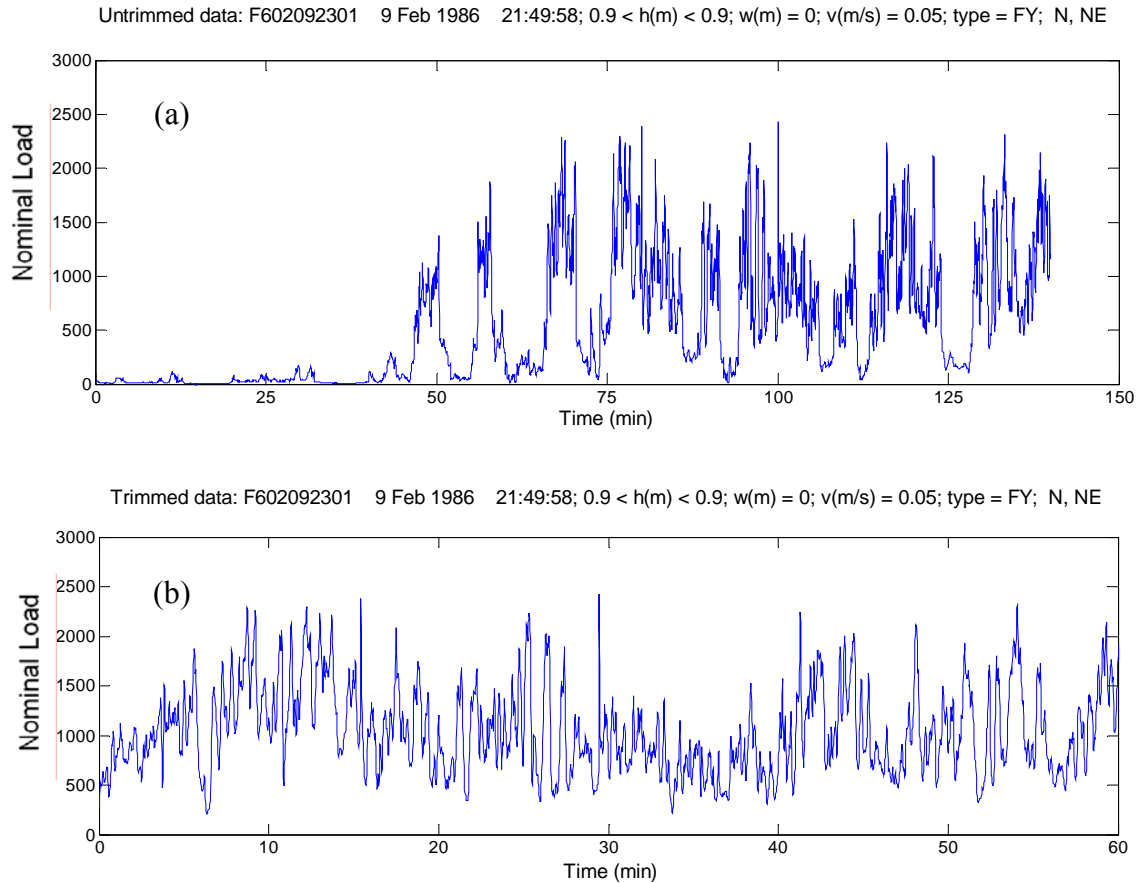
Figure 6-6   **Plots showing a sample Molikpaq event with: (a) linked untrimmed data, and (b) linked trimmed data.**

The Molikpaq fast files used in this analysis were collected at a sampling rate of 1 Hz. As noted by Jeffries and Wright (1988) the response time of the Medof panels to a step change in load was of the order of 5 to 10 seconds. Some of the high frequency loads were effectively damped out (averaged) and the panel could not capture processes with frequencies above about 0.5 Hz to 3 Hz. As a result, Medof panel measurements could not capture process frequencies over the same range as the STRICE instrumentation.

Given the lower effective sampling rate of the Molikpaq data, it would be expected that for similar events, the standard deviations of pressure should be higher for STRICE than for the Molikpaq. The extent to which the difference in sampling rate affects the data is not clear. For the present analysis, no correction has been made to account for the difference in sampling frequencies, since time series data are not available for STRICE. Should these data become available, this could be explored by comparing STRICE statistical parameters for unfiltered event data, as well as for data that is either resampled at the same rate as the Molikpaq data or alternatively averaged using a moving average with a time window that is representative of the Medof panel response time.

Comparing the sample Molikpaq event in Figure 6-6 with the sample STRICE event shown in Figure 6-7 illustrates the general agreement between the forms of the processed data for both datasets.
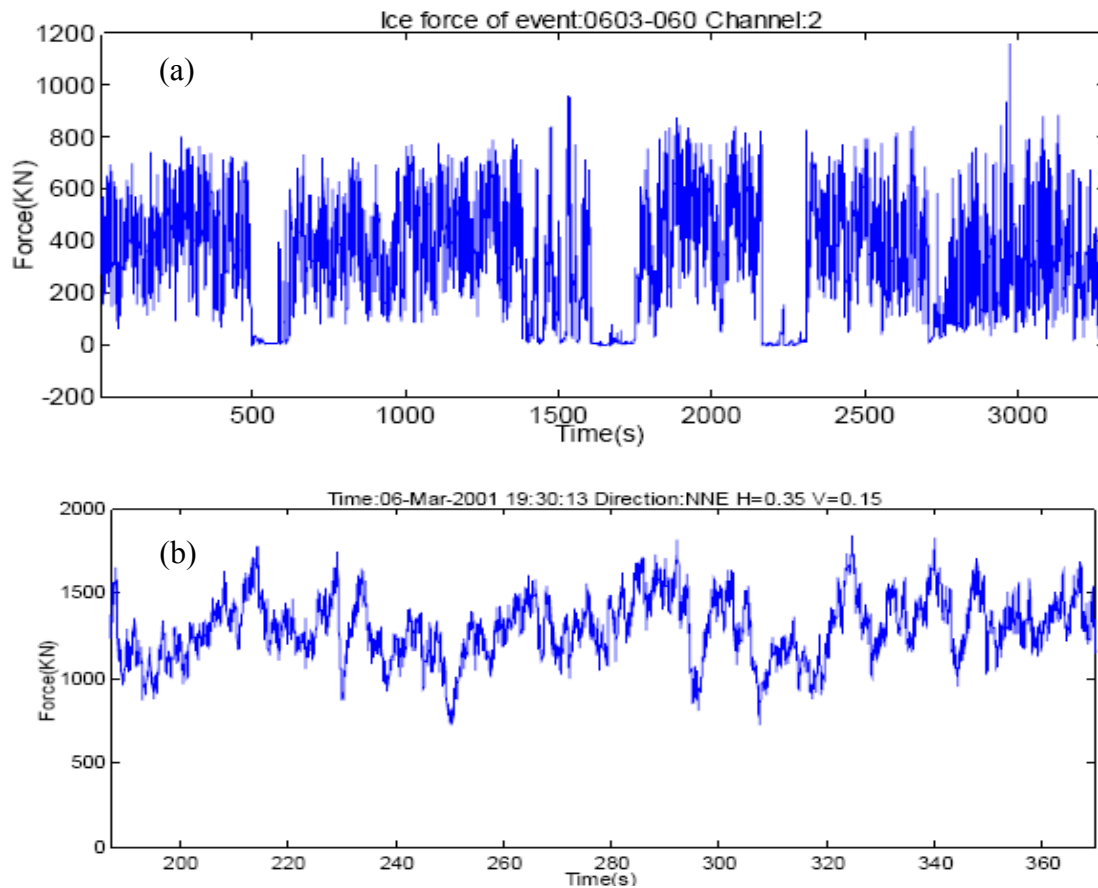
Figure 6-7   **Data for a sample STRICE event: (a) untrimmed data, and (b) a trimmed event (after Kärnä and Yan, 2006)**

The duration of individual events is also an important consideration. Short events do not provide a sufficiently large sample to give a representative estimate of the statistical parameters. This is an issue for all datasets, but this is of most relevance to the STRICE and Molikpaq datasets. Duration information is not available for the Cook Inlet dataset; these data were not included in analyses which studied the effects of duration. For the JOIA data, the duration of the events was determined by the stroke of the hydraulic ram used in the indentation tests. JOIA events are much shorter in duration than STRICE and Molikpaq events.

The issue of event duration was treated by weighting the means and standard deviations in determining averages to reflect the duration of individual events. This approach is preferred, since it does not completely remove the data but rather assigns more weight to the longer duration events. The premise here is that longer duration events have greater statistical significance since they represent larger samples of the processes of interest.

Duration weighting is accomplished by populating an array containing event means (or standard deviations) where the number of repeat entries for each given event is proportional to the duration. The number of replications of an event n_i, is equal to the duration of the ith event in minutes truncated to one decimal place and multiplied by 10. For instance, an event with a duration of 15.6 minutes has its event mean entered into the overall mean pressure array 156 times. A second event, having a duration of 10.3 minutes would have 103 entries in the overall mean pressure array. In this manner, longer duration events have a proportionally larger influence on the overall mean. This option can only be applied to data where duration information is available (i.e. not for Cook Inlet). Using this technique it is possible to examine if duration effects significantly affect the mean and standard deviation estimates.

Another difference between the STRICE and Molikpaq data is related to the configuration of panels. The STRICE program used a contiguous arrangement of panels (see Figure 6-9), while the Molikpaq panels were distributed across the face of the structure in clusters of two columns as shown in Figure 6-4. Consideration of temporal and spatial correlations is important when combining pressures from adjacent or remote columns to estimate pressures acting over a wider area, as with the probabilistic averaging analysis in Chapter 4. Since the emphasis here is on pressures corresponding to a single panel width, such correlations do not enter into the analysis. Trimmed data for the Molikpaq columns were linked in series to give a representative single panel event with an effective duration. These data were then analyzed in a manner consistent with the single panel data analyzed from STRICE.

Softening Correction:
To account for the softening of panels, an optional softening correction factor was implemented in the analysis. The purpose of this correction factor is to allow for an assessment of the degree of consistency between Molikpaq and other datasets both with and without the Molikpaq softening corrections. When this option is used final pressure estimates (means and standard deviations) for the Molikpaq data are reduced by half (i.e. multiplied by 0.5). When this option is turned off, the Molikpaq pressure values given are the uncorrected values.

6.2.2 STRICE

Field data were collected from the lighthouse Norstromsgrund, shown in Figure 6-8 (a), during two European Union funded projects carried out over four winter seasons from 1999-2003. The lighthouse Norstromsgrund is founded at a water depth of about 14 m and has a water line diameter of about 7.2 m. It is located in the Northern Baltic Sea approximately 60 km offshore of Lulea in Sweden; see Figure 6-8 (b).
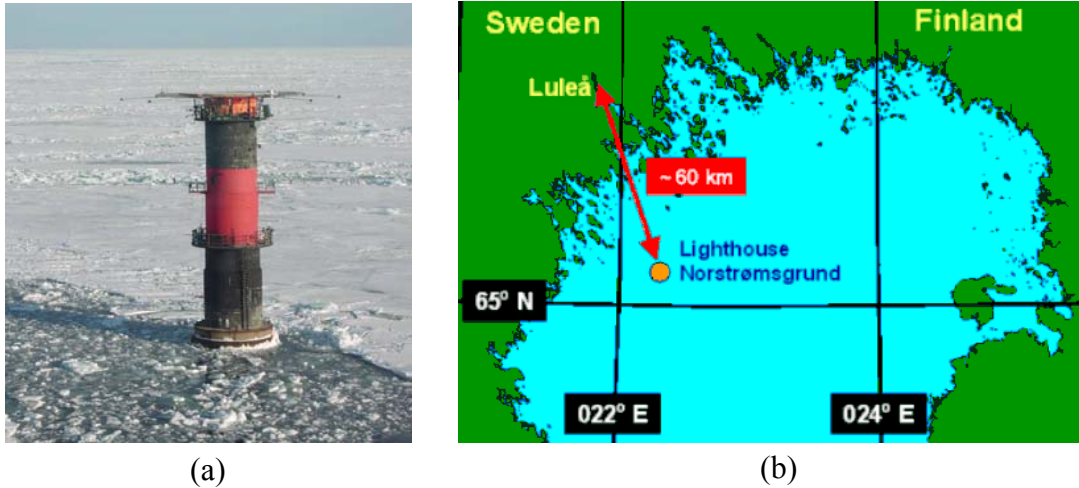
Figure 6-8   (a) Norstromsgrund lighthouse; (b) lighthouse location (Kärnä and Yan, 2006).

The lighthouse was outfitted with nine force measuring load panels, each with an individual area 1.2 m wide x 1.6 m high and a load capacity of 3000 kN. As illustrated in Figure 6-9 (a), the panel array covered approximately 167 degrees of the structure. The northern Baltic Sea has a salinity of about 1ppt and experiences about 1000 freezing-degree-days (based on 2002-2003 season). At this location, only first year ice is encountered, with a maximum level thickness of approximately 0.6m.

The primary source of ice crushing data gathered from the lighthouse during the winters of 1999-2003 is Kärnä and Yan (2006). In this report, the authors used spectral characteristics of the signals to identify stationary events of continuous ice crushing. The authors identified events as being either brittle crushing or low velocity crushing. In this report load panel data was converted into mean ice pressures and mean standard deviations of pressure using the following expressions:

$$\text{Mean Ice Pressure [MPa]} = \frac{\text{Mean Ice Force [kN]}}{\text{Panel Width [m]} \times \text{Ice Thickness[m]} \times 1000}$$

$$\text{Mean Standard Deviation [MPa]} = \frac{\text{Mean Standard Deviation [kN]}}{\text{Panel Width [m]} \times \text{Ice Thickness[m]} \times 1000}$$

Based on information presented in Kärnä and Yan (2006) it has been determined that only events where the panels were measuring the full load were used in the STRICE analysis.
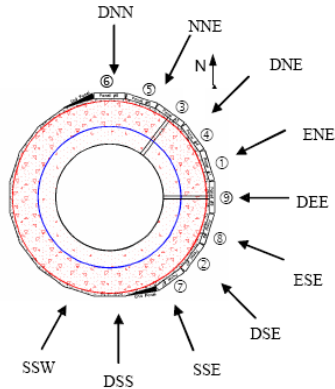
Figure 6-9 **STRICE measurement panels: (a) schematic of panel numbering and orientation; (b) mounting configuration (Kärnä and Yan, 2006).**

Based on information presented by Kärnä and Yan (2006) it was determined that data corresponding to ice thickness greater than 1.5 m or less than 0.2 m should be omitted. For this reason, all events with thickness above 1.5 m or below 0.2 m have been discarded. The authors also suggested that while rafted ice can have more or less the same strength as corresponding level ice, there is uncertainty associated with both the extent of consolidation of the rafted ice, and its strength. Since the competent level ice has an upper limit of approximately 0.6 m for this region, an optional level ice filter was used for some analysis cases, as is discussed below. From the STRICE data obtained from Kärnä and Yan (2006) relevant brittle crushing and low velocity crushing events were selected. The events used in this analysis are summarized in Taylor (2010).

Two optional filters, one for level ice and the other for event duration were implemented for the STRICE dataset.

Level Ice Filter
Given the ice conditions in the Baltic Sea, an upper limit on level ice thickness was taken as $h \leq 0.6m$. This filter removes all thicker (likely rafted) ice from the analysis.

Duration Filter:
This option is used to remove events which have an overall duration of less than 10 minutes to study the effect of removing short duration events.

6.2.3 JOIA

The Japan Ocean Industries Association (JOIA) medium-scale field indentation test (MSFIT) project consisted of over thirty tests carried out over a five year timeframe (1996-2000). These tests were conducted by mounting an indentation apparatus on the side of a fishing dock in the harbor of Notoro Lagoon in Hokkaido, Japan; see Figure 6-10. The average ice thickness during these tests was approximately 30 cm. Details of the ice conditions during the program, as well as the physical properties of the ice are presented in Kamio et al. (2000). The natural ice in Notoro Lagoon is brackish first-year

ice, with some natural snow cover. In some test cases the natural ice was removed and a refrozen ice sheet was grown, while other tests simply used the naturally grown ice. In the case of natural ice, a layer of snow ice was sometimes present; this was not present on refrozen sheets (Takeuchi et al., 1997).
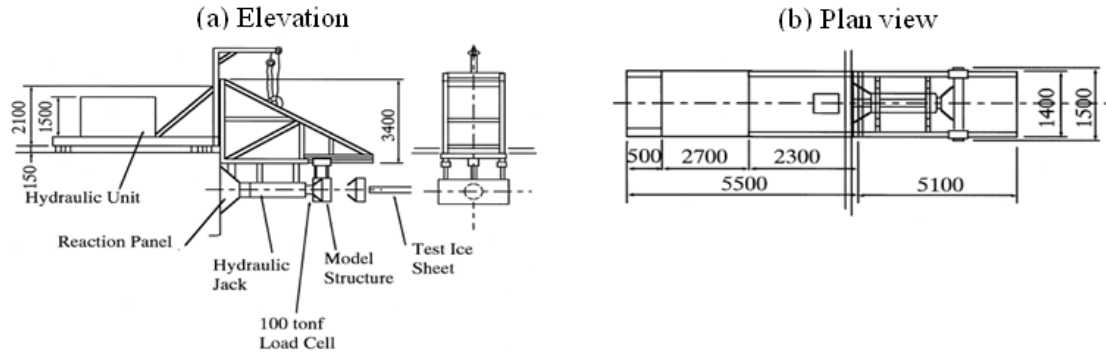
Figure 6-10   Indentation instrumentation and structure (a) elevation view; (b) plan view (Sodhi et al., 1998).

Displacement rates were held constant for a given test and ranged between 0.03 cm/s to 3 cm/s. In many instances several tests were conducted for a given ice sheet by dividing the stroke into three 35-40 cm sections (maximum stroke was 120 cm). By testing at a different speed for each section, multiple conditions could be studied for each prepared section of ice. A 100 ton-force load cell was mounted between the hydraulic ram and the test beam to measure global loads, though it was later discovered that this load cell did not work for many of the tests. Of interest to the present analysis is the segmented indenter, which consisted of fifteen 10 cm wide panels mounted on a 1.5 m beam. Each local panel was fitted with a 10 metric ton load cell and had a total area of 10 cm (wide) by 40 cm (high); see Figure 6-11.
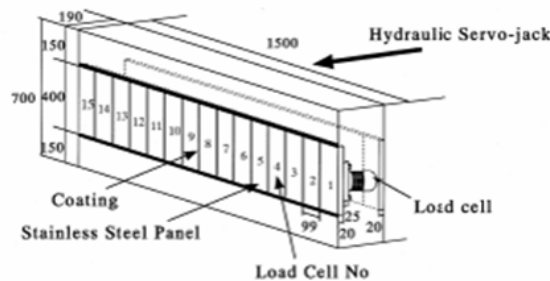
Figure 6-11   Segmented indenter used in MSFIT program (Sodhi et al., 1998)

In 2006, selected data from 1998, 1999 and 2000 seasons became publicly available. During the 1999 season 60 cm wide indenters were used, and thus these results are not considered here. Only results corresponding to tests with the 150 cm wide indenter (1998, 2000) are included in the present analysis. As discussed in Taylor (2010), each of the end panels of the indenter exhibited significant edge effects and data from these panels have been excluded from the analysis. Only data corresponding to the center 13 panels were included in the analysis. For the JOIA events, no screening parameters were required since the tests were conducted under controlled conditions and the relevance of individual

events to the present work could be more clearly determined. Details of the selected events and the event definition process used are provided in Taylor (2010).

6.2.4 Cook Inlet

Cook Inlet has been the site of concentrated oil and gas development since the early 1960s (Sanderson, 1988). The ice cover in Cook Inlet is typically thin first-year ice with maximum thickness often less than 0.5m. The salinity is in the range of 4-6 ppt and the ice is subject to vigorous tidal action. During the mid-1960s, 14 offshore structures were built in this region, with several being instrumented for ice forces during the 1963-1969 period. Instrumented piles were typically fitted with strain gauges to measure bending strain under load. The primary source of published data for this region is Blenkarn (1970).

Time series data are not available for the Cook Inlet measurements. In the following analysis, the steady ice load values reported by Blenkarn (1970) have been used to estimate mean pressures on the test structure. Standard deviations of pressure were not reported. These data were originally reported in units of thousands of pounds (kip) per foot in diameter and a corresponding value of thickness was provided. These values were converted into units of pressure (MPa) for an area of unit width (m) by converting the force per unit width to metric units and dividing by thickness.

Level Ice Filter
Blenkarn (1970) indicated that the limit of ice growth for the Cook Inlet region is on the order of 0.5 m. For this reason, an optional filter was used to remove data corresponding to ice thicknesses above 0.5m. Beyond this thickness, the ice is assumed to be rafted ice or refrozen brash ice.

The processing options used with this dataset are summarized in Table 6-1 for the various analysis cases presented in this report. It is noted that standard deviations of pressure and event durations are not available for these data. Cook Inlet data is absent from all portions of the analysis related to discussion of standard deviation of pressure and event duration.

6.3 Analysis

In light of the above assessment of the datasets, an analysis matrix was set-up to compare data processed using various combinations of the identified event screening criteria; see Table 6-1. These combinations of screening criteria were selected to illustrate the relationship between the Molikpaq and other datasets, while examining the influence of various factors on the observed trends. Results for individual cases have been grouped into pairs which have used similar analysis option. These are discussed below.

Table 6-1: **Description of cases considered in analysis**

Case	Molikpaq	STRICE	JOIA	Cook Inlet
1	Softening Correction Off Unweighted Mean	Level Ice Filter On Duration Filter Off	No Filters	Level Ice Filter On
2	Softening Correction On Unweighted Mean	Level Ice Filter On Duration Filter Off	No Filters	Level Ice Filter On
3	Softening Correction Off Weighted Mean	Level Ice Filter On Duration Filter Off	No Filters	Excluded
4	Softening Correction On Weighted Mean	Level Ice Filter On Duration Filter Off	No Filters	Excluded
5	Softening Correction On Unweighted Mean	Level Ice Filter On Duration Filter On	No Filters	Level Ice Filter On
6	Softening Correction On Weighted Mean	Level Ice Filter On Duration Filter On	No Filters	Excluded
7	Softening Correction On Unweighted Mean	Level Ice Filter Off Duration Filter Off	No Filters	Level Ice Filter Off
8	Softening Correction On Unweighted Mean	Level Ice Filter On Duration Filter On	No Filters	Excluded
9	Softening Correction Off Unweighted Mean	Level Ice Filter On Duration Filter On	Excluded	Excluded
10	Softening Correction On Unweighted Mean	Level Ice Filter On Duration Filter On	Excluded	Excluded
11	Softening Correction Off Weighted Mean	Level Ice Filter On Duration Filter On	Excluded	Excluded
12	Softening Correction On Weighted Mean	Level Ice Filter On Duration Filter On	Excluded	Excluded

For each of the above analysis cases, power law curves were fitted to the data. The assumed forms for the power law curves were:

$$P_{avg} = C\,h^{D}; \; P_{std} = E\,h^{F}$$

Values of these parameters are discussed below for each of the analysis cases.

6.3.1 Analysis Pair 1: Case 1 and Case 2

Data for this pair were analyzed using unweighted means for the assessment of mean pressure and standard deviations. The STRICE data were filtered to only include level ice, but were not filtered by event duration. JOIA data were not filtered and the Cook Inlet data only included results corresponding to level ice thicknesses. Molipaq data were analyzed with the softening correction turned off for Case 1, and turned on for Case 2.

For Case 1, a softening correction was not applied to the Molikpaq data. Results for the mean pressure data for this case are shown in Figure 6-12(a) and standard deviation of pressure data are in Figure 6-12 (b). As may be observed in Figure 6-12 (a), the

uncorrected Molikpaq mean pressure data are significantly higher than the other data and have a wider degree of variability. The power law fitted to the mean pressure data has parameters $C = 0.407$ and $D = -0.128$. Similarly for standard deviation of pressure data shown in Figure 6-12 (b), the Molikpaq dataset has significantly higher values than the standard deviations for other datasets. The power law fitted to the standard deviation of pressure data has parameter values $E = 0.228$ and $F = 0.106$.

For Case 2, a softening correction factor was used for the Molikpaq data. The mean pressure and standard deviation of pressure data are shown in Figure 6-13(a) and Figure 6-13 (b), respectively. As shown in Figure 6-13 (a), the corrected Molikpaq mean pressure data are much more consistent with the STRICE, JOIA and Cook Inlet data and a distinct pressure-thickness effect is observed. Similarly the standard deviation data for the corrected Molikpaq results in Figure 6-13 (b) are in much better agreement with STRICE and JOIA than were the uncorrected results shown for Case 1. For this case the curve fit parameters for the mean pressure data were found to be $C = 0.287$ and $D = -0.401$, and $E = 0.15$ and $F = -0.185$ for the standard deviation of pressure.

6.3.2 Analysis Pair 2: Case 3 and Case 4

For these cases duration weighted means were used in the assessment of mean pressure and standard deviations. The STRICE data were filtered to only include level ice, but were not filtered by event duration. The JOIA data were not filtered and Cook Inlet data are excluded, since event durations are not known for these data. Molikpaq data were included with the softening correction turned off for Case 3, and turned on for Case 4.

Case 3 did not include corrections to the Molikpaq data for panel softening. From Figure 6-14 (a) and (b) it may be observed inconsistencies between the uncorrected Molikpaq mean pressure data and other datasets dominates the trends for this case. The use of weighted means has little impact on these results, since the mismatch between the uncorrected Molikpaq and other datasets dominates the results. The curve fit parameters were found to be $C = 0.392$ and $D = -0.058$ for the mean pressure data and $E = 0.345$ and $F = 0.273$ for the standard deviation of pressure.

In Case 4, a softening correction was applied to the Molikpaq data. It may be observed from the mean pressure data in Figure 6-15 (a) and the standard deviation of pressure data in Figure 6-15 (b) that there is more consistency between the Molikpaq, STRICE and JOIA data for this case. Both mean and standard deviation results support a decreasing pressure-thickness trend. The curve fit parameters for this case were found to have values of $C = 0.212$ and $D = -0.429$ for the mean pressure and $E = 0.179$ and $F = -0.098$ for the standard deviation of pressure.

6.3.3 Analysis Pair 3: Case 5 and Case 6

This analysis pair used softening corrected Molikpaq data. STRICE data were filtered using the level ice and all events with duration less than 10 minutes were filtered out. JOIA data were not filtered.

For Case 5, unweighting means were used, and Cook Inlet data were filtered to include only level ice. From Figure 6-16 (a) it is observed that a good fit to the mean pressure data is obtained. The mean pressure data were well represented by a curve with parameter values $C = 0.299$ and $D = -0.384$. The standard deviation of pressure data are plotted in Figure 6-16 (b). Power law parameter values of $E = 0.167$ and $F = -0.182$ were obtained for a curve fitted to these data. A distinct decreasing pressure-thickness trend is observed for both mean and standard deviation results.

For Case 6, duration weighting was used and Cook Inlet data were excluded, since no duration information is available for this set. It may be observed from Figure 6-17 (a) that the curve fitted to the mean pressure data has parameters $C = 0.211$ and $D = -0.392$. While these parameter values well model the data for thin ice, the curve does not well bound the pressure values for thicker ice. The standard deviation of pressure results are plotted in Figure 6-17 (b). A power law curve of the form $P = Eh^F$ was fitted to these data and yielded parameter values of $E = 0.179$ and $F = -0.11$. While a trend of decreasing pressure with increasing thickness is observed for these results, the resulting power law fit does not bound the data as well as the curve fit parameters obtained for Case 5.

6.3.4 Analysis Pair 4: Case 7 and Case 8

For these analysis cases, corrected Molikpaq data were used, along with STRICE and JOIA data. Case 7 did not include any filtering for duration or for thicker rafted ice. Unfiltered Cook Inlet data were also included for this case. In Case 8, level ice and duration filters were used for the STRICE data and Cook Inlet data were excluded. In both cases, unweighted means were used in the assessment of overall mean and standard deviation of pressures.

The mean pressure data, along with associated mean curve and 95% confidence intervals on future response for Case 7 are shown Figure 6-18 (a). The parameter values for the curve fitted to these data are $C = 0.242$ and $D = -0.539$. From this plot it may be observed that the fitted curve tends to provide a better representation of the data for thinner ice, than for thick ice. Similarly in Figure 6-18 (b) a power law curve and associated confidence intervals were fitted to the unweighted standard deviation of pressure data. The fitted curve had parameter values of $E = 0.116$ and $F = -0.387$ for the standard deviation results. As may be observed in this plot, a decreasing pressure-thickness trend is evident, with the curve well bounding the data for this analysis case.

The unweighted mean pressure curve, confidence intervals on future response and mean pressure data for Case 8 are given in Figure 6-19 (a). A curve with power law parameter values of $C = 0.273$ and $D = -0.377$ were fitted to these data. The standard deviation results, along with the fitted power law curve and associated confidence intervals are shown in Figure 6-19 (b). The curve shown in this figure has parameter values of $E = 0.167$ and $F = -0.182$. As in previous analysis cases, a trend of decreasing pressure with

increasing thickness is evident. It may be observed from Figure 6-19 that the fitted curves well bound the data over the range of thicknesses included in this analysis.

6.3.5 Analysis Pair 5: Case 9 and Case 10

A main focus of this analysis pair was to examine results based solely on the STRICE and Molikpaq data (JOIA and Cook Inlet were excluded). STRICE data were filtered using both the level ice filter and the duration filter. The overall mean and standard deviation of pressures were evaluated using unweighted means for both cases. For Case 9, Molikpaq data were not corrected for softening. A softening correction factor was applied to the Molikpaq data for Case 10.

The unweighted mean and standard deviation of pressure curves for Case 9 are given in Figure 6-20. The power law curve parameters for the mean pressure data are $C = 0.44$ and $D = -0.113$, and $E = 0.286$ and $F = 0.022$ for the standard deviation results. As in other cases which did not use a softening correction, the Molikpaq data are not consistent with the other datasets and data are not well represented by the curve fits.

The results for Case 10 are given in Figure 6-21 (a) for mean pressure, and Figure 6-21 (b) for standard deviation of pressure. Parameter values of $C = 0.278$ and $D = -0.408$ were obtained for the mean pressure power law fit. Similarly for the standard deviation results, parameter values were found to be $E = 0.172$ and $F = -0.273$. From these data a clear trend of decreasing pressure with increasing thickness is observed. As shown in Figure 6-21, the above power law curves well bound the data for both mean and standard deviation results. As with other analysis cases, the Molikpaq data to which a softening correction factor had been applied were much more consistent with the STRICE results than were the uncorrected data.

6.3.6 Analysis Pair 6: Case 11 and Case 12

This analysis pair also examined results based solely on the STRICE and Molikpaq data (JOIA and Cook Inlet were excluded). The STRICE data were filtered using both the level ice filter and the duration filter. For these cases, duration weighted means were used for both cases. Molikpaq data were not corrected for softening for Case 11. For Case 12 a softening correction factor was applied to the Molikpaq data.

The mean pressure and standard deviation of pressure results for Case 11 are given in Figure 6-22(a) and Figure 6-22 (b), respectively. For the mean pressure power law fit, parameter values of $C = 0.392$ and $D = -0.038$ were obtained. Similarly, parameter values of $E = 0.348$ and $F = 0.229$ were obtained for the standard deviation results. It is again observed that uncorrected Molikpaq data are not consistent with the STRICE data and are not well represented by the fitted curves.

The softening corrected Molikpaq data used in Case 12 showed much better agreement with the STRICE data. The mean pressure data for this case is given in Figure 6-23 (a),

along with the associated power law curve and 95% confidence intervals on future response. Power law parameter values of $C = 0.211$ and $D = -0.383$ were fitted to the mean pressure data. As shown in Figure 6-23 (b), standard deviation of pressure data have been fitted with a power law curve ($E = 0.179$ and $F = -0.117$). A trend of decreasing pressure with increasing thickness is evident. As in earlier analysis cases using duration weighted means, the confidence intervals on future response do not bound the data as well as the unweighted analysis. Improved techniques for weighting should be explored.
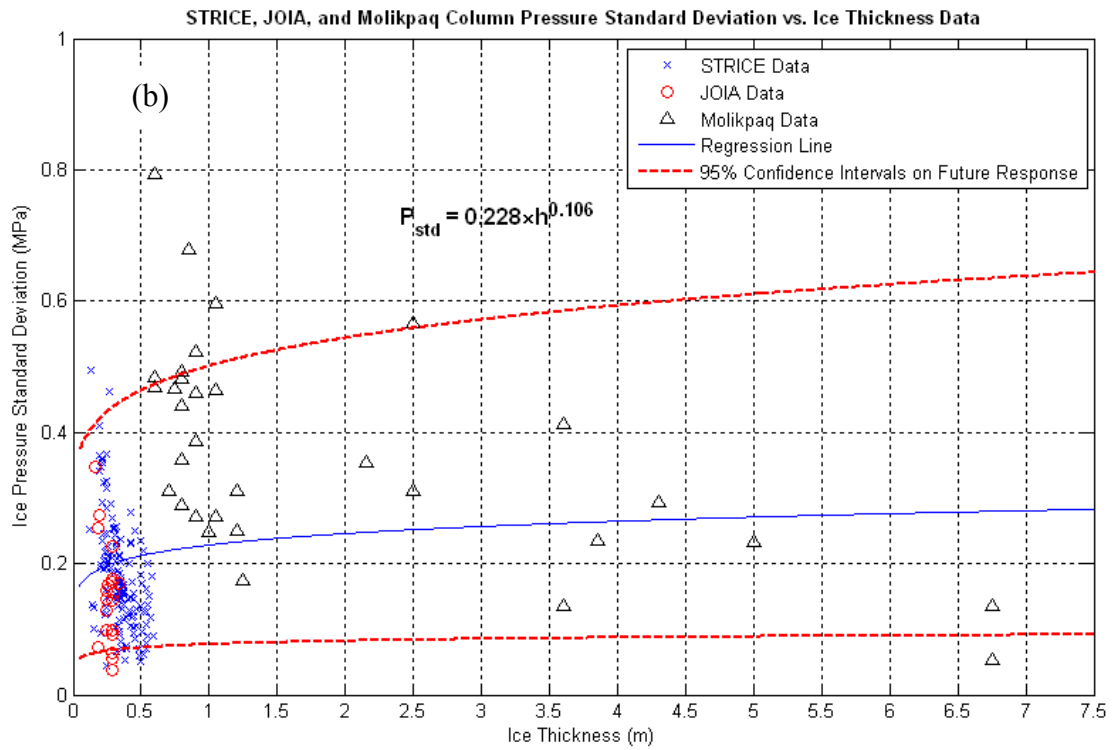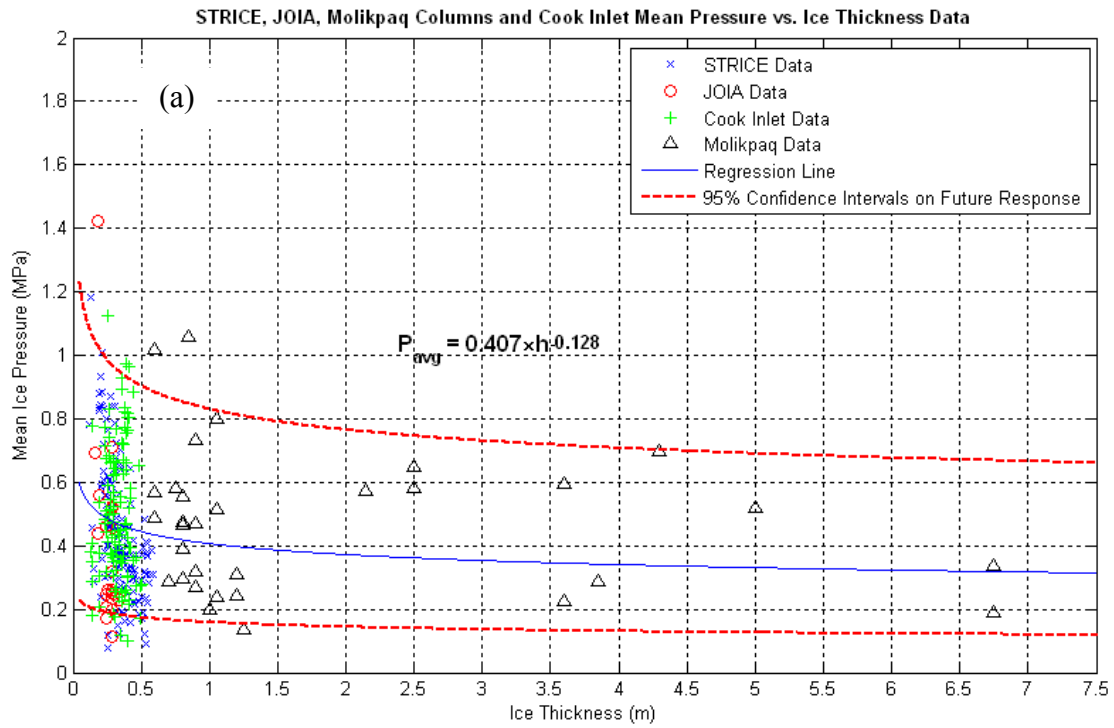
Figure 6-12 Case 1 (Molikpaq softening correction off; STRICE level ice filter on, duration filter off; JOIA unfiltered; Cook Inlet level ice filter on; unweighted mean) data and curve fits for: (a) mean pressure results; (b) standard deviation of pressure results.
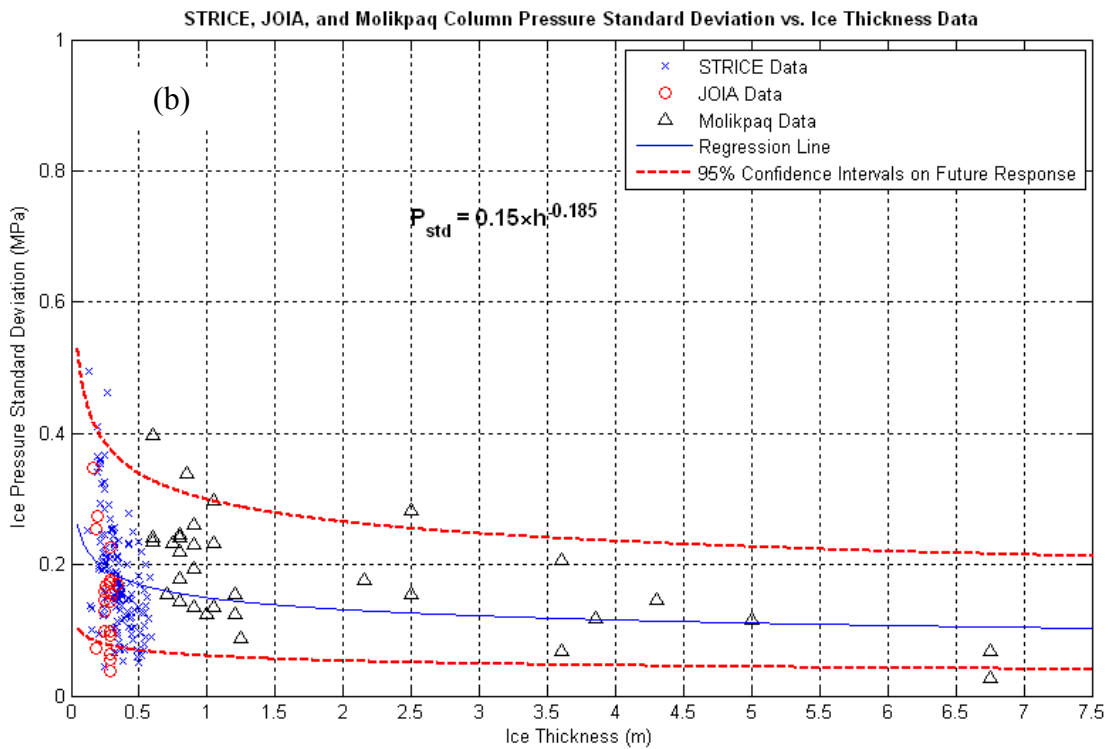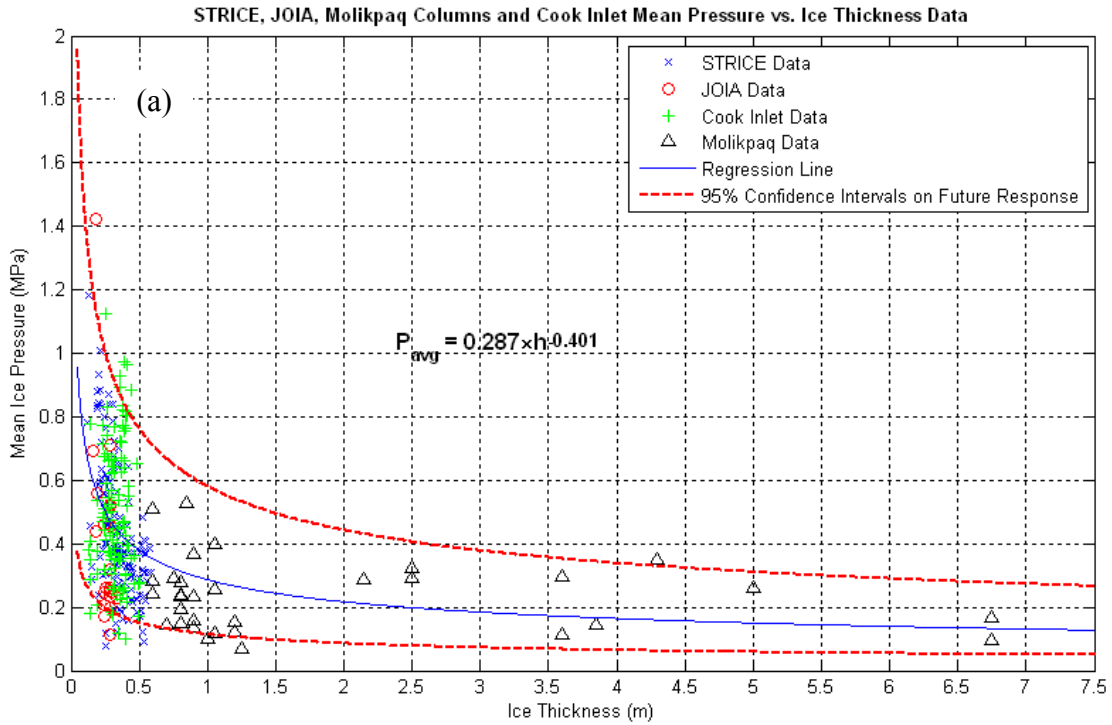
Figure 6-13   Case 2 (Molikpaq softening correction on; STRICE level ice filter on, duration filter off; JOIA unfiltered; Cook Inlet level ice filter on; unweighted mean) data and curve fits for: (a) mean pressure results; (b) standard deviation of pressure results.
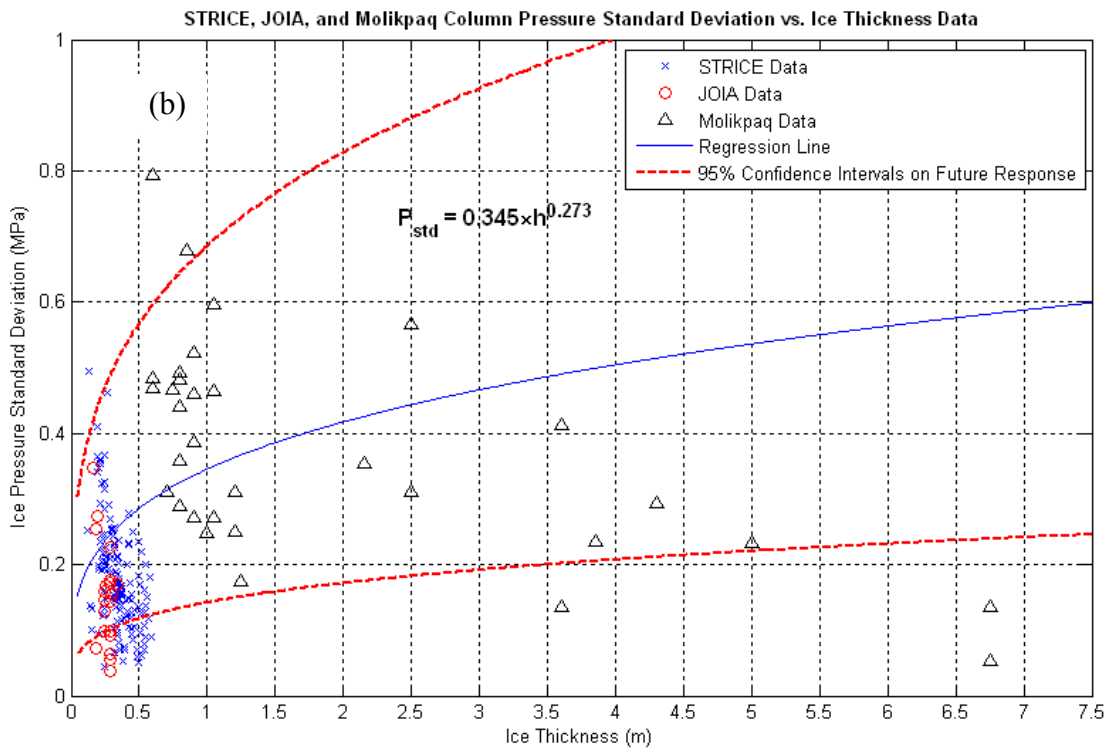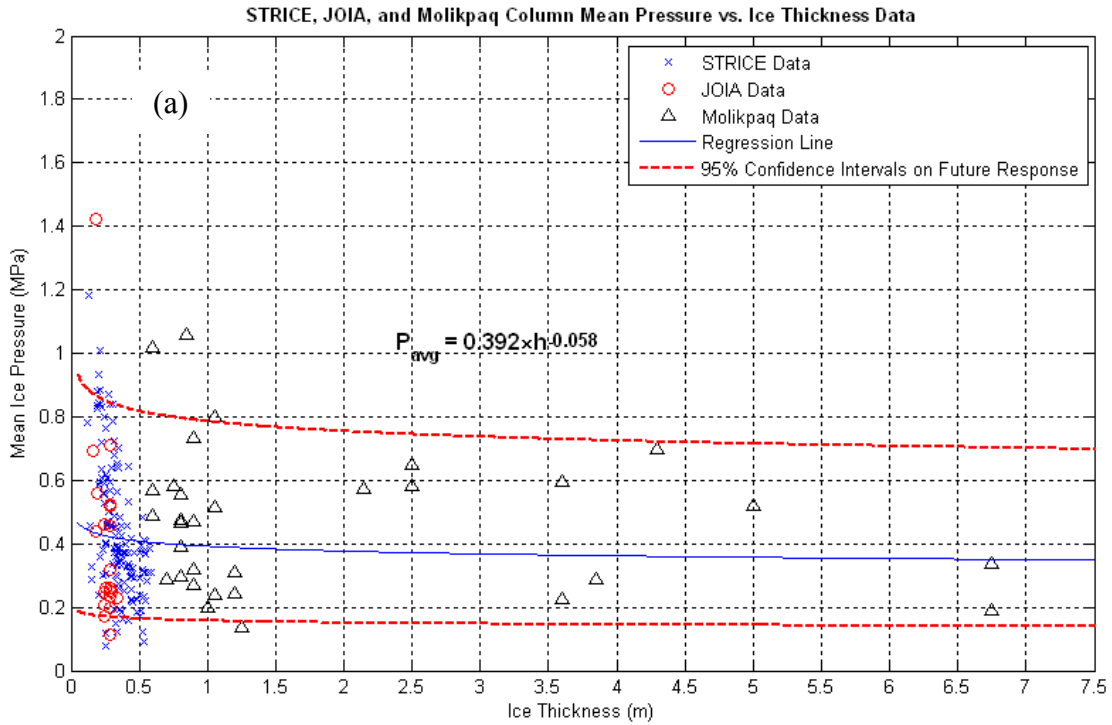
Figure 6-14 Case 3 (Molikpaq softening correction off; STRICE level ice filter on, duration filter off; JOIA unfiltered; Cook Inlet data excluded; weighted mean) data and curve fits for: (a) mean pressure results; (b) standard deviation of pressure results.
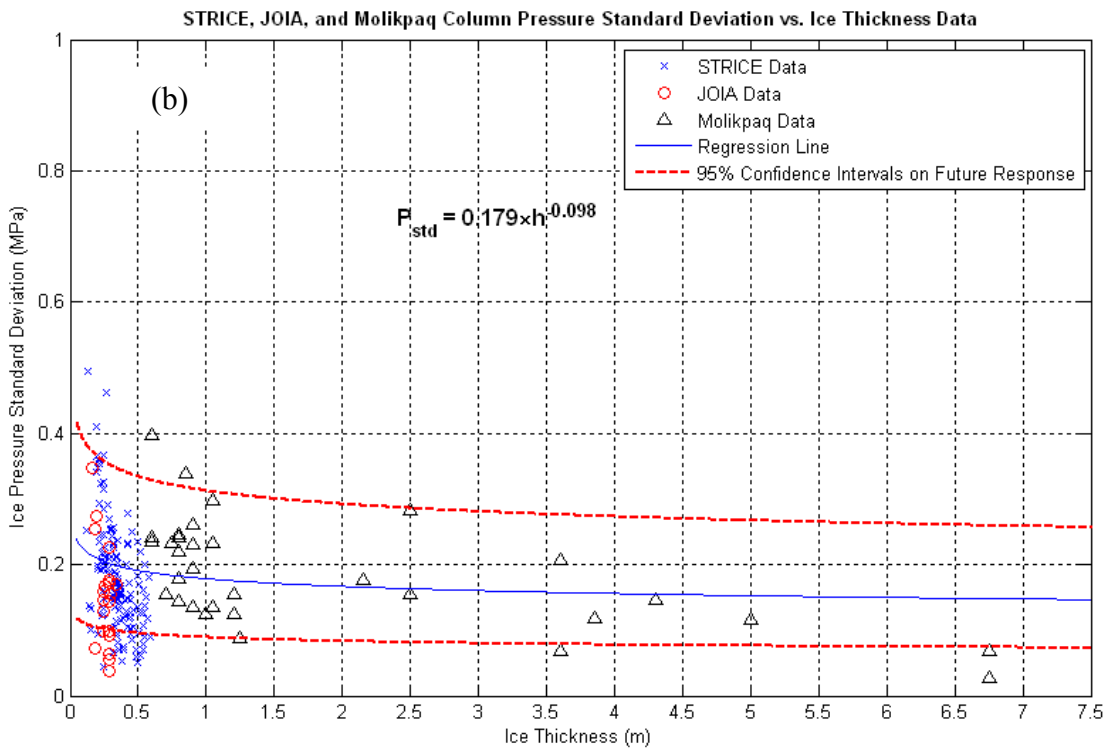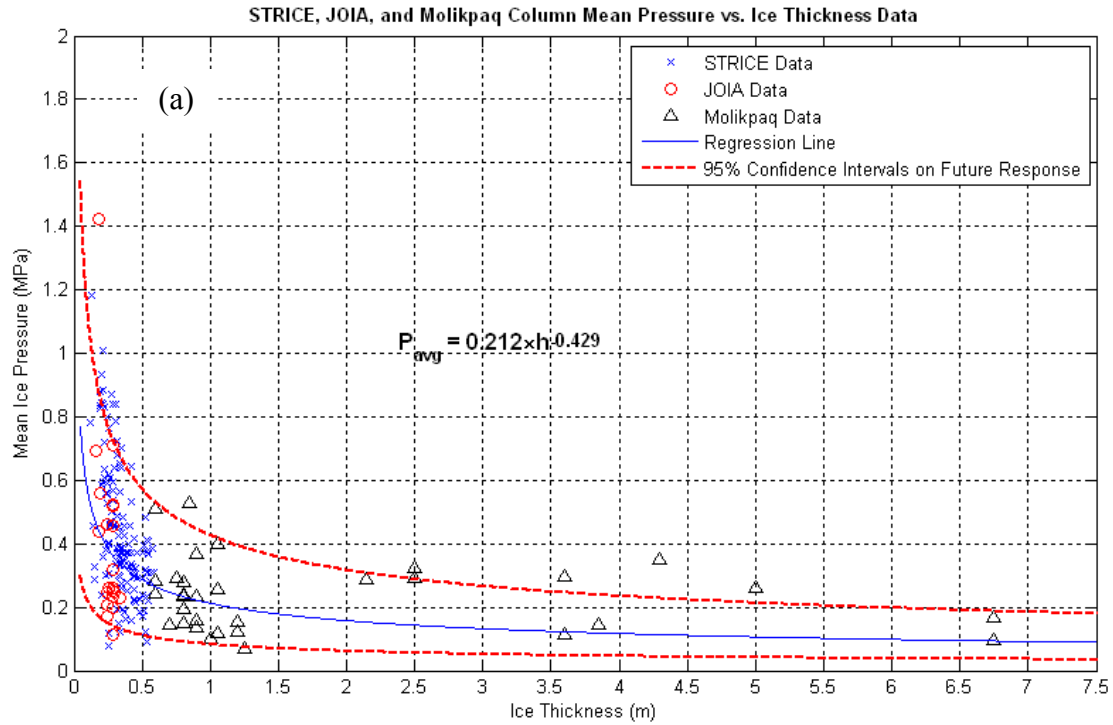
Figure 6-15 **Case 4 (Molikpaq softening correction on; STRICE level ice filter on, duration filter off; JOIA unfiltered; Cook Inlet excluded; weighted mean) data and curve fits for: (a) mean pressure results; (b) standard deviation of pressure results.**
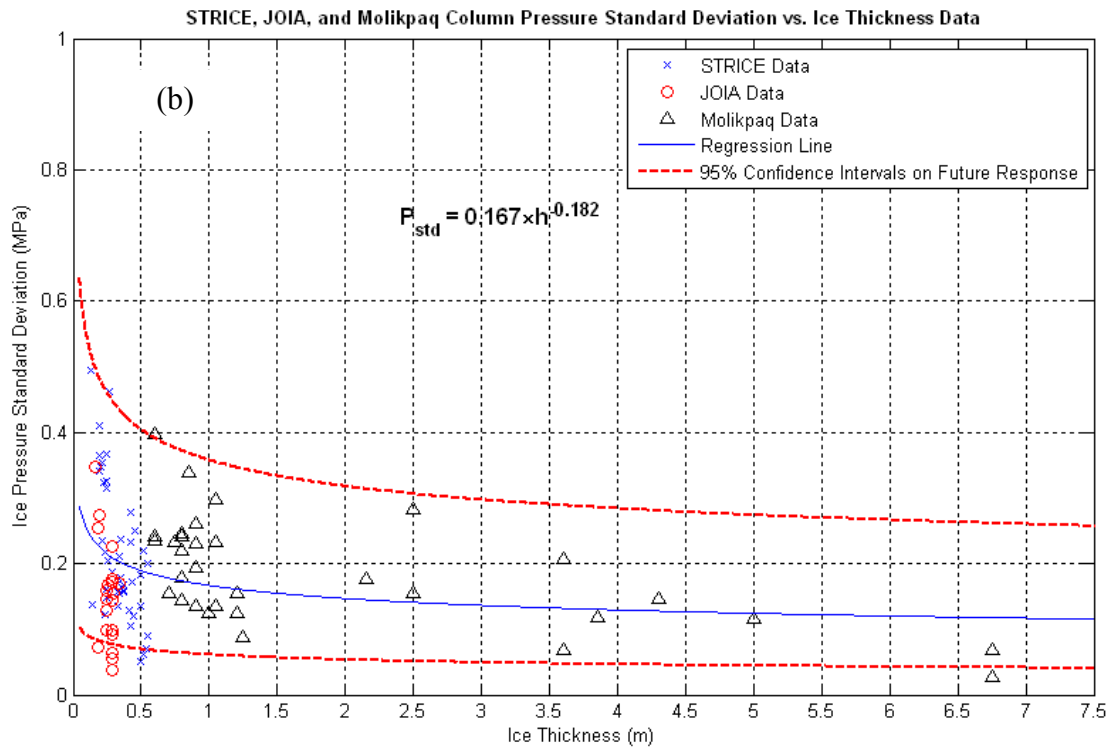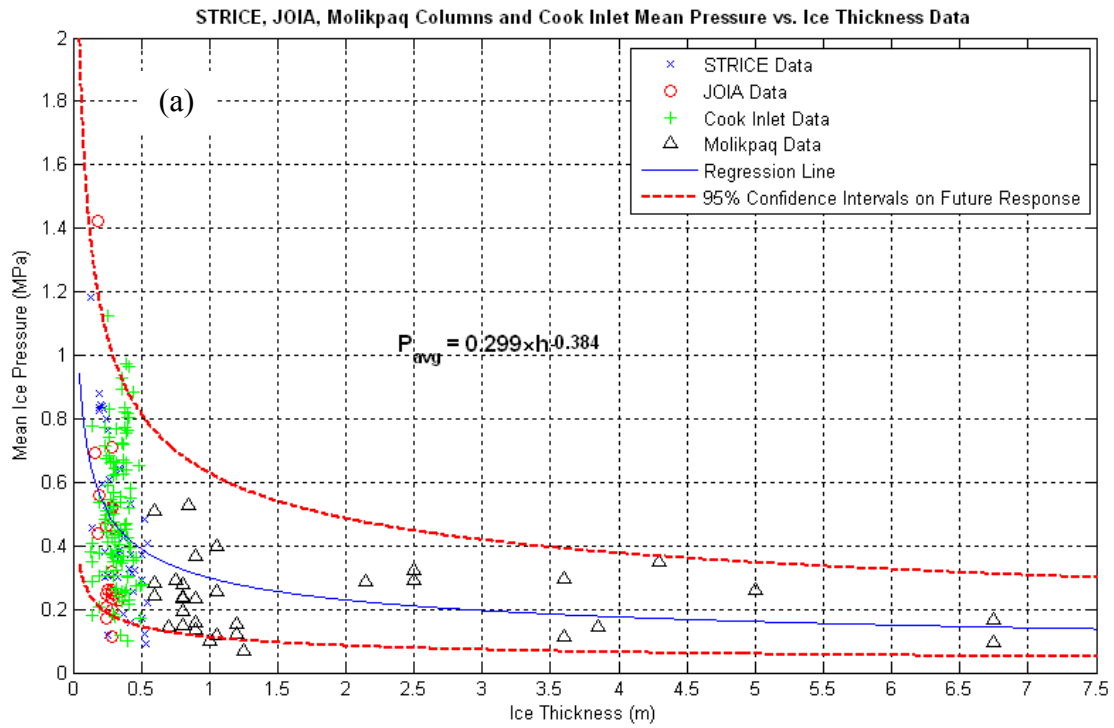
Figure 6-16   Case 5 (Molikpaq softening correction on; STRICE level ice filter on, duration filter on; JOIA unfiltered; Cook Inlet level ice filter on; unweighted mean) data and curve fits for: (a) mean pressure results; (b) standard deviation of pressure results.
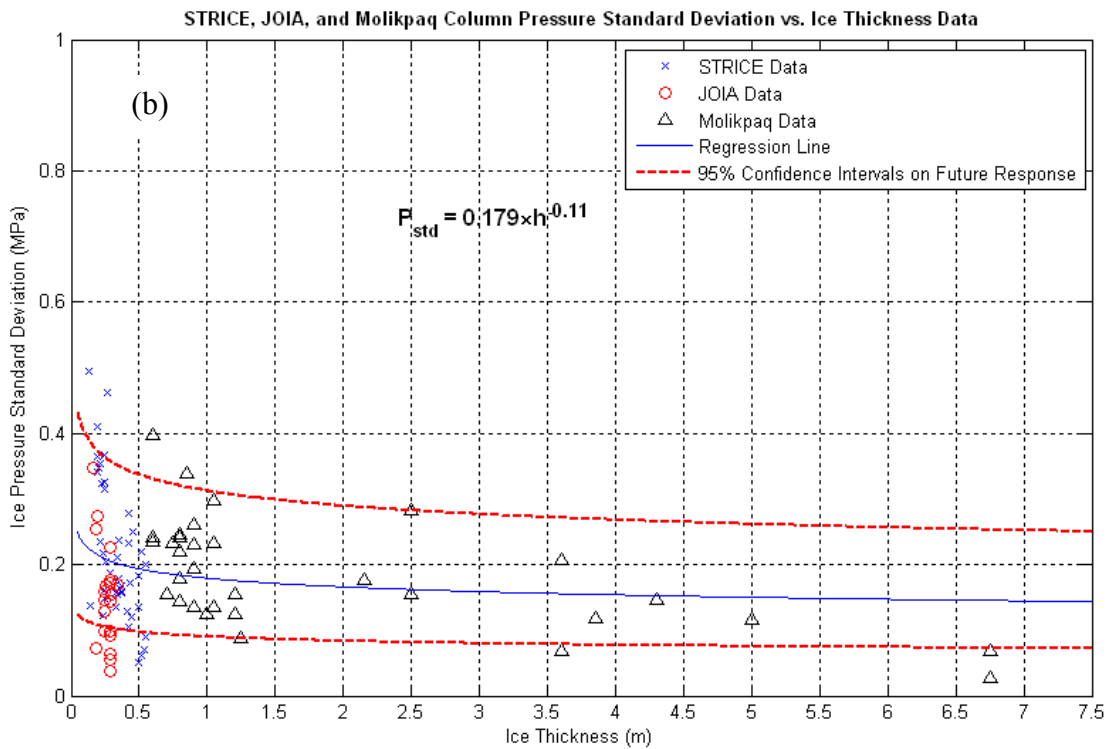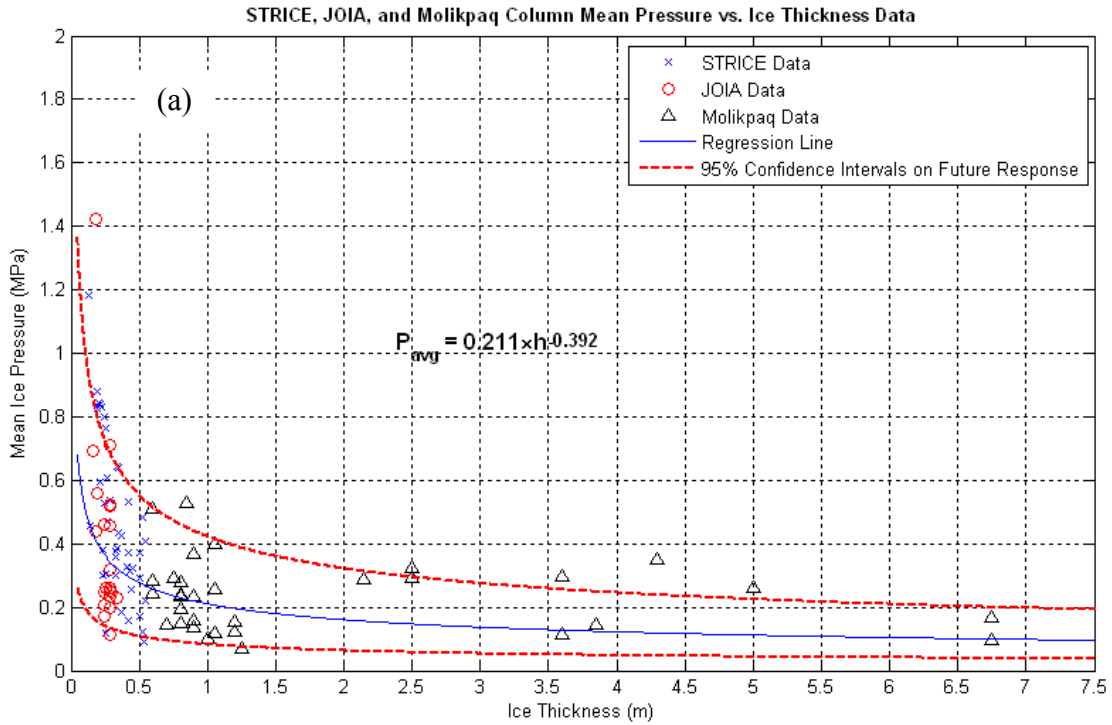
Figure 6-17 **Case 6 (Molikpaq softening correction on; STRICE level ice filter on, duration filter on; JOIA unfiltered; Cook Inlet data excluded; weighted mean) data and curve fits for: (a) mean pressure results; (b) standard deviation of pressure results.**
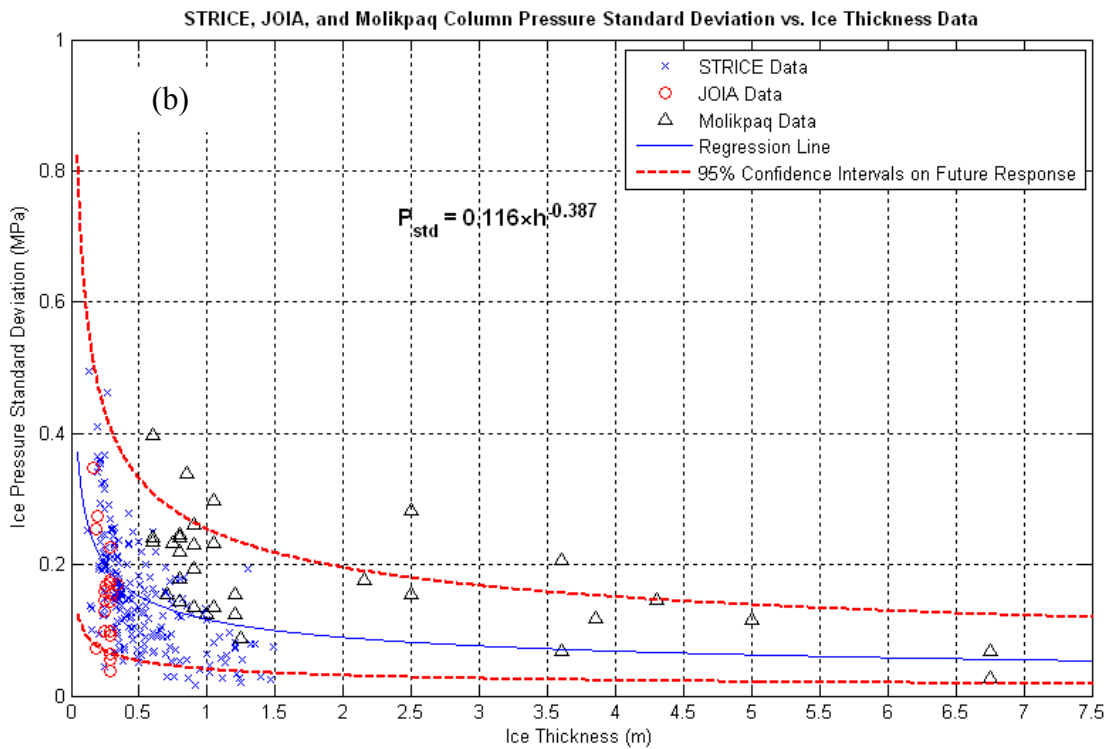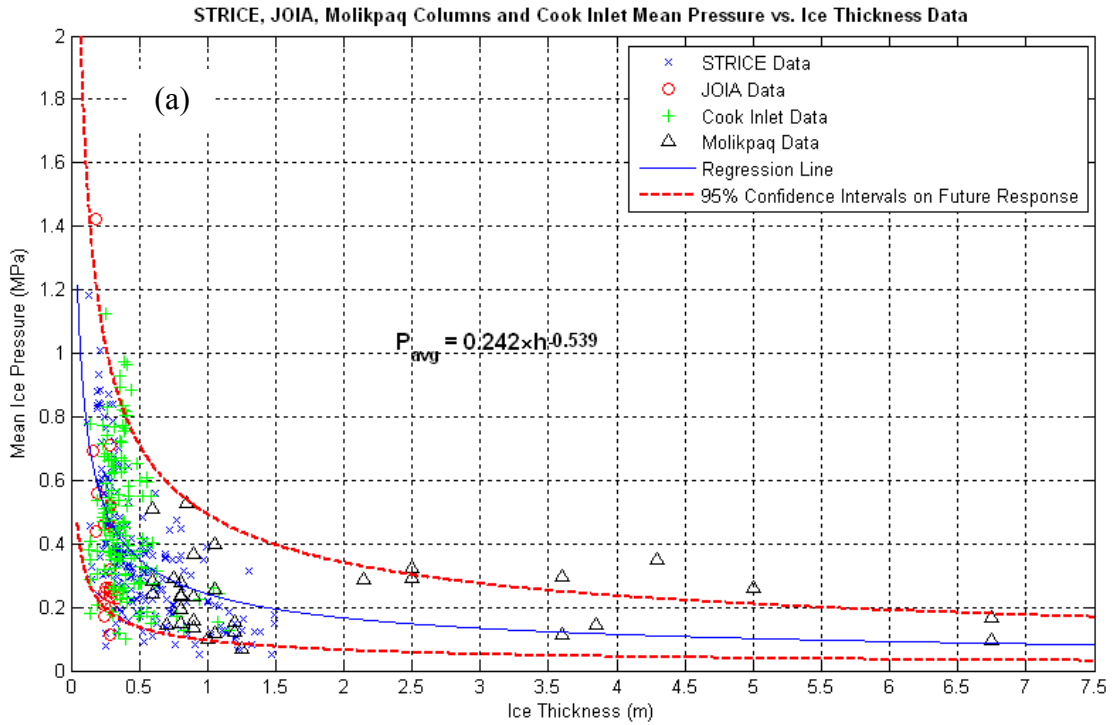
Figure 6-18 **Case 7 (Molikpaq softening correction on; STRICE level ice filter off, duration filter off; JOIA unfiltered; Cook Inlet data level ice filter off; unweighted mean) data and curve fits for: (a) mean pressure results; (b) standard deviation of pressure results.**
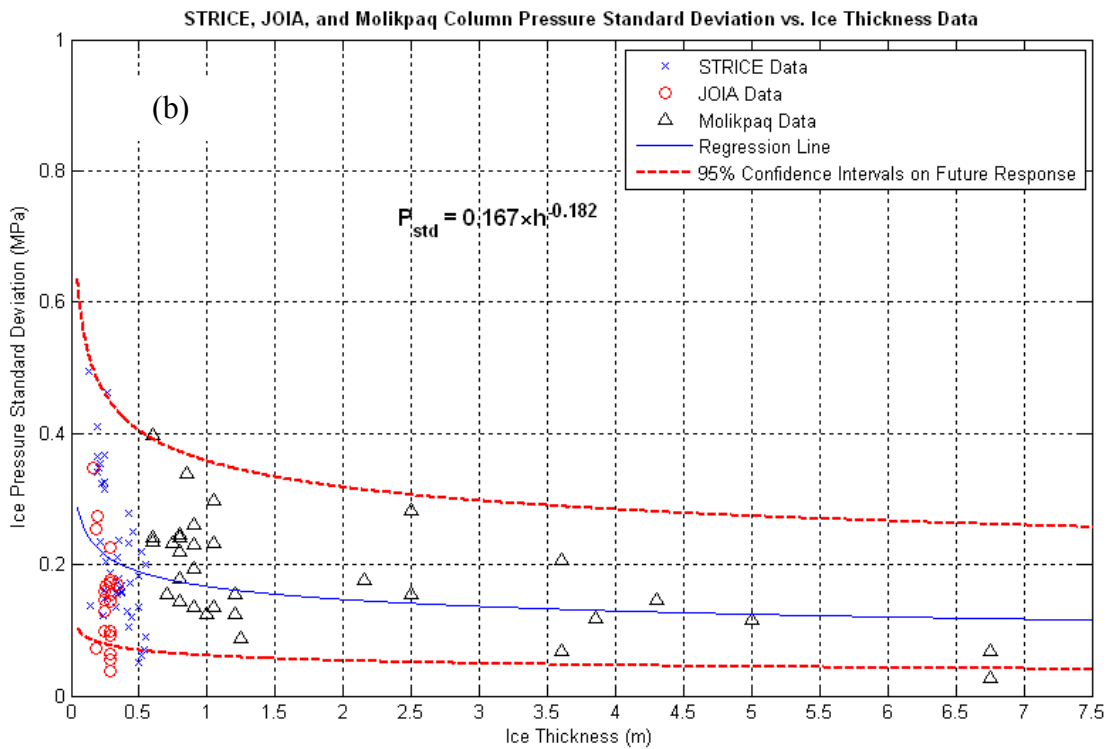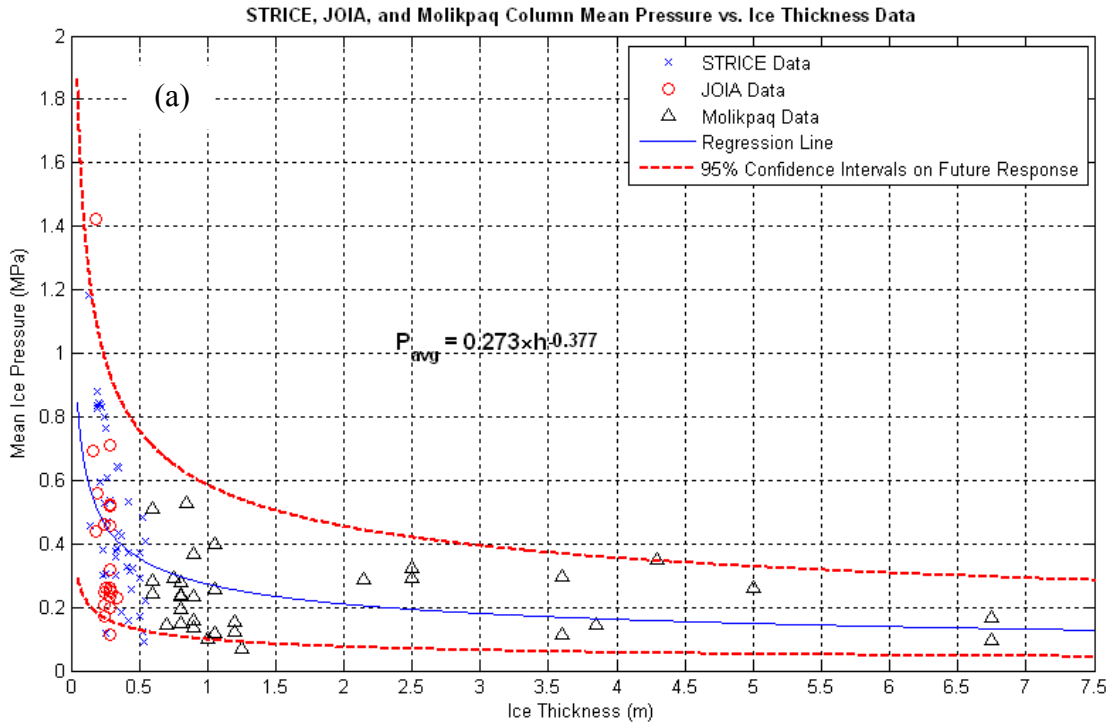
Figure 6-19   Case 8 (Molikpaq softening correction on; STRICE level ice filter on, duration filter on; JOIA unfiltered; Cook Inlet data excluded; unweighted mean) data and curve fits for: (a) mean pressure results; (b) standard deviation of pressure results.
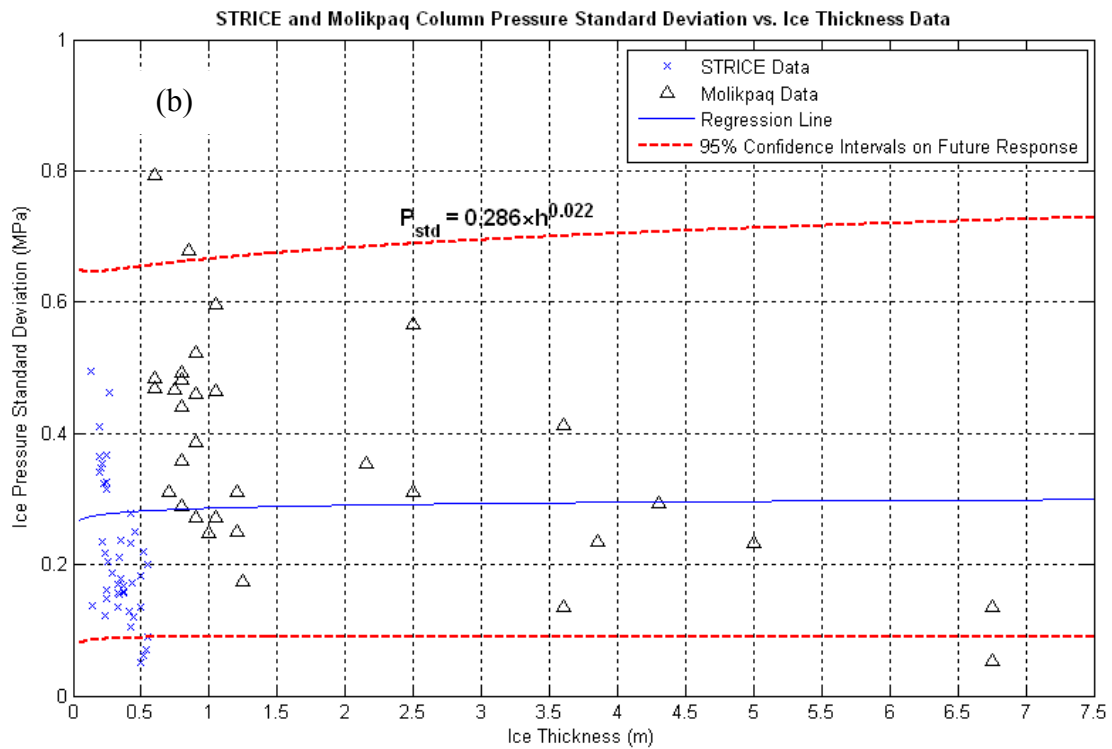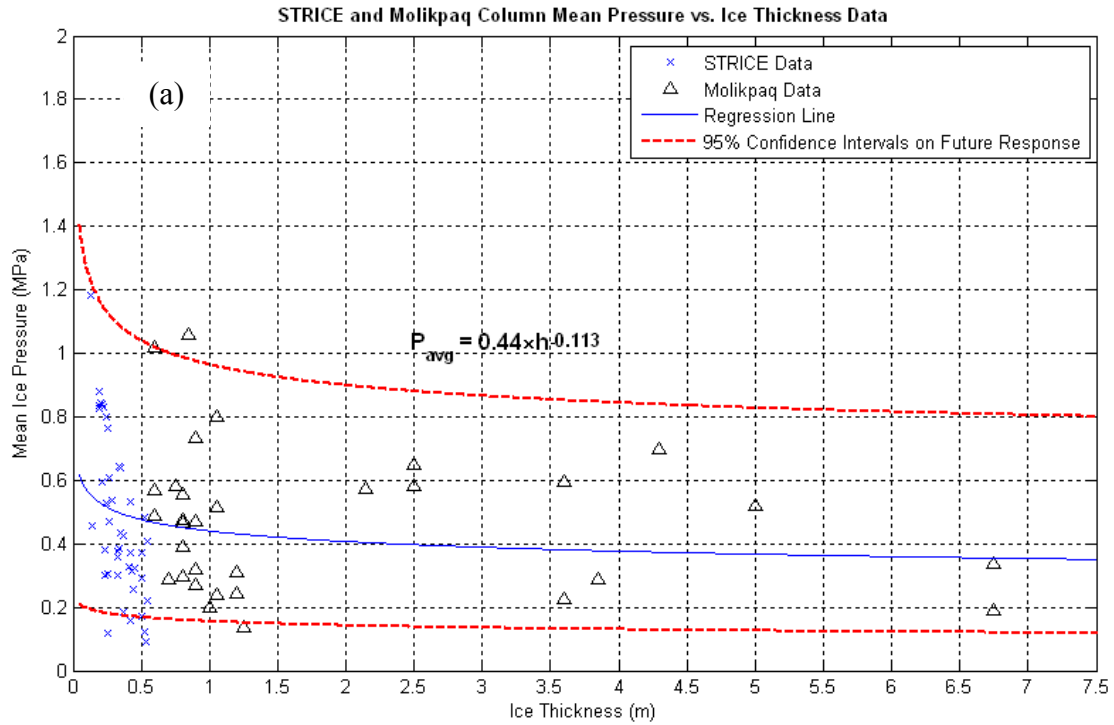
Figure 6-20 **Case 9 (Molikpaq softening correction off; STRICE level ice filter on, duration filter on; JOIA excluded; Cook Inlet data excluded; unweighted mean) data and curve fits for: (a) mean pressure results; (b) standard deviation of pressure results.**
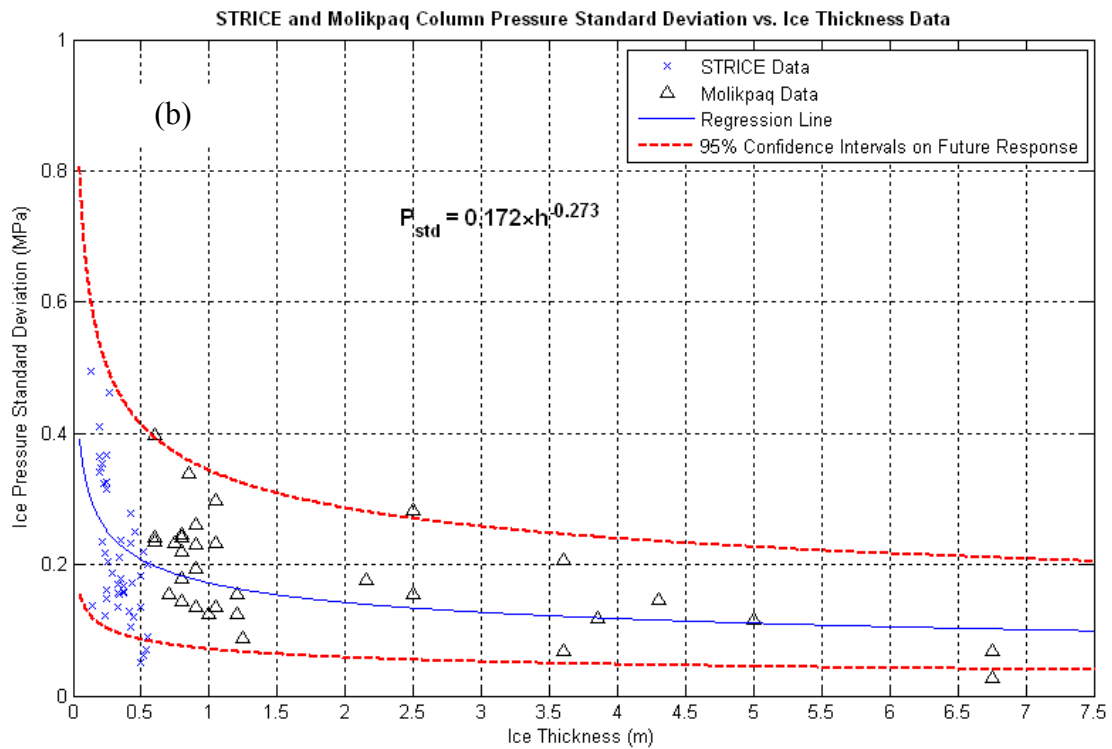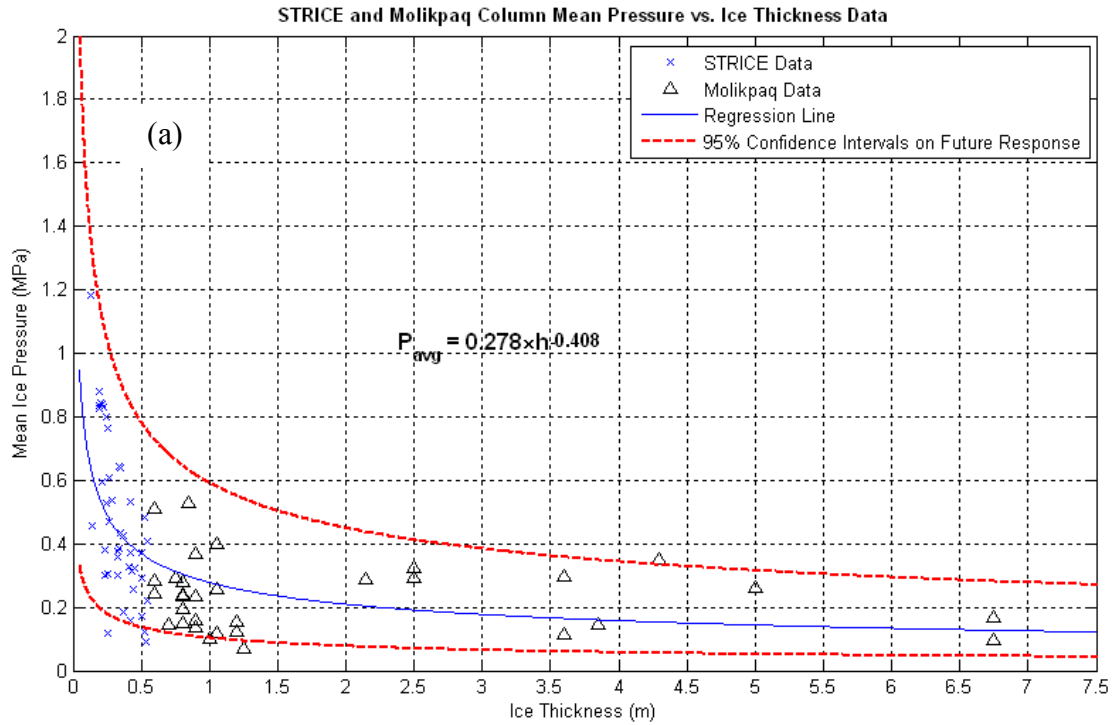
Figure 6-21   Case 10 (Molikpaq softening correction on; STRICE level ice filter on, duration filter on; JOIA excluded; Cook Inlet data excluded; unweighted mean) data and curve fits for: (a) mean pressure results; (b) standard deviation of pressure results.
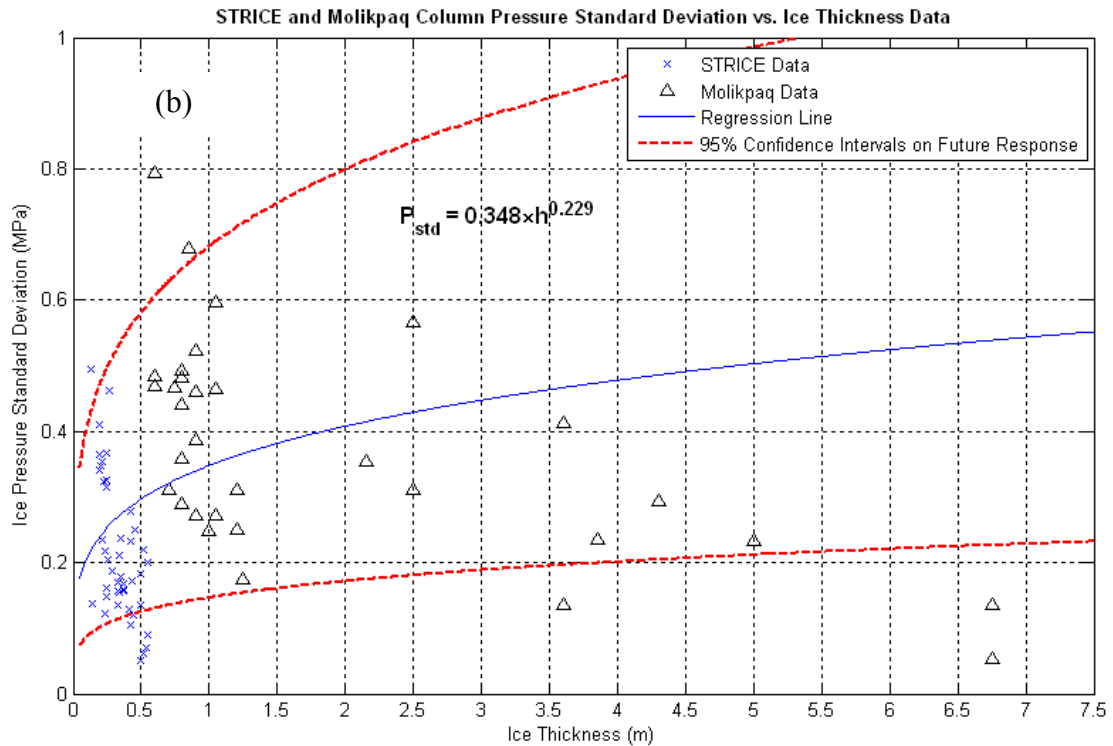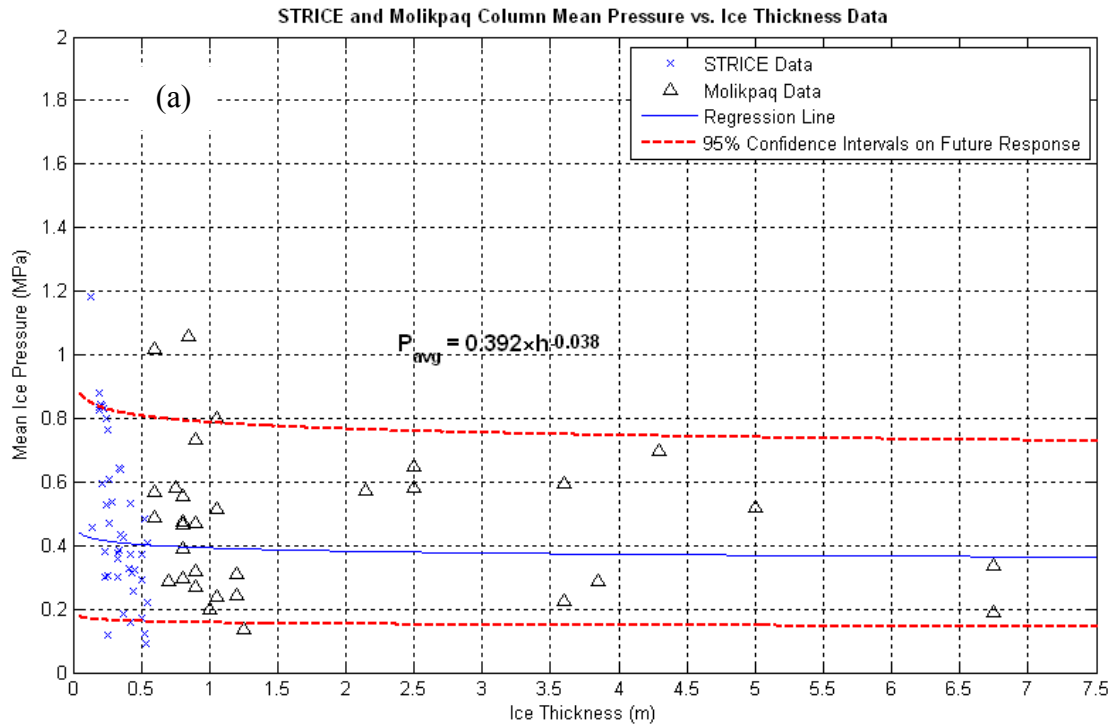
Figure 6-22   Case 11 (Molikpaq softening correction off; STRICE level ice filter on, duration filter on; JOIA excluded; Cook Inlet data excluded; weighted mean) data and curve fits for: (a) mean pressure results; (b) standard deviation of pressure results.

STRICE and Molikpaq Column Mean Pressure vs. Ice Thickness Data

(a)

$P_{avg} = 0.211 \times h^{-0.383}$

STRICE and Molikpaq Column Pressure Standard Deviation vs. Ice Thickness Data

(b)

$P_{std} = 0.179 \times h^{-0.117}$
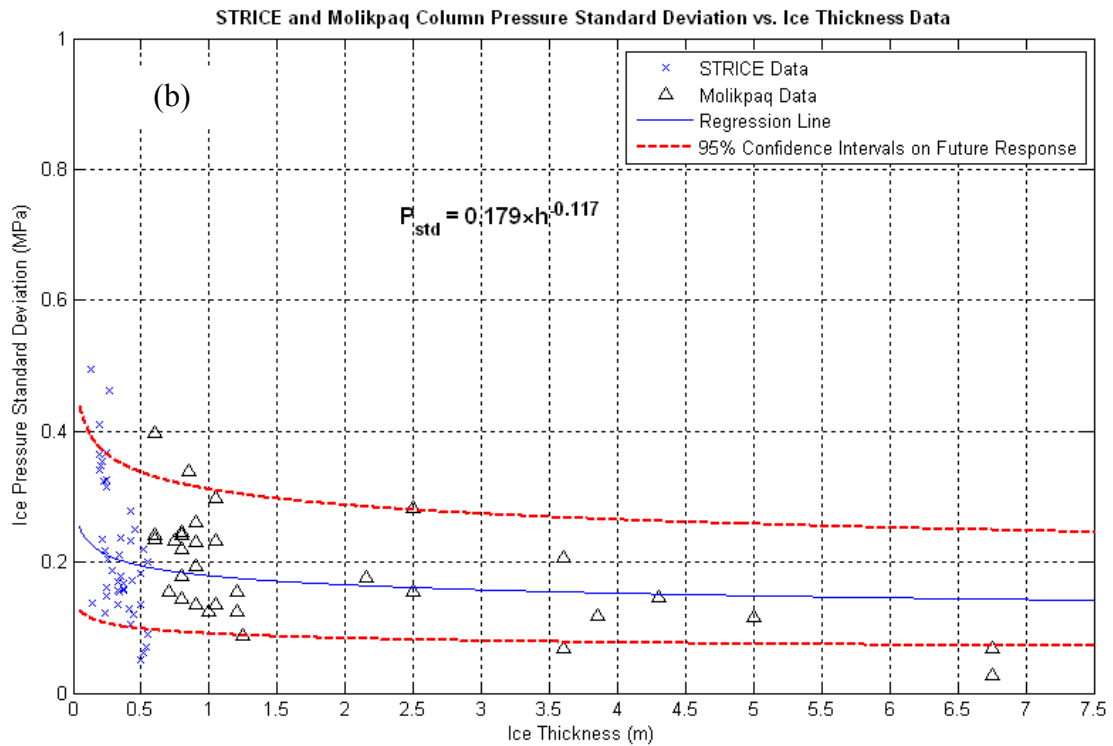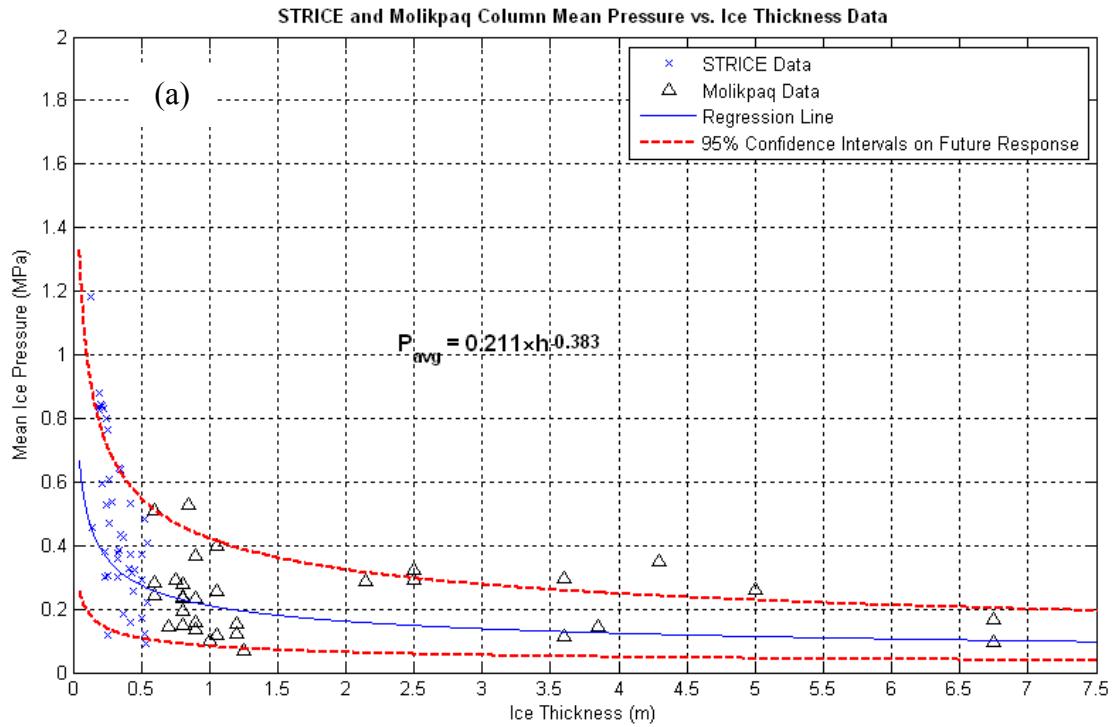
**Figure 6-23   Case 12 (Molikpaq softening correction on; STRICE level ice filter on, duration filter on; JOIA excluded; Cook Inlet data excluded; weighted mean) data and curve fits for: (a) mean pressure results; (b) standard deviation of pressure results.**

6-30

6.4 Discussion

To assess which analysis case is most representative of the observed pressure-thickness trends, a discussion of different analysis options is given below. The aim in comparing the different cases is to assess which set of analysis criteria produce the most appropriate power law fit to represent the observed pressure-thickness scale effect. Parameter values for each analysis case have been summarized in Table 2.

Table 6-2: **Power law parameters fit to mean and standard deviation data for analysis cases**

Case	$P_{avg} = C\,h^{D}$		$P_{std} = E\,h^{F}$	
	C	D	E	F
1	0.407	-0.128	0.228	0.106
2	0.287	-0.401	0.150	-0.185
3	0.392	-0.058	0.345	0.273
4	0.212	-0.429	0.179	-0.098
5	0.299	-0.384	0.167	-0.182
6	0.211	-0.392	0.179	-0.110
7	0.242	-0.539	0.116	-0.387
8	0.273	-0.377	0.167	-0.182
9	0.440	-0.113	0.286	0.022
10	0.278	-0.408	0.172	-0.273
11	0.392	-0.038	0.348	0.229
12	0.211	-0.383	0.179	-0.117

Effect of panel softening correction
Examining the power law parameters given in Table 6-2, as well as the data presented in Figure 6-12 through Figure 6-23, it is evident that the softening correction has a considerable impact on the consistency between the Molikpaq and other datasets. This is particularly evident for standard deviation data (compare for instance Case 11 with Case 12). For cases with uncorrected data, the fitted power law curves for the standard deviation of pressure data often have positive exponents, and yield very poor agreement with the data; see for example Figure 6-22 (b). By comparison, when the Molikpaq data is corrected to account for panel softening (i.e. Figure 23 (b)) significant improvements in the agreement between the Molikpaq and other data results. On this basis it may be concluded that correcting the Molikpaq data to account for panel softening results in more consistency between the Molikpaq, STRICE, JOIA and Cook Inlet datasets.

Effect of duration weighting
As discussed earlier in the chapter, duration weighting was used in some analysis cases to assign more statistical weight to events with longer durations. For most cases, (i.e. Case 3 and Case 4) using weighted means did not improve the accuracy of the curve fits in bounding the datasets. Depending on the filtering criteria used, different numbers of datapoints from each dataset are used in the analysis. Sets with more points, or longer total duration have more influence on the fitted curve. In some cases, the result of duration weighting was to produce trendlines which provided a good fit to the data for

thin ice, but which did not well bound the data for thick ice events. This may be observed by comparing the unweighted values from Case 10 (Figure 6-21) with those found using weighted means in Case 12 (Figure 6-23). From these figures it is evident that the thin ice events dominate in the weighting process, which results in poor agreement for thicker ice. In general it may be concluded that there are less data for thick ice events, and events in this range have shorter total duration, resulting in a weighting scheme which is biased towards thin ice events.

Effect of STRICE event duration
The effect of removing short duration events from the STRICE dataset may be assessed by comparing Case 2 and Case 5. Duration filters for short STRICE events (less than 10 minutes) were used for Case 5, but not used for Case 2. Comparing Figure 6-13 with Figure 6-16, it may be observed that filtering the short duration STRICE events results in curve fits which better bound the datasets. On this basis it is recommended that the short duration events should be filtered out.

Effect of level ice filters
While thicker ice event data are available within the STRICE and Cook Inlet datasets, the main focus here has been placed on competent level ice. The effect of including the thicker, rafted ice in the analysis may be assessed by comparing Case 7 (level ice filters off; Figure 6-18) with Case 2 (level ice filters on; Figure 6-13). As may be observed from Figure 6-18, including the thicker ice data in the analysis results in more inconsistencies between the datasets and results in trendlines which do not bound the data as well as those in Figure 6-13. As discussed earlier in the chapter, uncertainties are associated with the degree of consolidation and strength of the thicker, rafted ice. Based on these results it may be concluded that level ice filters are appropriate and only competent ice should be included in the pressure-thickness analysis.

Effect of Excluding Cook Inlet and JOIA data
Limited information is available for the Cook Inlet dataset making it difficult to assess which factors influence the data. For instance, if very short duration events were used in the calculation of mean pressures the resulting values may not well represent the true mean pressure during the interaction. In addition, it is not clear if the events correspond to continuous crushing, creep or other failure modes. JOIA events have very short durations and only cover a very narrow range of ice thicknesses. For these reasons, the effects of excluding the Cook Inlet and JOIA datasets have been considered here to gauge how strongly they influence the power law fits to the mean pressure data. Examining the trendlines and confidence intervals for Figure 6-12 through Figure 6-23, it may be observed that the analysis cases that include only the STRICE and Molikpaq data yield the most definitive results.

6.5   Summary and Conclusions

Based on the above analysis it may be concluded that a panel of constant width experiences decreasing pressure over the loaded area for increasing ice thickness. This is in general agreement with the well known pressure-area scale effect for ice. In the

absence of a correction for Medof panel softening, the trends of the Molikpaq data are not consistent with the STRICE. To illustrate this point, uncorrected Molikpaq data corresponding to first-year ice (thicknesses less than 0.8 m) and STRICE data have been plotted in Figure 6-24. As may be observed, the uncorrected Molikpaq data are significantly higher than those from STRICE (greater by more than a factor of two).

STRICE and Molikpaq Column Mean Pressure vs. Ice Thickness Data
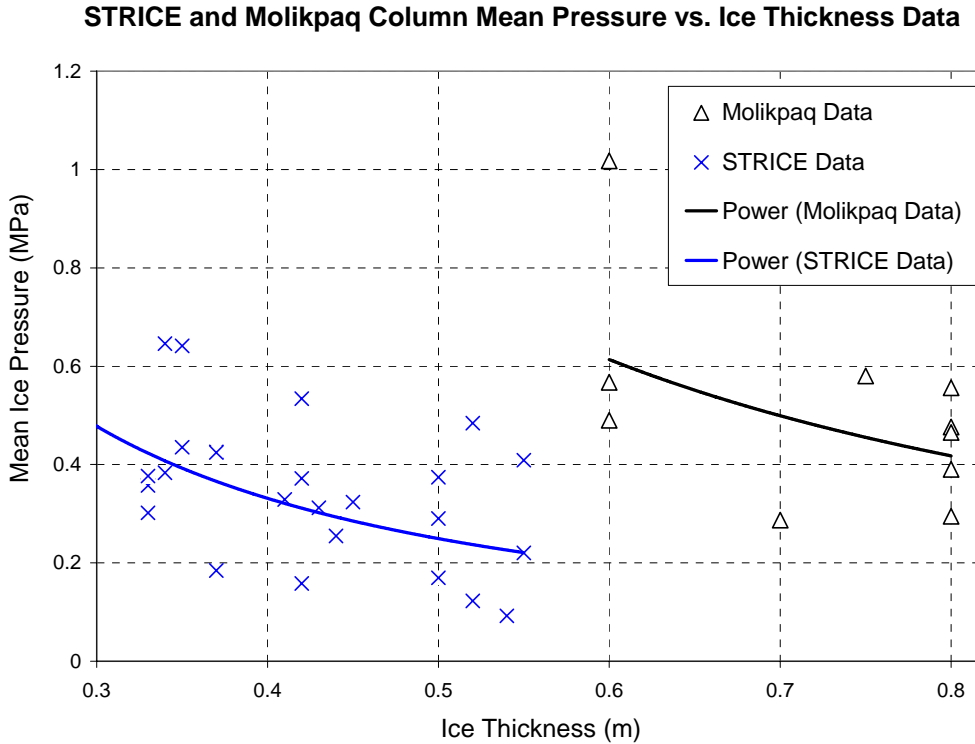
Figure 6-24 **STRICE data (level ice filter on, duration filter on) and Molikpaq data (softening correction off) with power law trendlines.**

Accounting for panel softening yields results that are much more consistent with those observed from the STRICE, JOIA and Cook Inlet datasets. Results corresponding to Case 10 are judged to provide the best fit to the data. A representative power law for the pressure-thickness effect observed in the STRICE and corrected Molikpaq data for Case 10 may be modeled using the power law curves:

$$P_{avg} = 0.278\,h^{-0.408}$$
$$P_{std} = 0.172\,h^{-0.273}$$

Further work is recommended to examine more fully the influence of duration weighting and determine a more effective approach. For the analyses performed here, more data exists for thin ice events than for thick ice. As a result, duration weighting results in trends that are highly influenced by the thin ice events. For the datasets considered in this analysis, duration weighting often produced curves which did not bound the thick ice event data as well as curves based on unweighted values. It was also noticed during the above analysis that time based weighting assigns a higher weight to the slower speed

events (this was particularly the case for the JOIA results). A possible alternative approach to explore in future work is the use of interaction distance (duration x speed) as a weighting measure in the assessment of overall mean and standard deviations.

7   CONCLUSIONS

The data from the Medof panels on the Molikpaq were subjected to statistical analysis to determine the variation of correlation with distance. This was carried out for creep and crushing events. The values of the correlation coefficient were used in an analysis to account for the averaging effect, resulting in a model of probabilistic averaging. Then the events were analyzed to determine the effect of probabilistic averaging, as compared to linear (or simple) averaging. The latter is based on extrapolation of the averaged Medof panel loads to the full structure width by the ratio of structure width to Medof panel total width. It is noted that the Medof panel width is about 10% of the structure width.

Results are shown in the following table, where LA = linear averaging and PA = probabilistic averaging. The values are face loads, but are not given dimensions because of the uncertainty in the Medof panel calibration constant (the original calibration was used). Although reduced global ice loads were found, probabilistic averaging had little effect on creep loads (as expected) but a greater effect in the case of crushing ice failures. The reduction in load was of the order of 15-20%. This was not enough to account for the differences in load estimates noted above.

Event	Failure Mode	Maximum Nominal Load		Maximum Nominal Load	
		LA	LA	PA	PA
		No Bottom	Uniform	No Bottom	Uniform
Mar-25-N-1	Creep	103.1	103.1	101.9	101.9
Apr-12-E-1	Crushing	168.6	168.6	139.1	139.1
Apr-12-E-2	Crushing	187.5	374.5	158.2	319.6
Apr-12-E-3	Crushing	83.9	92.1	73.3	82.4
May-12-N-1	Crushing	168	343.9	140.9	295.9
May-22-N-1	Creep	108.4	140.3	107.4	139.2
May-22-N-2	Crushing	123.1	213.8	103.2	180.1
Jun-02-E-1	Crushing	127.7	128.9	113.9	115.8
Jun-02-E-2	Creep	86.3	87.2	84.8	85.8

In the table, an adjustment has been made for the fact that in some cases, loads were measured on the lower Medof panels. These did not cover the same lateral width as the main set of panels, in fact were only present on one set of Medof panels per face. The term "Uniform" in the table is a method of allowing for the fact that the lower Medof panel is present for only one set of Medof panels, using a linear extrapolation. The "No Bottom" results do not account for bottom panel loads. Another method, the Ratio method, extrapolates on the basis of the ratio of the lower Medof load to the other loads above it. Neither of these methods (Uniform or Ratio) is satisfactory, particularly for ice crushing. The ice failure process consists of high-pressure zones generally concentrated near the centre of the ice sheet, with occasional excursions towards the edges. Both methods fail to recognize this, and generally overestimate the face loads. It is considered that the increase in loads in the table above under the heading "Uniform", where there are bottom loads, is overestimated.

A review has been conducted of the load measuring devices. The strain gauges have been calibrated to the Medof panel loads in the past, as have the extensometers. The strain gauge readings correlate well with the Medof panel loads, but the calibration factor varies considerably. The figure below, based on the data from all S09 strain gauges, shows the uncertainty in calibration factor (CF). Some differences can be explained by differences in structural details but individual gauges show substantial variation, and taken overall, the figure gives a reasonable illustration of the uncertainty. The variance in the calibration factor results from the fact that the same strain can be achieved in the gauge from a multitude of local ice loads at various positions and intensity.

An investigation into the past recalibrations of the Medof panels at the Tarsuit location (Tarsiut Island Research Program, 1982-3) has been undertaken. This led to the conclusion that softening of this material has very likely taken place. The conclusion is reinforced by the very high variability of stiffness in the calibration reports indicating variability in manufacturing quality. In addition there was evidence of softening in the recalibrations and under repeated loadings.

A review was undertaken of the behaviour of the polyurethane material used as part of the construction of the Medof panels. The panels were composed of two parallel steel plates with Adiprene L100 urethane buttons sandwiched between the plates. The outside plate had a thickness of 12.5 mm (1/2") while the Adiprene L100 buttons had a thickness of 2.54mm (1/10") and a diameter of 9.5 mm (3/8") while the back plate had a thickness of 4.5mm (0.179in). This was in contact with the hull of the structure and welded to it. The urethane buttons were closely spaced at 12.7 mm (1/2") centre to centre, and carried most of the load from the outer surface to the structure.

The original calibration was carried out at a maximum nominal stress on the panel of about 1.86 MPa, resulting in a maximum stress on the polyurethane buttons of about 4 MPa. These stress levels, if uniformly distributed over the panel, might lead to acceptable performance, possibly with small damage or nonlinearity in the material. At the same time, creep is significant for longer term loadings. The original calibrations did not show nonlinearity but nonlinearity was identified in later work by Spencer. In all cases, the stress levels were too low to identify any softening, and none of the programs included meaningful repeated-load tests. A viscoelastic model was developed by Spencer based on his tests, but this is applicable only to low stress levels and one-time loading. The Medof panels in the field received many cycles of loading and high stress levels as will now be outlined.

Ice crushing in particular and mixed-mode failure involve highly localized pressures, so that the pressures are significantly amplified over regions of the panel under these ice failure modes. Crushing in particular will apply loadings akin to "panel beating" with repeated and randomly placed high-pressure zones across the face of the panel. In the literature, and particularly the work of Qi and Boyce, it is found that the stress and strain under plausible conditions for the Medof panels, reached levels that would result in nonlinearities in stress-strain behaviour and in softening associated with the Mullins effect. Further, in most instances, the loads were repeated in many cycles, which would add to the softening effect.

Many results have in the past been premised on the basis that the Medof panels are strictly correct. The analysis in this report shows this to be a questionable assumption as a result of possible softening of the panels. Data gathered using other instruments may form a better basis of load estimation. The following hypotheses were proposed in this work for consideration.

1. The Medof panels form the basis of load estimation, with other devices calibrated to them.
2. The extensometer readings form the basis of load estimation, with other devices calibrated to them.
3. The strain gauges form the basis of load estimation, with other devices calibrated to them.
4. A best estimate compromise between the three estimates form the basis of load estimation.

Our evaluation based on the evidence is that the extensometers form the best method of calibration (item 2 above), with a much higher credibility than the other devices. It is a reasonable conclusion that the Medof panel calibrations changed with time, in the sense of a softening process, giving readings that indicated higher loads than previously thought. The errors are of the order of magnitude two.

It is accepted generally that hydraulically placed sand pumped through a pipeline is loose and not dilative (see Hewitt, 2009), and furthermore, prone to liquefaction. While there are disagreements as to the precise state of the sand core, the estimates based on a loose fill agree in essentials with our current estimates of load. In general terms: our advice from Ryan Phillips is that the three significant load events (March 7/8, April 12, and May 12) exceeded the "basal shear resistance" (say 140 to 180 MN), "but not by very much" (C-CORE Technical Memorandum, July 14, 2009). Our current best estimates of global load for these events based on the extensometer readings are somewhat less than 180 MN (120-160 MN) except for the April 12 event which is greater (about 235 MN). The decelerating floe analysis suggests that the load in the May 12 event might be substantially less than 180 MN, but other estimates are closer to this value. The geotechnical estimates fall more in line with these values and all estimates are beginning to fall into the same "ballpark".

The Medof panels have been used for the calibration of the correlation model used for probabilistic averaging. If panels have softened, the correlation structure should remain unchanged, even if different softening of two panels has occurred. If two panels softened in a significantly different way during a loading event, this might have some effect on the correlation analysis. But this scenario is unlikely since most of the softening would have occurred in the early stages of loading, in the 1984-5 season or early in the 1985-6 season, and the change thereafter not very rapid.

The main factors affecting the choice of stiffness are:

1. core stiffness, and
2. proportion and distribution of load on the base and the consequent load path.

It is difficult to obtain a definitive estimate of the structure stiffness from the Sandwell report for use with the extensometer readings. In our calibration work, the values of stiffness (Load Distortion Ratio) equal to 2.2, 2.6 and 3.0 $MNmm^{-1}$ have been chosen. Our best estimate is of the order of 2.6 $MNmm^{-1}$ but the surrounding uncertainty has been taken into account by using a range of values. The values just quoted are for face loads. In the case of global loads, the inclusion of a lateral force in the Sandwell analysis of the forces on the corners tends to make the structure stiffer than it is in reality. As a result, the load distortion ratios for global loads would tend to be too high and exaggerate them.

The loading pattern in the loading case under consideration must be carefully considered in choosing the appropriate factor. A methodology based on matrix methods for dealing with biaxial loading and superposition on multiple faces has been developed successfully, but does suffer from difficulties in the calibration based on the Sandwell report mentioned in the preceding paragraph.

A new finite element analysis with well chosen boundary conditions would be most useful.

In the following, a summary is presented of the main conclusions of the analysis of the three selected events, as decided by clients in the June, 2008 meeting.

May 12th Floe Deceleration Event

The event of May 12th, in which a large floe in open water impacted the Molikpaq, presented a unique opportunity to assess independently the stiffness of the Molikaq in terms of global load versus extensometer readings. Because the floe was in open water, and the size and velocity of the floe were provided, the initial kinetic energy of floe can be estimated. Assuming that the load during the interaction is proportional to the north-south ring distortion and assuming a linear response, the stiffness (in MN applied force per mm ring distortion) required so that the floe stops in the observed time can be calibrated. The necessary global stiffness (load distortion ratio) is 2.2 $MNmm^{-1}$, corresponding to a maximum load of 105 MN. Our best estimate of the value of load

distortion ratio (2.6 MNmm^{-1}) results in a load of 123 MN. This is a face load, and in the present event the loading was mainly concentrated on the north-east face of the structure.

A sensitivity analysis of uncertainty in the time during which the floe deceleration proper occurred, was undertaken. To do this, the first 12 minutes of the impact was removed. The contribution for these first 12 minutes appears to correspond to small loads based on the extensometer ring distortion. It was assumed that the floe stopped in 15 minutes as opposed to the 27 minute approach described previously. A structural stiffness of 2.9 MNmm^{-1} with a maximum global load of 130 MN is the result of this analysis. The matrix model has also been applied to the May 12, 1986 data set. Using this approach a global load estimate of 126 MN results. This approach considers the predominant loading on the North face in addition to the loading occurring on the North East and East faces. In reality, the load seems to have been mainly a face load so that this is likely to be an overestimate.

The deceleration analysis supports the case that ice loads have been overestimated, giving grounds for using significantly lower stiffness values (load distortion ratios).

Analysis of March 25 Event

On March 25th, there were two significant creep loading ice events which were analyzed. For the first event, a face load of 34 MN was obtained, with a value of 55 MN in the second. The second creep event from March 25 was considered in further detail to examine the reasons for the bilinear slope between the Medof loads and ring distortions and the apparent hysteresis effect. By plotting the Medof column loads against ring distortion for given loading and unloading cycles of the north face, it is seen that there is first loading on the east side of the north face, then the west side and finally the center. The difference in loading times may result from the direction of ice movement and the observed fact that in creep type loads, loading occurs at the edges of a face before the center. The net effect is to produce an apparent bilinear slope in the curve giving total Medof load as a function of ring distortion. The analysis also showed that there were considerable differences in the Medof loads for adjacent columns, and that the non-zero intercepts for the Medof load versus ring distortion may be a function of differences in the time of loading and the fact that only 10% of the face was instrumented.

Analysis of March 7th Event

On March 7th there were two significant events which were considered. The ice came from the North impacting the North, North West and West faces. Due to the loading being on the West face, there were no Medof panels to consider. As a result of there being loading on more than one face, the method of calibrating Medof loads on the North face to the face load determined from the N-S ring distortion was not successful. The matrix method was also used as this has the capability of using extensometer ring distortions from multiple faces. The result was very sensitive to the initial offsets which were chosen. The resulting load was 165 MN for the first event and 95 MN for second.

The table below lists the factors which were used to adjust the Medof panel loads for softening. These were achieved by calibrating the Medof panels to the face loads determined by the extensometers for various ring distortion ratios chosen based on the results presented by Sandwell (1991). The Medof panel loads include appropriate averaging.

Event Number	Date	Fast File	Max Face Load for 2.6 MN/mm Ring Distortion Ratio	Factor used to reduce the Medof panel face load to account for softening		
				Ring Distortion Ratio = 2.2	Ring Distortion Ratio = 2.6	Ring Distortion Ratio = 3.0
0325A	25-Mar-86	f603250801	34 MN	0.27	0.32	0.37
0325B	25-Mar-86	f603251302	55 MN	0.44	0.52	0.60
0512A	12-May-86	f605120301	123 MN	0.44	0.52	0.60
0307A	7-Mar-86	f603071520	100 MN	N/A	N/A	N/A
0307B	7-Mar-86	f603071603	81 MN	N/A	N/A	N/A

Note: Those events with N/A were events for which this method was considered to be inappropriate as there was load on multiple faces and limited contact with Medof panels. The matrix method was adopted for these cases.

With regard to the matrix method, the authors feel that the method is promising, and could be much improved by more work on zeroing, and by adjustments to the stiffness matrix.

While there are disagreements as to the precise state of the sand core, the estimates based on a loose fill agree in essentials with our current estimates of load. In general terms: our advice from Ryan Phillips is that the three significant load events (March 7/8, April 12, and May 12) exceeded the "basal shear resistance" (say 140-180 MN), "but not by very much" (C-CORE Technical Memorandum, July 14, 2009). The state of the core would also be affected by the dynamic shaking during these events. Our current best estimates of load for these events based on the extensometer readings are somewhat less than 200 MN except for the April 12 event which is somewhat greater. The decelerating floe and other analyses suggest that the load in the May 12 event is less than 140 MN. But the geotechnical estimates are beginning to fall into the same "ballpark" as other estimates.

In the absence of a correction for Medof panel softening, the trends of the Molikpaq data are not consistent with the other data. Figure A below, with power-law trendlines, illustrates the discrepancy. Accounting for panel softening yields results that are much more consistent with those observed from the STRICE, JOIA and Cook Inlet datasets. Based on a comparison with other data sets, it has been concluded that a panel of constant width experiences decreasing pressure over the loaded area for increasing ice thickness. This is in general agreement with the well known pressure-area scale effect for ice.

The main conclusion of the work is that design pressures based on the Medof panels attached to the Molikpaq structure, for the 1985-86 deployment, overestimate the loads by about 50%. The more detailed approach based on probabilistic methods, given in our Appendix IJA – A, should also be adjusted to give appropriate input values. The methodology for local pressures, as analyzed in the paper (Jordaan, Bruce, Masterson and Frederking, 2010, Cold Regions Science and Technology, in press) based on the Medof panels, is also relevant for this future work.

STRICE and Molikpaq Column Mean Pressure vs. Ice Thickness Data

Figure A

8 REFERENCES

Ashour, M. and Norris, G. 2003. Lateral loaded pile resistance in liquefiable soil. Journal of Geotechnical and Geoenvironmental Engineering, ASCE, May; 129:6, pp 404-414.

Blenkarn, K.A., (1970). Measurements and analysis of ice forces on Cook Inlet structures. In Offshore Technology Conference 1970, Houston, Paper No. OTC 1261, pp. 365-378.

CANATEC, 1991. *Error Analysis of Medof Panels.* CHC 10-54.

Derham C.J. and Thomas A.G. (1977), Creep of rubber under repeated stressing. Rubber Chemistry and Technology 30, 397-402.

Fenco, 1983a. May 16, 1983. *Ice Load Panels for MAC System.* Prepared for Gulf Canada Resources Ltd.

Fenco, 1983b. September 22, 1983. *Recalibration of 10 Tarsiut Medof Panels.* Prepared for Gulf Canada Resources Ltd.

Frederking, R. and Sudom, D., 2006. Maximum ice force on the Molikpaq during the April 12, 1986 event. Cold Regions Science and Technology. 46 147–166.

Gerber, T.M. and Rollins, K.M. 2006. Lateral subgrade moduli for liquefied sand under cyclic loading. Seismic Performance and Simulation of Pile Foundations, ASCE pp 149-160

Hetényi, M., 1946. *Beams on Elastic Foundation*. University of Michigan Studies, Scientific Series, Vol XVI, The University of Michigan Press.

Hewitt, K., 1994. Molikpaq ice interactions: predicted and actual performance. IAHR Ice Symposium 1994. Trondheim, Norway.

Hewitt, K. 2009. *Estimates of Ice Loads on the Molikpaq based on Geotechnical Analyses and Responses*, Report September 2009.

Jefferies, M.G., Wright, W.H., 1988. Dynamic response of Molikpaq to ice-structure interaction. Proceedings OMAE, 1988. Vol IV, pp. 201-220. Houston, TX,USA.

Jordaan, I.J. 2001. Mechanics of ice-structure interaction. Engineering Fracture Mechanics, 68:1923-1960

Jordaan, I.J., 2005. *Decisions under Uncertainty*. Cambridge University Press.

Jordaan, I.J., Li, C., Mackey, T., Nobahar, A. and Bruce, J. 2006. *Design Ice Pressure-Area Relationships; Molikpaq Data,* Report prepared for Canadian Hydraulics Centre, National Research Council of Canada, PERD/CHC Report 14-121, Version 2.2

Jordaan, I.J., Frederking, R., Li, C., 2006. Mechanics of ice compressive failure, probabilistic averaging and design load estimation. IAHR, Ice Symposium 2006.

Jordaan, I.J., Bruce, J.E., Masterson, D and Frederking, R, 2010. Local ice pressures for multiyear ice accounting for exposure. Cold Regions Science and Technology, 2010 (in print).

Kärnä, T. and Yan, Q., (2006). *Analysis of the size effect in ice crushing – edition 2., Technical Research Centre of Finland*, VTT Building and Transport, February 20th, 2006. [Confidential until December 31, 2008]

Kamio, Z., Takawaki, T., Matsushita, H., et al. (2000). Medium scale field indentation tests: physical characteristics of first-year sea ice at Notoro Lagoon, Hokkaido. Proceedings of the Tenth International Offshore and Polar Engineering Conference. 2000. p. 562.

Khan, A.S., and Lopez-Pamies, O., 2002. Time and temperature dependent response and relaxation of a soft polymer. International Journal of Plasticity, Vol 18. pp. 1359.

Klohn-Crippen, 1998. *DynaMAC: Molikpaq Ice Loading Experience.* PERD/CHC Report 14-62. Calgary, Alberta, Canada.

Klohn Crippen Berger, 2009. *Molikpaq Ice Loading 1986 JIP Canadian Beaufort Sea Summary Document.* Report submitted to Conoco Phillips Canada.

Marcellus, R.W. and Morrison, T.B., 1982, *Ice design statistics for the Canadian Beaufort Sea. In Beaufort Sea Environmental Impact Statement (EIS)* 1982, Report No. RWI 15. Calgary: Pallister Resource Management Ltd

Plumtree, A., and Cheng, G.X., 1998. Monotonic and cyclic compressive behaviour of elastomers. Plastics, Rubber and Composites Processing and Applications. Vol 27. No 8. pp 349.

Qi, H.J. and Boyce, M.C., 2005. Stress-strain behaviour of thermoplastic polyurethanes. Mechanics of Materials 37, pp. 817-839.

Rogers. B, Hardy, M.D., Jefferies, M.G, Wright, B.D., 1998. see Klohn-Crippen 1998.

Sanderson, T.J.O 1991. *Ice Mechanics: Risks to Offshore Structures*. Graham Trotman.

Sandwell 1991. *Extensometer Calibration for Ice Load Measurement*, Report 112451, for Gulf Canada Resources Ltd., May 1991.

Smyth M. and Spencer,P. 1987. *Review of Ice Load Measurement Techniques on the Gulf Molikpaq.* Prepared for Gulf Canada Resources Ltd.

Sodhi, D.S., Takeuchi, T., Nakazawa, N., Akagawa, S., Saeki, H. (1998). Medium-scale indentation tests on sea ice at various speeds. *Cold Regions Science and Technology.* 1998. 28. pp. 161-182.

Spencer, P. 1988. *Laboratory Testing of Medof Panels.* Report by Geotech for Gulf Canada.

Takeuchi, T., Masaki, T., Akagawa, S., et al. (1997). Medium-scale indentation tests (MSFIT) - ice failure characteristics in ice/structure interactions. Proceedings of the Seventh International Offshore and Polar Engineering Conference. 1997. v2. p. 376.

Taylor, R.S., (2010). *Investigation and Modeling of Compressive Ice Failure in Offshore Engineering Applications.* Ph.D. Thesis. Memorial University of Newfoundland. St. John's, NL, Canada. (In preparation)

Timco, G., Johnston, M. and Wright, B., 2005. Multi-year ice loads on the Molikpaq: May 12, 1986 event, POAC '05, Vol.1, pp 453-462

Vinogradov, A.M., Jenkins, C.H.M., Winter, R.M., 2000. Cyclic loading effects on durability of polymer systems. Proceedings of the Durability Workshop, Berkeley, California, pp. 159.